SCALABLE TECHNIQUES FOR THE FORMATION OF POLYMER-NANOPLATELET HYBRID MEMBRANES AND CHARACTERIZATION THEREOF

A Dissertation
Presented to
The Academic Faculty

By

J.R. Johnson

In Partial Fulfillment
Of the Requirements for the Degree
Doctor of Philosophy in the School of
Chemical & Biomolecular Engineering

Georgia Institute of Technology

December 2010

SCALABLE TECHNIQUES FOR THE FORMATION OF POLYMER-NANOPLATELET HYBRID MEMBRANES AND CHARACTERIZATION THEREOF

Approved By:

Dr. William J. Koros
School of Chemical &
Biomolecular Engineering
Georgia Institute of Technology

Dr. Chris Jones
School of Chemical &
Biomolecular Engineering
Georgia Institute of Technology

Dr. Victor Breedveld
School of Chemical &
Biomolecular Engineering
Georgia Institute of Technology

Dr. Sankar Nair
School of Chemical &
Biomolecular Engineering
Georgia Institute of Technology

Dr. Wallace Carr
School of Materials Science and
Engineering
Georgia Institute of Technology

Date Approved: 1 October 2010

Aerodynamically, the bumblebee shouldn't be able to fly, but the bumblebee doesn't know that, so it goes on flying anyway.

-Mary Kay Ash

DEDICATION

I would like to dedicate this work to my loving parents, Anthony Johnson and Merri Compton, who have given me the opportunity to be here. Their support (emotionally and financially) and guidance has made me the person that I am today.

A special dedication goes to my high school chemistry teacher, Ms. Laura Miller, and my best friend Ms. Joanna Begin. Ms. Miller pushed me in the right direction early on and I never looked back. Joanna has been a great friend over the years no matter the circumstances. She has provided me with more encouragement than I can every repay.

Thank You.

ACKNOWLEDGEMENTS

Before I name names and recognize all of those people that made my graduate experience amazing, I have to recognize those that are truly responsible – the sponsors. At the onset, this project was sponsored by the National Science Foundation (NSF) as part of the Nanoscale Interdisciplinary Research Team (NIRT) program via NSF/CTS Grant #0403574. After expiration, the project was continued under the King Abdullah University of Science and Technology Global Research Partnership (KAUST-GRP), Award #KUS-I1-011-21.

Now that we have got the formalities out of the way, we should move forward into the heart of the matter. First and foremost I have to thank Dr. Koros – for everything. The moment I met him I was sold on membrane technology. His relentless energy, excitement, wealth of knowledge and "not-so-normal" sense of humor has made the experience over the years absolutely amazing. I can honestly say that I have never met anyone so dedicated to their job while simultaneously focused on student development (and of course, Ann). His guidance over the years has shaped me into the researcher that I am today.

It would be far too easy to go on an Oscar winning tirade in attempts to acknowledge everyone who has played a role in the success of my project over the years. I will do my best to recognize those who have had the biggest impact. From colleagues to friends and of course family, there is a laundry list of people that deserve recognition.

Colleagues

First, I would like to credit the Koros Research Group – past and present. I realize that this is a blanket a statement, so I will do my best to recognize those members that have been particularly influential.

Past: Shabbir Husain for transferring his vast knowledge of hollow fiber spinning to me (and many others). John Perry, Raymond Chafin and Adam Kratochvil – who were senior members when I joined the group – for their advice and direction during my startup period. I owe a great deal of gratitude to Madhava Kosuri for his fundamental teachings of all things chemical engineering. And of course, I can't forget Jason Ward and Ryan Adams for teaching me the "dense film" ropes and everything else that they were willing to share.

Present: I am very grateful to Oğuz Karvan for all of his help alleviating my other workload which has allowed me to finish this project in less than a decade. I would also like to recognize Dhaval Bhandari, Jong Suk Lee and Ryan Lively for their various efforts over the past few years.

Friends & Family
It goes without saying that I wouldn't be here without my parents, who took the time to bring me into the world. I would also like to thank my brother Jeremy and my close friend Joe Hill for their tireless efforts to put food on the table of America. There is a list of friends that have made the grad school experience more than just work, the notable contestants include (in no particular order): Harty, Petey, Jason, K-Reed, Cash Money, RaRa, Catherine, JohnBoy, RyanL and of course Ronnie. There are two more people of particular importance. First, my best friend, Bananahead, for any and everything. Please keep being you. Finally, Rybi, whom is probably a worse influence than anything, has been a great friend since day one. The yarn we could spin would be leagues in length. I only hope the carousals continue over the years.

Honorable Mention
I would like to thank my committee members for their input and feedback over the years. Dr. Alexander Moukasian and Ms. Tatyana Orlova at the University of Notre dame were critical in the TEM characterization portion of this work. Without their help, I would only have half a story to tell. Additional TEM support was provided by Dr. Sunho Choi while he was at the University of Minnesota. Michelle Martin, the group administrative assistant, makes this place tick and tock. We couldn't do it without her. Finally, I would like to recognize the efforts of the most important man in the building: Hot Rod Sefton. Thanks for all of the terrible jokes and package deliveries.

Let's eat.

TABLE OF CONTENTS

LIST OF TABLES

LIST OF FIGURES

SUMMARY

Membrane technology has become an essential alternative for efficient gas separation processes versus traditional thermally-driven processes. Although polymeric membranes have received the most attention, researchers have found that combining highly separation selective inorganic, metal-organic (MOFs) or carbon molecular sieving materials with polymeric materials can improve membrane performance. These multi-component membranes are often referred to as *mixed matrix* or *hybrid membranes*. Traditional hybrid membrane filler materials have size and aspect ratio characteristics that are less favorable for the production of asymmetric membranes that utilize a thin (~100nm) permselective layer. Recent developments have considered high aspect ratio sieving materials (i.e. *flakes* or *platelets*) as alternative inorganic fillers in hybrid membrane systems. Polymer-nanoplatelet hybrid membranes show promise as the next generation of membranes, but in order to make these realizable, methods to produce these materials on a large scale are necessary. In this study it was our objective to develop scalable techniques for creating polymer-nanoplatelet membranes.

There has been extensive research in the area of these hybrid materials. Moreover, many authors have been successful at producing gas separation membranes. Typically these reports have utilized melt blending, *in situ* polymerization or solution blending. Few, however, have utilized solution blending for creating membranes via phase inversion. And to date, there have not been any reports regarding the fabrication of asymmetric membranes containing nanoplatelet filler materials. In this work we have developed a solution-based procedure for the formation of hybrid polymer-nanoplatelet dopes for dense film and asymmetric hollow fiber membrane formation. To our knowledge, we are the first to report the formation of successful polymer-nanoplatelet membranes containing unmodified filler materials.

Dense film membrane studies were used to prove the effectiveness of our exfoliation and dispersion process developed for this work. Permeation measurements showed the hybrid membranes have desirable transport properties that are on par with mathematical model predictions. Additionally, TEM characterization provided strong evidence supporting the efficacy of our preparation procedures to produce an exfoliated system of nanoplatelets. We also showed that these procedures are applicable to different polymer systems (cellulose acetate and Torlon®) of commercial relevance. Demonstrating the successful production of dense films set the stage for asymmetric hollow fiber membrane formation. We report the first production of asymmetric hollow fiber membranes containing nanoplatelet fillers; indicating that the process can be applied in a realistic membrane formation platform. These accomplishments serve as the groundwork for future nanocomposite formation. We believe that the results from this work strongly indicate that the methods are flexible, diverse and scalable.

CHAPTER 1

INTRODUCTION & MOTIVATION

1.1 Motivation

Gas and vapor separation processes have received significant attention in recent years.[1,2] Traditional thermally-driven processes are effective but lack the desired energy efficiency and may also have associated environmental consequences. Membrane technology has become an essential alternative for efficient gas separation processes.[3] Polymeric membranes have received the most attention in this field due to the manufacturability, low material costs and robust physical characteristics. These membranes can be manufactured into various module types, including: plates, spiral wound and hollow fibers.[4]

Albeit polymeric membranes are a great alternative to thermal separation systems, it has been shown that known materials have a performance limit. As both energy costs and the demand for increased separation performance rise, the need for enhanced membrane performance is growing. In order to surpass these limitations researchers have found that combining highly separation selective inorganic, metal-organic (MOFs) or carbon molecular sieving materials with polymeric materials can provide such a solution. These multi-component membranes are often referred to as *mixed matrix membranes*. However, for the purposes of this study we will use the more general term *hybrid membranes*.

Hybrid membranes show promise as the next generation of membranes, but in order to make these realizable we must develop methods to produce these materials on a large

scale. In this study it was our objective to develop such a method for creating advanced hybrid membranes.

1.2 Asymmetric Membranes

It was elucidated by Loeb and Sourirajan in the 1960s that a high flux membrane could be produced by forming an ultra-thin selective layer on top of a porous support layer.[4] This process is successful because membrane permeability/permeance (productivity) is governed by the thickness of the membrane itself (see Chapter 2 for additional transport theory). Membranes of this type are referred to *anisotropic* or *asymmetric* membranes. We will use the latter term for this document.[4]

Typically, asymmetric membranes are comprised of a thin (50-500nm) *permselective* skin layer supported by a porous, non-selective substrate. Figure 1.1 shows a schematic example of an asymmetric hollow fiber membrane.

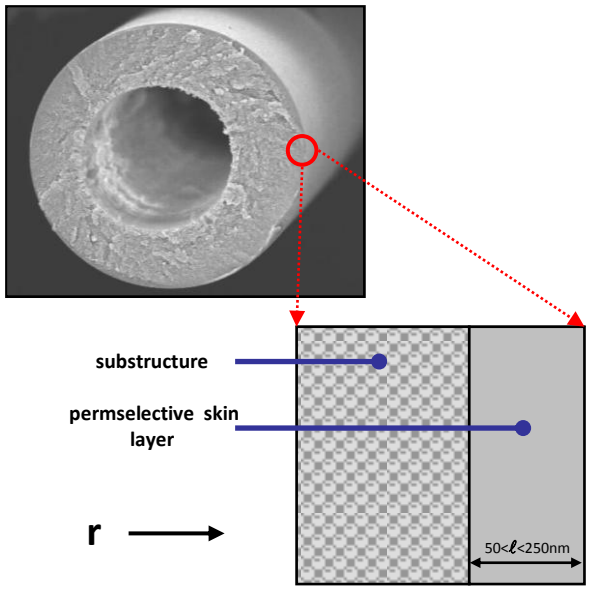

Figure 1.1: Asymmetric hollow fiber membrane

The asymmetric form of membranes is actively used in most separation applications (e.g., water, gas, liquid).[4] In the previous section we identified the three most common formats used industrially to be plate-in-frame, spiral wound and hollow fiber. Each of these morphologies has been shown to have specific applications where one may be preferred over the other. However, if one were to consider surface area to volume trade-offs – in other words, the potential productivity versus the size of the separation unit – it is clear that the hollow fiber format is the clear leader. This trade-off also has particular economic importance in aggressive separations because flanges and membrane module shells are made from expensive stainless steel or alloys. If the operation is large, the cost of the separation unit quickly outweighs the cost of the membrane and therefore it is desirable to reduce the number of modules necessary.

1.3 Hybrid Membranes

Pure polymer materials have been the focus for the production of a majority of membranes. Robeson awakened the membrane community by identifying tradeoff limitations of the selectivities (efficiency) and permeabilities (productivity) of solution processible polymers.[5,6] With rising energy costs and the need for advanced separations, the noted limitations of pure polymer membranes have indeed imposed an upper bound. Multi-component membranes utilizing organic and inorganic (or carbon) materials offer opportunities to achieve these goals.[7] An example of the suggested polymeric efficiency trade-off is plotted as a function of productivity in Figure 1.2. Moreover, we include the proposed productivity and efficiency enhancements for hypothetical hybrid membranes.

Hybrid membranes incorporate molecular sieving filler materials into an efficient polymer matrix. The filler materials provide advanced selectivity characteristics and the polymer matrix lends the desired processibility required to manufacture membranes. These hybrid membranes have received significant attention in the literature recently.[8-18]

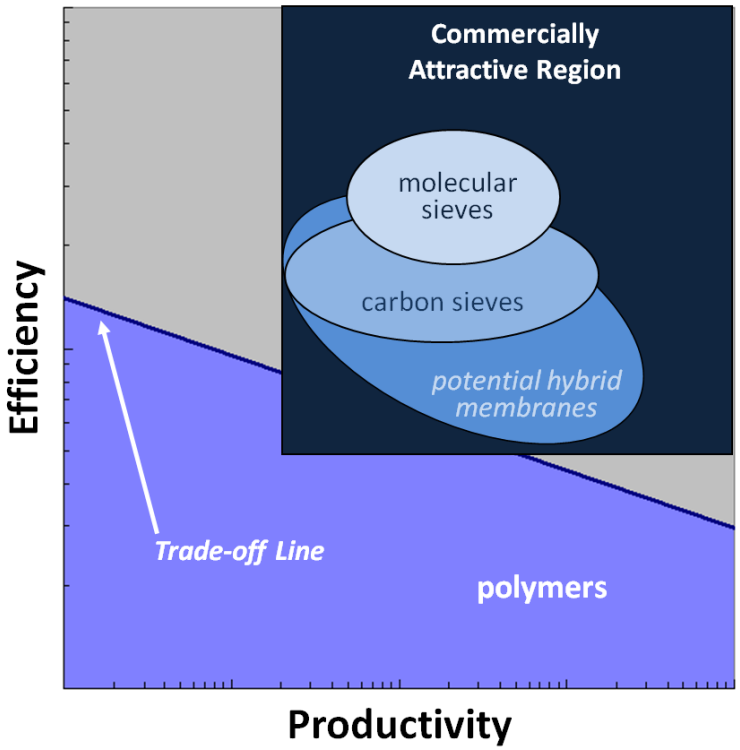

Figure 1.2: Hypothetical polymer trade-off curve and the corresponding capabilities of hybrid membrane materials.

1.3.1 Transport Mechanisms in Hybrid Membranes

In some instances, transport in hybrid membrane materials can be extremely complicated to interpret accurately.[19-21] However, for the sake of simplicity, we can consider the scenario that would ideally contribute to the greatest permselectivity enhancement in these materials. This case is strongly rooted in the diffusion of independent molecular species through the membrane – specifically we consider comparative path of *tortuosity* for each species. In Figure 1.3 we have drawn a simple cartoon that demonstrates the effect of a selective insert in a non-selective matrix.

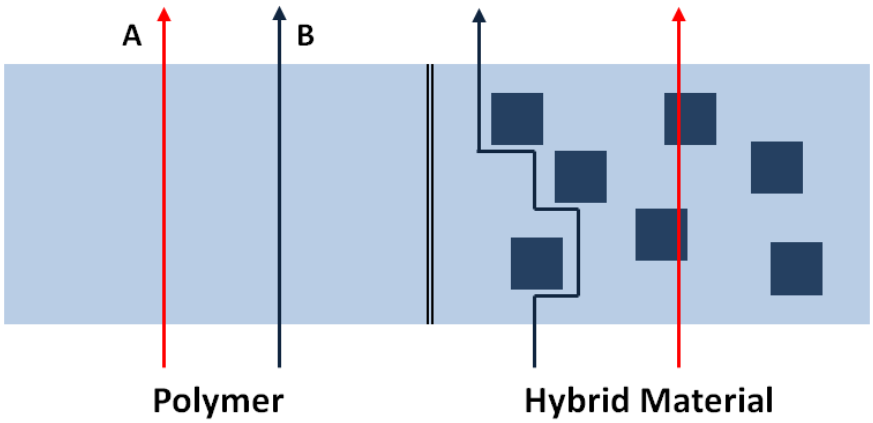

Figure 1.3: Comparative transport pathways of molecular species in polymer and hybrid materials containing molecular sieving fillers.

From the figure we see that in the polymer matrix, the two species have similar transport pathways. Alternatively, in the second system we have introduced a size-selective filler material. Species "B" is unable to permeate through the filler material and therefore is forced to take a more tortuous path through the membrane. Species "A" on the other hand continues to travel a direct path through the membrane, thereby increasing the permselectivity of the membrane.

1.3.2 Formation Challenges in Hybrid Membranes

On paper, hybrid membranes provide an excellent opportunity to enhance the properties of traditional polymeric materials. There are, however, a number of challenges in producing these membranes without defects. Problems arise in the pre- and/or post-membrane formation stages. Pre-formation challenges are largely related to solution formulation and processing and post-formation challenges are predominated by polymer-filler interactions. These challenges have been significant attention in the literature over the years.[7,15,21-23] In the following two sub-sections we will elucidate the primary challenges.

1.3.2.1 Pre-Formation Challenges

In order to create a hybrid membrane with idealized permselectivity enhancements we must begin with an extrudable “dope” that will yield a membrane with the desired properties. To that effect it is imperative that we create a solution containing a well dispersed and stable filler phase. It is unlikely that simply adding filler particles to a solution of polymer and solvent will produce the desired hybrid dope without additional preparation. In all likelihood the filler phase will remain in an agglomerated form and/or precipitate out of solution. These two circumstances are presented as a simple cartoon in Figure 1.4.

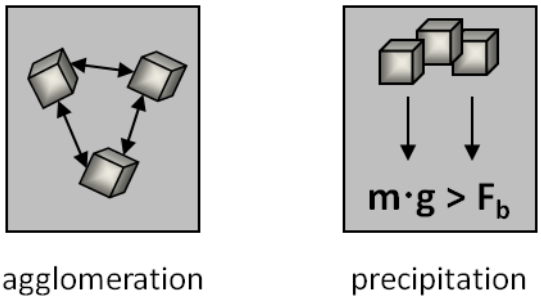

Figure 1.4: Examples of pre-formation challenges in hybrid membrane solutions.

Particle agglomeration is the most common challenge related to dispersing fillers in solution.[24] In most cases the filler being added is already in an agglomerated state and must first be fragmented down to the desired size and simultaneously dispersed evenly in the host medium. This is general accomplished via mechanical energy input (e.g., blending, sonication, shaking).[24] After creating the desired blend it is imperative that the filler phase remains dispersed throughout the membrane formation process. Dispersant stabilization can be achieved using a variety of methods which will be discussed in further detail in the next chapter.

Precipitation of the dispersant phase is function of final particle size and density after proper dispersion and the buoyant forces provided by the host medium. In the case of hybrid membranes this is generally not a prevalent issue because (1) the molecular sieving filler should be nano-sized in order to produce an effective asymmetric membrane and (2) the polymer solution host medium typically has a high viscosity. Regardless, it is important to consider the negative effects of poor dispersion and particle-host matching.

1.3.2.2 Post-Formation Challenges

For the purposes of this discussion we will assume that the well-dispersed phase that we created in the pre-formation stage will survive after the membrane formation process. If true, the primary source of hybrid membrane defects is related to the interfacial region between the host matrix and the filler phase. More specifically, there are four major cases to consider and their effects on membrane performance.[7,9] These cases and their corresponding permselective consequences are exemplified in Figure 1.5 with discussion to follow.

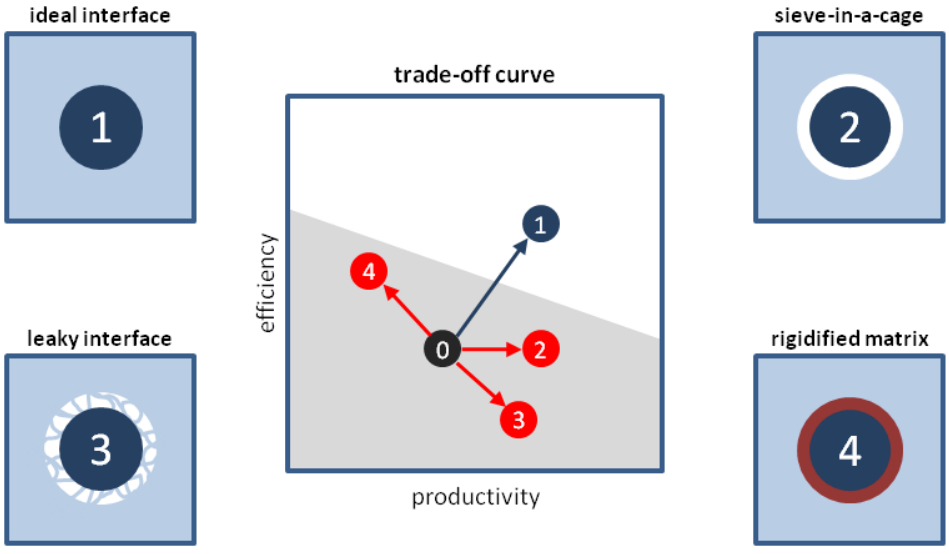

Figure 1.5: Interfacial morphologies in hybrid membrane materials and their apparent effects on membrane performance.

Case 1: Ideal Interface

This is the desired morphology that will produce the desired enhancements in both productivity and efficiency. For this morphology to occur, the polymer and filler must be compatible or the filler needs to be modified in order to create a surface leading to the ideal interface.

Case 2: Sieve-in-a-cage

This phenomenon generally occurs if the polymer and filler phases are incompatible, but may also be caused by surface delamination during the formation process. If the sieve-in-a-cage morphology occurs, then the membrane will show an increase in permeability but no gain in selectivity. In some cases, the selectivity may even decrease if Knudsen diffusion contributions become significant (i.e. higher particle loadings). Many researchers have studied this side effect and solutions to prevent it. Successful solutions include sieve surface modification, polymer-sieve grafting and chemical functionalization of the sieve surface.

Case 3 & 4: Leaky Interface & Rigidified Matrix

These two cases are often considered to be parts of the *zone-of-influence* phenomenon wherein the polymer phase around the filler material is either less or more densely packed than the bulk phase. In the former case, the polymer shows some affinity for the sieve surface, but not enough to create a defect-free interface. In fact, the poorly absorbed chains create a polymer lean phase that lends to a non-selective increase in permeability via Knudsen diffusion. Alternatively, the polymer chains may pack more densely around the sieve thereby creating a more rigid interphase, which is referred to as chain immobilization. The rigid interphase will produce barrier-like properties, compared to the bulk phase, thus leading to a decrease in membrane productivity. Coincidently, the membrane may exhibit increases in selectivity.

Plugged Sieves

An additional post-formation non-ideality in hybrid membranes is related to the sieve itself. Depending on the size of the sieve pore window and the kinetic diameters of the other system components, it is possible to create a dispersion of plugged sieves. In this regard the filler phase will behave like a barrier and a depression in productivity will be observed. Plugged pores are generally a result of solvent ingress (e.g., water, solvent, functionalization agents) and/or polymer chains sorption.

1.4 Hybrid Membranes Containing Non-Unit Aspect Ratio Fillers

As noted, hybrid membranes containing molecular sieving materials offer the potential to provide greater separation selectivities. A majority of the literature has focused on the incorporation of standard zeolite or carbon molecular sieve materials and more recently, metal-organic framework (MOF) sieves. These materials have the potential to yield the desired results, but their size and aspect ratio is less favorable for the production of asymmetric membranes that utilize a thin (~100nm) permselective layer. Moreover, such hybrids require achieving high sieve loadings in order to provide properties that approach those of the pure component high performance dispersed sieve phase itself. Recent developments have considered high aspect ratio sieving materials (i.e. *flakes* or *platelets*) as alternative organic fillers in hybrid membrane systems.[25-31]

Traditional molecular sieving materials generally have an aspect ratio (A_r) of ~1. This geometry limits particle packing within the skin layer. Moreover, these materials are usually greater than 100nm in lateral dimensions (diameter) which imposes further limitations when manufacturing asymmetric membranes. When larger diameter particles are used, the risk of producing defects in the permselective skin increases. Finally, if these particles are not dispersed well (e.g., if there are particle agglomerates) the probability of defect formation increases further. On the plus side, the functionality of sieves with A_r~1 is not usually affected by orientation within the polymer matrix.

High aspect ratio (A_r>10) and thin (~1 nm) nanoplatelet sieves offer many advantages over traditional molecular sieves.[28,29] The small thickness is critical when producing asymmetric membranes where thinner skins yield greater productivity.[32] Figure1.6 demonstrates the packing differences between A_r~1 and A_r>10 materials within the permselective layer of an asymmetric membrane. (Note: $\ell_1 > \ell_2$) If we analyze this characteristic further we see that nanoplatelets also provide filler loading advantages. Recognizing that molecular sieves predominately separate molecules based on size and shape, the pore window of the sieve is the critical characteristic.[33] A longer transport path length through the sieve does not improve the separation selectivity of material; therefore, a thinner sieving material can achieve the same separation if the critical pore windows are equal to those in an A_r~1 material. Applying this principle permits one to incorporate less filler material without sacrificing selectivity. Alternatively, one may also use more material and take advantage of the packing capability of the platelets in order to increase selectivity and productivity even further.

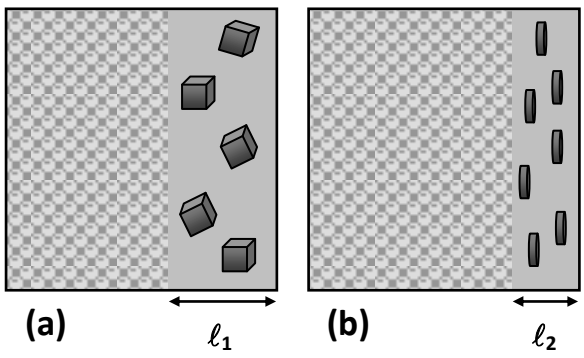

Figure 1.6: (a) Asymmetric membrane containing molecular sieves with A_r~1 (b) Asymmetric membrane containing nanoplatelet molecular sieves

Like A_r~1 materials, nanoplatelets are susceptible to membrane defects caused by particle agglomeration and improper polymer-sieve interfacial contact; therefore proper formulation of the casting/spinning solutions is critical. Nanoplatelets can provide significant improvement in membrane mechanical properties.[34] Considerable research

has focused on the benefits of adding impermeable layered silicate materials to polymer matrices as highlighted in the literature.[35-38] To our knowledge, however, no one has extended this work with nanoplatelets to small diameter hollow fibers.

1.4.1 Formation Challenges in Hybrid Membranes Containing Nanoplatelets

In Section 1.2.2 we discussed the formation challenges associated with hybrid membranes. When working with nanoplatelet materials, rather than A_r~1 materials, the same challenges described above apply with the *addition of two others*: exfoliation and orientation. The cartoon in Figure 1.7 is used to demonstrate the difference between a well-dispersed, exfoliated system and that of an unexfoliated or unoriented system. Further explanation of these system non-idealities is provided in the next two subsections.

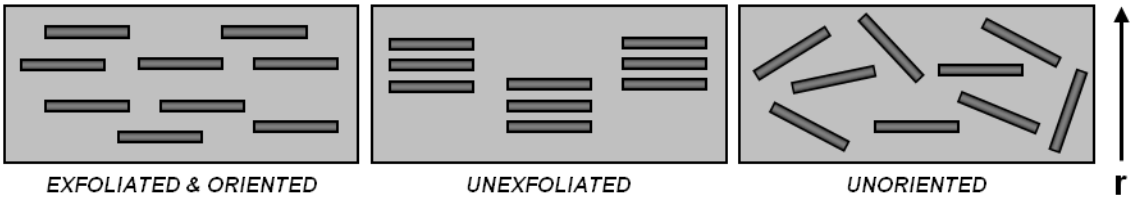

Figure 1.7: Possible nanocomposite formations

1.4.1.1 Exfoliation

This is the most difficult challenge associated with nanoplatelets. Due to the nature of their geometry and crystallography, nanoplatelet materials are usually synthesized or occur in a stacked formation; like a deck of cards.[39,40] The layers are held together by charge neutralizing cations or anions or by the template structuring agents used during synthesis. In order to utilize the favorable characteristics of these materials in a membrane platform, these stacks of layers must be disrupted in order to yield an exfoliated state.[38] This process has received significant attention in the literature.[35,37]

However, the success of particle exfoliation greatly depends on the procedures and other materials used.

1.4.1.2 Orientation

In order to utilize the geometric benefits of nanoplatelet molecular sieves, it is critical that the face of the particles be oriented orthogonal to the direction of molecular transport.[29,41] Unoriented particles can still increase the tortuosity of the molecular transport path, but this makes transport modeling extremely difficult and reduces the efficacy of the membrane as a torturous barrier for the undesired component. Rheological studies have shown that under high shear stresses nanoplatelets can be oriented.[42,43] Fortunately, if nanoplatelets are incorporated into the hollow fiber morphology, there is a high probability that the particles will orient due to the very high shear stresses that occur within the annulus of an extrusion spinneret. This applies to commercial film casting as well. Figure 1.8 is a drawing of the truncated cross section of a spinneret. The shear force gradient in the polymer solution is represented by the shaded profile. A shear force gradient applied to the surface of the particle leads to an axial rotation and ultimately the particle will orient in the solution. Macosko discusses this principle in-depth.[42]

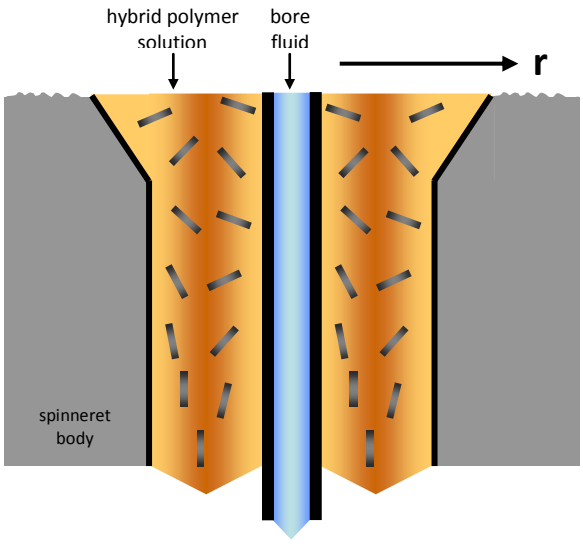

Figure 1.8: Truncated cross section of fiber spinneret showing shear alignment of nanoplatelets during spinning process.

1.5 Research Objectives

At the onset of this project, the goal was to develop an engineering understanding of the principles governing production of polymer-nanoplatelet hybrid asymmetric hollow fiber membranes and their applications in efficient gas separations. To achieve this goal, we identified three objectives that we hypothesized would generate the desired results.

1. *Develop a method(s) to successfully exfoliate and disperse inorganic nanoplatelets into a polymer solution for membrane formation.*

   It has been highlighted throughout this Chapter that there are numerous challenges associated with hybrid membrane formation. This is especially true for hybrid membranes containing nanoplatelet fillers. Therefore in order to produce membranes with the desired morphology we had to first identify an effective method to produce an exfoliated, dispersed and stable polymer solution containing an significant quantity of nanoplatelets filler.
2. *Produce and characterize hybrid dense-film membranes to verify the efficacy of the preparation techniques developed.*

   Keeping with the traditional process of membrane development, we must first explore and understand the properties of dense film membranes before moving forward into asymmetric morphologies. This step is important in determining the fundamental transport properties of a new material set. Furthermore, this step provides us with the opportunity to screen the efficacy of the solution preparation techniques without the added complications of hollow fiber spinning.

3. *Spin and characterize hybrid asymmetric hollow fiber membranes containing exfoliated and dispersed nanoplatelet filler materials.*

The ultimate membrane morphology for gas separations is the asymmetric hollow fiber. To prove the value of the method developed in Objective 1, we must show that the method is in fact scalable. Successful application of this method will serve as the final validation.

1.6 Dissertation Organization

Following this introductory Chapter we will be presenting seven additional Chapters. As is customary we will provide a concise literature review of the material pertaining to our objectives in Chapter 2. This will be followed by a description of the materials used in this work and the various investigatory methods used to qualify and quantify our work. Chapters 4-7 will serve as the core and highlight the results of this work. More specifically, Chapter 4 will focus on the characterization of the preparation methods used to form the hybrid membranes that are presented in Chapters 5 & 6. In the final body Chapter we will discuss the hollow fiber membranes that were produced using the as-developed preparation techniques. Conclusions and potential paths forward will be presented in Chapter 8. There will be numerous Appendices of supplemental and/or complimentary material.

1.7 References

1. Panel on Separations, *Separation Technologies for the Industries of the Future*. (National Academy Press, Washington, D.C., 1998).

2. R.W. Baker, "Membrane Technology in the Chemical Industry: Future Directions", in *Membrane Technology in the Chemical Industry*, edited by Suzana Pereira Nunes and Klaus-Viktor Pienemann (WILEY-VCH, Weinhiem, Germany, 2006), pp. 305-335.

3. W.J. Koros, "Evolving Beyond the Thermal Age of Separation Processes: Membranes Can Lead the Way," *AIChE Journal* **50** (10), 2326 (2004).

4. R.W. Baker, *Membrane Technology and Applications*. (John Wiley & Sons, Inc., New York, 2004), 2nd ed.

5. L.M. Robeson, "The Upper Bound Revisited," *Journal of Membrane Science* **320** (1-2), 390-400 (2008).

6. L.M. Robeson, "Correlation of Separation Factor versus Permeability for Polymeric Membranes," *Journal of Membrane Science* **62**, 165-185 (1993).

7. T. T. Moore, R. Mahajan, D. Q. Vu, and W. J. Koros, "Hybrid Membrane Materials Comprising Organic Polymers with Rigid Dispersed Phases," *AIChE Journal* **50** (2), 311-321 (2004).

8. C.M. Zimmerman, A. Singh, and W.J. Koros, "Tailoring Mixed Matrix Composite Membranes for Gas Separations," *Journal of Membrane Science* **137**, 145-154 (1997).

9. S. Shu, "Engineering the Performance of Mixed Matrix Membranes for Gas Separations," *PhD Dissertation*, Georgia Institute of Technology, 2007.

10. D. Sen, H. Kalipcilar, and L. Yilmaz, "Development of Polycarbonate Based Zeolite 4A Filled Mixed Matrix Gas Separation Membranes," *Journal of Membrane Science* **303** (1-2), 194-203 (2007).

11. T. Merkel, B. Freeman, R. Spontak, Z. He, I. Pinnau, P. Meakin, A. Hill, "Ultrapermeable, Reverse-Selective Nanocomposite Membranes," *Science* **296** (5567), 519-522 (2002).

12. J. Liu, T-H. Bae, W. Qiu, S. Husain, S. Nair, C. Jones, R. Chance, W.J. Koros, "Butane Isomer Transport Properties of 6FDA-DAM and MFI-6FDA-DAM Mixed Matrix Membranes," *Journal of Membrane Science* **343** (1-2), 157-163 (2009).

13. S. S. Kulkarni, S. M. Tambe, A. A. Kittur, and M. Y. Kariduraganavar, "Preparation of Novel Composite Membranes for the Pervaporation Separation of Water-Acetic Acid Mixtures," *Journal of Membrane Science* **285** (1-2), 420-431 (2006).

14. L. Y. Jiang, T. S. Chung, and S. Kulprathipanja, "Fabrication of Mixed Matrix Hollow Fibers with Intimate Polymer-Zeolite Interface for Gas Separation," *AIChE Journal* **52** (8), 2898-2908 (2006).

15. S. Husain and W.J. Koros, "Mixed Matrix Hollow Fiber Membranes Made with Modified HSSZ-13 Zeolite in Polyetherimide Polymer Matrix for Gas Separation," *Journal of Membrane Science* **288** (1-2), 195-207 (2007).

16. C. V. Funk and D. R. Lloyd, "Zeolite-filled Microporous Mixed Matrix (ZeoTIPS) Membranes: Prediction of Gas Separation Performance," *Journal of Membrane Science* **313** (1-2), 224-231 (2008).

17. T. S. Chung, L. Y. Jiang, Y. Li, and S. Kulprathipanja, "Mixed Matrix Membranes (MMMs) Comprising Organic Polymers with Dispersed Inorganic Fillers for Gas Separation," *Progress in Polymer Science* **32** (4), 483-507 (2007).

18. R. Adams, C. Carson, J. Ward, R. Tannenbaum, W.J. Koros, "Metal Organic Framework Mixed Matrix Membranes for Gas Separations," *Microporous and Mesoporous Materials* **131** (1-3), 13-20 (2010).

19. R. Pal, "Permeation Models for Mixed Matrix Membranes," *Journal of Colloid and Interface Science* **317** (1), 191-198 (2008).

20. S. Hashemifard, A. Ismail, T. Matsuura, "A New Theoretical Gas Permeability Model Using Resistance Modeling for Mixed Matrix Membrane Systems," *Journal of Membrane Science* **350** (1-2), 259-268 (2010).

21. R. H. B. Bouma, A. Checchetti, G. Chidichimo, and E. Drioli, "Permeation Through a Heterogeneous Membrane: The Effect of the Dispersed Phase," *Journal of Membrane Science* **128** (2), 141-149 (1997).

22. P. Rittigstein and J. M. Torkelson, "Polymer-Nanoparticle Interfacial Interactions in Polymer Nanocomposites: Confinement Effects on Glass Transition Temperature and Suppression of Physical Aging," *Journal of Polymer Science Part B-Polymer Physics* **44** (20), 2935-2943 (2006).

23. S. Matteucci, R. D. Raharjo, V. A. Kusuma, S. Swinnea, and B. D. Freeman, "Gas Permeability, Solubility, and Diffusion Coefficients in 1,2-polybutadiene Containing Magnesium Oxide," *Macromolecules* **41** (6), 2144-2156 (2008).

24. R. Nelson, *Dispersing Powders in Liquids*. (Elsevier, New York, NY, 1988).

25. C. Wang, W. M. Hua, Y. H. Yue, and Z. Gao, "Delaminated Microporous Aluminophosphate-Filled Polyvinyl Alcohol Membrane for Pervaporation of Aqueous Alcohol Solutions," *Microporous and Mesoporous Materials* **105** (1-2), 149-155 (2007).

26. B. R. Vaughn and E. Marand, "Transport Properties of Polymer-Aluminophosphate Nano-Composites Prepared by Simple Mixing," *Journal of Membrane Science* **310** (1-2), 197-207 (2008).

27. S. Maheshwari, E. Jordan, S. Kumar, F. S. Bates, R. L. Penn, D. F. Shantz, and M. Tsapatsis, "Layer Structure Preservation During Swelling, Pillaring, and Exfoliation of a Zeolite Precursor," *Journal of the American Chemical Society* **130** (4), 1507-1516 (2008).

28. H-K Jeong, W. Krych, H. Ramanan, S. Nair, E. Marand, and M. Tsapatsis, "Fabrication of Polymer/Selective-Flake Nanocomposite Membranes and Their Use in Gas Separation," *Chemistry of Materials* **16** (20), 3838-3845 (2004).

29. E.L. Cussler, "Membranes Containing Selective Flakes," *Journal of Membrane Science* **52**, 275-288 (1990).

30. S. H. Choi, J. Q. Coronas, Z. P. Lai, D. Yust, F. Onorato, and M. Tsapatsis, "Fabrication and Gas Separation of Polybenzimidazole (PBI)/Nanoporous Silicates Hybrid Membranes," *Journal of Membrane Science* **316** (1-2), 145-152 (2008).

31. S. Choi, J. Coronas, E. Jordan, W. Oh, S. Nair, F. Onorato, D. F. Shantz, and M. Tsapatsis, "Layered Silicates by Swelling of AMH-3 and Nanocomposite Membranes," *Angewandte Chemie-International Edition* **47** (3), 552-555 (2008).

32. J.R. Johnson, W.J. Koros, "Utilization of Nanoplatelets in Organic-Inorganic Hybrid Separation Materials: Separation Advantages and Formation Challenges," *Journal of Taiwan Insitute of Chemical Engineers* **40** (3), 268-275 (2009).

33. D.W. Breck, *Zeolite Molecular Sieves*. (John Wiley & Sons, Inc., New York, 1974).

34. H. Stretz, D. Paul, R. Li, H. Keskkula, P. Cassidy, "Intercalation and Exfoliation Relationships in Melt-Processed poly(styrene-*co*-acrylonitrile)/Montmorillonite Nanocomposites," *Polymer* **46** (8), 2621-2637 (2005).

35. T.J. Pinnavaia and G.W. Beall, *Polymer-Clay Nanocomposites*. (John Wiley & Sons, Ltd., New York, 2000).

36. D.R. Paul, L.M. Robeson, "Polymer Nanotechnology: Nanocomposites," *Polymer* **49** (15), 3187-3204 (2008).

37. Y.C. Ke and P. Stroeve, *Polymer-Layered Silicate and Silica Nanocomposites*. (ELSEVIER Inc., San Diego, 2005).

38. F. Hussain, M. Hojjati, M. Okamoto, and R. E. Gorga, "Review Article: Polymer-Matrix Nanocomposites, Processing, Manufacturing, and Application: An Overview," *Journal of Composite Materials* **40** (17), 1511-1575 (2006).

39. H. van Olphen, *An Introduction to Clay Colloid Chemistry*. (John Wiley & Sons, Ltd., New York, 1977), 2nd ed.

40. A. Newman, G. Brown, *Chemistry of Clays and Clay Minerals*. (John Wiley & Sons, New York, 1987).

41. J. A. Sheffel and M. Tsapatsis, "A Model for the Performance of Microporous Mixed Matrix Membranes with Oriented Selective Flakes," *Journal of Membrane Science* **295** (1-2), 50-70 (2007).

42. C. Macosko, *Rheology Principles, Measurements and Applications*. (Wiley-VCH, Inc., New York, 1994).

43. I. Frankel and H. Brenner, "Taylor Dispersion of Orientable Brownian Particles in Unbounded Homogeneous Shear Flows," *Journal of Fluid Mechanics* **255**, 129-156 (1993).

CHAPTER 2

THEORY & LITERATURE REVIEW

2.1 Overview

Polymeric and hybrid membranes are subjects of great interest because of their current and potential applications in efficient separation processes. As such, literature exists that describes the fundamental aspects of these materials at great length.[1-5] In this section, we aim to provide a concise background on the governing transport principles that we used to calculate membrane properties and the formation techniques used. Particular attention will be paid to membranes containing platelet (high aspect ratio) filler materials.

2.2 Gas Transport in Membrane Materials

By definition, permeation refers to the flow rate (flux, N) of a material through a unit area as a function of the concentration gradient.[5] Equation 2.1 may be used to illustrate this definition for a gas (i) in a membrane, where P_i is the rate of permeation (*permeability*), ℓ is a characteristic length (thickness) of the membrane and Δp_i represents the partial pressure driving force across the membrane.

$$P_i = \frac{N_i \cdot \ell}{\Delta p_i} \qquad \text{Eq. 2.1}$$

A caveat related to this equation applies to asymmetric membranes. It is often the case that the thickness of the selective skin layer is unknown because it is comprised of a dense layer that transitions into a less dense morphology. This makes delineating the boundary between the skin and substructure difficult. Therefore, the term *permeance* is used to describe transport in these cases (see Equation 2.2).[6]

$$P_i = \frac{N_i}{\Delta p_i} \qquad \text{Eq. 2.2}$$

Both permeability and permeance are measured in this work. Due to the widespread use of the permeation term, it is common to report values using a variety of units. However, for consistency we will report measured values in units of Barrer and Gas Permeation Units (GPU) for permeability and permeance respectively. Definitions of these units are provided in Table 2.1.

Table 2.1: Definition of permeation and permeance units used in this work

Barrer	Gas Permeation Unit (GPU)
$\frac{cc_{STP} \cdot cm}{cm^2 \cdot s \cdot cmHg} \cdot 10^{-10}$	$\frac{cc_{STP}}{cm^2 \cdot s \cdot cmHg} \cdot 10^{-6}$

2.2.1 Permeation in Polymers

For a membrane to be successful it must exhibit high productivity and efficiency. These characteristics are generally governed by the solution diffusion mechanism responsible for the permeation process (see Equation 2.1).[5] In this mechanism a penetrant sorbs into the membrane, diffuses through it and desorbs at the opposite face. Therefore, the diffusion (D_i) and the solubility (S_i) coefficients of the penetrant in the material dictate the permeability coefficient, viz.,

$$P_i = D_i \cdot S_i \qquad \text{Eq. 2.3}$$

Let us examine these two coefficients more closely. The equilibrium solubility coefficient is equivalent to the concentration (C_i) of the penetrant with respect to a given driving force for sorption.[7] In gas phase separations, the driving force is the locally acting equilibrium partial pressure (p_i). This relationship is shown as Equation 2.4. Gas

solubility in glassy polymers may be described using more complex models, which will be discussed in Section 2.1.1.1.

$$S_i = \frac{C_i}{p_i} \qquad \text{Eq. 2.4}$$

The other factor in the solution-diffusion mechanism – diffusion – is controlled by transient openings between polymers chains.[7] Thermal fluctuations in the membrane create mobility in the polymer chains, which leads to randomly occurring local openings that the gas molecule can move through in a *random walk*. Frequency (f_i) of these fluctuations and the activated jump length (λ_i) that a molecule can achieve determines the rate of diffusion. This relationship is represented as Equation 2.5, wherein a geometric coefficient (1/6) is included to account for the "random walk" of a molecule in homogenous media.

$$D_i = \frac{f_i \cdot \lambda_i^2}{6} \qquad \text{Eq. 2.5}$$

Albeit diffusion and solubility may be measured independently, we traditionally measure the rate of permeation directly because our ultimate concern is the membrane productivity. Furthermore, for selective membranes we are interested in the separation efficiency (selectivity or permselectivity) for two components (i,j). The ideal selectivity for a gas pair is represented as the ratio of two permeabilities (see Equation 2.6) that have been measured independently.

$$\alpha_{i/j} = \frac{P_i}{P_j} = \frac{D_i \cdot S_i}{D_j \cdot S_j} \qquad \text{Eq. 2.6}$$

For the purpose of this study we will use the ideal selectivity of two penetrants. However, in more realistic separation studies with aggressive swelling feeds (e.g. natural gas, hydrocarbon, etc.) one must conduct mixed gas permeation tests, in which case ideal selectivity calculations are only a first approximation to performance properties.

2.2.1.1 Dual-Mode Sorption

In the previous section we alluded to the utility of using more complex models to describe gas sorption in glassy polymers. Solubility, as we noted, is a function of the concentration of sorbed species in the membrane. An idealized explanation of molecular sorption in glassy polymers occurs in a dual-mode fashion.[7] In other words, the membrane consists of two idealized regions where sorption can occur: (1) a densified equilibrium matrix and (2) a region of molecular gaps (see previous section for further explanation). Existence of these two regions led to the development of the dual-mode sorption theory (Equation 2.7) which is the sum of Henry's and Langmuir parameters. Concentration (C_i) is presented as a function of the partial pressure (p_i) of the sorbate.

$$C_i = k_{D,i} p_i + \frac{C'_{H,i} b_i p_i}{1 + b_i p_i} \qquad \text{Eq. 2.7}$$

The first term in this equation corresponds to the Henry's region as indicated by the Henry's coefficient, k_D. Henry's sorption sites are associated with the densified matrix. Langmuir sorption, which occurs due to packing disruptions, is represented by the second term in the equation. Two coefficients are used to describe Langmuir sorption: the Langmuir sorption capacity ($C'_{H,i}$) and the Langmuir affinity parameter (b_i).

Sorption tests (pressure-decay, gravimetric) are generally used to determine the equilibrium concentration of a penetrant. Curve fitting is then used to determine the corresponding dual-mode sorption coefficients for a penetrant over a pressure range of interest. Completing these tests also allows one to accurately calculate diffusion coefficients if corresponding permeation data is available.

2.2.2 Permeation in Polymer-Platelet Nanocomposites

Changes in molecular transport through hybrid membranes containing high aspect ratio platelet fillers is largely governed by the alteration of diffusive path length.[8] *Tortuosity* in the transport is used to describe this effect. Equation 2.8 provides a correlation between

diffusion (D) and the tortuosity (τ) with respect to the intrinsic diffusion coefficient (D_0) of the polymer matrix.

$$D = \frac{D_0}{\tau} \qquad \text{Eq. 2.8}$$

Tortuosity is dependent on the aspect ratio and orientation (with respect to the transport path) of the nanoplatelet filler. Mathematically, this is expressed as the ratio between the diffusive path length (ℓ) when filler is present and when it is not (ℓ_0) – as shown in Equation 2.9.[9]

$$\tau \equiv \frac{\ell}{\ell_0} \qquad \text{Eq. 2.9}$$

In the case of nanocomposites containing impermeable filler with no contributing solubility effects, the permeability of the hybrid may be simply represented as function of the filler volume fraction (ϕ) in the membrane and the contributing tortuosity.[9] Equation 2.10 shows this idealized equation, where P_0 is the intrinsic permeability of the polymer matrix in the absence of fillers.

$$P = D_0 \cdot \left(\frac{1-\phi}{\tau} \right) \cdot S_0(1-\phi) \qquad \text{Eq. 2.10}$$

To improve the accuracy of estimating permeability in these complex systems one should consider other geometric characteristics, such as: distribution of the filler, platelet orientation and solubility effects.

2.2.2.1 Predicting Separation Performance

Mathematical models serve a dual purpose when working with hybrid membranes. If the materials are preselected and well-known, one can estimate the expected change in permeabilities which provides initial insight into the efficacy of the chosen materials. Alternatively, if the membrane has already been fabricated and tested, models may be used to qualitatively deduce the efficacy of the preparation methods used in membrane

formation. Numerous authors have developed mathematical models to predict the transport properties of polymer-platelet composites.[8-15] These models vary in complexity. Some are based purely on geometric assumptions while others account for anisotropies using empirical data. For our purposes, we have identified several equations that have been extensively used in the literature and that account for different variables.

In traditional mixed matrix membranes containing permeable unit aspect ratio fillers, the *Maxwell* model (Equation 2.11) is frequently used to predict permeability of the hybrid.[16] In this equation P_D represents the permeability of the dispersed filler phase. If the filler phase is impermeable, then this equation reduces to Equation 2.12.

$$\frac{P}{P_0} = \frac{P_D + 2P_0 - 2\phi(P_0 - P_D)}{P_D + 2P_0 + \phi(P_0 - P_D)} \qquad \text{Eq. 2.11}$$

$$\frac{P}{P_0} = \frac{1-\phi}{1+\frac{\phi}{2}} \qquad \text{Eq. 2.12}$$

An important advantage of hybrid membranes containing platelet materials is that they provide additional diffusive resistance at low loadings because the tortuous path is greatly influenced by the particle aspect ratio. The Maxwell model does not account for this geometric benefit and therefore severely under predicts the performance of well made polymer-platelet hybrid membranes.

In the 1960s, *Nielsen* developed one of the first models to account for filler aspect ratio in a composite material.[8] It was assumed that the filler was an array of impermeable and evenly distributed overlaying plates with infinite length (ribbons). Moreover, the diffusive path of transport was orthogonal to the longest dimension of the filler. The Nielsen model is represented by Equation 2.13, where A_r is the aspect ratio (diameter over thickness) of the filler and ϕ is the contributing volume fraction in the membrane.

$$\frac{P}{P_0} = \frac{1-\phi}{1+\frac{A_r}{2}\cdot\phi} \qquad \text{Eq. 2.13}$$

After Nielsen work several other authors reported variations to account for the geometry of filler dispersion more accurately. In 1990 *Cussler* proposed a model (Equation 2.14) that accounted for the high aspect ratio geometry and incorporated a permeability term for the filler phase to predict *diffusion* in hybrid membranes.[12]

$$\frac{D}{D_0} = \left[1-\phi+\left(\frac{1}{\delta\phi}+\frac{1-\phi}{A_r^2\cdot\phi^2}\right)^{-1}\right]^{-1} \qquad \text{Eq. 2.14}$$

In this equation, A_r is the radius of the particle divided by its thickness. Additionally, the term δ represents the ratio of diffusion coefficients, D_0/D_D where D_D corresponds to the filler material. When the filler is impermeable, such as a polymer-clay nanocomposite, this equation will reduce to:

$$\frac{D}{D_0} = \left[1-\phi+\left(\frac{A_r^2\cdot\phi^2}{1-\phi}\right)\right]^{-1} \qquad \text{Eq. 2.15}$$

Recalling that permeability is the product of the diffusion and solubility coefficients, we should expand Equation 2.15 with a solubility term in order to predict permeability. We have assumed that solubility in the polymer and filler are additive and are only dependent on the volume fraction of filler. After expansion we have the following expression:

$$\frac{P}{P_0} = \left[1-\phi+\left(\frac{A_r^2\cdot\phi^2}{1-\phi}\right)\right]^{-1}\cdot\frac{S_0(1-\phi)+S_D\cdot\phi}{S_0} \qquad \text{Eq. 2.16}$$

Although we have accounted for the solubility term to calculate permeability from the reduced Cussler model, it is typically assumed that the filler phase in a polymer-clay nanocomposite is does not have a contributing sorption property.[9] If this is true, then Equation 2.16 simplifies to the form shown as Equation 2.17.

$$\frac{P}{P_0} = \left[\left(\frac{A_r \cdot \phi}{1-\phi} \right)^2 + 1 \right]^{-1} \qquad \text{Eq. 2.17}$$

Both the Cussler and Nielsen models sufficiently account for the shape factor of high aspect ratio fillers, but both models are based on the assumption that the filler is in an optimum uniform distribution and orientation normal to the direction of permeation. In practical applications it is very difficult to satisfy both of these assumptions. If the volume fraction of filler is very dilute ($\phi << 1$) then the distribution assumption approaches reality. Otherwise, empirical correlations based on measured values are more appropriate. To create a perfectly oriented matrix would require high shear forces during casting or spinning to align the platelets. This is theoretically achievable. However, to account for any inadequacies in the particle orientation, *Bharadwaj* proposed a model (Equation 2.18) that includes a shape factor (S) which is derived from trigonometric correlations.[13] Examples of particle orientations and their corresponding shape factors are shown in Figure 2.1.

$$\frac{P}{P_0} = \frac{1-\phi}{1+\frac{A_r}{2} \cdot \phi \left(\frac{2}{3} \cdot \left(S + \frac{1}{2} \right) \right)} \qquad \text{Eq. 2.18}$$

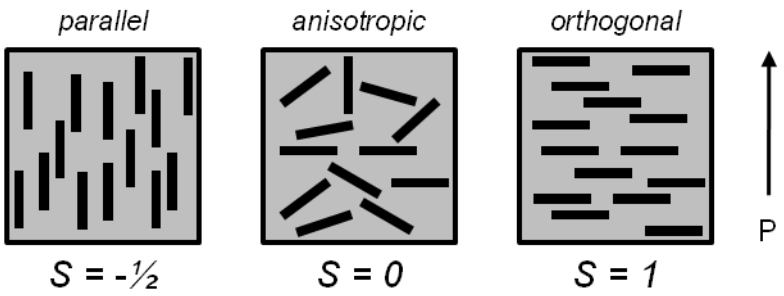

Figure 2.1: Example orientations of well dispersed platelet fillers in a polymer matrix. Shape factors (S) are related to solutions for Equation 2.18. The direction of permeation (P) is noted.

2.2.2.2 Additional Considerations

Regardless of the mathematical model used, there are numerous types of anisotropic characteristics for us to consider that may have contributing effects on the measured permeability of a polymer-platelet hybrid membrane. Unless additional characterization is available, it is difficult to account for the realities of an actual system. The following factors include:

1. **Orientation:** With respect to diffusion the observed particles are not perpendicular to the path of transport. This effect is accounted for in the Bharadwaj equation in principle and can be accounted for if microscopic inspection reveals the orientation
2. **Diameter:** Effective particle diameter whereby two overlapping flakes would contribute to a greater diameter and therefore a much greater apparent aspect ratio.
3. **Thickness:** If *tactoids* (unexfoliated platelets) are present, then the apparent particle thickness will be much greater and therefore the aspect ratio smaller. Moreover, if exfoliated platelets flocculate during processing they may form stacks yielding the same effect as a tactoid.
4. **Agglomeration:** This non-ideality has aspects related to the previous anisotropic conditions wherein a group of particles with varying orientation, thickness and apparent diameter are “joined” to form a larger fractal structure. During diffusion an agglomerate may appear as a large amorphous or even spherical filler with respect to the penetrant. In some cases, by-pass through poorly consolidated agglomerates can occur, thereby increasing permeability. In other cases, consolidated agglomerates can provide an impediment beyond the simple volume fraction of the individual platelets.

2.3 Polymer–Platelet Composites

Hybrid materials comprised of high aspect ratio, platelet-type fillers in a polymer matrix have been topics of interest for decades.[17] These materials have shown promise for increasing mechanical properties, improved flame retardancy, UV resistance, enhanced barrier materials and recently for advanced membranes.[18,19] Particular focus has been given to polymer-clay composites. Clays are naturally occurring, readily available and inexpensive additives that provide beneficial properties. As a result of the widespread application of these materials, there have been significant contributions in synthesis, formation and characterization. Numerous authors have published exhaustive reviews and books on this subject entirely.[17-24] For the purposes of this study we will review the base formation techniques as well as some defining characteristics as they apply to our project objectives.

2.3.1 Formation

For a polymer-platelet composite to provide optimal properties, it must contain an exfoliated, well-dispersed inorganic phase that also exhibits good adhesion between the polymer and filler.[25] There are a variety of methods used to achieve this morphology. Melt blending, wherein clays are combined with molten polymer, is the most frequently used technique.[18] This has particular relevance in composite formation for reinforced plastics and mouldings. Alternatively, *in situ* polymerization may be used to chemically incorporate platelets into the polymer matrix.[24] Albeit effective, this method can be time intensive and costly. A more general approach for platelet incorporation is via solution blending where the polymer and clay are combined in a solvent or solvent blend that will dissolve the polymer phase and ideally exfoliate the clay phase.[24] Solution based techniques are especially favorable for the formation of films, coatings and membranes. All of these techniques will ideally create a well dispersed filler phase. Moreover, if the materials have been selected based on expected or pre-determined miscibility, then good adhesion should be achievable. Therefore, exfoliation is often the most difficult – and most important – step in creating a polymer-platelet composite. For the duration of

this section we will be using clay materials as our reference platelet, unless otherwise noted.

2.3.1.1 Exfoliation

The first challenge in creating polymer-platelet composites is the exfoliation of the platelet materials. Most clay materials – whether natural or synthetic – exist as stacks or tactoids wherein the individual layers are constrained by cations or anions in the interstices that are satisfying a charge imbalance.[26,27] Imbalance occurs as a result of isomorphous substitutions in the lattice structure of the clay layer. Figure 2.2 shows a cartoon of the tactoid formation with coordinated ions.

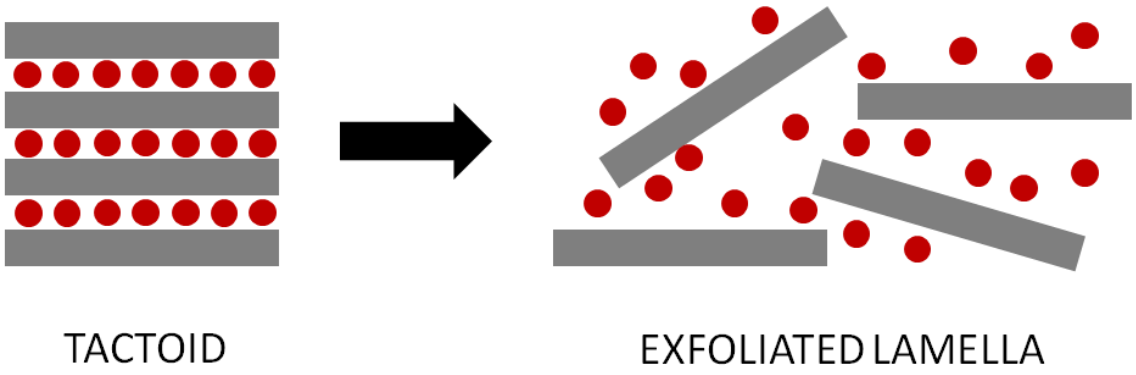

Figure 2.2: Cartoon depicting (i) clay tactoid with interstitial charge balancing ions and (2) tactoid after exfoliation into individual lamella

As a tactoid, platelet fillers will not produce a composite with desired properties. Exfoliation of the layers, as shown in the second part of Figure 2.2, is necessary to fully benefit from high aspect ratio fillers. There are three primary conditions that must be satisfied to produce an exfoliated state: particle surface wetting, deagglomeration and stabilization.[28]

1. Surface Wetting: Occluded gas (usually air) in the clay interstices must be displaced by a solvent system that will hydrate the ions and the clay surface.[27,28] Capillary forces are the primary driving force for this mechanism. Once the surface is wetted, the layers are not necessarily exfoliated, but wetting does provide sufficient force to overcome the first energy barrier.
2. Deagglomeration: There are cases where the layers will spontaneously exfoliate if the system is dilute and the solvent is sufficiently polar.[29] However, it is more often the case that additional energy is necessary to achieve exfoliation. If the particles are sufficiently large or if the ionic bridging after wetting is weak, then mechanical methods (sonication, mixing) may be used to deagglomerate the tactoids. Alternatively, bulky chemical reagents may be used to create further separation via ionic or electrostatic interactions with the clay surface that are stronger than the bridging forces.
3. Stabilization: Once deagglomeration has been achieved, the platelets are exfoliated. At this stage the particles must be stabilized to prevent flocculation in the solvent system.[28] There are numerous stabilization options. If the particle concentration in the solvent medium is sufficiently dilute, then the probability of particle collision is minimized; but this is usually not practical. Continuous mechanical energy input (sonication, stirring) will also work. Adjusting the system pH or inducing an electrical current may provide electrostatic stabilization; but at high particle concentrations diffusion can still cause flocculation. Steric stabilization (closely related to chemical based deagglomeration) is the last choice.[30,31] In this manner, macromolecules are added to the platelet suspension and either electrostatically stabilize via surface sorption or bulky molecules induce depletion stabilization which prevents the particles from colliding.

One of the most widely used methods for deagglomerating and stabilizing clay materials is organo-modification of the surface.[32] After the clay surface has been wetted, a bulky organic salt (usually an alkyl ammonium) is added to the suspension medium. The salt

intercalates into the wetted interstice and ionically sorbs to the clay surface, creating an organic layer (see Figure 2.3) and expanding the separating distance between platelets. This organic layer also makes the clay surface hydrophobic which can promote miscibility in the polymer matrix. Organo-modification can, however, limit the available techniques for dispersion into a polymer matrix. For additional details, see comments in Section 2.2.1.2.

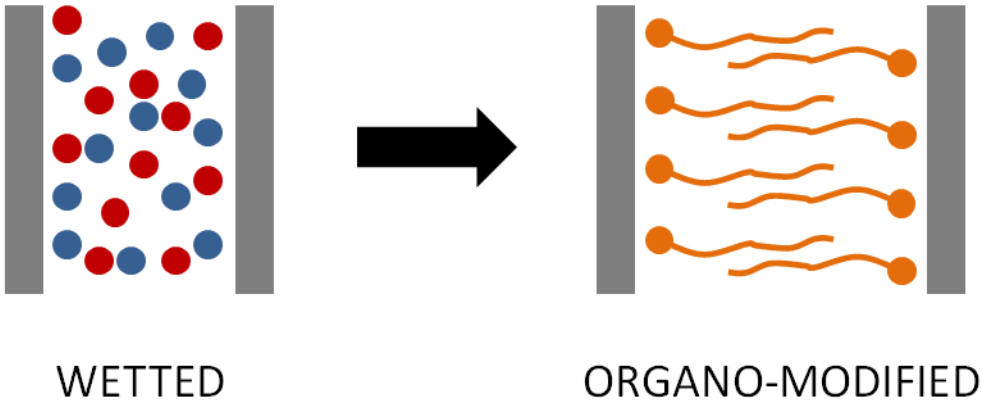

Figure 2.3: Deagglomeration and stabilization of a wetted tactoid via organo-modification

Similar effects as the organo-modification route may be attained if the composite matrix polymer has an affinity for the particle surface and/or if it is bulky enough to induce depletion stabilization.[30] Regardless of the method used to exfoliate and stabilize the particles, one must be able to incorporate polymer without inducing flocculation in order to create an effective hybrid material.

2.3.1.2 Dispersion

Once an exfoliated system of nanoplatelets has been achieved, one can move forward to the dispersion stage. For the purposes of this discussion, dispersion will coincide with the blending of filler with a polymer matrix. (In some instances dispersion may refer to a solvent based system where polymer is not part of the desired system.) Before

reviewing the different dispersion methods, we should consider the different composite morphologies that may occur. In Figure 2.4 we present a cartoon that exemplifies the three circumstances: unexfoliated, intercalated and exfoliated. [18] If exfoliation is not achieved in the first step, the platelet tactoid will appear unaffected by the polymer phase. In other words, polymer will not exist in the gallery spaces. Alternatively, if the particles are swollen or partially exfoliated, then polymer may intercalate into the gallery space.[18] This morphology will yield some improved mechanical properties for the composite, but limited transport advantages will be obtained. If a high degree of exfoliation is achieved, the polymer and particle phase will appear well blended. Moreover, the particles should appear to be well spaced (at low loadings). A number of methods may be used to achieve the desired morphology.

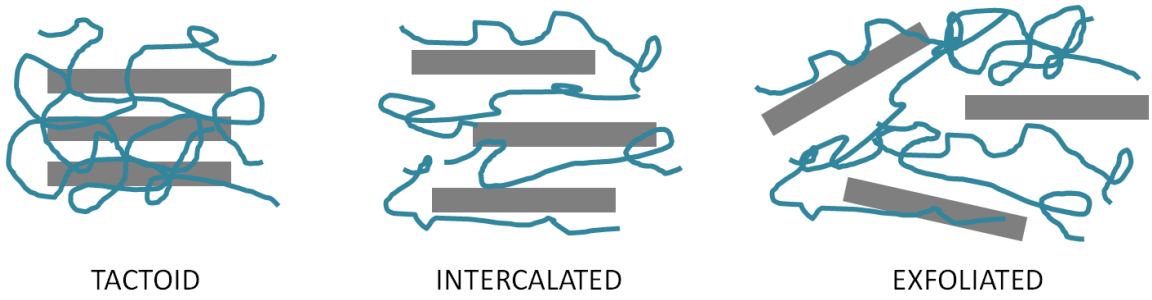

Figure 2.4: Potential morphologies with respect to particle exfoliation in a polymer-platelet composite. (i) unexfoliated tactoid (ii) partially exfoliated with polymer intercalation (iii) complete exfoliation and stabilization

It was previously noted that organo-modification of clays (organoclays) is commonly used for creating hybrid materials.[24] In most instances, organoclays are dispersed into the polymer matrix via melt blending/extrusion. (Significant literature exists on this subject.) This process is highly desirable because it may be done using existing equipment for extrusion and moulding applications.[18] Conversely, this method is less desirable for traditional solution-based membrane formation for obvious reasons. We should consider alternative approaches that are more accommodating.

The original dispersion method used, *in situ* polymerization, is receiving increasing attention once again.[23] The matrix polymer or a secondary stabilization polymer is created in solution in the presence of the nanoclays. In some cases the clay serves as a seeding site for polymer growth. *In situ* polymerization is an attractive solution to ensure sufficient polymer incorporation and even promotion of polymer-filler adhesion. This method, however, can be complex and time consuming depending on the polymer of interest.

Previously we alluded to the possibility of using the desired polymer matrix to induce steric and/or depletion stabilization. The easiest approach for this type of system is solution blending. For this to be successful, though, the polymer must be miscible in the solvent system used to exfoliate the platelets; otherwise the polymer will precipitate in solution. Polymer may be added during the deagglomeration step or after if the suspension stability has an acceptable working time. If the matrix polymer is not miscible with the nanoclay one may observe depletion induced flocculation.[30] This may be resolved by using organoclays as evidenced in the literature.[18] A more vigorous mixing procedure may also be a solution.[33]

There are many methods for creating a well-dispersed composite matrix. Determining which method to use will depend on the final product and the materials of interest. Ultimately, though, the materials dictate the performance of the composite. An ideal matrix may be achievable, but the organic-inorganic miscibility governs the final composite properties.

2.3.1.3 Adhesion

In Chapter 1 we introduced the importance of polymer-particle compatibility and its effect on gas transport in membrane materials. As a general rule, the miscibility between polymer and filler is the deciding factor in the ultimate efficacy of a hybrid membrane. Four scenarios exist to describe the state of adhesion between the two phases: strong

adhesion, good adhesion, poor adhesion and immiscibility.[34-36] A cartoon depicting these scenarios is shown in Figure 2.5.

Figure 2.5: Possible polymer chain conformations in an organic-inorganic hybrid material.

If good adhesion exists between the polymer and impermeable filler, molecular transport will exhibit model properties because the filler will act as a non-selective diffusive barrier. Strong adhesion and poor adhesion, on the other hand, may lead to non-ideal transport properties due to the existence of rigidified or leaky interfaces.[37] Depending on the loading fraction of the inorganic phase, immiscibility between the two components can lead to equivalent or enhanced permeabilities. Moreover, the permselectivity would decrease due to Knudsen diffusion through the nano-sized interfacial gap.

For membrane and barrier studies, using permeation tests to probe the interface between the polymer and filler is the most reliable and pertinent method. Alternatively, interfacial characteristics may be identified using thermal analytical methods (dynamic mechanical analysis, differential scanning calorimetry) as well.[17] If desirable adhesion exists between the two phases, the composite will exhibit an increase in the glass transition temperature (T_g) as compared to the pure polymer.[25] A decrease in the T_g indicates poor interfacial adhesion.

Careful material selection is critical. It may be possible to create an exfoliated system of platelets and even disperse them well into a polymer matrix, but in the end the compatibility between polymer and filler is the absolute limitation for hybrid membrane performance.

2.3.2 Rheological Properties

The rheological properties of a solution containing rigid (insoluble) particles can provide insight into the degree of exfoliation and dispersion and even the interactions between dissolved polymer and the filler.[38] Work by Einstein showed that the addition of rigid spheres had a dramatic effect on solution viscosity as a function of volume fraction in the solution.[39] Systems containing platelet fillers exhibit additional characteristics of interest. At low shear rates, nanosized platelet materials will effectively behave as spheres in solution due to rapid free rotation in the suspending medium.[39,40] This effect produces viscosities that are significantly higher than the medium. When the shear rate is increased the viscosity will decrease due to the shear thinning nature of platelet materials in solution, because platelets orient along the flow direction.[39] This rheological phenomenon is represented in Figure 2.6 with corresponding platelet orientations.

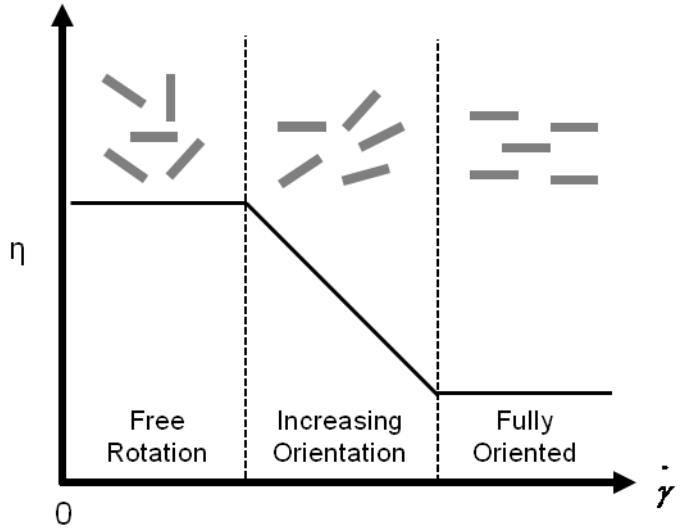

Figure 2.6: Viscosity of a solution containing rigid platelet filler presented as function of increasing shear rate. Corresponding geometries of platelets are presented with respect to the solution viscosity.

Details regarding platelet exfoliation may also be inferred from viscosity data. If the platelets are still in the tactoid formation, viscous contributions will be less prominent

compared to a highly exfoliated system.[17] Figure 2.7 aids in elucidating this concept. If we consider a tactoid of five lamellas, we see that it has an effective volume, V_1. At low shear rates this tactoid will behave like a spheroid with an effective hydrodynamic radius only slightly larger than a single platelet. Now, if this tactoid was fully exfoliated, it would yield five particles with equivalent hydrodynamic radii as the tactoid. Therefore, the exfoliated platelets will occupy roughly five times the effective volume of the tactoid. This observation can be used to compare solutions with like weight fractions of filler but with varying low shear viscosities. When the shear rate is increased the viscosity will rapidly decrease due to shear thinning, as previously shown in Figure 2.6. A system with a greater degree of exfoliation will therefore exhibit a lower viscosity at high shear rates.

As a final note, it is also possible to observe strong polymer attraction to the particle surface from shear viscosity measurements. If the attraction is sufficiently high, it has been observed that the relative viscosity, η/η_s, where η_s is the polymer solution viscosity, is less than one.[36] A relative viscosity less than one can be used as evidence that the bulk composition of the suspending medium is changed by the addition of the filler.

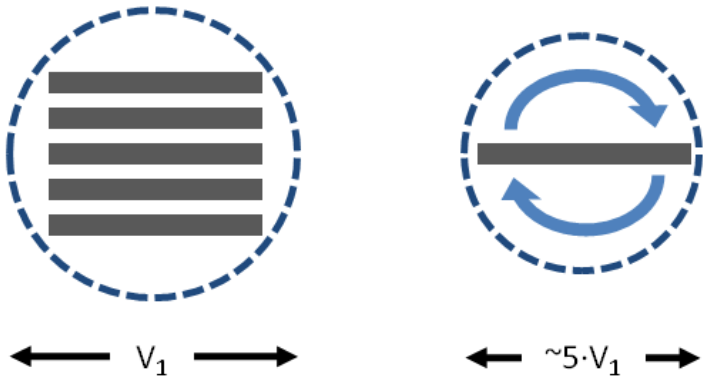

Figure 2.7: Comparison of the volume contribution of a nanoclay tactoid and a single clay nanoplatelet. Note that a tactoid comprised of five platelets will have approximately five times the apparent volume when fully exfoliated and dispersed in suspension.

2.4 Asymmetric Membranes

In Chapter 1 we provided an introduction into the topic of asymmetric membranes and their importance in the development of energy efficient separation systems. Moreover, we provided an economic justification for hollow fibers versus flat sheet membranes. Regardless of the morphology, the principles of membrane formation are similar. A selective skin layer is desired with a mechanical robust support layer. There are numerous fabrication methods used to create the asymmetric morphology, including: phase inversion, interfacial polymerization, solution coating, plasma deposition.[4,41] For the purposes of this project we will focus on the phase inversion technique. For simplicity we will use terminology related to *dry-wet quench fiber spinning*, which is the method typically used for asymmetric membrane formation in the Koros Research Group. A simplified diagram of this process is shown in Figure 2.8. Additional details of the spinning process and apparatus are provided in Chapters 3 and 7.

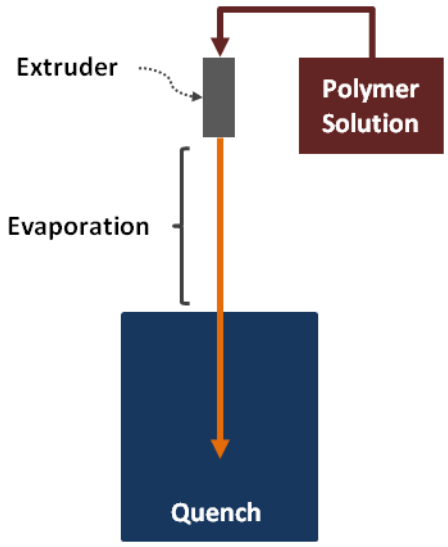

Figure 2.8: Dry-wet quench fiber spinning process. In this cartoon the critical membrane formation steps (evaporation and quench) are highlighted.

2.4.1 Formation Principles

Both hollow fiber and flat sheet asymmetric membranes may be formed using the Loeb-Sourajan phase inversion process.[4,41] There are two primary pathways in this process: (1) skin layer formation and (2) substructure formation. The skin layer is formed first during the evaporation step followed by rapid formation of the substructure during the quench step.[41] Let us refer to Figure 2.9 as a graphical tool to describe this process.

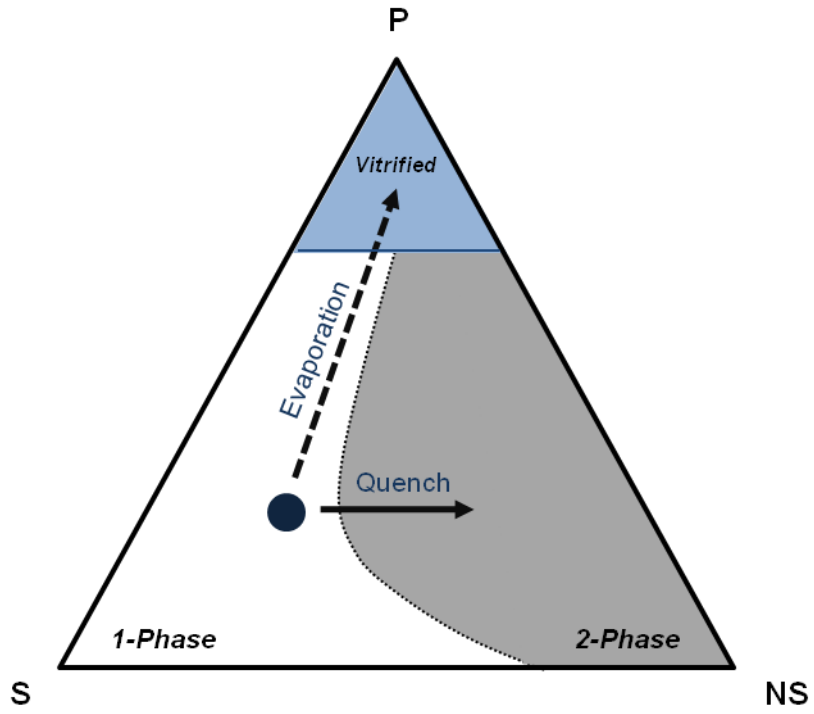

Figure 2.9: Ternary phase diagram depicting phase transition pathways during the dry-wet fiber spinning process. (P = polymer, S = solvent, NS = non-solvent/coagulant)

Skin Layer Formation

The selective layer of an asymmetric membrane forms when solvent egress is sufficiently higher than non-solvent ingress at the surface during the spinning process. If this occurs, the solution enters the vitrified region (see dashed line pathway in Figure 2.9).[41] If quench bath conditions and the dope composition have been highly optimized,

this may occur without the aid of an evaporative step; but this circumstance increases the difficulty of defect-free membrane formation. An evaporative step is typically used to promote skin formation via loss of a volatile solvent in the dope. Using an evaporative step for skin layer formation provides flexibility in the skin layer properties as well. Adjusting the evaporation time via the *air gap* height can dictate the skin layer thickness and the presence of defects.

Substructure Formation

Typically, a ternary mixture of polymer, solvent and non-solvent is used as the starting solution or dope. (In the case of hybrid membranes, this mixture is tertiary but it is generally assumed that the inorganic phase does not contribute significantly to the phase inversion process.) To ensure rapid phase separation in the quench medium, the ratio of components in the ternary mixture should produce a solution that is near the phase boundary. The cloud point technique is commonly used to determine where this boundary exists for a particular system of materials.[42] During the extrusion process, the fiber experiences an evaporative process where the skin layer forms and then enters a quench bath where phase separation is completed. Phase separation occurs because the quench bath solution is a non-solvent/coagulant for the polymer. A chemical potential difference forces the solvent in the spin line – which must be miscible with the quench medium – to rapidly demix and enter the quench medium.[43] Simultaneously, the quench medium diffuses into the spin line thereby driving the solution into the two phase region as shown in Figure 2.9.

Additional Considerations

The fiber spinning process has many controlling variables that influence defect-free membrane formation. We have only mentioned the air gap and quench bath conditions. Other variables include temperature, draw ratio, and bore fluid composition. Effects of these variables on membrane formation are discussed in more depth elsewhere, and for brevity are not discussed in detail here.[41-45]

2.5 Summary

Transport in membrane materials is based on the well-known solution-diffusion mechanism. Numerous authors have proposed models to predict transport in hybrid membranes containing inorganic filler in a polymer matrix. Moreover, models for hybrid membranes containing high aspect ratio materials exist, but with stringent assumptions regarding the system morphology.

Polymer-platelet composites are of particular interest to a variety of communities. There has been substantial work in the field of polymer-clay nanocomposites in particular. Methods exist for the exfoliation and dispersion of platelet materials in polymer matrices. Melt blending and *in situ* polymerization are the most common approaches. However, for the formation of phase inversion membranes solution based techniques are preferred.

A review of the literature shows that solution blending to create polymer-nanoplatelet composite has been extensively used. Moreover, there have recently been reports of membranes formed via phase inversion of solutions containing nanoplatelets.[46,47] These membranes, however, were not for gas separations. More importantly, the authors used melt-blending to create a composite that was then dissolved into a solvent system. To date there is no literature that reports a purely solution based procedure for the formation of phase inversion membranes containing high aspect ratio fillers. Moreover, there has been minimal success related to membranes containing unmodified platelet fillers in a hydrophobic polymer matrix.

2.6 References

1. M. Porter, *Handbook of Industrial Membrane Technology*. (William Andrew Publishing, Norwich, NY, 1991).

2. N. Li, A. Fane, W. Ho, T. Matsuura (ed), *Advanced Membrane Technology and Applications*. (John Wiley & Sons, Inc., Hoboken, NJ, 2008).

3. W. Ho (ed), *Membrane Handbook*. (Springer, New York, NY, 1992).

4. R.W. Baker, *Membrane Technology and Applications*. (John Wiley & Sons, Inc., New York, 2004), 2nd ed.

5. M. Mulder, *Basic Principles of Membrane Technology*. (Kluwer Academic Publishers Group, Norwell, MA, 2003), 2nd ed.

6. Y. Yampolskii, I. Pinnau, B. Freeman (ed), *Materials Science of Membranes for Gas and Vapor Separation*. (John Wiley & Sons Inc., Hoboken, NJ, 2006).

7. W.J. Koros (ed), *Barrier Polymers and Structures*. (American Chemical Society, Washington, D.C., 1990).

8. L. Nielsen, "Models for the Permeability of Filled Polymer Systems," *Journal of Macromolecular Science: Part A, Pure & Applied Chemistry* **1** (5), 929-942 (1967).

9. G. Choudalakis, A. Gotsis, "Permeability of Polymer/Clay Nanocomposites: A Review," *European Polymer Journal* **45** (4), 967-984 (2009).

10. B. Xu, Q. Zheng, Y. Song, Y. Shangguan, "Calculating Barrier Properties of Polymer/Clay Nanocomposites: Effects of Clay Layers," *Polymer* **47** (8), 2904-2910 (2006).

11. C. Lu, Y-M. Mai, "Influence of Aspect Ratio on Barrier Properties of Polymer-Clay Nanocomposites," *Physical Review Letters* **95** (8), 088303/088301-088303/088304 (2005).

12. E.L. Cussler, "Membranes Containing Selective Flakes," *Journal of Membrane Science* **52**, 275-288 (1990).

13. R. Bharadwaj, "Modeling the Barrier Properties of Polymer-Layered Silicate Nanocomposites," *Macromolecules* **34** (26), 9189-9182 (2001).

14. G. Fredrickson, J. Bicerano, "Barrier properties of Oriented Disk Composites," *Journal of Chemical Physics* **110** (4), 2181-2188 (1999).

15. W. Wakeham, E. Mason, "Diffusion Through Multiperforate Laminae," *Industrial & Engineering Chemistry Fundamentals* **18** (4), 301-305 (1979).

16. J. Maxwell, *A Treatise on Electricity and Magnetism*. (Clarendon Press, Oxford, UK, 1873).

17. T. Pinnavaia, G. Beall (ed), *Polymer-Clay Nanocomposites*. (John Wiley & Sons, Inc., New York, NY, 2000).

18. D.R. Paul, L.M. Robeson, "Polymer Nanotechnology: Nanocomposites," *Polymer* **49** (15), 3187-3204 (2008).

19. C. Sanchez, B. Julian, P. Belleville, M. Popall, "Applications of Hybrid Organic-Inorganic Nanocompsites," *Journal of Materials Chemistry* **15**, 3559-3592 (2005).

20. F. Hussain, M. Hojjati, M. Okamoto, and R. E. Gorga, "Review Article: Polymer-Matrix Nanocomposites, Processing, Manufacturing, and Application: An Overview," *Journal of Composite Materials* **40** (17), 1511-1575 (2006).

21. Y.C. Ke and P. Stroeve, *Polymer-Layered Silicate and Silica Nanocomposites*. (ELSEVIER Inc., San Diego, 2005).

22. J. Koo, *Polymer Nanocomposites*. (McGraw Hill, New York, NY, 2006).

23. S. Pavlidou, C. Papaspyrides, "A Review on Polymer-Layered Silicate Nanocomposites," *Progress in Polymer Science* **33** (12), 1119-1198 (2008).

24. S. Ray, M. Okamota, "Polymer/Layered Silicate Nanocomposites: A Review from Preparation to Processing," *Progress in Polymer Science* **28** (11), 1539-1641 (2003).

25. P. Rittigstein and J.M. Torkelson, "Polymer-Nanoparticle Interfacial Interactions in Polymer Nanocomposites: Confinement Effects on Glass Transition Temperature and Suppression of Physical Aging," *Journal of Polymer Science Part B-Polymer Physics* **44** (20), 2935-2943 (2006).

26. A. Newman (ed), *Chemistry of Clays and Clay Minerals*. (John Wiley & Sons, Inc., New York, NY, 1987).

27. H. van Olphen, *An Introduction to Clay Colloid Chemistry*. (John Wiley & Sons, Inc., New York, NY, 1977), 2nd ed.

28. R. Nelson, *Dispersing Powders in Liquids*. (Elsevier, New York, NY, 1988).

29. S. Olejnik, A. Posner, J. Quirk, "Swelling of Montmorillonite in Polar Organic Liquids," *Clays and Clay Minerals* **22**, 361-365 (1974).

30. R. Hunter, *Foundations of Colloid Science*. (Oxford University Press, New York, NY, 1991).

31. D. Napper, A. Netschey, "Studies of the Steric Stabilization of Colloidal Particles," *Journal of Colloid and Interface Science* **37** (3), 528-535 (1971).

32. S. Yariv, H. Cross (ed), *Organo-Clay Complexes and Interactions*. (Marcel Dekker, Inc., New York, NY, 2002).

33. S. Tunc, O. Duman, "Preparation and Characterization of Biodegradeable Methyl Cellulose/Montmorillonite Nanocomposite Films," *Applied Clay Science* **48** (3), 414-424 (2010).

34. P. de Gennes, "Conformations of Poymers Attached to an Interface," *Macromolecules* **13** (5), 1069-1075 (1980).

35. P. de Gennes, "Polymers at an Interface: A Simplified View," *Advances in Colloid and Interface Science* **27** (3-4), 189-209 (1987).

36. P. Dubin, P. Tong (ed), *Colloid-Polymer Interactions*. (American Chemical Society, Washington, D.C., 1993).

37. T. Moore, W.J. Koros, "Non-Ideal Effects in Organic-Inorganic Materials for Gas Separation Membranes," *Journal of Molecular Science* **739** (1-3), 87-98 (2005).

38. J. Vermant, S. Ceccia, M. Dolgovskij, P. Maffettone, C. Macosko, "Quantifying Dispersion of Layered Nanocomposites via Melt Rheology," *Journal of Rheology* **51** (3), 429-450 (2007).

39. C. Macosko, *Rheology Principles, Measurements, and Applications*. (Wiley-VCH, Inc., New York, NY, 1994).

40. R. Pal, *Rheology of Particulate Dispersions and Composites*. (CRC Press, Boca Raton, FL, 2007).

41. I. Pinnau, B. Freeman (ed), *Membrane Formation and Modification*. (American Chemical Society, Washington, D.C., 1999).

42. D. Clausi, W.J. Koros, "Formation of Defect-Free Polyimide Hollow Fiber Membranes for Gas Separations," *Journal of Membrane Science* **167** (1), 79-89 (2000).

43. S. Pesek, "Aqueous Quenched Asymmetric Polysulfone Flat Sheet and Hollow Fiber Membranes Prepared by Dry/Wet Phase Separation," *PhD Dissertation*, University of Texas - Austin, 1993.

44. S. Carruthers, "Integral-skin Formation in Hollow Fiber Membranes for Gas Separations," *PhD Dissertation*, University of Texas - Austin, 2001.

45. S. Carruthers, G. Ramos, W.J. Koros, "Morphology of Integral-Skin Layers in Hollow-Fiber Gas-Separation Membranes," *Journal of Applied Polymer Science* **90** (2), 399-411 (2003).

46. L. Cheng, D. Lin, K. Yang, "Formation of Mica-Intercalated Nylon-6 Nanocomposite Membranes by Phase Inversion Method," *Journal of Membrane Science* **172** (1-2), 157-166 (2000).

47. A. Leite, L. Maia, E. Araujo, H. Lira, "Nylon 6/Brazilian Clay Membranes Prepared by Phase Inversion," *Journal of Applied Polymer Science* **113** (3), 1488-1493 (2009).

CHAPTER 3

MATERIALS & EXPERIMENTAL PROCEDURES

3.1 Overview

The overarching goal of this work was to produce hybrid membranes containing nanoplatelet filler materials. To accomplish this goal we first carefully selected materials that would allow us to develop membranes that satisfied our objectives. A technique was developed that promoted the production of polymer-nanoplatelet materials that is commercially appealing for the manufacture of asymmetric hollow fiber membranes. Before discussing the promising results that were obtained, we will first provide an explanation regarding the materials used and why they were selected followed by a description of the methods used throughout this work to characterize the hybrid membranes.

3.2 Materials

Both the polymers and inorganic filler that were used in this work are commercially available. Solvents and other chemical reagents were also readily available from commercial suppliers. To promote ease of scalability, the polymers, fillers and reagents presented in the body of this work were not chemically modified. Before use, polymers, nanoclays and salts were dried at 100ºC overnight in a vacuum oven. Solvents were used as received. Additional specifics regarding the materials used are provided in this section.

3.2.1 Polymers

Two different commercially available glassy polymers (T_g<300 K) were used in this work: cellulose acetate and Torlon® 4000T (polyamide-imide). The former material was obtained from Sigma-Aldrich and the latter from Solvay Advanced Polymers (Alpaharetta, GA). Backbone structures of these polymers are shown in Figure 3.1. Additional details regarding the physical properties of these two materials are provided in Table 3.1.[1,2]

Table 3.1: Some physical properties for Torlon® and Cellulose Acetate polymers

Polymer	M_n (kDa)	M_w (kDa)	Density (g/cm^3)	T_g (K)
Cellulose Acetate	50	--	1.3	~473
Torlon® 4000T	18.4	43.7	1.38	546

Cellulose acetate is a naturally derived polymer from pure cellulose.[2] The R-groups shown on the polymer backbone (see Figure 3.1) are entirely hydrogen constituents in pure cellulose. If all of the R-groups are substituted with acetate, the polymer is commonly referred to as cellulose triacetate and has a degree of substitution (D.S.) of three. However, for this work we used a cellulose acetate containing 39.7wt% acetyl content (D.S.~2.5).[3]

Torlon® is a robust polyamide-imide polymer often used in aggressive environments where solvent and temperature resistance is of concern.[4] This polymer is often melt-processed and used to form engine and electrical components. Solvay Advanced Polymers also produces other versions with different molecular weights and/or that include glass or graphite fillers for enhancing mechanical properties. We used a pure form of the polymer for our work.

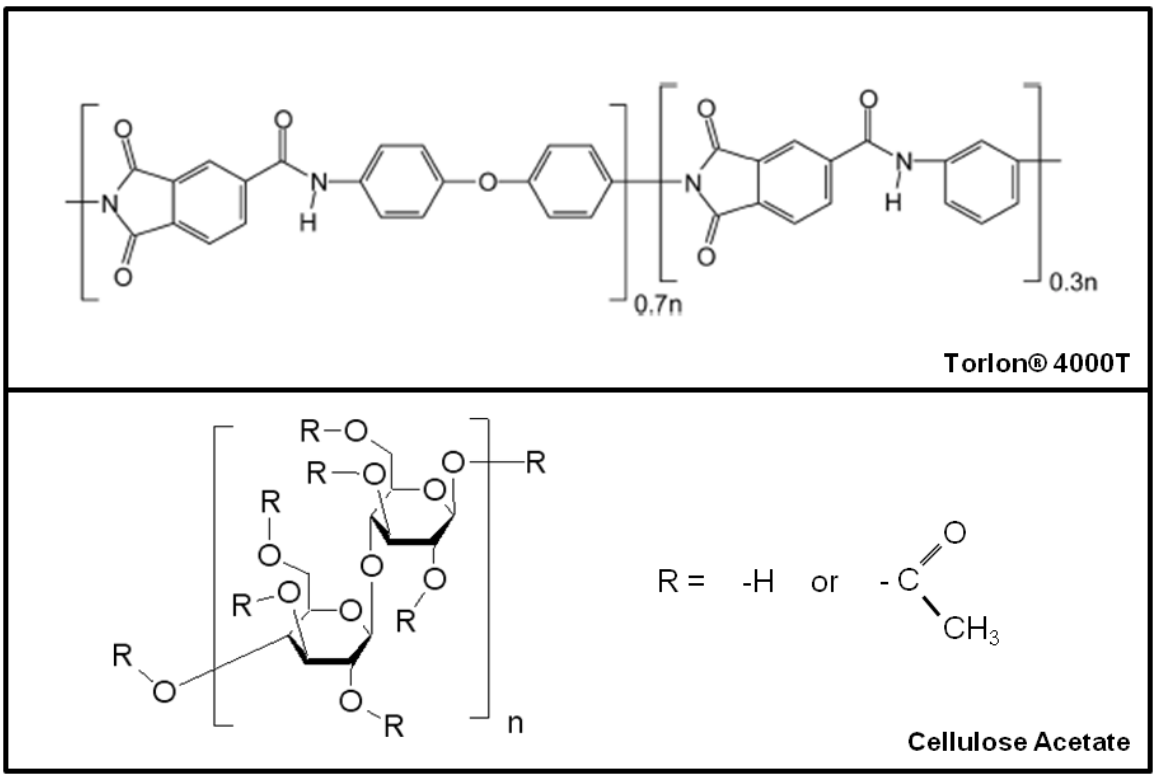

Figure 3.1: Molecular structures for Torlon® 4000T and Cellulose Acetate polymers

3.2.2 Inorganic Filler

Nonporous clay particles were chosen as a representative nanoplatelet material for our work. There is a vast array of different clays with variable properties available commercially. For our work we chose Laponite® RD; which is synthetically produced and was provided by Southern Clay Products (Gonzales, TX). Laponite® is a *trioctahedral smectite* – a subgroup of the 2:1 group of phyllosilicates.[5] Additional classification claims Laponite® in the *hectorite* family of clay materials. This information tells the reader that these clays have a net negative charge in their crystal structure that is balanced by cations in the gallery spaces. According the manufacturer, the empirical molecular formula for Laponite® is $Na_{+0.7}[(Si_8Mg_{5.5}Li_{0.3})O_{20}(OH)_4]_{-0.7}$ wherein sodium serves as the charge balancing cation.[6]

A single Laponite® RD platelet reportedly has a diameter between 25-30nm and an average thickness of 1nm.[7,8] In the transport modeling portion of this work, we made the assumption that the clay particles are 30nm in diameter and therefore have an aspect ratio of 30. It is difficult to obtain an accurate density of a single platelet, but the manufacturer reports a specific density of 2.53 g/cm^3 for Laponite® RD.[6]

3.2.3 Solvents & Chemical Reagents

All of the chemicals used in this study were of ACS reagent grade or higher. For the preliminary exfoliation work and the dense film formation, anhydrous n-methyl-2-pyrrolidone (NMP) and dimethyl sulfoxide (DMSO) were used. Deionized (DI) water was always used. Table 3.2 provides some of the physical properties of interest pertaining to the different solvents used.[9] Polyvinylpyrrolidone (PVP) with a M_w of ~55,000 g/mol was used during the spinning process as a pore forming agent. Lithium nitrate salt was used as well in subsequent experiments.

Table 3.2: Selected physical properties for solvents used this work

Compound	Chemical Formula	Molar Mass (g/mol)	Density (g/cm^3)	Boiling Point (ºC)
Water	H_2O	18.01	0.997	100
DMSO	$(CH_3)_2OS$	78.13	1.101	189
NMP	C_5H_9NO	99.13	1.026	202
Acetone	CH_3COCH_3	58.08	0.790	56.2
Ethanol	CH_3CH_2OH	46.07	0.789	78.5
n-Hexane	C_6H_{14}	86.18	0.660	69

3.2.4 Penetrants for Transport Measurements

All of the separation studies carried out during this project were based on gas phase transport. The gases used were helium, oxygen, nitrogen and carbon dioxide. Their respective kinetic diameters and critical temperatures are listed in Table 3.3.[10,11] Throughout the course of experimentation the gases used were either *ultra high purity* or *research* grade.

Table 3.3: Kinetic diameters and critical temperatures for gases used in this work

Property	He	CO_2	O_2	N_2
Kinetic Diameter (Å)	2.6	3.3	3.46	3.64
Critical Temperature (K)	5.2	304.2	154.4	126.1

3.3 Motivation for Material Selection

The original motivation for this project stems from the concept of hybrid membranes containing size selective nanoplatelets for enhanced gas separations. In Chapter 1 we recognized some of the work that has been done in this field to date. Creating these membranes is challenging, but synthesizing the nanoplatelet sieves is even more difficult. There are numerous researchers that are still exploring and optimizing the synthesis of these materials.[12-15] We chose to work in parallel with these researchers. Sufficient scalable techniques are not presently available to create hybrid dopes containing nanoplatelets for the formation of asymmetric membranes. Our approach to this problem was to identify materials that are commercially relevant and to develop a process that would be scalable for industrial membrane fabrication. Polymers, model nanoplatelets and solvent systems were selected to satisfy this approach.

3.3.1 Nanoclay Exfoliation

To produce an effective polymer-nanoplatelet membrane, the most crucial step is exfoliation.[16-18] Polymer-nanoplatelet adhesion is important too. Exfoliation dictates whether the membrane can provide separation enhancements. Water may be used to easily achieve exfoliation, but large quantities of water will limit the polymers that may be used for membrane formation because water is a strong non-solvent. Therefore, either an organic or semi-aqueous system is necessary to create desirable hybrid membranes.

Researchers have shown that many organic solvents induce swelling (an indication of surface wetting) effects in charged clays.[19-21] Moreover, the swelling effect generally correlates to the solvent polarity. Water, being highly polar, is the most efficient for hydration of interstitial cations and charge neutralization of the clay surface. Considering

this information, we chose solvents with very high polarity indices that are also valuable for polymer dissolution. The latter constraint limited the options to only a few because Torlon® is very solvent resistant. DMSO and NMP were specifically chosen because they have the highest polarities and are good solvents for both of the polymers used in this work.[22]

It was observed early on in this project that pure organic solvent would not exfoliate the nanoclays. Alternatively, we found that a blend of solvent and water would produce an exfoliated system. A solvent's high degree of miscibility with water and polarity contribute to the hydration and charge neutralization.[21] In Figure 3.2 we present a cartoon depiction of the hypothesized nanoclay hydration via a water and DMSO co-solvent system.

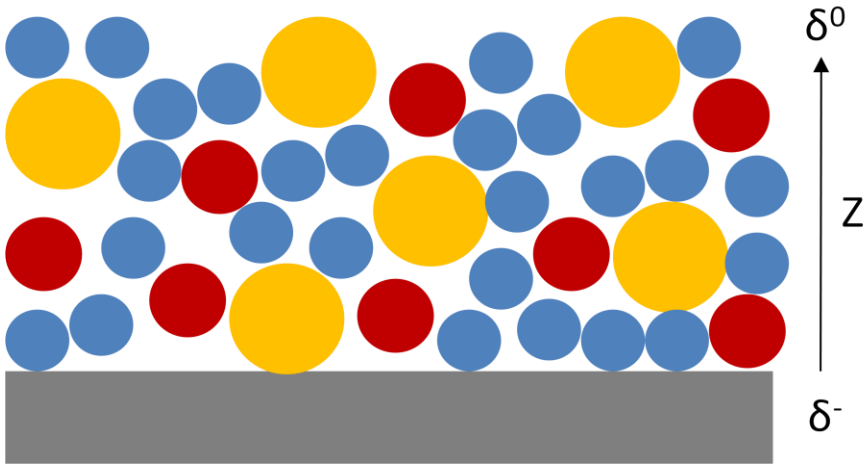

Figure 3.2: Schematic illustration of nanoclay (grey) and sodium cation (red) hydration via a blend of water (blue) and DMSO (yellow). The electrostatic field charge, δ, is a f(z).

3.3.2 Polymer-Nanoplatelet Compatibility

Cellulose acetate and Torlon® were selected for a number of reasons: both are commercially available and have relevance as membrane materials. More importantly, both polymers have constituent groups that hypothetically would exhibit desirable

interfacial characteristics with the nanoclay. By proving the efficacy of each polymer, we would be able to demonstrate the flexibility of our dope preparation methodology.

Macromolecule adhesion to clay surfaces is a topic of extensive study.[23-26] Primarily, researchers have focused on the surface modification of clays using long-chain quaternary ammonium salts.[17,24] This mechanism is successful because the surface of these clays has a net negative charge and the ammonium salts are positive. Alternatively, researchers have shown that polymers can adsorb via numerous mechanisms. These identified mechanisms played a vital role when we were selecting polymers to use in this work.

Cellulose acetate (di- and tri- substituted) has several potential absorption mechanisms according the literature.[24,27] However, in the absence of water, there are two primary routes: protic bridging between the hydroxyl groups of the polymer and the negatively charged clay surface and carbonyl complexation via cations on the clay surface. We have schematically represented these two mechanisms in Figure 3.4 below. In the former case, the hydroxyl group acts as a proton donor that links to the broken Si-O-Si edges of the clay surface.[24] The second route requires the presence of a cation, which serves as the link between the clay and the polymer.[27] This linkage is stronger in the presence of water, but was shown to survive without. Hybrid membrane properties will improve if one or both of these linkages occur.

Torlon® is a polyamide-imide that does not contain any hydroxyl groups, but does have carbonyl and amide groups. We propose that a similar carbonyl linkage may occur between the polymer and clay as described above.[27] In addition, the amide group has been shown to have strong hydrogen bonding characteristics, which we hypothesize may coordinate with the negatively charged clay surface (see Figure 3.4).[1] Although not necessarily applicable in our system, it has been shown that amide groups can form cationic *d*-complexes with clay surfaces.[24] However, the literature shows this route to exist in the presence of transition metals (X^{+2}) only.

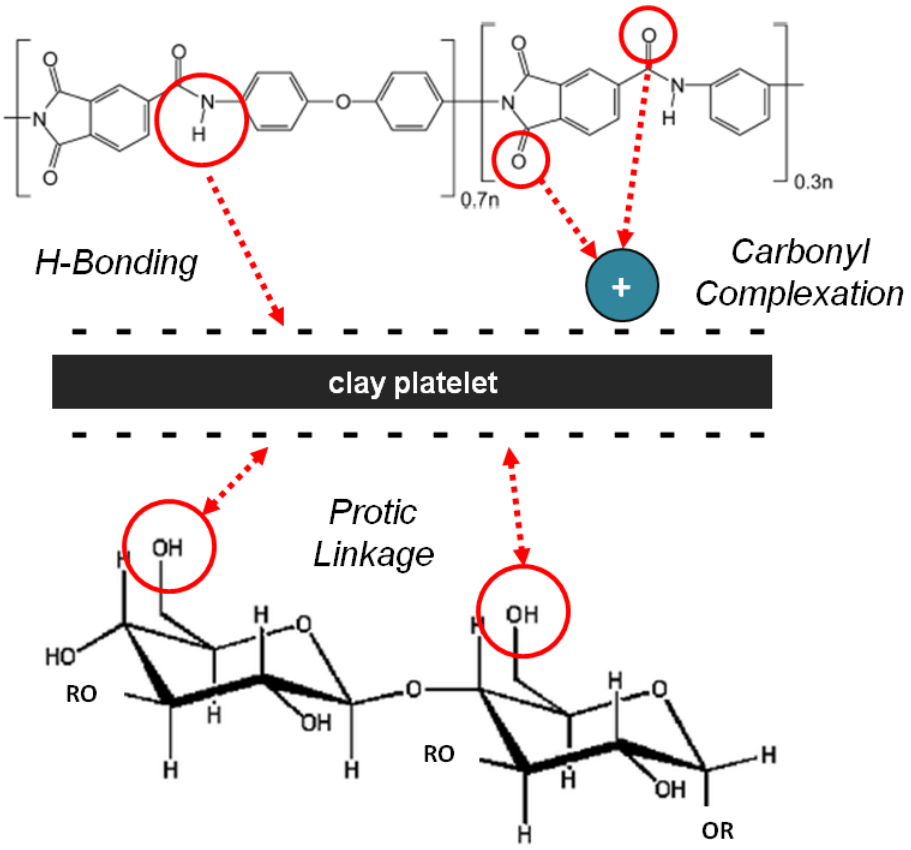

Figure 3.4: Polymer-Clay adhesion mechanisms. (1) Protic bridging between hydroxyl groups and the negatively charged clay surface (2) H-bonding between amide groups and the negatively charged clay surface (3) Carbonyl complexation with hydrated interlayer cations

3.4 Membrane Formation

There exists a delicate balance in the component ratios when creating solution based polymer-nanoclay dispersions (see Figure 3.5). One must consider several aspects when determining the formulation for these systems. Before we discuss the techniques used for creating solutions and forming membranes, it is useful to understand the compositional balance needed for success.

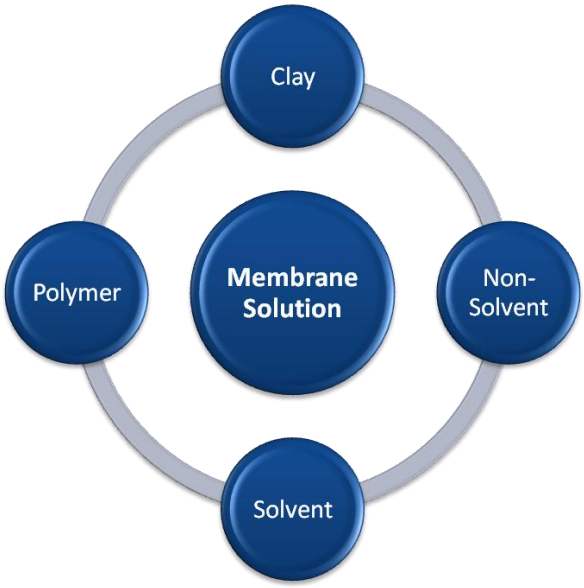

Figure 3.5: Tertiary component balance for hybrid membrane solution containing nanoclays in a polymer matrix.

The first step one must take is to determine the desired polymer-to-clay ratio in the membrane. This sets the stage. We have identified an aqueous organic co-solvent that will sufficiently create an exfoliated system of nanoclays; but this imposes other limits. Water is an essential element in clay exfoliation, regardless of the organic solvent polarity. There exists, though, a limit to the quantity of clay that can be exfoliated per quantity of water. Moreover, a secondary boundary condition exists with respect to the upper limit of organic solvent concentration in the blend. Assuming these two conditions can be satisfied, we must then consider the polymer.

Polymers used in gas separations are generally hydrophobic in nature. This is not to say that water cannot be present in the dope, but that it is severely limited to low quantities. Considering the minimum amount of water that is necessary to exfoliate the clays in the first step, we must then choose a polymer dope concentration that is one phase on a ternary phase diagram. Next we should re-evaluate the polymer and clay concentrations. Based on the polymer and non-solvent limitations, will the polymer-clay

ratio still yield the desired membrane? If not, the easy solution is the addition of strong solvent.

Adding strong solvent after the exfoliation step – followed by additional mixing – did not negatively affect the degree of exfoliation and actually improved dispersion via destruction of the gel structure. The quantity of additional solvent is important for the final stage though. If too much solvent is used, then the hybrid solution will have a low viscosity, which may not be desirable in some applications. Alternatively, if too little solvent is added then the polymer will not fully dissolve, thereby rendering a two phase solution. As noted in the exfoliation step, solvent quantities must be thoroughly considered.

At this point, if the solvent and clay compositions satisfy the limits (the water portion must be such that a one phase polymer solution will form) then polymer may be incorporated via additional high shear blending. This final mixing may be correlated to traditional melt blending extrusion in that polymer and clay are being combined using a high energy mixing process. Incorporation of the polymer into the clay suspension may be done in a sequentially optimized manner (similar to a priming procedure); in this work complete addition was chosen instead to seek the simplest approach.

Determining the correct ratios for the tertiary system can be challenging and is heavily dependent on the specific materials of interest as well as the desired hybrid membrane composition. In traditional polymer membranes the components are plotted on a ternary phase diagram (see Figure 3.6) wherein the apexes of the diagram represent polymer, solvent and non-solvent. Based on our observations, a second ternary phase diagram exists for clay, solvent and non-solvent (water). In this regard, we propose that there exists a phase boundary that differentiates a *highly exfoliated suspension of nanoclays* from a swollen precipitate. If true, then when the two independent systems (polymer & clay) are combined, there exists a region where all limits are satisfied. This overlapping region may be identified by combining two ternary plots. Alternatively, we suggest that

that the system may be represented as a tetrahedral diagram (see Figure 3.6) with clay anchoring the fourth apex.

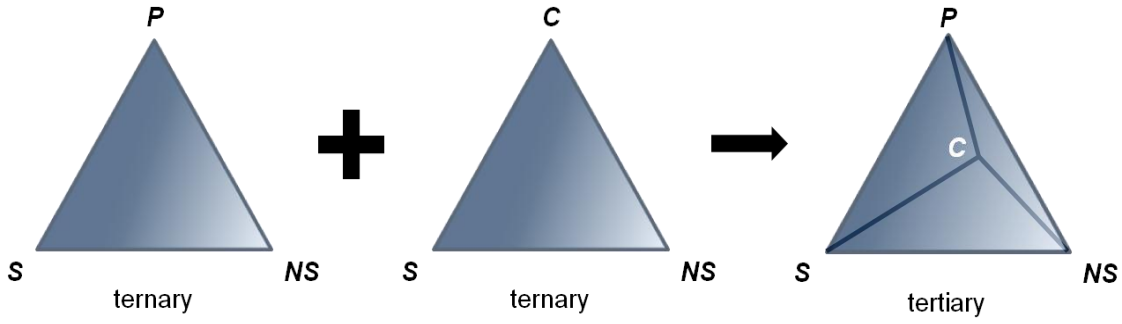

Figure 3.6: Ternary phase diagrams for polymer and clay blends and hypothetical tertiary diagram for hybrid membrane solution. (P = polymer, S = solvent, NS = non-solvent, C = clay)

It should be noted that we did consider using traditional organo-modification methods in this work, versus a purely solution based technique. We found that this approach did not yield the desired results. Moreover, this approach is more involved, making it less desirable industrially. Details and discussion of this study are provided in Appendix A as well as in the literature.[28]

3.4.1 Solution Development and Preparation

Success in this project was largely due to the identification of preparation procedures that were developed for creating stable hybrid dopes. Inspired by reports in the literature, we developed a process that, when executed precisely, will yield a polymer-nanoclay solution that can be used to produce hybrid membranes with excellent performance.[29-35] This is a novel contribution, but it relies heavily on "art" and experience. There are two critical components of this process that make it successful. First, the nanoclays must be *exfoliated* in an aqueous organic co-solvent – and the solvent ratios are important. Second, a high shear mechanical mixing process is necessary for the destruction and *dispersion* of flocculated clay gel and for the

incorporation of the polymer into the clay-solvent suspension. A generalized flowchart (Figure 3.7) is used to illustrate the steps in this process. Identification of the critical solvent ratios seems to be potentially achievable based on fundamental analysis; however, even this is a rather complex goal.

High shear mixing was achieved by using a Silverson Model L5M-A Lab Mixer that was fitted with a 5/8" Micro mixing head working with 10-50ml sample volumes. (Other configurations are available for various batch volumes.) The mixing protocol for each step was 7500RPM for 30 minutes. It was not in the scope of this work to explore alternative mixing speeds and times, although this may lead to improved membranes.

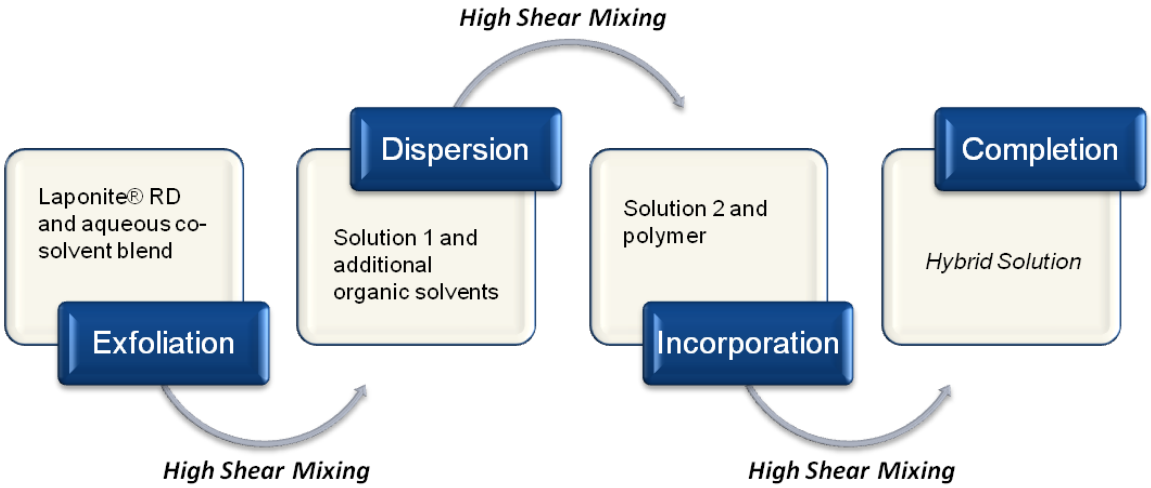

Figure 3.7: Flow diagram describing the necessary steps for creating a polymer-nanoclay hybrid solution for membrane formation: exfoliation (solution 1), dispersion (solution 2) and incorporation (solution 3).

Speaking specifically about the exact procedure used in this work, Laponite® RD was added to a 50/50 weight ratio blend of DI water and DMSO. This suspension was mixed for 30min using a speed of 7500RPM. After exfoliation, a portion of this suspension was combined with additional organic solvent to create a dilute system that would accommodate polymer dissolution (the solvent ratios are key to creating a one phase

dope). The solvent-clay dispersion was mixed further using the same protocol to destroy any gelled floccs. Afterwards, polymer was combined with the suspension in the second step. A final blending step was used to ensure polymer-clay homogenization. Pure polymer solutions were also created – but only mixing in the final step was used – to produce control films.

As a final comment, there was concern early on that the high intensity mixing would damage the polymer (i.e. reduced molecular weight). We confirmed that the molecular weight before and after blending was consistent via gel permeation chromatography (GPC) analysis. In other words, the high shear mixing process does not "chop" the polymer chains.

3.4.2 Dense Film Formation

Two methods were used for the formation of dense films as dictated by qualitative visual viscosity assessment. For low viscosity solutions the ring casting technique was used. All other membranes were made using the draw casting technique. General procedural details may be found elsewhere.[36] However, for this work there are a number of specifics that should be covered. The procedural specifics are applicable to all membranes in this work.

Casting Plate Preparation

All films were cast on heat treated glass plates. These plates may be cleaned and used as is or some authors report surface treatment of the glass to reduce membrane adhesion after vitrification.[37] For this work an abrasive paste (Colgate® Total Advanced Whitening Toothpaste) was used to polish the glass plates before film casting. The casting plate was then placed on a level support table prior to film casting.

Casting, Drying and Removal

Since the casting solutions contained low volatility solvents (DMSO, NMP), the films were vitrified and dried in a vacuum oven. Films were cast on the as-prepared plate on

the bench top and then immediately moved to a vacuum oven for solvent removal. The solvent removal process was carried out under continuous vacuum using a gradual, ramping temperature protocol (see Table 3.4) to minimize stress accumulation. After the final drying temperature, the oven temperature was reduced to room temperature and allowed to cool naturally. Once cool, the casting plates were submerged in DI water to remove the film. Fully vitrified films were further dried under vacuum at 100ºC overnight to remove water.

Table 3.4: Drying protocol used for film vitrification

Elapsed Time	0-24hrs	24-48hrs	48-72hrs	72-96hrs
Temperature	25ºC	50ºC	100ºC	180ºC

3.4.3 Asymmetric Hollow Fiber Formation

The dry-wet quench spinning process was used for hollow fiber formation in this work.[38] More specifically, dual layer (or composite) hollow fibers were produced. In this process, a hybrid solution containing polymer and nanoplatelet filler was co-extruded with a pure polymer solution using a spinneret that was designed and developed by members of the Koros Research Group. To obtain our desired morphology the hybrid layer was on the fiber periphery and the pure polymer was on this inside. Commonly these layers are referred to the sheath and core layers, respectively. A thermodynamically neutral bore fluid comprised of a blend of water and NMP was used to produce the bore of the fiber. Figure 3.8 provides a cartoon depicting the multi-layer fiber composition. After spinning, the fibers were removed from the collection drum and were post-processed to remove any residual solvent using a multi-step solvent exchange process. Details of this process are presented in Chapter 7.

Sheath dope formulations were based on the developments in the dense film portion of our work. As an extension to the process described in Section 3.3.1, acetone was used in conjunction with DMSO or NMP during the dilution/dispersion step. Acetone was used as the necessary volatile solvent for skin layer formation during the spinning

process. Further details on the sheath dope compositions are described in Chapter 7. Core dope formulations (also listed in Chapter 7) were derived from work by a fellow Koros Group Member – Dhaval Bhandari.[39] It was not necessary to prepare these dopes using the high mixing technique. Rather, solvent (NMP) and $LiNO_3$ salt – when used – were combined in a jar and the salt was allowed to fully dissolve. Polymer(s) was then added to the mixture and allowed to dissolve while slowly mixing on an in-house built rolling apparatus.

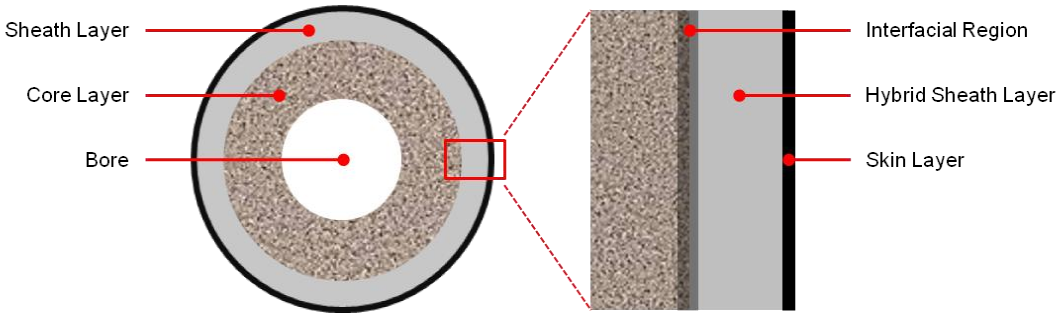

Figure 3.8: Cartoon depicting the cross-section of a hybrid dual layer hollow fiber membrane.

Additional details regarding the dual layer hollow fiber spinning process are provided in Chapter 7. Specifics of the spinning equipment used in the Koros Research Group are provided elsewhere.[38,40,41]

3.5 Membrane Testing

In this work we used several different procedures to characterize gas transport properties in membranes. Permeation experiments were used to determine the permeability in the dense film membranes and permeance in the hollow fiber membranes. Additionally, pressure-decay sorption was used to determine the solubility coefficient in some materials. All measurements were conducted using single gas feedstreams and operating temperatures were maintained at 35ºC.

3.5.1 Dense Film Permeability Measurements

An isochoric (constant volume, variable pressure) permeation system was used to measure the permeability in dense film membranes. Thorough descriptions of the permeation system used and sample preparation procedures are provided elsewhere.[36,42] However, for the reader's benefit we will provide an explanation of the governing principles and measurement apparatus.

A cartoon depicting the basic components of a permeation system is shown in Figure 3.9. For the sake of brevity, we have neglected to include the entire schematic. Since permeability correlates to pressure normalized flux, the device is used to measure the change in pressure in the downstream as a function of time. A volume of gas (V_1) at a known pressure is feed to the membrane and allowed to permeate until the flux is confidently at steady state ($t \geq 10$ time lags). The gas is collected in the downstream volume (V_2) and the pressure is measured continuously. In this configuration $V_1 >> V_2$ such that p_1 remains constant during the course of the measurement. Moreover, $p_1 >> p_2$ because the downstream is initially at vacuum ($p \sim 10$mtorr) and data is collection is limited to pressures less than 10torr. These constraints ensure that the base assumptions – wherein Δp across the membrane is equal to p_1 – are true. Based on the measurements performed and principles of the system we can calculate permeability as illustrated by the correlation in Equation 3.1.

$$\frac{dp}{dt} \propto \frac{dn}{dt} \rightarrow \frac{N \cdot L}{A \cdot t \cdot P_1} = Permeability \qquad \text{Eq. 3.1}$$

In this equation *dp/dt* is the measured change in pressure in the downstream volume, which can be converted to moles (*dn/dt*) and in the final form is converted to the number of moles, N (reported at STP), that permeated (see Table 2.1 for units and Chapter 2 for additional details on transport theory). Specific membrane characteristic values of area (A) and thickness (L) are measured. And as before, p_1 is the feed pressure during the experiment.

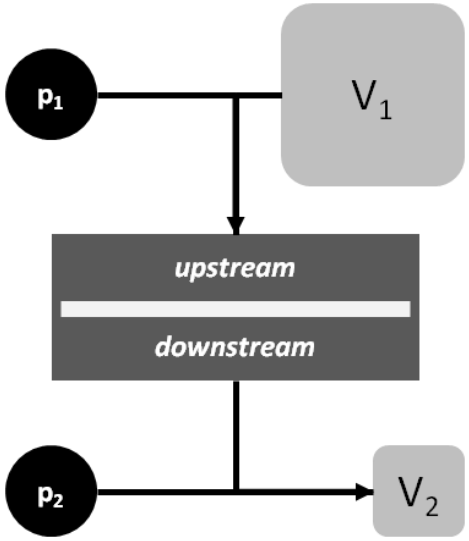

Figure 3.9: Cartoon of a permeation apparatus (without valves and communication). In this figure p_1 and p_2 represent pressure transducers. V_1 and V_2 are the feed and collection volumes respectively, where $V_1 >> V_2$

3.5.2 Asymmetric Hollow Fiber Permeance Measurements

Compared to dense films, measuring permeation in an asymmetric hollow fiber membrane is considerably simpler. To test this membrane morphology we used an isobaric system (constant pressure, variable volume) wherein a constant delivery pressure is applied and the volumetric flow rate (*dv/dt*) of the permeate is measured using a bubble flow meter and converted to moles or volume (measured at STP). A simplified cartoon of a hollow fiber membrane test module is shown in Figure 3.10. In this case, we are depicting a single gas feed because the end is capped and thus there is no retentate. Also, we used a *bore side* feed because the test pressures of interest were sufficiently low.

Preparation of the test modules may be more difficult than dense film test cells. Detailed descriptions of the module preparation procedures have been provided adequately elsewhere.[40,41] In this work, fiber modules generally contained 10-20 fibers and the modules were on the order of 15-25cm in length.

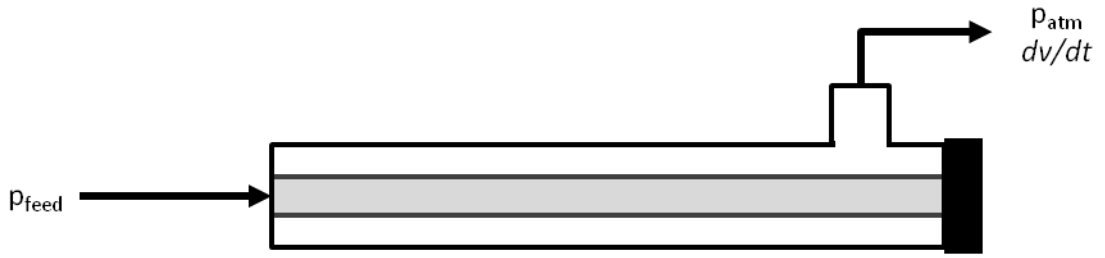

Figure 3.10: Cartoon of permeation in a hollow fiber membrane module using a single gas feed on the bore side.

3.5.3 Pressure-Decay Sorption

In non-porous polymeric materials, permeability is best described using solution-diffusion theory. As such, the permeability is a function of the diffusion and solubility coefficients ($P=D\cdot S$). Diffusion coefficients may be calculated from measured permeability data using the time-lag model.[43] This then allows one to calculate the solubility coefficient. A more rigorous and accurate alternative to determine the solubility coefficient is by measuring the sorption capacity using pressure-decay sorption. In this procedure, a known quantity of gas is exposed to a sample and the concentration in the bulk is measured over time to determine the change – and therefore the amount sorbed into the sample. A basic cartoon of the configuration is shown in Figure 3.11 with the corresponding experimental intervals of interest. Pressure and time (*dp/dt*) are measured continuously.

At time zero (t=0) the sample cell, which contains a known quantity of sample, is isolated from the reservoir. A quantity of gas (p_1,n_1) is charged to the reservoir and the system is allowed to thermally equilibrate. The isolation valve is then quickly opened (t=1) to feed gas from the reservoir to the sample cell and then closed. For this initial moment, the bulk of the sample cell has some quantity of gas (p_2, n_2). Over time the sample will sorb gas until it reaches a steady state capacity ($t\rightarrow\infty$, p_3, n_3). During this time the reservoir concentration will remain constant (p_2, n_2) because there are no sorbing components.

Completing a mole balance on the system allows us to determine the amount of gas sorbed into the sample. Solubility is generally reported as volume of gas sorbed (measured at STP) per volume of sample for polymeric materials.

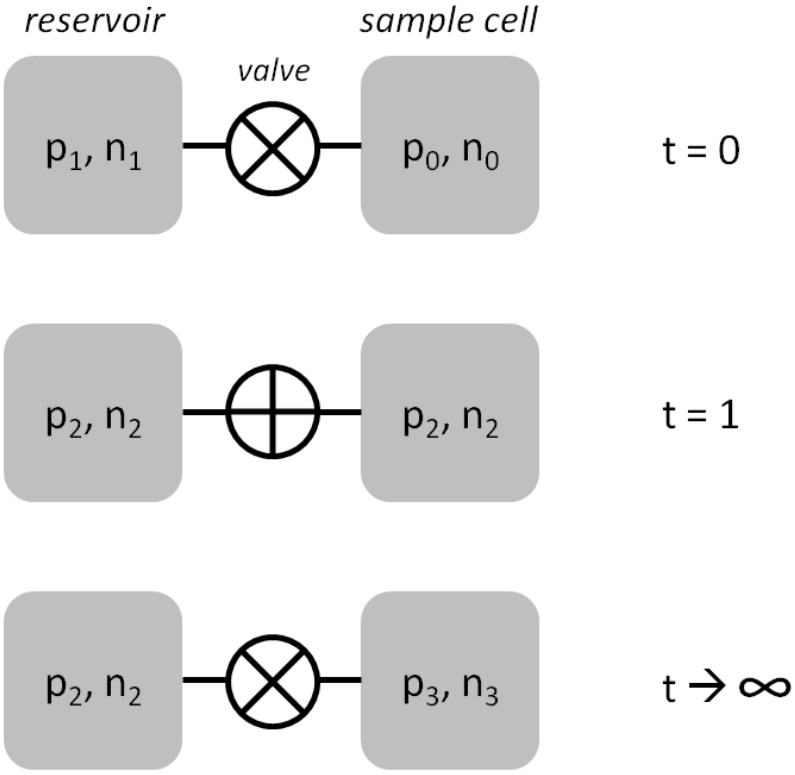

Figure 3.11: Cartoon of the steps during a pressure-decay sorption experiment. In this image, p_i is the pressure in the chamber at some time (t) and n_i are the number of moles of gas in the bulk (outside the sorbing component). Reservoir and sample cell volumes are constant.

Specific details of the experimental apparatus and sample preparation are reported elsewhere.[36] It should be noted, though, that for sorption experiments on nanoclays, a sintered stainless steel filter is used with an aluminum cover to prevent dispersion of the inorganic powder into the system. Moore has described this in greater detail.[36] Also, for sorption experiments using CO_2, the *virial equation of state* was used to determine the compressibility factor.

3.6 Complementary Characterization Techniques

Permeation and other gas transport tests serve as the ultimate technique for characterizing membrane materials. In hybrid materials, permeation tests may readily provide insight into the organic-inorganic interface because angstrom sized defects may be observed from transport properties and the deviations from transport theories for defect free dense materials. Despite the value of permeation measurements, additional characterization techniques were used to evaluate the membrane solutions and preparation procedures. Also, microscopic characterization was a critical element for determining structural information.

3.6.1 Rheological Evaluation

Two types of rheological measurements were made to characterize the efficacy of the solution preparation techniques. The primary measurement type was viscosity as a function of shear rate, which was applied to the polymer-clay hybrid solutions. Storage and loss modulii were measured as a function of frequency on the clay-solvent dispersions. All measurements were conducted in the laboratory of the Complex Fluids Group (PI: Dr. Victor Breedveld) in the School of Chemical & Biomolecular Engineering at Georgia Tech using an Anton-Paar MCR-300 rheometer. The instrument was operated at 25ºC for all measurements.

Viscosity measurements were made using the CC10 C*ouette geometry* (inner diameter: 10mm, outer diameter: 10.84mm, volume: 0.97cc). Measurements were made using a shear rate range of 0.1-1000 s^{-1} – forward and reverse to show hysteresis. It was found that Torlon®-based samples could not be accurately measured when the shear rate was less than 1 s^{-1} due to sensitivity limitations of the instrument. Data in this range will not be presented for these samples.

Moduli measurements were made using a *cone-and-plate geometry* (cone diameter: 50mm, cone angle: 1.01º). After loading each sample, a high shear was applied (1000 s^{-1} for 1min total) to remove any structural history before starting oscillatory

deformations. Oscillatory amplitude (0.1) and angular frequency (2π rad/s) were kept constant during the measurement.

3.6.2 Scanning Electron Microscopy

The concentricity, porosity, interfacial adhesion and skin layer of the dual layer asymmetric hollow fibers were all characterized using scanning electron microscopy (SEM). Samples were prepared using the technique discussed by Husain.[41] All measurements were made at Georgia Tech in the Center for Nanostructure Characterization.

3.6.3 Transmission Electron Microscopy

One of the most widespread characterization techniques for polymer nanocomposites is transmission electron microscopy (TEM).[16] The high magnification capabilities of TEM allow the user to visualize individual clay platelets that are 1nm thick. Dispersion and the degree of exfoliation can be illustrated via careful TEM analysis. Preparing samples for analysis can be difficult because of the amorphous nature of the polymer component. Ultra-microtomy is commonly used to produce ultrathin slices for analysis.[44] These capabilities are not available at Georgia Tech. So for this work we collaborated with researchers at the University of Minnesota and the University of Notre Dame.

The hollow fiber TEMs presented in Chapter 7 were provided by Dr. Sunho Choi while he was in residence at the University of Minnesota. He used ultra-microtomy to prepare the samples for analysis. Images in Chapters 5 and 6 were provided by Ms. Tatyana Orlova at the University of Notre Dame. She and Dr. Alexander Moukasian developed a unique procedure for preparing the samples using *focused ion beam milling* (FIB) which is a derivative of the procedure reported by Hashemi, et al.[44] During this process a section of the hybrid membrane is milled into an ultra-thin lamella by etching away the surrounding material. The etched sample was then mounted to a TEM sample inside the FIB chamber using an omni probe (nanotweezers) and a platinum spot weld to affix the sample to the grid. A glimpse of this process is shown in Figure 3.12. Additional

details are provided in Appendix B. After mounting on the grid, additional milling was done to provide a clean sample for analysis. Imaging was done using a Titan TEM from FEI Company.

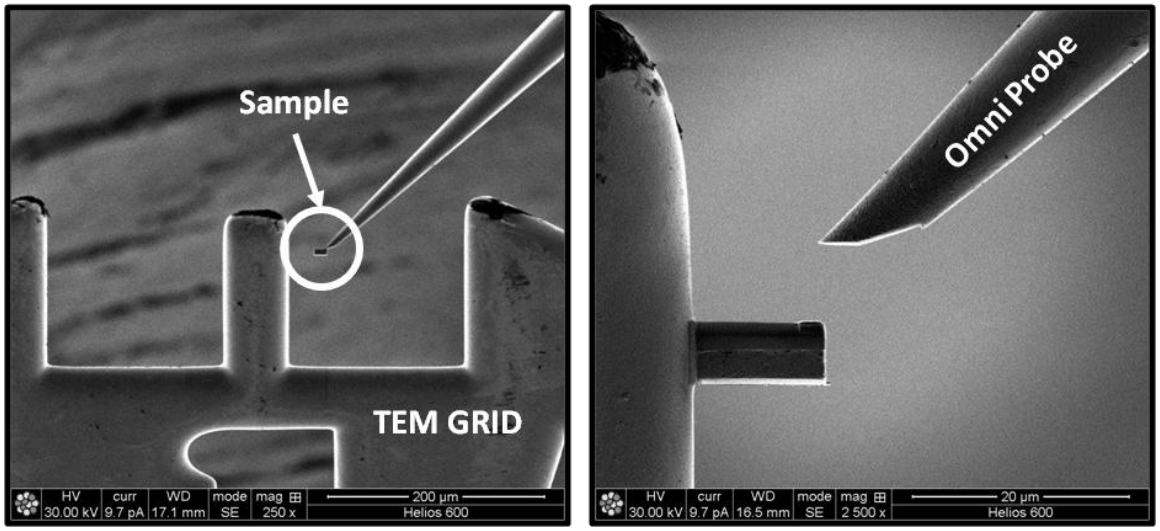

Figure 3.12: SEM images showing (1) the process of transferring a FIB milled nanocomposite sample to a TEM grid using the omni probe and (2) the attached sample after platinum welding to the TEM grid

3.6.4 Solvent Swell Tests

Swell tests are a quick method that can be used to qualitatively determine the affinity of a solvent and nanoclay. A measured quantity of Laponite® RD was added to an 8ml glass vial. The initial fill height of the clay is then measured as the reference height (h_0). A known volume of solvent is then slowly added to the vial, as to not disturb the packing of clay, and allowed to rest for 24 hours unperturbed. If the nanoclay completely exfoliates, then it will no longer be easily visible. However, in an organic solvent this does not occur, but rather the clays swell. This swelling effect is determined by measuring the expanded fill height (h_1) of the clay precipitate in the solvent. The swell height with respect to the initial height can be used to determine a swelling factor. Additional details are provided in Chapter 4, Section 4.1.1.1.

3.7 References

1. M. Kosuri, "Polymeric Membranes for Super Critical Carbon Dioxide ($scCO_2$) Separations," *PhD Dissertation*, Georgia Institute of Technology, 2009.

2. J. Mark (ed), *Polymer Data Handbook*. (Oxford University Press, New York, NY, 1999), 1st ed.

3. O. Olabisi (ed), *Handbook of Thermoplastics*. (Marcel Dekker, Inc., New York, NY, 1997).

4. Solvay Advanced Polymers, "http://catalog.ides.com/datasheet.aspx?I=42041&FMT=PDF&E=135275", (2010).

5. A. Newman (ed), *Chemistry of Clays and Clay Minerals*. (John Wiley & Sons, Inc., New York, NY, 1987).

6. Southern Clay Products, "http://www.laponite.com"

7. A. Mourchild, A. Delville, J. Lambard, E. Lecolier, and P. Levitz, "Phase Diagram of Colloidal Dispersions of Anisotropic Charged Particles: Equilibrium Properties, Structure, and Rheology of Laponite Suspensions," *Langmuir* **11** (6), 1942-1950 (1995).

8. J. Ramsay, S. Swanton, and J. Bunce, "Swelling and Dispersion of Smectite Clay Colloids: Determination of Structure by Neutron Diffraction and Small-Angle Neutron Scattering," *Journal of the Chemical Society, Faraday Transactions* **86**, 3919-3926 (1990).

9. R. Weast (ed), *CRC Handbook of Chemistry and Physics*. (CRC Press, Inc., Boca Raton, FL, 1986), 67th ed.

10. C. Yaws (ed), *Chemical Properties Handbook*. (McGraw-Hill Professional, Columbus, OH, 1998), 1st ed.

11. D. Breck, *Zeolite Molecular Sieves: Structure, Chemistry, and Use*. (Robert E. Krieger Publishing Co., Malabar, FL, 1974).

12. M. Tsapatsis and W. Fan, "A New, Yet Familiar, Lamellar Zeolite," *ChemCatChem* **2** (3), 246-248 (2010).

13. J. Coronas, "Present and Future Synthesis Challenges for Zeolites," *Chemical Engineering Journal* **156** (2), 236-242 (2010).

14. S. Choi, J. Coronas, J. Sheffel, E. Jordan, W. Oh, S. Nair, D. Shantz, M. Tsapatsis, "Layered Silicate by Proton Exchange and Swelling in AMH-3," *Microporous and Mesoporous Materials* **115** (1-2), 75-84 (2008).

15. L. Liu, S. Ferdov, C. Coelho, Y. Kong, L. Mafra, J. Li, J. Dong, U. Kolitsch, R. Ferreira, E. Tillmanns, J. Rocha, and Z. Lin, "New Crystalline Layered Zinc Phosphate with 10-Membered-Ring Channels Perpendicular to Layers," *Inorganic Chemistry* **48** (11), 4598-4600 (2009).

16. T. Pinnavaia and G. Beall (eds), *Polymer-Clay Nanocomposites*. (John Wiley & Sons, Inc., New York, NY, 2000).

17. D.R. Paul and L.M. Robeson, "Polymer Nanotechnology: Nanocomposites," *Polymer* **49** (15), 3187-3204 (2008).

18. S. Pavlidou and C. Papaspyrides, "A Review on Polymer-Layered Silicate Nanocomposites," *Progress in Polymer Science* **33** (12), 1119-1198 (2008).

19. H. van Olphen, *An Introduction to Clay Colloid Chemistry*. (John Wiley & Sons, Inc., New York, NY, 1977), 2nd ed.

20. S. Olejnik, A. Posner, and J. Quirk, "Swelling of Montmorillonite in Polar Organic Liquids," *Clays and Clay Minerals* **22**, 361-365 (1974).

21. G. Brindley, K. Wiewiora, A. Wiewiora, "Intracrystalline Swelling of Montmorillonite in Some Water-Organic Mixtures," *The American Mineralogist* **54**, 1635-1644 (1969).

22. A. Barton, *Handbook of Solubility Parameters and Other Cohesion Parameters*. (CRC Press, Inc., Boca Raton, FL, 1983).

23. S-H. Chang, M. Ryan, R. Gupta, B. Swiatkiewicz, "The Adsorption of Water Soluble Polymers on Mica, Talc, Limestone, and Various Clay Minerals," *Colloids and Surfaces* **59**, 59-70 (1991).

24. S. Yariv and H. Cross (eds), *Organo-Clay Complexes and Interactions*. (Marcel Dekker, Inc., New York, NY, 2002).

25. N. Schamp and J. Huylebroeck, "Adsorption of Polymers on Clays," *Journal of Polymer Sicence: Polymer Symposia* **42** (2), 553-562 (1973).

26. B. Theng, "Clay-Polymer Interactions: Summary and Perspectives," *Clays and Clay Minerals* **30** (1), 1-10 (1982).

27. M. Onikata, M. Kondo, N. Hayashi, and S. Yamanaka, "Complex Formation of Cation-Exchanged Montrmorillonites with Propylene Carbonate: Osmotic Swelling in Aqueous Electrolyte Solutions," *Clays and Clay Minerals* **47** (5), 672-677 (1999).

28. J.R. Johnson, W.J. Koros, "Utilization of Nanoplatelets in Organic-Inorganic Hybrid Separation Materials: Separation Advantages and Formation Challenges," *Journal of Taiwan Insitute of Chemical Engineers* **40** (3), 268-275 (2009).

29. N. N. Herrera, J. M. Letoffe, J. L. Putaux, L. David, and E. Bourgeat-Lami, "Aqueous Dispersions of Silane-Functionalized Laponite Clay Platelets. A First Step Toward the Elaboration of Water-Based Polymer/Clay Nanocomposites," *Langmuir* **20** (5), 1564-1571 (2004).

30. E. S. H. Leach, A. Hopkinson, K. Franklin, and J. S. van Duijneveldt, "Nonaqueous Suspensions of Laponite and Montmorillonite," *Langmuir* **21** (9), 3821-3830 (2005).

31. A. Manninen, H. Naguib, A. Nawaby, and M. Day, "CO_2 Sorption and Diffusion in Polymethyl Methacrylate-Clay Nanocomposites," *Polymer Engineering and Science* **45** (7), 904-914 (2005).

32. S. Liff, N. Kumar, G. McKinley, "High-Performance Elastomeric Nanocomposites Via Solvent-Exchange Processing," *Nature Materials* **6**, 76-83 (2007).

33. D. Burgentzle, J. Duchet, J. Gerard, A. Jupin, B. Fillon, "Solvent-based Nanocomposite Coatings I. Dispersion of Organophillic Montmorillonite in Organic Solvents," *Journal of Colloid and Interface Science* **278** (1), 26-39 (2004).

34. M. McAlpine, N. Hudson, J. Liggat, R. Pethrick, D. Pugh, and I. Rhoney, "Study of the Factors Influencing the Exfoliation of an Organically Modified Montmorillonite in Methyl Methacrylate/Poly(Methyl Methacrylate) Mixtures," *Journal of Applied Polymer Science* **99** (5), 2614-2626 (2006).

35. I. Rhoney, S. Brown, N. Hudson, and R. Pethrick, "Influence of Processing Method on the Exfoliation Process for Organically Modified Clay Systems I. Polyurethanes," *Journal of Applied Polymer Science* **91** (2), 1335-1343 (2004).

36. T. Moore, "Effects of Materials, Processing, and Operating Conditions on the Morphology of Gas Transport Properties of Mixed Matrix membranes," *PhD Dissertation*, University of Texas - Austin, 2004.

37. S. Shu, "Engineering the Performance of Mixed Matrix Membranes for Gas Separations," *PhD Dissertation*, Georgia Institute of Technology, 2007.

38. S. Pesek, "Aqueous Quenched Asymmetric Polysulfone Flat Sheet and Hollow Fiber Membranes Prepared by Dry/Wet Phase Separation," *PhD Dissertation*, University of Texas - Austin, 1993.

39. D. Bhandari, "Hollow Fiber Sorbents for the Desulfurization of Pipeline Natural Gas," *PhD Dissertation*, Georgia Institute of Technology, 2010.

40. I. Omole, "Crossliked Polyimide Hollow Fiber Membranes for Aggressive Natural Gas Feed Streams," *PhD Dissertation*, Georgia Institute of Technology, 2008.

41. S. Husain, "Mixed Matrix Dual Layer Hollow Fiber Membranes for Natural Gas Separation," *PhD Dissertation*, Georgia Institute of Technology, 2006.

42. T. Moore, S. Damle, P. Williams, and W.J. Koros, "Characterization of Low Permeability Gas Separation Membranes and Barrier Materials: Design and Operation Considerations," *Journal of Membrane Science* **245** (1-2), 227-231 (2004).

43. J. Crank, G. Park, *Diffusion in Polymers*. (Academic Press, Inc, 1968).

44. S. Hashemi, R. Sahraian, P. Lafleur, K. Stoeffler, "Focus Ion Beam Preparation of Transmission Electron Microscope Sample in Polymer Clay Nanocomposite," *Iranian Polymer Journal* **15** (7), 539-545 (2006).

CHAPTER 4

PREPARATION & CHARACTERIZATION OF POLYMER-NANOPLATELET SOLUTIONS FOR HYBRID MEMBRANE FORMATION

4.1 Overview

The production of polymer-nanoclay composites has been topic of investigation for many years. Typical methods for exfoliation and dispersion include (1) melt blending (2) *in situ* polymerization and (3) solution dispersion.[1,2] All of these methods have been proven successful for various material applications. It was our objective to use the developmental history of these methods to create a unique, efficient and effective method for the creation of polymer-platelet nanocomposites that can be easily scaled for the production of advanced membrane materials. In this chapter we aim to illustrate the efficacy of our preparation method prior to membrane formation.

It is important for the progression of this investigation to follow a well-defined path towards dope development. Our study begins with an evaluation of solvents because platelet exfoliation must be achieved before the addition of polymer, which is determined in the initial solvent system. Once a solvent or co-solvent has been identified, polymer can then be incorporated to create a membrane dope. All the while, we must establish an effective mixing protocol for making a dope containing well-exfoliated nanoclays in a polymer matrix.

4.2 Methods for Dispersing and Exfoliating Nanoclays and Their Efficacy

Early on in this investigation we chose to eliminate melt blending and extrusion as an option for nanocomposite formation. This method, albeit very common industrially, requires an extensive mechanical energy and material preparation via functionalization.[2] In that same vein, we also removed *in situ* polymerization from the list. We wanted to utilize commercially available polymers in order to broaden the applicability of our procedure. The in situ polymerization technique requires a series of complex steps which do not scale easily. By eliminating these two methods we reduced our options to one base method of interest: solution dispersion. This approach is generally applicable, so it is very attractive relative to the other approaches noted.

With respect to membrane formation – especially asymmetric hollow fiber membranes - solution dispersion is a popular technique. Literature has even showed the viability of this method in the production of molecular sieve containing mixed matrix membranes.[3-5] Sonication homogenization and/or low shear mixing are the most prevalent techniques used in these works. We have found that these traditional methods do not yield the desired results when applied to polymer-nanoclay hybrid membrane formation. Using these other studies as inspiration and considering developments in the literature, we have created a successful method that employs high shear mixing for the dispersion process and a co-solvent blend for nanoclay exfoliation.[6-11] We have validated the true effectiveness of this technique using gas permeability tests (see Chapters 5 and 6).

4.2.1 Analysis of Solvent Systems Used for Nanoclay Exfoliation

It is well known that many types of clay materials will readily exfoliate when dispersed into water.[12] This fact has been employed to create water soluble polymer-clay nanocomposites for a variety of applications.[13-15] Unfortunately these systems are not applicable to our case. Typical membrane polymers are hydrophobic. Our objective in this portion of the study was to identify a solvent or co-solvent system that would promote excellent particle exfoliation and allow us to add non-water soluble polymer in

order to create a hybrid solution that is suitable for membrane formation – with the ultimate target being phase inversion membranes.

Reports in the literature have shown that solvent polarity contributes to exfoliation potential.[16] Water being highly polar has the greatest capabilities for exfoliation in hydrophilic clays. (Clay exfoliation via cationic hydration is discussed in greater detail in Chapter 2 of this work.) Recalling that our ultimate objective is to form a solution for membrane formation, we were limited in our choice of solvents. Therefore we identified two solvents with high polarity indices that could also be used for polymer dissolution: dimethyl sulfoxide (DMSO) and n-methylpyrrolidone (NMP). Their respective molecular structures are shown in Figure 4.1.[17]

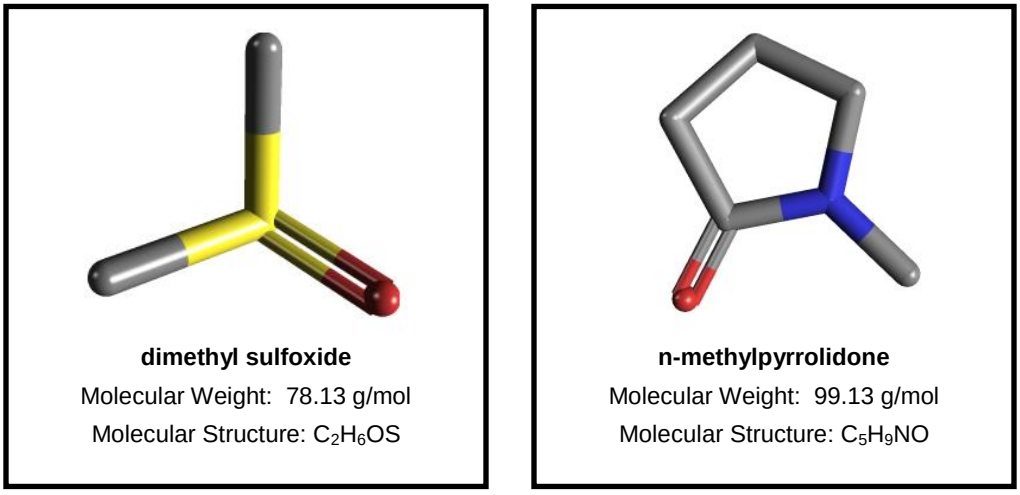

Figure 4.1: Molecular structures of dimethyl sulfoxide (DMSO) and n-methylpyrrolidone (NMP). Colors in structure correspond accordingly: ● = carbon, ● = nitrogen, ● = oxygen, ● = sulfur

After dispersing Laponite® RD into these solvents, we found that they did not exfoliate (a precipitate was evident). This observation let us to the conclusion that an aqueous solvent blend would be necessary to exfoliate the nanoclays. Meanwhile, we had to ensure that the quantity of water was kept to a minimum to ensure polymer dissolution at

later stages in the membrane formation process. Analysis of solvent blend ratios will be discussed in greater detail later. We must first determine which solvent will provide a greater contribution towards the exfoliation of Laponite® RD.

4.2.1.1 Qualitative Analysis of Solvent Systems for Nanoclay Exfoliation via Swell Tests

It was predetermined which solvents were available for this work based on the defined constraints (must be a good solvent for our polymers). Based on the literature, the solvent with the highest polarity should induce the most swelling.[18] Thus, we initially hypothesized that DMSO would be more favorable because its Polarity Index (P') is higher (see Table 4.1).[19] To verify this hypothesis we used swelling tests (the experimental procedure has been previously described in Chapter 3, Section 3.5.4) to draw a qualitative conclusion. The results of these tests are presented in Figures 4.2 and 4.3 and Table 4.1.

The free swelling factor (S_f) for Laponite® RD in the test solvents was calculated using Equation 4.1, where h_0 is observed height of clay before adding solvent, h_1 is the swollen height of the clay in solvent without mixing and h_2 is the swollen height after brief agitation. It is important to keep in mind that these are qualitative measurements. Values for h_0 were estimated separately for each solvent system to improve accuracy.

$$S_i = \frac{(h_i - h_0)}{h_0} \qquad \text{Eq. 4.1}$$

If we only consider the second frame of Figure 4.2, it is clear that water exhibits the best swelling capability followed by DMSO, NMP and acetone. This fits the original hypothesis that swelling is a function of solvent polarity. There is one important caveat regarding this analysis. In the second frame of the image (part *a*) it appears that water has a finite swelling factor. At these clay concentrations that is actually not true. The clear head volume of the framed portion is actually a transparent gel. Formation of the gel layer imposed swelling resistance thereby limiting the overall swelling of the clay.

Table 4.1: Calculated Free Swelling Factors (S_f) for each solvent system in this study and the corresponding Snyder Polarity Index.

Solvent	Free Swelling Factor (S_f)	Snyder's Polarity Index (P')
Deionized H_2O	4.45	10.2
Dimethylsulfoxide	2.8	7.2
n-Methylpyrrolidone	1.4	6.7
Acetone	0.75	5.1

To roughly emulate the mixing conditions of the actual formulation process, we vigorously mixed each sample after the first 24 hour window. After doing so we see that all solvent systems show an increase in the observed swelling factor. Water behaved as expected and fully exfoliated the clays; hence there is no observed precipitate. Regardless of the improvements, the order of potency did not change. We have represented the observed free swelling factor as a function of solvent polarity in Figure 4.3 for each case.

This simple characterization technique provided a very good insight into which solvents induce the most swelling – and the results matched our expectations. More importantly, these tests reaffirmed our suspicion that an aqueous solvent blend is necessity for creating an exfoliated system of nanoclays. We can utilize these observed solvent properties and create an aqueous solvent blend that would promote exfoliation and allow for polymer incorporation later in the solution formation process.

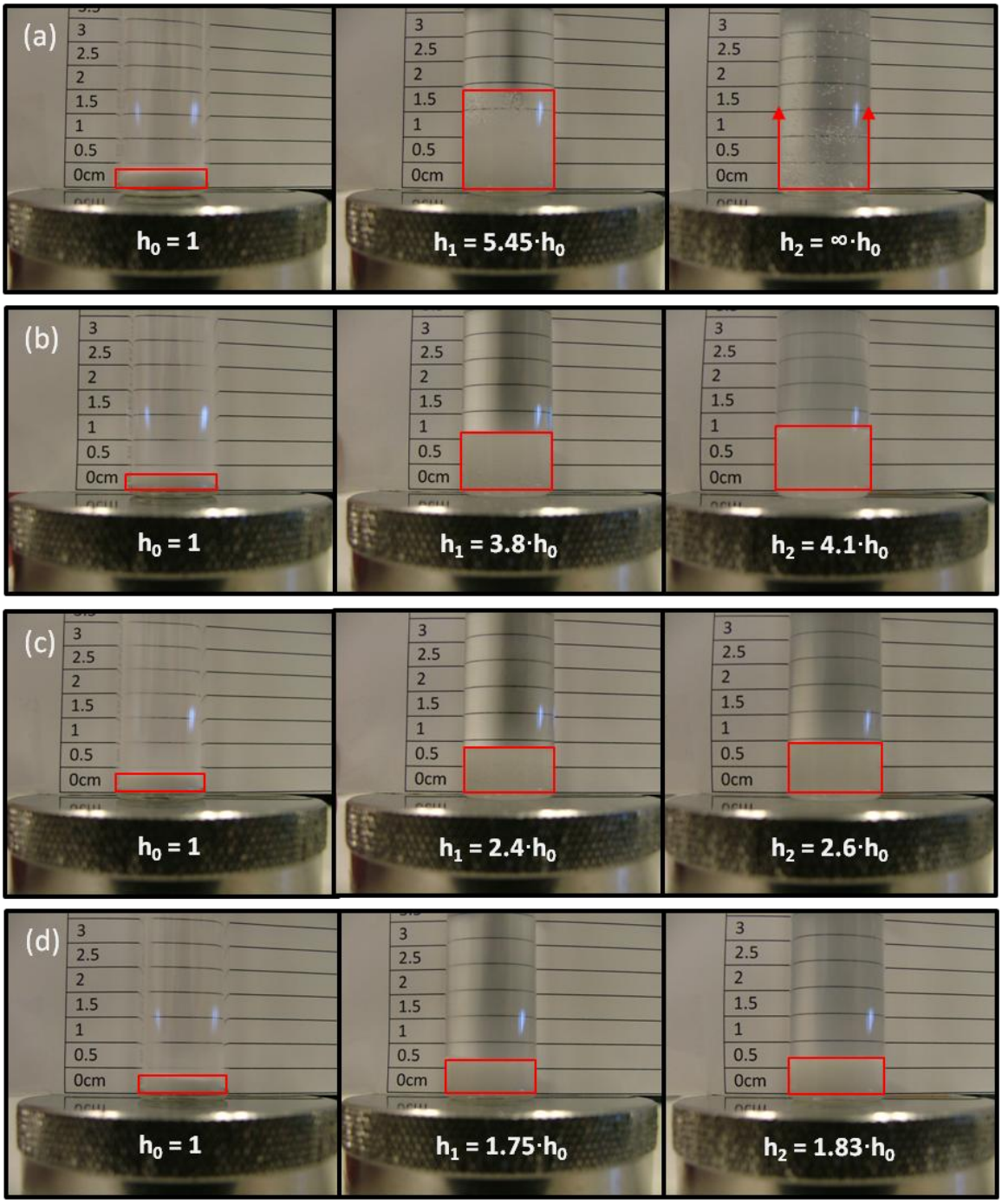

Figure 4.2: Free Swelling Factor of Laponite® RD in Different Solvents. (a) DI water (b) DMSO (c) NMP (d) Acetone. [Frame 1: no solvent, Frame 2: swelling after 24hrs unperturbed in solvent, Frame 3: swelling after additional 24hrs wherein the system was mixed briefly]

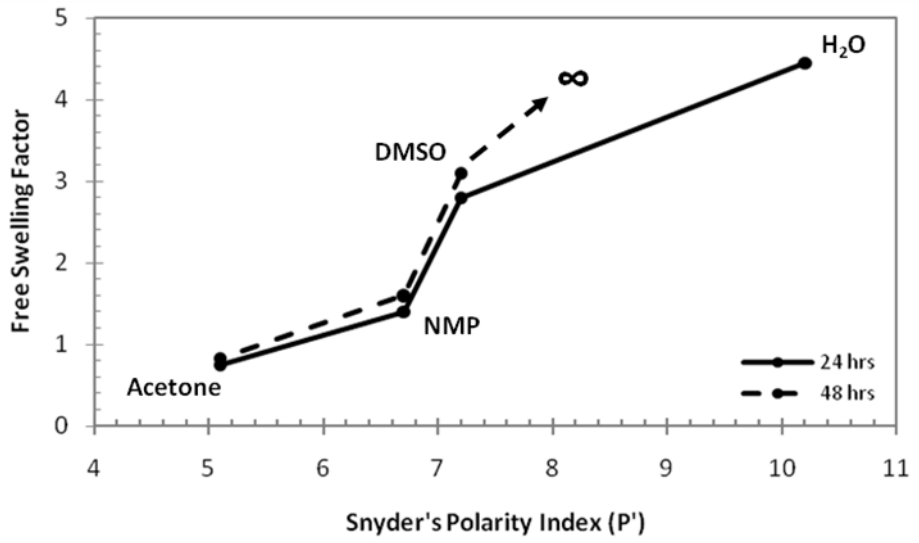

Figure 4.3: Free Swelling Factor of Laponite® RD in Different Solvents as a Function of the Snyder Polarity Index for each Solvent. The dashed line indicates that the Swelling Factor approaches infinity at high polarity because not limit was observed in this study.

4.2.1.2 Qualitative Analysis of Solvent Systems for Nanoclay Exfoliation via Microscopy

To complement the swelling study that was presented in previous section, we prepared dispersions of Laponite® RD in different solvent systems and used scanning electron microscopy (SEM) to characterize. Corresponding images for each system are shown in Figure 4.4. The micrographs provide further proof that pure solvents are not sufficient for exfoliating clays, but that a co-solvent system is the correct choice.

Images shown in Figure 4.4 correspond to water, DMSO, hexane and a DMSO/water blend. To prepare these samples we dispersed a small amount (<1wt%) of Laponite® RD in the respective solvent and allowed the samples to rest overnight. Next, several drops of each suspension were deposited on a standard flat SEM sample mount. The mounts were then dried in a vacuum oven to remove the solvents. Please note that in Figure 4.4c we are presenting results for a hexane (P'=0.1) dispersion; in the swelling study we used acetone. Hexane was used here to show an extreme case.

A frame-by-frame analysis of the images shown in Figure 4.4 is provided in Table 4.2. In summary, we see that neither hexane nor DMSO sufficiently exfoliate Laponite® RD, which agrees well with our previous study. Water provided a well exfoliated state as expected. More importantly, we see that a blend of water and DMSO provides a semi-aqueous solution to the exfoliation issue. This concept will be discussed in further detail in the next section.

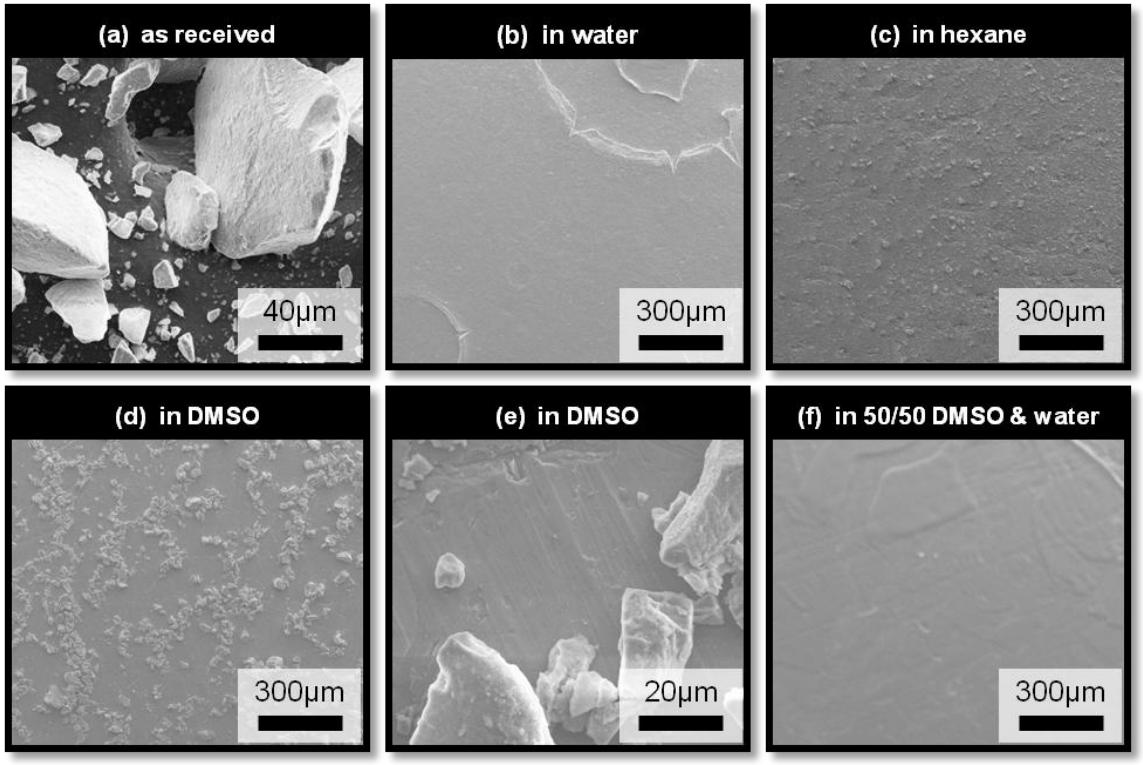

Figure 4.4: Scanning electron micrographs of as received Laponite® RD and after dispersing in various solvents. (a) as received (b) dispersed in water (c) dispersed in hexane (d) dispersed in DMSO (e) dispersed in DMSO – magnified view (f) dispersed in 50/50 (w/w) blend of DMSO and water

Table 4.2: Frame-by-frame analysis of Figure 4.4.

Image	Analysis
4.4a	In this image we can see that the as received material is highly polydisperse with particle agglomerates ranging from ~1μm to hundreds of microns in diameter.
4.4b	After dispersing in water and drying we can no longer see the presence of clay at a moderate magnification. This observation agrees with the literature. It is known that after exfoliating, nanoclays will not re-form into stacks. Rather, the platelets will dry into a film-like morphology. If we were to use a very high resolution we would see that the morphology would be likened to the scales of a snake.
4.4c	Without further discussion, one would think that hexane provides good exfoliation based on the image here; on the contrary. In this image the white spots represent clay agglomerates that are sufficiently small such that buoyant forces kept them present in the sample head space. Most of the clays precipitated during dispersion.
4.4d	We identified during the swelling study that DMSO has a good affinity for Laponite® RD. However, in this image we see that the clays are still highly agglomerated form.
4.4e	Magnification of 4.4d provides further evidence that the clays are not exfoliated.
4.4f	A blend of DMSO and water was used (50/50 by weight fraction) to disperse the nanoclays. Results were very positive as evidenced by the lack of large agglomerates. In fact, we see a similar morphology as that of 4.4b – which is the best case scenario.

4.2.1.3 Effects of Co-Solvent Ratios on Nanoclay Exfoliation

It has been clearly demonstrated that an aqueous solvent system is necessary for the exfoliation of Laponite® RD. However, we have not identified the optimum ratio of solvents. To prevent polymer phase separation in the dope we must carefully consider the quantity of water used during the exfoliation process. Simultaneously, we must create an exfoliated state of nanoclays in solution. In Chapter 3 we suggested that a tertiary phase boundary exists that can satisfy both of these conditions. It is our intent to consider this trade-off and identify an aqueous blend that will meet the constraints.

Laponite® RD will readily form a gel if the solution conditions are right (i.e. higher clay concentrations, solution pH).[20] We can use this phenomenon to our advantage to gain insight into the degree of exfoliation. Measuring the development of the storage (G') and loss (G") moduli as a function of time, can provide information regarding the evolution of gel strength when a constant oscillatory amplitude and angular frequency are applied.[21,22] For this study we measured the storage modulus of four samples containing equal quantities of clay but with different ratios of solvent. Measurements were made

using the cone-and-plate configuration in the rheometer (see Chapter 3 for more details). Immediately after loading a sample, a constant shear of 1000 s^{-1} was applied for 60 seconds. This was done to break down any history dependent structure formation.[22] After pre-shearing, the oscillatory strain amplitude was set very low (γ_o = 0.1) to ensure that minimal deformation was applied to the solution. Higher amplitudes could prevent the formation of low strength gels in the test cell. A standard angular frequency ($\omega = 2\pi$ rad/s) was used during this portion of the measurement.[22] Results of this study are shown in Figures 4.5 and 4.6.

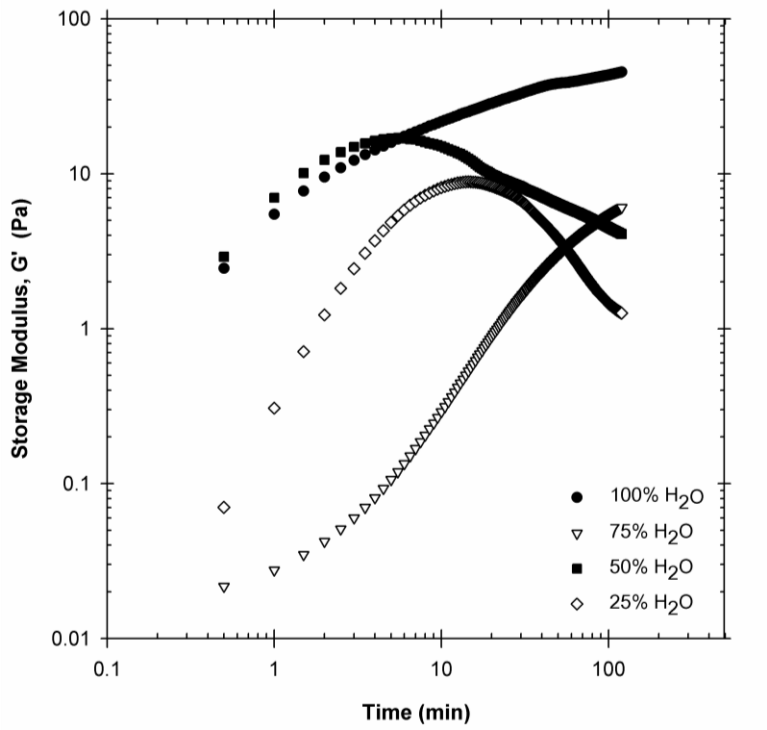

Figure 4.5: Developing storage modulus (G') as function of time for suspensions of 1% (w/v) Laponite® RD in DMSO and water blends. Legend indicates mass fraction of water in the solvent phase (mass of clays excluded). γ_o = 0.1; $\omega = 2\pi$ s^{-1}

We consider the pure water sample to be the "best case scenario" because it is well known that the clays fully exfoliate in this environment. The storage modulus at t~0min and the trajectory indicates that the gel structure begins to form quickly after perturbation

and continues to form (as evidenced by the increasing G') on long time length scales. If the measurement was allowed to continue for many hours (or even days) a maxima in the curve may appear. Our second sample (75% H_2O) shows a similar trend, but with a lower beginning modulus. It is probable that if the measurement continued that a maximum would appear, but at a lower value than the pure water case. To produce a membrane solution, though, the water content should be lower to ensure complete dissolution of the polymer in the final solution. The third and fourth samples in this study correspond to a water content of 50% and 25% respectively. Storage modulus trends indicate that both of these sample of maxima under these operating conditions. Comparing these maxima, we see that 50% water produces an altered state of exfoliation – as expected. It can be assumed that samples containing between 50% and 75% water will exhibit a transition in the trajectory patterns.

An alternative evaluation of these data is shown in Figure 4.6 wherein we have plotted both modulii (G' and G") for each co-solvent system. From these plots were sought to identify the initial and secondary (where applicable) cross-over times for the two moduli. According to Winter and Chambon, the point of gelation (GP) occurs at the initial time when G'=G".[23,24] Identifying the GP provides information regarding the history dependence. The second cross-over, on the other hand, indicates that the gel structure is not stable and begins to collapse. For the reader's reference, Laponite® RD and other hydrophilic clays are known to form a *house of cards* structure based largely on electrostatic interactions, which lends to the formation of a gel.[12,25]

In the first plot where pure water was used to suspend the nanoclay we do not see the initial crossover, which indicates that the gelation is fast (<<1min). Moreover, there is no apparent secondary intersection in the measured time frame, suggesting that the gel is sufficiently stable. When water content is reduced to 75%, the GP occurs much later (~20min), but there does not appear to be a second cross-over in this time frame either. Once the quantity of water is decreased to 50%, we see that the GP also decreases (<1min). More importantly though, there is an observed secondary cross-over (~10min).

Similar phenomena appear in the sample containing only 25v% water wherein there are two intersections of the elastic and viscous moduli (~1min and 20min). If our objective was to form a stable gel, we know that the less aqueous co-solvent is not suitable. Fortunately, we are trying to prevent gel formation while creating an exfoliated system.
So what is the take-home message from these data? Both plots (Figures 4.5 and 4.6) provide evidence indicating that there is a finite working time before the onset of gelation and that the gel structure is not stable when the amount of water in the co-solvent is reduced. This is important for processing and dope development wherein there are several mixing steps throughout. If an exfoliated system is left to rest for extended periods we would see the onset of gelation, which means that the system would require additional mixing to destroy the gel structure. The lack of gel stability in some samples, however, suggests that the gel structure can be destroyed via rigorous mixing; this is favorable for the next step.

There are opportunities to conduct additional studies related to solvent systems to further elucidate co-solvent interactions and their affects on exfoliation. However, this is outside the scope of this project. Thus, noting the results that were obtained, it was decided that for the scope and objectives of this project that the 50/50 blend would be a suitable choice because it shows evidence of sufficient exfoliation and promoted polymer dissolution in the later stages of solution development.

As a complementary technique to these rheological measurements we did consider small angle x-ray scattering (SAXS). Many authors in the literature quantify exfoliation in these systems using SAXS.[25-28] Correlations exist for platelet materials that relate the slope of SAXS data to the degree of exfoliation. These capabilities are not available at Georgia Tech. Preliminary measurements were conducted by researchers at the University of Minnesota. Unfortunately the resolution of data did not yield any conclusive findings.

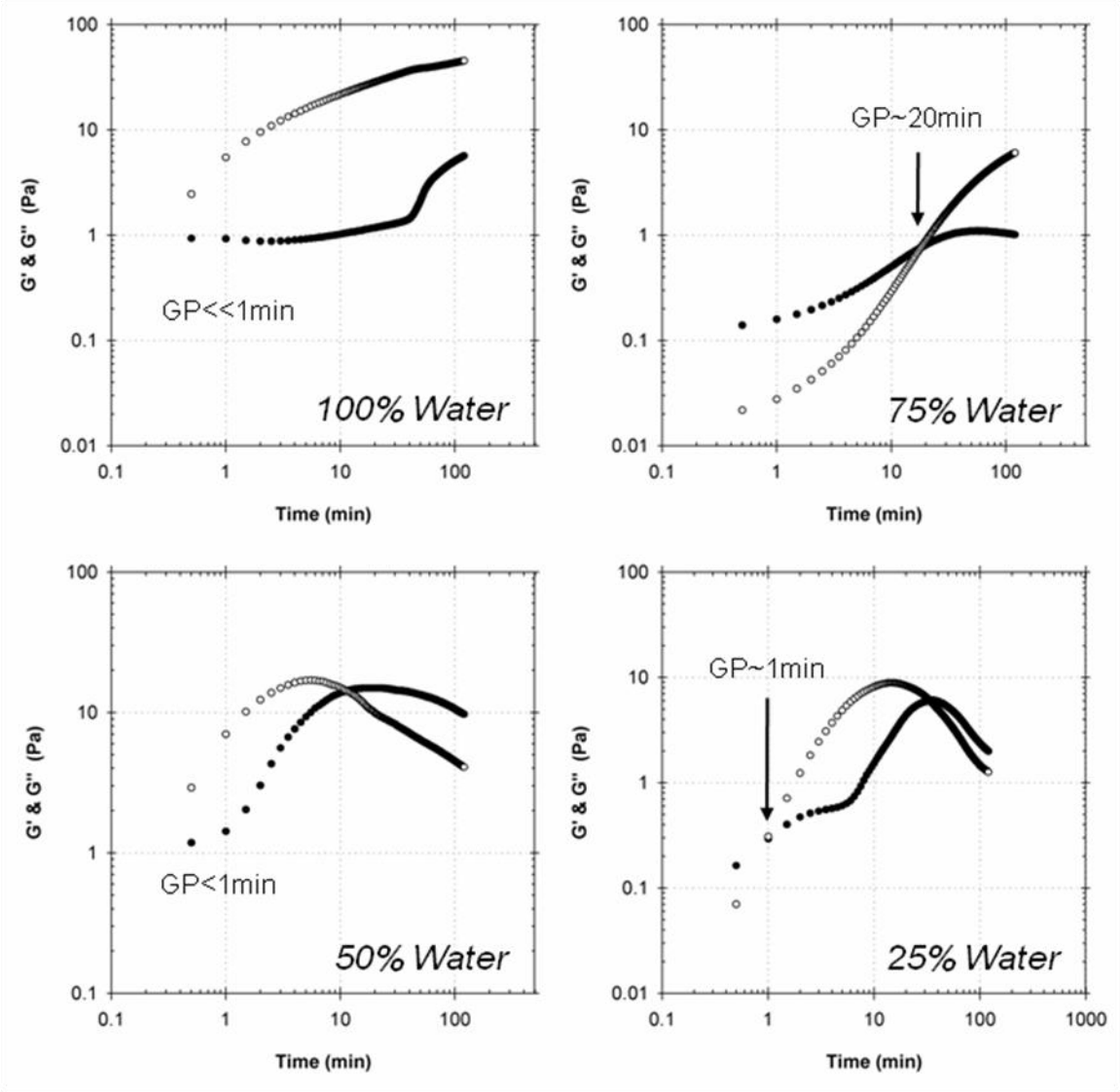

Figure 4.6: Storage (G'=○) and loss (G"=●) moduli for suspensions of 1% (w/v) Laponite® RD in DMSO and water blends. The gel point (GP) and equivalent time (min) for each system is indicated on each plot. $\gamma_o = 0.1$; $\omega = 2\pi\ s^{-1}$

4.2.2 Comparison of Dispersion Methods

It has been duly noted that there are a variety methods capable of creating a suspension of particles in solution. In this section we will investigate the efficacy of several different methods in the preparation of polymer-nanoclay solutions for membrane formation. Rheological measurements are a very useful tool for quantifying and comparing the

different processes. Moreover, rheology studies may serve as a preliminary verification that can be completed prior to membrane formation and permeation testing.

A series of protocols utilizing three different dispersion methods were applied in this investigation. We have highlighted the steps involved for the three approaches in Figure 4.7 below. (Note: An in-depth explanation of Method 3 was provided in Chapter 3.) Method 1 in this scheme represents the "traditional" solution preparation procedure for hollow fiber spinning. In this case mixing is predominately driven by shear thinning inside the mixing vessel at the walls as it slowly rotates; we have denoted this as low shear mixing. The second method is based on sonication techniques wherein the suspension of clays and solvent was placed in a sonication bath for 24 hours. High power sonication tools are available, but were not explored in this study for the sake of brevity. Also, it should be noted that the components in Step 1 for Methods 2 and 3 are equivalent to the combination of Steps 1 and 2 for Method 3. The product from Step 1 in Method 3 yields a gel material if it is allowed to rest. High shear mixing provides sufficient mechanical energy to homogenize and thin this material. On the other hand, we observed that sonication does not provide the same mechanical energy and therefore is not sufficient for the homogenization of the product. Hence, we combined all of the solvents and clay for the dispersion stage in Method 2. These processes were repeated for both polymers of interest – Cellulose Acetate and Torlon® - to verify expandability. All solutions were created under the assumption that they could be used to produce a hybrid membrane with 5wt% nanoclay loading in a polymer matrix. The mass fractions for polymer, clay, NMP, DMSO and water were 9.5%, 0.5%, 80%, 5% and 5% respectively.

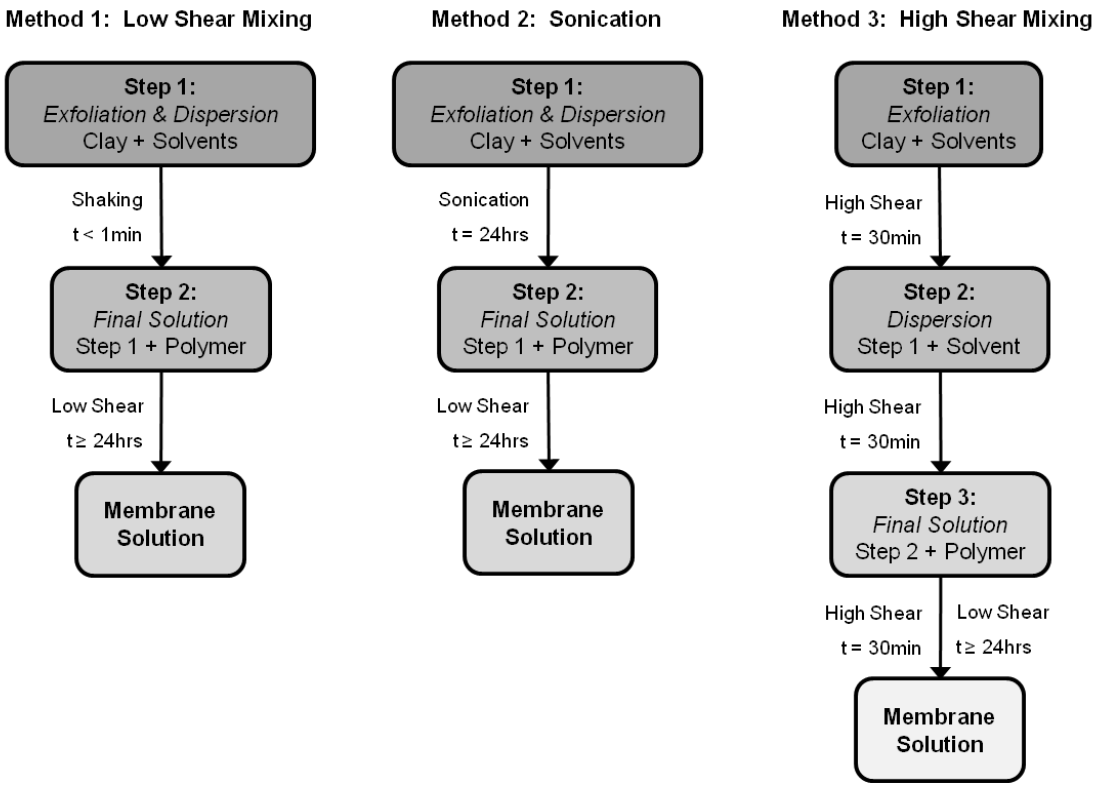

Figure 4.7: Flowchart illustrating steps in the three mixing and dispersion processes used in this work. (1) low shear mixing (2) sonication bath mixing (3) high shear mixing

The viscosity of each test solution was measured as a function of shear rate in a CC10 Couette measurement cell (details provided in Chapter 3). Results for the cellulose acetate and Torlon® hybrid solutions are illustrated in Figures 4.8 and 4.9 respectively. Recall in Chapter 2 that we explained that a tactoid, although larger than a single platelet, has a smaller effective volume than the sum of its constituent platelets. In other words, five individual, freely rotating platelets has five times the effective volume of five stacked platelets. We see in both cases that the solutions produced using high shear mixing have a significantly higher viscosity when measured at low shear rates. This is indicative of a higher effective volume of dispersed rigid particles.[29] In the cellulose acetate samples we see that sonication increased the viscosity more than low shear mixing. The Torlon® samples, on the other hand, do not show conclusive evidence that sonication is better than low shear mixing.

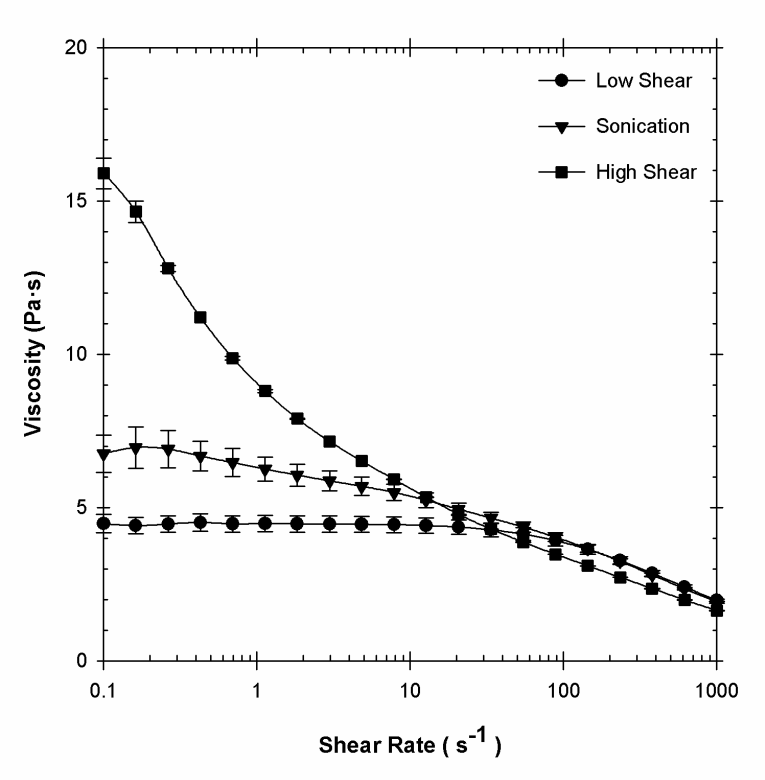

Figure 4.8: Comparison of mixing methods for hybrid solutions containing Laponite® RD in a solution Cellulose Acetate and solvent. Symbols represent average values. All solutions contain 9.5wt% polymer and 0.5wt% nanoclay.

Viscosity measurements for both systems clearly indicate that the high shear mixing process developed in this work is most effective method for producing hybrid solutions with the highest degree of exfoliation. This is apparent in our measurements because the viscosity of "high shear" samples is significantly higher than the other preparation methods. The sharp decrease in viscosity, as a function of shear rate, provides additional evidence that the exfoliation process is effective because this trend corresponds with theories for solutions containing platelet dispersants. (See Chapter 2 for additional explanation.) These measurements verify the efficacy of the mixing procedure, but permeation tests are necessary to truly confirm the validity of this process.

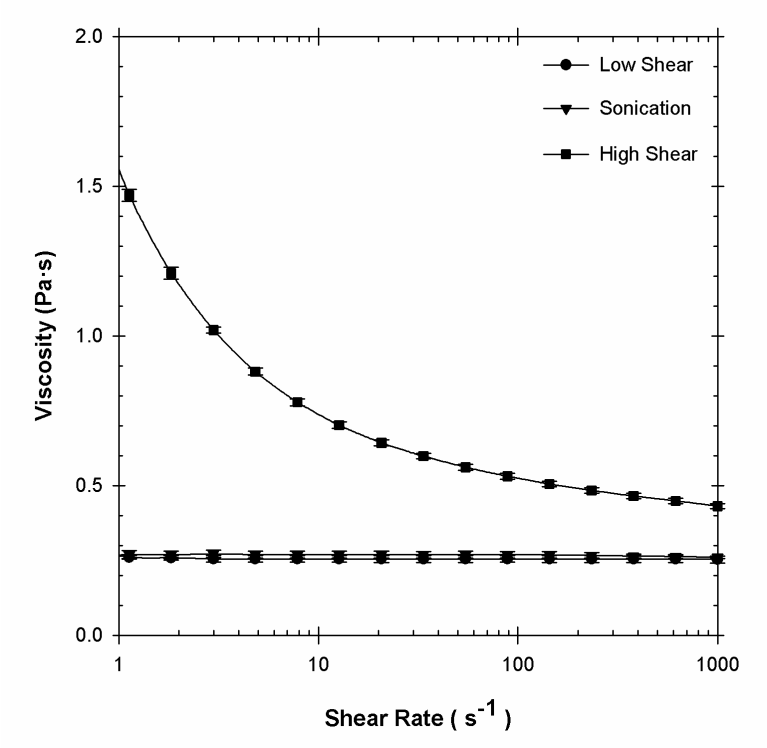

Figure 4.9: Comparison of mixing methods for hybrid solutions containing Laponite® RD in a solution of Torlon® and solvent. Symbols represent average values. All solutions contain 9.5wt% polymer and 0.5wt% nanoclay.

4.3 Effect of Nanoclay Content on Hybrid Solution Rheology

In the previous section we showed experimental results wherein we used solution viscosity to analyze and validate the efficacy of different dispersion methods. Similar measurements may be used to characterize and compare solutions comprised of different inorganic filler content. This information serves two primary purposes: (1) validate that the determined exfoliation/dispersion method is applicable to different nanoclay loadings and (2) probe the microscopic structural influences with respect to nanoclay content in the solution. The measurements and analyses were repeated for both polymers of interest (cellulose acetate and Torlon®).

For the membrane portion of this work we made hybrid membranes containing 1, 3 and 5wt% Laponite® RD in a polymer matrix. The clay content in the casting solutions was

significantly lower due to the presence of solvent. To study the influence of clay content on solution viscosity we prepared casting solutions that would correlate to those used for membrane formation. Additionally, we prepared the same solutions without clay. These latter solutions were used to determine the solvent (suspending media) viscosity (η_s) in order to calculate the relative viscosity ($\eta_r = \eta/\eta_s$) for each sample. Reporting relative viscosity normalizes any discrepancies due to solvent effects for more accurate comparison. Component ratios for each hybrid sample are shown in Tables 4.3 and 4.4 in terms of mass and volume fractions for convenience. We should note that the volume fractions were calculated based on the reported independent densities for each component, as previously reported in Chapter 3.

Table 4.3: Component breakdown of Torlon® test solutions in terms of ϕ_{mass} and ϕ_{volume}

Component	1wt% Membrane		3wt% Membrane		5wt% Membrane	
	ϕ_{mass}	ϕ_{volume}	ϕ_{mass}	ϕ_{volume}	ϕ_{mass}	ϕ_{volume}
Torlon®	9.9%	7.6%	9.7%	7.4%	9.5%	7.3%
Laponite® RD	0.1	0.04	0.3	0.13	0.5	0.21
NMP	80.0	82.2	80.0	82.2	80.0	82.2
DMSO	5.0	4.8	5.0	4.8	5.0	4.8
Water	5.0	5.3	5.0	5.3	5.0	5.3

Table 4.4: Component breakdown of Cellulose Acetate test solutions in terms of ϕ_{mass} and ϕ_{volume}

Component	1wt% Membrane		3wt% Membrane		5wt% Membrane	
	ϕ_{mass}	ϕ_{volume}	ϕ_{mass}	ϕ_{volume}	ϕ_{mass}	ϕ_{volume}
Cellulose Acetate	9.9%	8.0%	9.7%	7.8%	9.5%	7.7%
Laponite® RD	0.1	0.04	0.3	0.13	0.5	0.21
NMP	80.0	81.9	80.0	81.9	80.0	81.9
DMSO	5.0	4.8	5.0	4.8	5.0	4.8
Water	5.0	5.3	5.0	5.3	5.0	5.3

Specific details regarding the calculation of relative viscosity and the reported error bars are provided in Appendix C. The plots presented in the following sections do not include hysteresis data. These measurements were made but it was found that data trends did not contribute to the discussions below. We have included complete plots for all of the following measurements in Appendix C for reference.

4.3.1 Torlon®–Laponite® RD Hybrid Solutions for Membrane Formation

The relative viscosities for Torlon®-Laponite® RD hybrid dopes are presented in Figure 4.11 as a function of shear rate. Additionally, the relative viscosity values for each solution at low and high shear rates (1.13 and 1000 s^{-1}) are plotted as a function of volume fraction (%) of clay in the solution in Figure 4.12. It should be noted that viscosity values corresponding to shear rates below 1 s^{-1} are not shown in these figures because of sensitivity limitations in the equipment.

At low shear rates the relative viscosity values in these samples exhibit behavior in good agreement with the theory of suspensions containing rigid particles.[29] We see an increase in viscosity as a function of filler loading: an increase of ~80% between the 1wt% and 3wt% samples and ~400% increase between the 1wt% and 5wt% samples. As the shear rate is increased we see a sharp decline in the viscosity which is attributed to orientation of the platelets.[29] (Recall that normalization of the solvent (η_s) has removed most of the polymer shear thinning effects from this analysis.) As expected, the 1wt% solution does not exhibit as strong a trend. We can attribute this characteristic to the very low quantity of platelets in the solution (0.04v%).

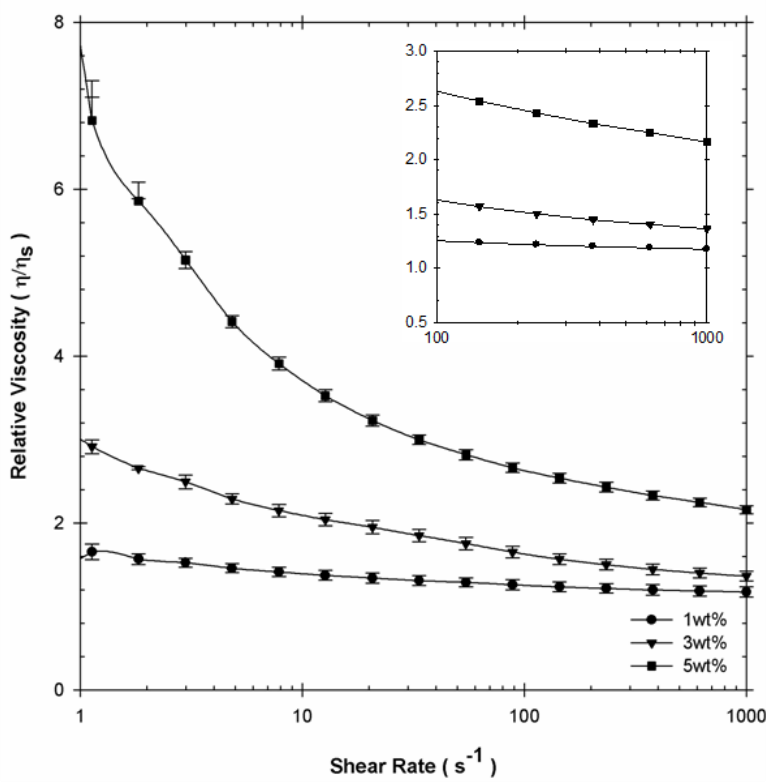

Figure 4.11: Relative viscosity of hybrid solutions containing Laponite® RD in a solution of Torlon® and solvent. Symbols represent average values. Legend nomenclature corresponds to the effective weight fraction of nanoclay in the hypothetical membrane after formation. *Figure inset displays a magnified view of the relative viscosities at higher shear rates.*

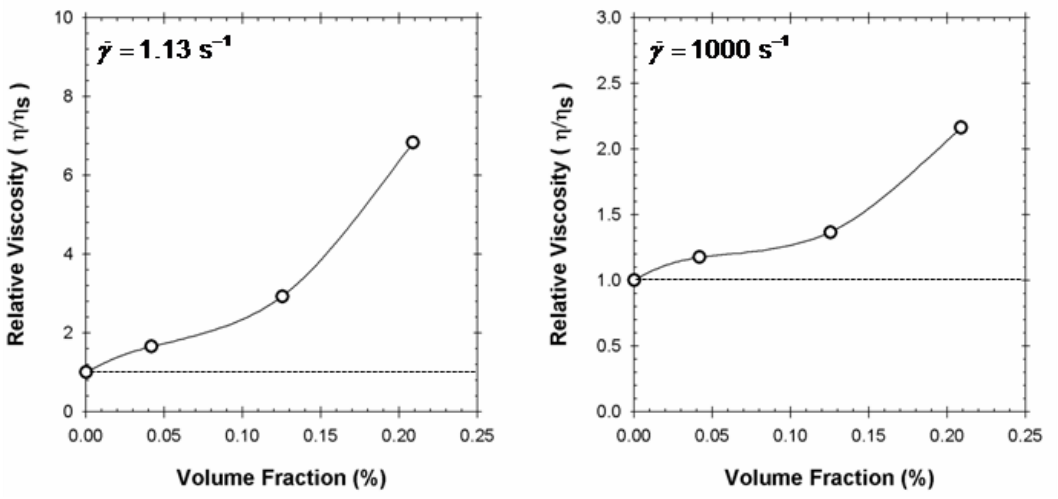

Figure 4.12: Relative viscosity for hybrid solutions containing Laponite® RD in a solution Torlon® and solvent presented as a function of volume fraction (%) of nanoclay in the measured solution. Plot 1 corresponds to the relative viscosity measured at shear rate of 0.1 s^{-1} and Plot 2 corresponds to relative viscosity measured at a shear rate of 1000 s^{-1}. Symbols represent average values.

4.3.2 Cellulose Acetate–Laponite® RD Hybrid Solutions for Membrane Formation

The previous samples containing Torlon® behaved according to accepted theory for solutions containing platelets. These measurements were repeated for samples containing cellulose acetate. Relative viscosities data for cellulose acetate-Laponite® RD hybrid dopes are presented in Figure 4.13 as a function of shear rate. Additionally, relative viscosities for each solution at low and high shear rates (0.1 and 1000 s^{-1}) are plotted as a function of volume fraction (%) of clay in the solution in Figure 4.14.

It was observed in Section 4.2.1 that increasing volume fractions of clay content solution equated to increases in relative viscosity. The same observations can made for the cellulose acetate hybrid solutions. In fact, we see very similar growth as function of weight fraction in the solution. Complementing results as such indicate that the mixing technique does translate well to other polymers and more importantly that the degree of exfoliation is similar. However, when we consider the relative viscosities at high shear rates (1000 s^{-1}) an interesting phenomenon appears for the 5wt% sample.

According to theory, the addition of rigid particles to a solution should increase the viscosity; therefore the relative viscosity cannot be less than one.[29] However, we see that the dope viscosity at high shear rates is below the limit. For this to be true, the bulk phase viscosity (η_s) is no longer the same between the hybrid and control dopes. One explanation for this phenomenon is bulk phase polymer depletion.[30] This indicates that the attractive forces between the polymer and clay are quite strong. We proposed various mechanisms in Chapter 3 that suggest cellulose acetate should be attracted to the electronegative surface of the clays. Evidence of polymer depletion coincides with the proposed absorptivity of polymer to clay.

To further convince the reader that this phenomenon is real – and not just an artifact of confidence limits – we have plotted the viscosity of the pure polymer solutions (which called the solvent earlier) in Figure 4.15. From these data we see that small changes

(0.2%) in the polymer concentration have a noticeable effect on the overall viscosity. As such, the data lends credibility to the hypothesis that bulk phase polymer is depleting in our hybrid dope containing 5wt% clay.

The data presented in this study show very credible evidence that cellulose acetate has a high affinity for the nanoclay surface without the addition of functional groups or grafting agents. Unfortunately this observation is only visible in one sample, at high clay loading. We suspect that the particle volume fraction in the other samples (1wt% and 3wt%) is too low to see the same depletion effects. Additional measurements on samples containing lower solids (polymer plus clay) concentrations may provide further insight into this phenomenon.

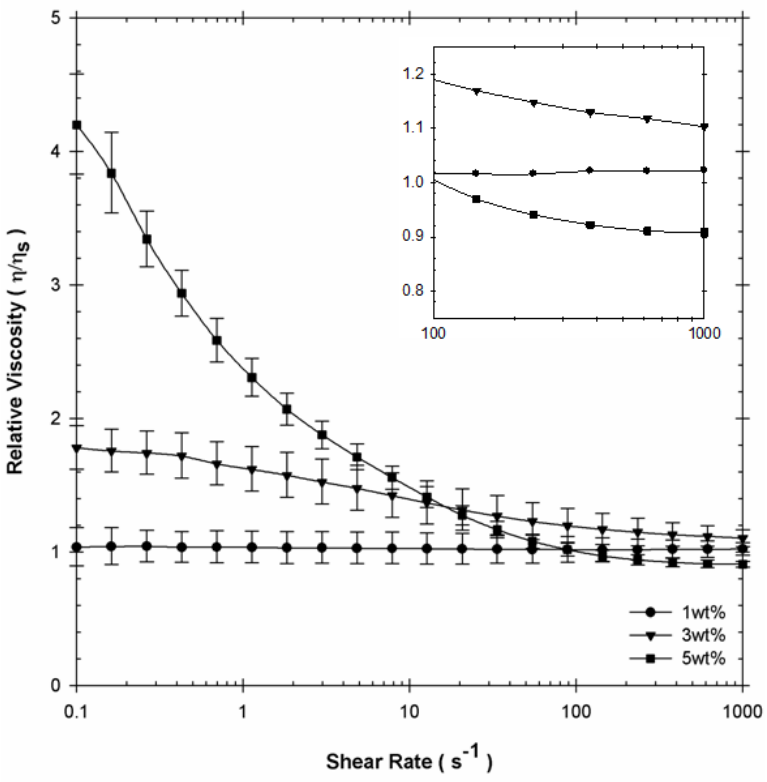

Figure 4.13: Relative viscosity of hybrid solutions containing Laponite® RD in a solution of Cellulose Acetate and solvent. Symbols represent average values. Legend nomenclature corresponds to the effective weight fraction of nanoclay in the hypothetical membrane after formation. *Figure inset displays a magnified view of the relative viscosities at higher shear rates.*

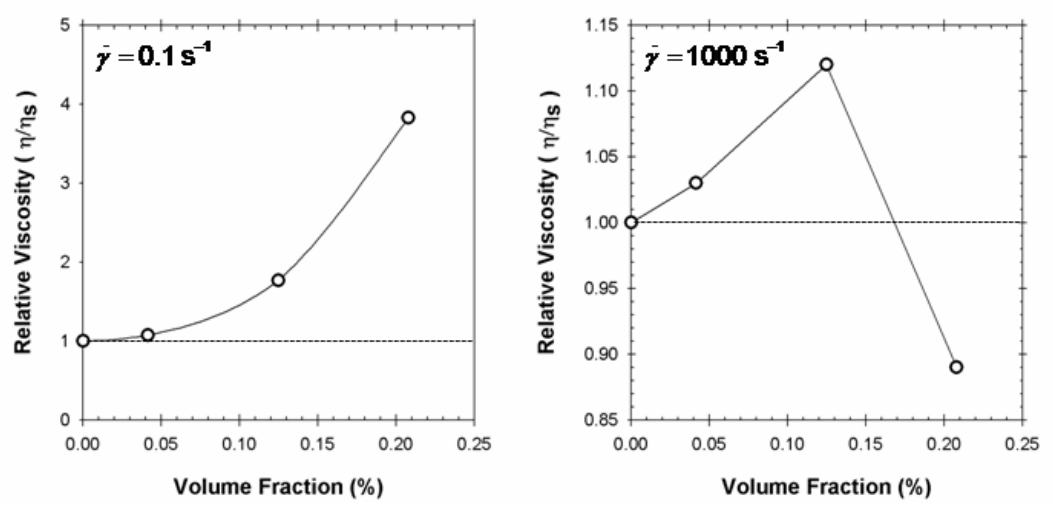

Figure 4.14: Relative viscosity for hybrid solutions containing Laponite® RD in a solution Cellulose Acetate and solvent presented as a function of volume fraction (%) of nanoclay in the measured solution. Plot 1 corresponds to the relative viscosity measured at shear rate of 0.1 s-1 and Plot 2 corresponds to relative viscosity measured at a shear rate of 1000 s-1. Symbols represent average values**.**

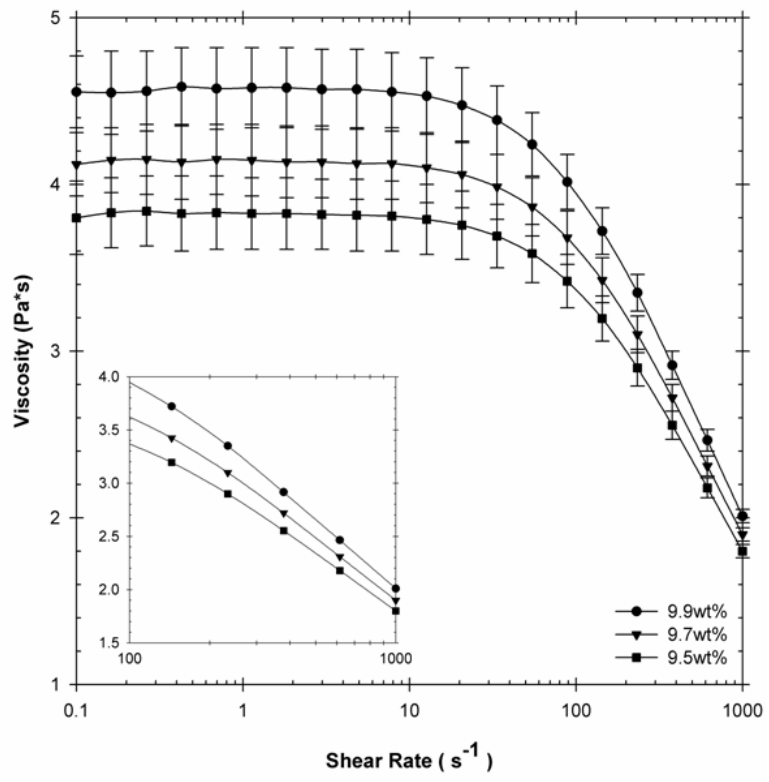

Figure 4.15: Viscosity of Cellulose Acetate polymer solutions with varying mass fraction in solvent. Symbols represent average values. *Figure inset displays a magnified view of the relative viscosities at higher shear rates.*

4.4 Summary & Conclusions

Throughout this chapter we have sought to prove the efficacy of high shear mixing versus other methods. Moreover, we have also explored organic solvents and aqueous blends and their effects on nanoclay exfoliation – specifically Laponite® RD. From the results presented it can be stated with confidence that the exfoliation and dispersion technique developed in our work meets the objective. Rheological measurements provide evidence that the mixing procedure creates a hybrid solution with well exfoliated nanoclays as evidenced by the significant increases in viscosity even at low loadings of nanoclay in solution.

It is important to verify that the proposed membrane solutions will in fact yield membranes with desirable properties. In Section 4.2.1 we provided evidence that suggests that cellulose acetate has a strong affinity for the clay surface via bulk density depletion of the polymer leading to a decrease in the relative viscosity at high shear rates. The same study completed on Torlon® based samples, however, did not yield the same conclusion. Gas permeation tests are necessary to provide further evidence of polymer-clay affinity. If permselectivity results meet the expected values for pure polymer membranes then we can further validate the conclusions from this chapter.

4.4.1 A First Glimpse at Hybrid Membranes

To give the reader an idea of what is to come, we would like to provide a brief look into permeation results obtained for a membrane prepared using the high shear mixing method. These results are compared to permeation results for a membrane that was prepared early in this work using a low shear method. The results are presented in Table 4.5. Ideally, the normalized permeabilities for a hybrid membrane containing a barrier material should yield values less than one. This trend is observed in the membrane prepared using high shear mixing, but not in the membrane prepared using low shear mixing. In the latter case we see significant increases in permeability, which is due to poor dispersion and exfoliation. The presence of large agglomerates produces

increased, non-selective molecular transport through interstitial spaces that are not filled with polymer. [11,31]

Table 4.5: Comparison of normalized permeability (P/P_0) and selectivity (α/α_0) results for Cellulose Acetate hybrid membranes containing 5wt% Laponite® RD nanoclay filler prepared using low shear and high shear mixing methods. P_{feed} = 100psia, T_{test} = 35ºC

	P/P_0 – Oxygen	P/P_0 – Nitrogen	α/α_0 – O_2/N_2
Low Shear	1.64	1.69	0.97
High Shear	0.77	0.75	1.03

Photographic evidence provides further confirmation that the membrane prepared using low shear methods contains visibly large agglomerates. Figure 4.16 shows a comparative perspective in the optical transparency between the two films with respect to a common background. It is expected that a hybrid film containing low mass fractions of Laponite® RD should yield a highly transparent film because the diameter of a single clay particle (d~30nm) is significantly lower than the wavelength of visible light (380-760nm). The high shear prepared membrane produces a transparent image whereas the other membrane produces an opaque picture. Albeit not conclusive, visual inspection for optical transparency – in both the membrane solution and the membrane itself – can serve as a preliminary analysis to predict the efficacy of a hybrid system containing nanoparticles in low concentrations.[1]

Figure 4.16: Photographs of hybrid membranes produced using low and high shear mixing methods. Optical transparency of each film is compared with a common background**.**

4.5 References

1. T. Pinnavaia and G. Beall (eds), *Polymer-Clay Nanocomposites*. (John Wiley & Sons, Inc., New York, NY, 2000).

2. D.R. Paul and L.M. Robeson, "Polymer Nanotechnology: Nanocomposites," *Polymer* **49** (15), 3187-3204 (2008).

3. J. Liu, T-H. Bae, W. Qiu, S. Husain, S. Nair, C. Jones, R. Chance, and W.J. Koros, "Butane Isomer Transport Properties of 6FDA-DAM and MFI-6FDA-DAM Mixed Matrix Membranes," *Journal of Membrane Science* **343** (1-2), 157-163 (2009).

4. L. Y. Jiang, T. S. Chung, and S. Kulprathipanja, "Fabrication of mixed matrix hollow fibers with intimate polymer-zeolite interface for gas separation," *Aiche Journal* **52** (8), 2898-2908 (2006).

5. S. Husain and W. J. Koros, "Mixed Matrix Hollow Fiber Membranes Made with Modified HSSZ-13 Zeolite in Polyetherimide Polymer Matrix for Gas Separation," *Journal of Membrane Science* **288** (1-2), 195-207 (2007).

6. E. S. H. Leach, A. Hopkinson, K. Franklin, and J. S. van Duijneveldt, "Nonaqueous Suspensions of Laponite and Montmorillonite," *Langmuir* **21** (9), 3821-3830 (2005).

7. S. Liff, N. Kumar, and G. McKinley, "High-Performance Elastomeric Nanocomposites Via Solvent-Exchange Processing," *Nature Materials* **6**, 76-83 (2007).

8. M. McAlpine, N. Hudson, J. Liggat, R. Pethrick, D. Pugh, and I. Rhoney, "Study of the Factors Influencing the Exfoliation of an Organically Modified Montmorillonite in Methyl Methacrylate/Poly(Methyl Methacrylate) Mixtures," *Journal of Applied Polymer Science* **99** (5), 2614-2626 (2006).

9. I. Rhoney, S. Brown, N. Hudson, and R. Pethrick, "Influence of Processing Method on the Exfoliation Process for Organically Modified Clay Systems I. Polyurethanes," *Journal of Applied Polymer Science* **91** (2), 1335-1343 (2004).

10. D. Burgentzle, J. Duchet, J. Gerard, A. Jupin, and B. Fillon, "Solvent-based Nanocomposite Coatings I. Dispersion of Organophillic Montmorillonite in Organic Solvents," *Journal of Colloid and Interface Science* **278** (1), 26-39 (2004).

11. A. Manninen, H. Naguib, A. Nawaby, and M. Day, "CO_2 Sorption and Diffusion in Polymethyl Methacrylate-Clay Nanocomposites," *Polymer Engineering and Science* **45** (7), 904-914 (2005).

12. H. van Olphen, *An Introduction to Clay Colloid Chemistry*. (John Wiley & Sons, Inc., New York, NY, 1977), 2nd ed.

13. S. Tunc and O. Duman, "Preparation and Characterization of Biodegradeable Methyl Cellulose/Montmorillonite Nanocomposite Films," *Applied Clay Science* **48** (3), 414-424 (2010).

14. J. Park, H. Lee, D. Chae, W. Oh, J. Yeh, Y. Deng, and J. Yeum, "Electrospinning and Characterization of Poly(vinyl alcohol)/Chitosan Oligosaccharide/Clay Nanocomposite Nanofibers in Aqueous Solutions," *Colloid and Polymer Science* **287** (8), 943-950 (2009).

15. J. Chang, T. Jang, K. Ihn, and G. Sur, "Poly(vinyl alcohol) Nanocomposites with Different Clays: Pristine Clays and Organoclays," *Journal of Applied Polymer Science* **90** (12), 3208-3214 (2003).

16. S. Olejnik, Posner, A., Quirk, J., "Swelling of Montmorillonite in Polar Organic Liquids," *Clays and Clay Minerals* **22**, 361-365 (1974).

17. National Institute of Health, "http://pubchem.ncbi.nlm.nih.gov/".

18. S. Olejnik, A. Posner, and J. Quirk, "Swelling of Montmorillonite in Polar Organic Liquids," *Clays and Clay Minerals* **22**, 361-365 (1974).

19. A. Barton, *Handbook of Solubility Parameters and Other Cohesion Parameters*. (CRC Press, Inc., Boca Raton, FL, 1983).

20. Southern Clay Products, "http://www.laponite.com"

21. J. Meng, X. Hu, F. Boey, and L. Lin, "Effect of Layered Nano-Organosilicate on the Gel Point Rheology of bismaleimide/diallylbisphenol A Resin," *Polymer* **46** (8), 2766-2776 (2005).

22. N. Willenbacher, "Unusual Thixotropic Properties of Aqueous Dispersions of Laponite RD," *Journal of Colloid and Interface Science* **182**, 501-510 (1996).

23. H. Winter, "Soft Polymeric Materials Near the Transition from Liquid to Solid State," *Korea-Australia Rheology Journal* **11** (4), 275-278 (1999).

24. H. Winter and F. Chambon, "Analysis of Linear Viscoelasticity of a Crosslinking Polymer at the Gel Point," *Journal of Rheology* **30** (2), 367-382 (1986).

25. M. Kroon, "Structure and Formation of a Gel of Colloidal Disks," *PhD Dissertation*, Universiteit van Amsterdam, 1998.

26. F. Pignon, A. Magnin, J-M. Piau, B. Cabane, P. Lindner, and O. Diat, "Yield Stress Thixotropic Clay Suspensions: Investigations of Structure by Light, Neutron, and X-Ray Scattering," *Physical Review E* **56** (3), 3281-3289 (1997).

27. C. Pizzey, S. Klein, E. Leach, J. van Duijneveldt, and R. Richardson, "Suspensions of Colloidal Plates in a Nematic Liquid Crystal: A Small Angle X-Ray Scattering Study," *Journal of Physics - Condensed Matter* **16** (15), 2479-2495 (2004).

28. L. Zhang, C. Jahns, B. Hsiao, and B. Chu, "Synchrotron SAXS/WAXD and Rheological Studies of Clay Suspensions in Silicone Fluid," *Journal of Colloid and Interface Science* **266** (2), 339-345 (2003).

29. C. Macosko, *Rheology Principles, Measurements, and Applications*. (Wiley-VCH, Inc., New York, NY, 1994).

30. E. Goddard and B. Vincent (eds), *Polymer Adsorption and Dispersion Stability*. (Amercian Chemical Society, Washington, D.C., 1984).

31. G. Choudalakis, A. Gotsis, "Permeability of Polymer/Clay Nanocomposites: A Review," *European Polymer Journal* **45** (4), 967-984 (2009).

CHAPTER 5

TORLON®-LAPONITE® RD HYBRID DENSE FILM MEMBRANES

5.1 Overview

In Chapter 3, we highlighted the benefits and motivation for using Torlon® polyamide-imide as the organic phase in a hybrid membrane material. In this chapter it is our intent to show the successes in the formation of Torlon®-Laponite® RD hybrid dense film membranes. Permeability studies show that all of the hybrid membranes exhibited permeability reductions – as expected. These permeation properties are complemented by microscopic characterization to prove the efficacy of the preparation techniques. Additionally, mathematical models were used to estimate the expected permeability properties of our hybrid films based on control membrane properties and other characteristic assumptions.

5.2 Characterization of Torlon® Dense Films: A Control Study

It is scientifically prudent of us to determine the base properties of a dense film that does not contain filler materials. This is especially important in the case of Torlon®. Previous studies have shown that Torlon® is highly prone to polar solvent retention.[1,2] The amide groups in the polymer backbone form strong hydrogen bonds with polar solvents (e.g., n-methyl-2-pyrrolidone, dimethyl sulfoxide, dimethyl acetamide, dimethyl formamide) which increase the difficulty in complete solvent removal using conventional techniques. However, as we described in previous chapters, highly polar solvents are necessary to effectively exfoliate and disperse the nanoclay materials.

For the scope of this work it was decided that residual solvent in the membranes would not be a showstopper. Our objective in this study was to prove (1) the efficacy of the exfoliation and dispersing procedure and (2) verify that Torlon® forms a proper interface with the nanoclay filler. By using the same preparation techniques for both the control and hybrid membranes it was assumed that any second order effects due to residual solvent on gas permeability would be negated.

Since the control films did not contain any filler materials, it was not necessary to use any additional microscopic techniques to study the nanoscale structure of the dense films.

5.2.1 Permeability of Control Membranes

Control films of pure polymer were made using the techniques highlighted in Chapters 3 & 4. Since there is no inorganic filler in these films, we bypassed the first two shear mixing steps. The prepared films showed sufficient mechanical properties (i.e., the crease test) with good optical clarity. Permeabilities and ideal selectivities are shown in Figure 5.1 as a function of test gas and feed pressure. These values are also summarized in Table 5.1 for convenience.

Table 5.1: Average Permeability (Barrers) & Selectivity values for Torlon® control film at different feed pressures.

Feed Gas	**Feed Pressure**		
	50 psia	*75 psia*	*100 psia*
Helium	3.58 ±0.23	3.48 ±0.29	3.46 ±0.28
Oxygen	0.132 ±0.013	0.127 ±0.012	0.124 ±0.013
Nitrogen	0.019 ±0.001	0.018 ±0.002	0.018 ±0.002
O_2/N_2 Selectivity	6.95 ±0.29	7.06 ±0.07	6.89 ±0.08

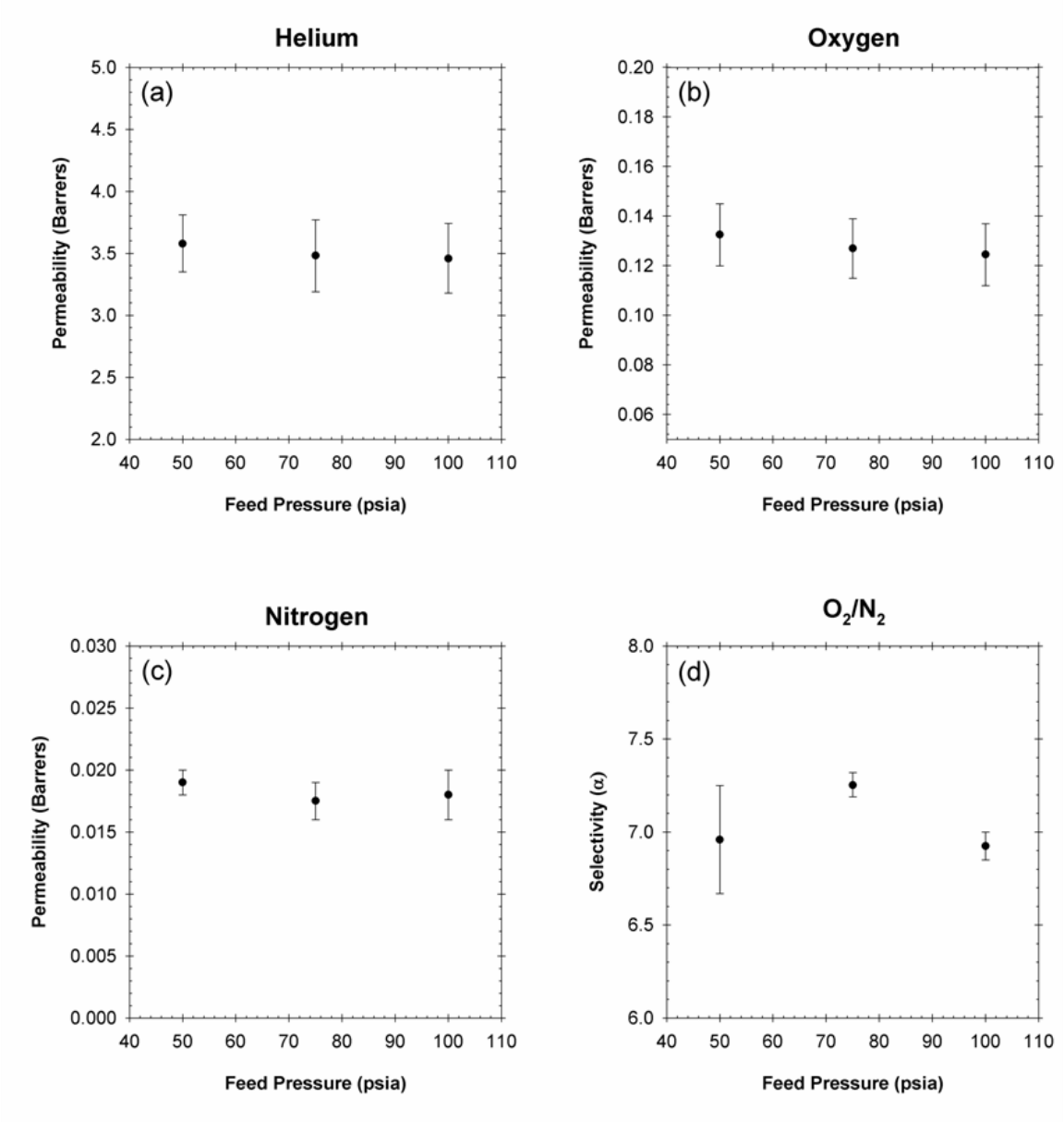

Figure 5.1: Permeability properties of Torlon® dense film membranes. (a) Helium (b) Oxygen (c) Nitrogen (d) O_2/N_2 Selectivity

Previous researchers in the Koros Group have found that Torlon® exhibits stronger sample-to-sample variations in transport properties than other common polymers; even when comparing membranes that were prepared nominally in the same fashion.[1,3] Therefore, we should stress that we rigorously kept the preparation protocol consistent for the control and hybrid films.

5.3 Characterization of Torlon®-Laponite® RD Dense Film Membranes Containing 1wt% Nanoclay

Transmission electron micrographs (TEM) show that the nanoclays are exfoliated, but do suffer from some agglomeration issues. Permeation tests showed further evidence that the nanoclays are exfoliated in the organic phase via non-negligible reductions in fluxes for the hybrid films.

5.3.1 Permeability of Hybrid Membranes Containing 1wt% Nanoclay

Following the protocol used to test the permeability of the Torlon® control film, we again measured the transport properties of several films in order to acquire an average curve for each test. The permeabilities of these films are represented in Figure 5.2 and summarized in Table 5.2 for convenience.

It was found that the hybrid films tested showed a permeability decrease for all of the gases tested. This is the first evidence to confirm our hypothesis that Torlon® is in fact compatible with unmodified Laponite® RD via the proposed bridge mechanism discussed earlier (see Figure 3.4).

If we consider the ratio of permeabilities P/P_0, wherein P is the permeability of the hybrid film and P_0 is the permeability of the pure polymer control film, we can see the evidence of successful exfoliation more clearly. In Table 5.3 we have compiled the P/P_0 and α/α_0 values based on the average permeabilities for the films tested. Trends in these will be discussed in greater detail in Section 5.5.

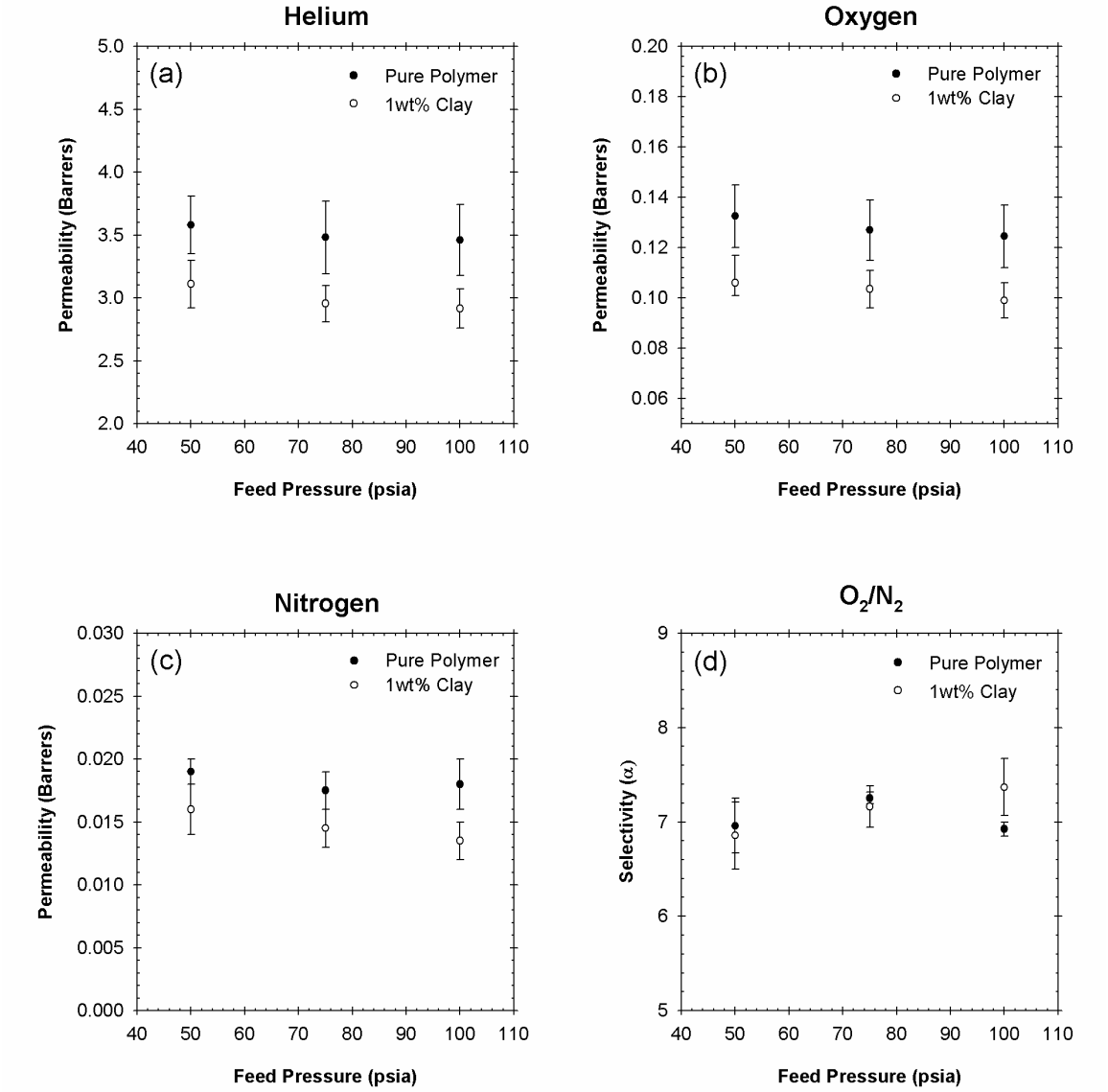

Figure 5.2: Permeability properties of Torlon®-Laponite® RD nanocomposite dense film membranes containing 1wt% nanoclay filler. (a) Helium (b) Oxygen (c) Nitrogen (d) O_2/N_2 Selectivity

Table 5.2: Average Permeability (Barrers) & Selectivity values for Torlon®-Laponite® RD nanocomposite films containing 1wt% nanoclay filler at different feed pressures.

Feed Gas	Feed Pressure		
	50 psia	*75 psia*	*100 psia*
Helium	3.11 ±0.19	2.95 ±0.15	2.91 ±0.16
Oxygen	0.106 ±0.011	0.103 ±0.007	0.099 ±0.007
Nitrogen	0.016 ±0.002	0.014 ±0.002	0.013 ±0.002
O_2/N_2 Selectivity	6.62 ±0.35	7.36 ±0.22	7.62 ±0.30

Table 5.3: Average P/P_0 and α/α_0 values for Torlon®-Laponite® RD nanocomposite films containing 1wt% nanoclay filler at different feed pressures.

Feed Gas	Feed Pressure		
	50 psia	*75 psia*	*100 psia*
Helium	0.87	0.85	0.84
Oxygen	0.80	0.82	0.80
Nitrogen	0.84	0.83	0.75
O_2/N_2 Selectivity	0.98	0.99	1.06

5.3.2 Microscopic Characterization of Hybrid Membranes Containing 1wt% Nanoclay

To obtain a visual perspective of these membranes, we used transmission electron microscopy to probe nanoclay exfoliation. Figures 5.3 and 5.4 represent two different areas of the membrane as observed by TEM. Each image provides evidence of exfoliation in the matrix and suggests that there are no major issues related to polymer-filler adhesion. These images correspond well to established conclusions in the literature that adhesion to such platelets is robust

In the first figure was can clearly see the nanoclay filler with respect to the polymer matrix based on the contrast (the nanoclays are the dark lines in the image).[4,5] If we carefully look at this image we can see that the clay layers are largely exfoliated in the matrix based on the lack of tactoid formations (swollen stacks of nanoclay). On the

other hand, if we consider the scale of the image, we can see that the clays in this image represent an example of particle flocculation with a flocc that has an effective diameter of ~150-200nm. Existence of particle flocculation will generally lead to less than desirable separation performance and mechanical properties.

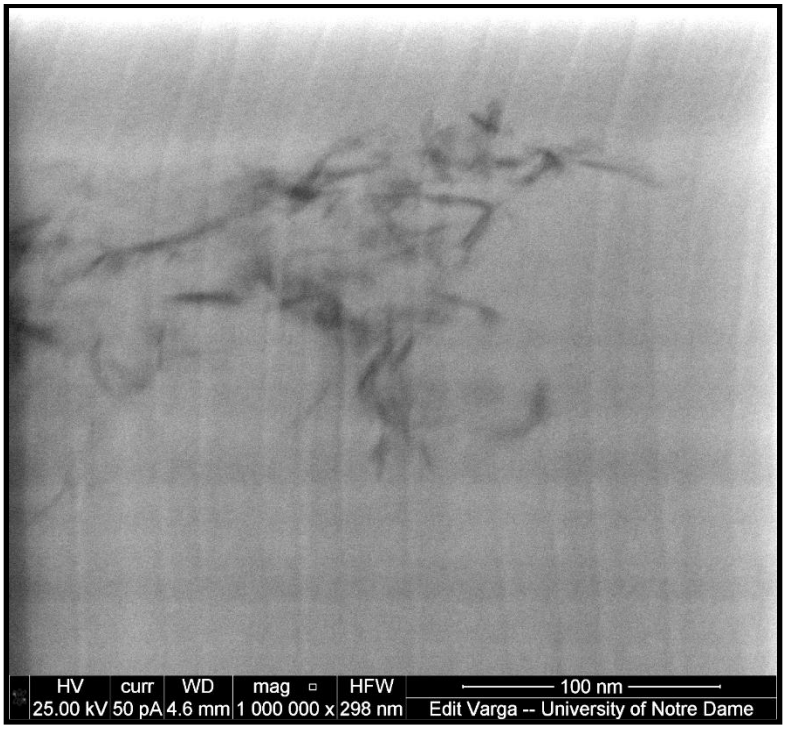

Figure 5.3: Transmission electron micrograph of Torlon®-Laponite® RD nanocomposite film containing 1wt% nanoclay filler showing evidence of exfoliation and polymer adhesion.

Based on the evidence shown in Figure 5.3 we know that we have created an exfoliated state of nanoclays but with the existence of flocculation. Figure 5.4 further supports the conclusion that the filler is exfoliated with the added benefit of improved dispersion. Again, the dark lines in the image represent the nanoclay filler. We can see in this image that the clays are still not perfectly distributed, but the presence of tight-packed floccs is less evident.

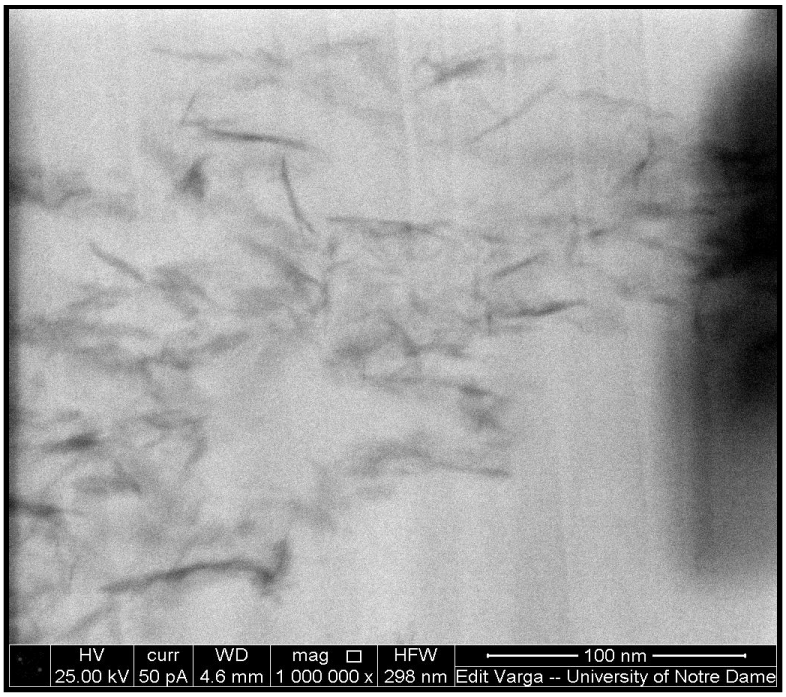

Figure 5.4: Transmission electron micrograph of Torlon®-Laponite® RD nanocomposite film containing 1wt% nanoclay filler showing evidence of dispersion in the host matrix.

If we consider the two images together we can clearly see that we have created a membrane with exfoliated nanoclays that are both well dispersed but also partially flocculated in the matrix. Such morphology would lead us to believe that the preparation procedure requires further tuning (increased mixing speed, longer mixing times).

5.3.3 Comparison of Experimental Permeation Results to Model Permeability Predictions

In Chapter 2 we highlighted four equations that would be used in this work to predict nanocomposite performance. Much to our surprise, when plotted against the model predictions we see that the membranes in this portion of the study greatly *outperformed* the mathematical expectations. We believe that the deviation from the model predictions may be due to (1) membrane morphology a la particle dispersion and orientation and/or (2) zone of influence effects at the particle interface. The latter will be embellished in Section 5.5.

Figure 5.5 graphically represents the predicted P/P_0 values for the four models of interest compared to the experimental values obtained in this work. We should note that the predicted values are constant for all pressures and gases because they are calculated based on assumed values for particle aspect ratio (A_r) and known values for volume fraction (ϕ_{vol}).[6] It is assumed that the sorption capacity does not change. Additionally, we assumed that the orientation parameter, *S*, in the Bharadwaj equation (see Equation 2.18) is zero. This assumption was based on the observed morphology of these samples via TEM. Please note that the Maxwell and Cussler models yielded very similar values – 0.994 and 0.992 respectively – and therefore are shown as overlapping in the figure.

The most interesting observation from these results is that our experimental values outperform the predicted values; which cannot occur without successful exfoliation. This result is of particular interest because all of the models are derived with the assumption that the nanoplatelet fillers are perfectly distributed within the matrix and of uniform geometry. However, if we consider the TEM images shown in Figures 5.3 and 5.4 it is quite clear that our membrane morphology does not meet the qualifications of a perfectly uniform system. Anisotropy or zone-of-influence (see Chapter 1) effects may cause such unexpected enhancements. At this point it is difficult to conclude the direct cause of the permeability deviations. A simple first analysis would be related to determining the apparent aspect ratio of the filler in the membrane.

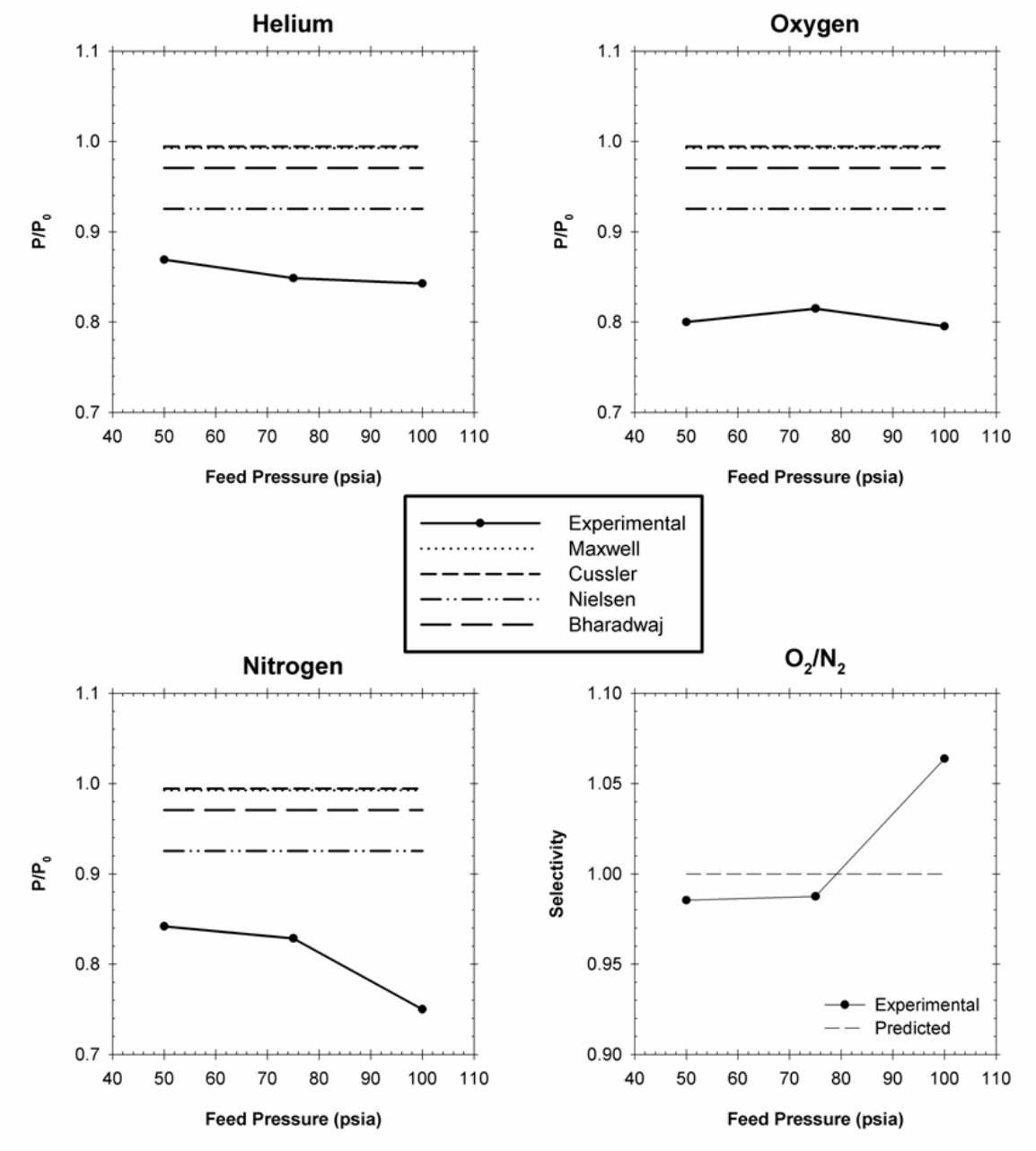

Figure 5.5: Average P/P_0 and α/α_0 values for Torlon®-Laponite® RD nanocomposite films containing 1wt% nanoclay filler at different feed pressures compared to predicted values using various transport models. Filler particle aspect ratio was assumed to be 30 for model calculations and S=0 for the Bharadwaj model.

It is reasonable to assume that the average aspect ratio of the nanoplatelet filler is not uniform. We can take this one step further and estimate the observed aspect ratio using the experimental values for P/P_0. Figure 5.6 represents the calculated aspect ratio based on these values. The Maxwell model has been neglected from this analysis because there is no shape factor built into the equation. As before, for the Bharadwaj equation we let S=0. Data in the figure is organized by the respective model used, the gas penetrant (y-axis) and the corresponding pressure for experimental P/P_0 values used.

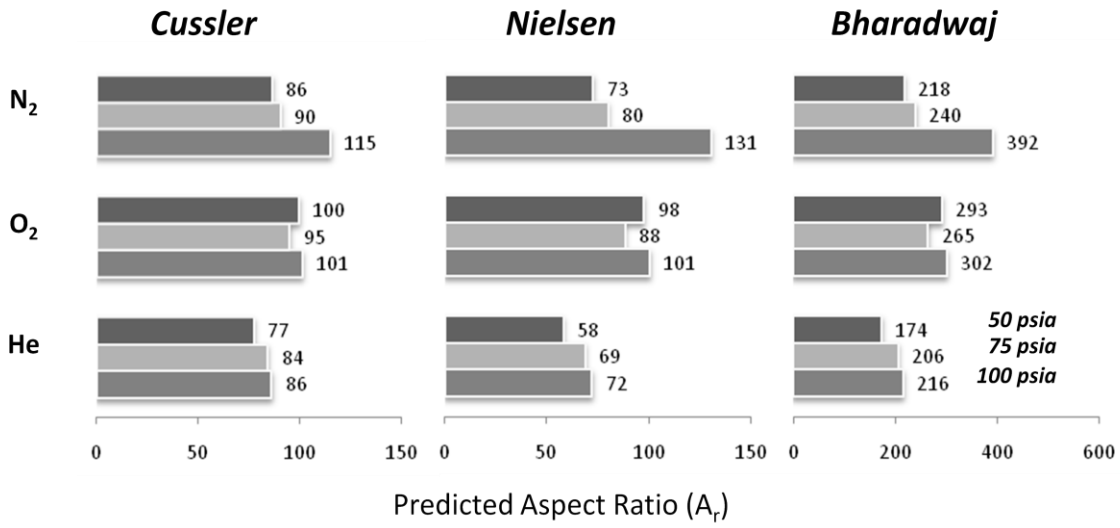

Figure 5.6: Predicted aspect ratio (A_r) of nanoclay in Torlon®-Laponite® RD nanocomposite film containing 1wt% filler based on three hybrid transport models. Experimental values of P/P_0 for each gas penetrant were used to calculate A_r.

Based on the results presented in Figure 5.6, the Cussler and Nielsen are in reasonable agreement for each penetrant and the respective feed condition. The Bharadwaj equation, on the other hand, predicts aspect ratio values on the order of 2-3 higher than either Cussler or Nielsen. Albeit none of these values precisely represent the actual membranes, it is more likely that the Bharadwaj equation serves as a better representation because it includes a coefficient to account for anisotropy. Further

analyses using all of these equations would be needed in order to more accurately back-calculate geometric characteristics of the membranes.

5.4 Characterization of Torlon®-Laponite® RD Dense Film Membranes Containing 3wt% Nanoclay

It was shown that a Torlon®-Laponite® RD hybrid membrane containing 1wt% nanoclay loading had desirable transport properties with permeability reductions on the order of 15-20%. Therefore, to further prove efficacy of this procedure we increased the nanoclay loading to 3wt%. With triple the loading we should even further depression in gas permeability. Unfortunately this was not the case. Permeability was reduced in most cases, but by a smaller margin than that of the first case. TEM characterization, on the other hand, did yield promising results.

5.4.1 Permeability of Hybrid Membranes Containing 3wt% Nanoclay

Considering the mathematical predictions shows that permeability depression does not scale linearly in these systems. In other words, if a film containing 1wt% filler has a 15% depression in permeability then a membrane containing 3wt% filler would not provide a 45% depression in permeability. However, we should see a permeability depression greater than that of the first case. Several films were tested and their corresponding results are shown in Figure 5.7 and Table 5.4 for convenience.

Table 5.4: Average Permeability (Barrers) & Selectivity values for Torlon®-Laponite® RD nanocomposite films containing 3wt% nanoclay filler at different feed pressures.

Feed Gas	**Feed Pressure**		
	50 psia	*75 psia*	*100 psia*
Helium	3.59 ±0.42	3.79 ±0.09	3.54 ±0.26
Oxygen	0.112 ±0.003	0.114 ±0.002	0.112 ±0.007
Nitrogen	0.014 ±0.000	0.011 ±0.000	0.014 ±0.001
O_2/N_2 Selectivity	8.00 ±0.17	7.80 ±0.06	8.00 ±0.38

We can see clear evidence of a depression in both oxygen and nitrogen permeabilities when comparing the hybrid and pure polymer films. These results prove that the nanoclays are in fact well exfoliated and dispersed within the polymer matrix and that the polymer chains are adhered to the nanoclay surface.[7] If we now consider the helium permeation study we can see that there is no depression in the permeability and in some cases there was a slight increase. This observation does not disprove the results for the other gases, but it does indicate that there may be sub-nanometer molecular scale defects within the membrane at the polymer-filler interface that are made more apparent by smaller molecules than larger ones.

Like the previous section (5.2.1), we have represented the ratio of change – whether greater or lesser than unity – between the pure polymer and the hybrid membranes. These results can be seen in Table 5.5. We will discuss the anomalies of these trends further in Section 5.5.

Table 5.5: Average P/P_0 and α/α_0 values for Torlon®-Laponite® RD nanocomposite films containing 3wt% nanoclay filler at different feed pressures.

Feed Gas	**Feed Pressure**		
	50 psia	*75 psia*	*100 psia*
Helium	1.00	1.09	1.02
Oxygen	0.85	0.92	0.90
Nitrogen	0.74	0.86	0.81
O_2/N_2 Selectivity	1.16	1.08	1.12

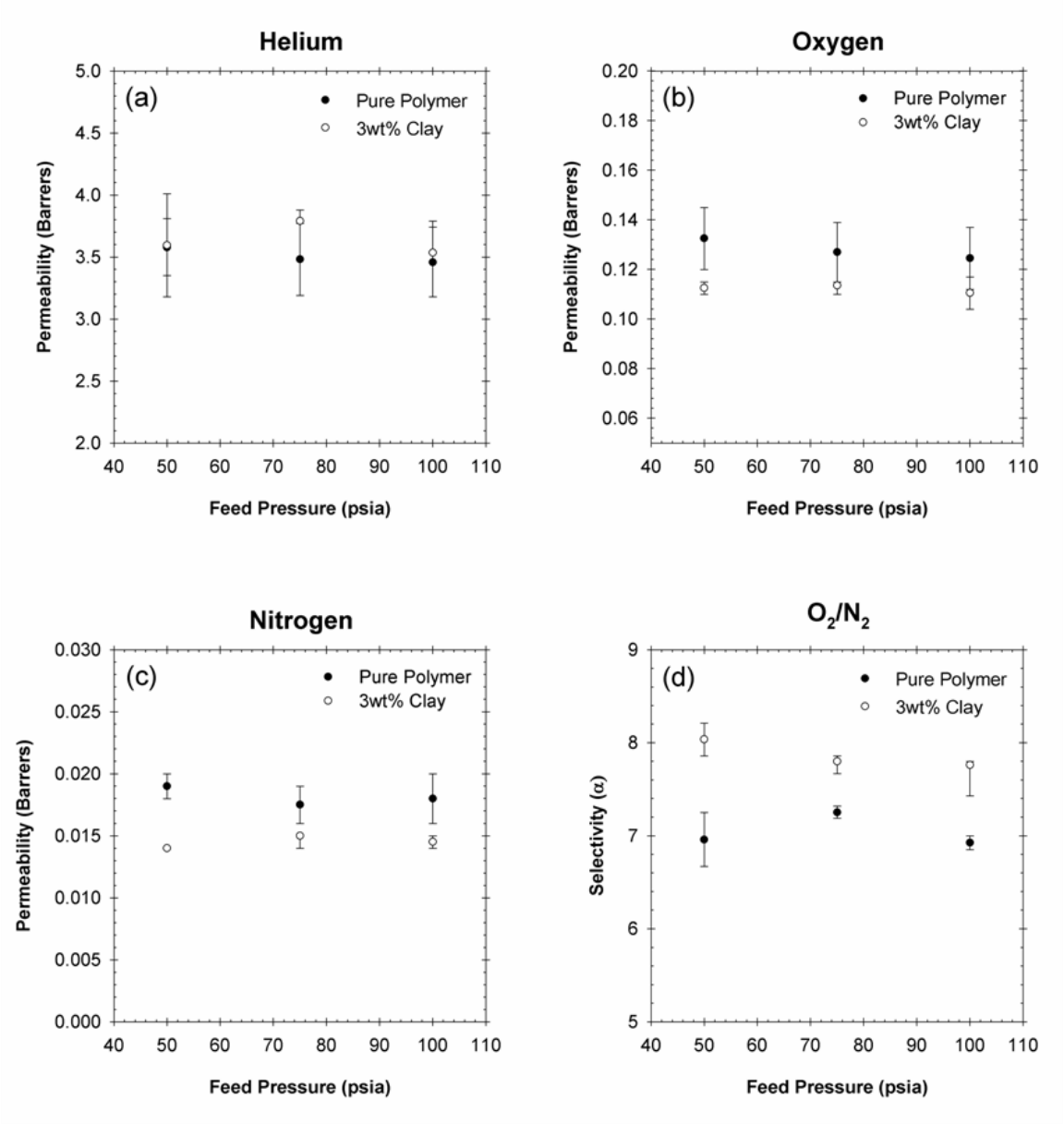

Figure 5.7: Permeability properties of Torlon®-Laponite® RD nanocomposite dense film membranes containing 3wt% nanoclay filler. (a) Helium (b) Oxygen (c) Nitrogen (d) O_2/N_2 Selectivity

5.4.2 Microscopic Characterization of Hybrid Membranes Containing 3wt% Nanoclay

According to the measured permeation results it is quite evident that we have created a hybrid membrane with a high degree of exfoliation and dispersion. This is further supported by the TEM images shown in Figures 5.8 and 5.9.

It was shown in Figure 5.4 that, despite promising permeation properties, there was evidence of imperfect nanoclay dispersion in the polymer. This trend is repeated for the membranes discussed in this section as illustrated in Figure 5.8. We were not surprised by this observation since the volume fraction is more than threefold higher. Regardless of the dispersive incongruities, it is still quite clear that we have achieved a high percentage of exfoliation.

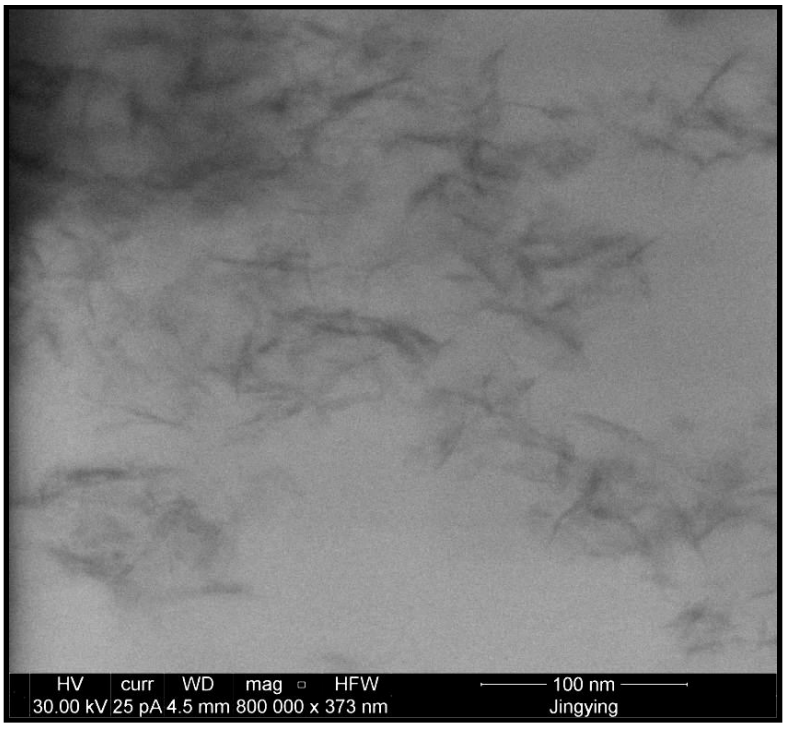

Figure 5.8: Transmission electron micrograph of Torlon®-Laponite® RD nanocomposite film containing 3wt% nanoclay filler showing evidence fractal dispersion.

The high magnification image shown in Figure 5.9 is good complement to the permeation results and the image in Figure 5.8. In this image we can see more clearly that the polymer is adhered to the particle surface. This conclusion is corroborated by the polymer density gradient (as represented by the image contrast) which is quite consistent as a function of proximity to the clay surface. Significant interfacial defects would be visible at this scale (and certainly via permeation measurements). It is still possible to have angstrom-size defects at the polymer-nanoclay interface, but this phenomenon generally leads to a slight decrease in permselectivity; which was not seen in the permeability results.[8-10]

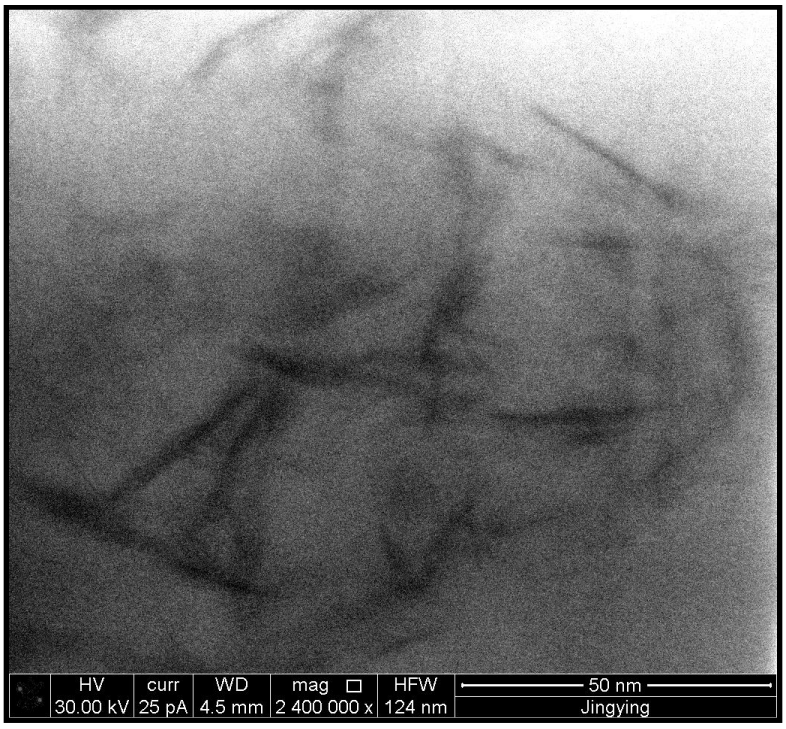

Figure 5.9: Transmission electron micrograph of Torlon®-Laponite® RD nanocomposite film containing 3wt% nanoclay filler showing evidence of exfoliation and polymer adhesion.

5.4.3 Comparison of Experimental Permeation Results to Model Permeability Predictions

Unlike the hybrid membranes containing 1wt% Laponite® RD filler, the membranes containing 3wt% filler did not outperform all of the model predictions for each case. In fact, as we discussed previously in this section, helium permeation tests actually had worse performance than expected whereas oxygen and nitrogen tests showed positive results. Comparisons of the model predictions and the corresponding experimental results are shown in Figure 5.11. Similar constraints and assumptions were applied in the model calculations as noted in Section 5.2.3.

In terms of the overall comparisons we can see that our materials perform within the bounds of the model predictions, which is expected for a nanocomposite membrane with a desired polymer-nanoplatelet interface. The obvious exception in this conclusion pertains to the helium permeability results. A hypothesis for these erroneous results was presented previously in this section. Oxygen and nitrogen permeation results exhibit the desired behavior – albeit their respective performances are not equal (as further illustrated by the change in the gas pair permselectivity versus the pure polymer). Further discussion on these results is presented in Section 5.5.

There is an anomaly present for both oxygen and nitrogen experimental values when the feed pressure was 50psia. In each case we see a departure from other points on the order of 10%. This is likely due to differences in permeability trends between the pure polymer and the hybrid membrane. The trend is not so obvious in the data trends presented in Figure 5.7 due to the y-axis scale in the figures. However, when normalized, it becomes more apparent. We believe that this deviation from expectations is due to the compounded uncertainty in the measured values of the pure and hybrid samples. Regardless of this trend, we can still say confidently that the hybrid membrane still shows the desired permeability decrease.

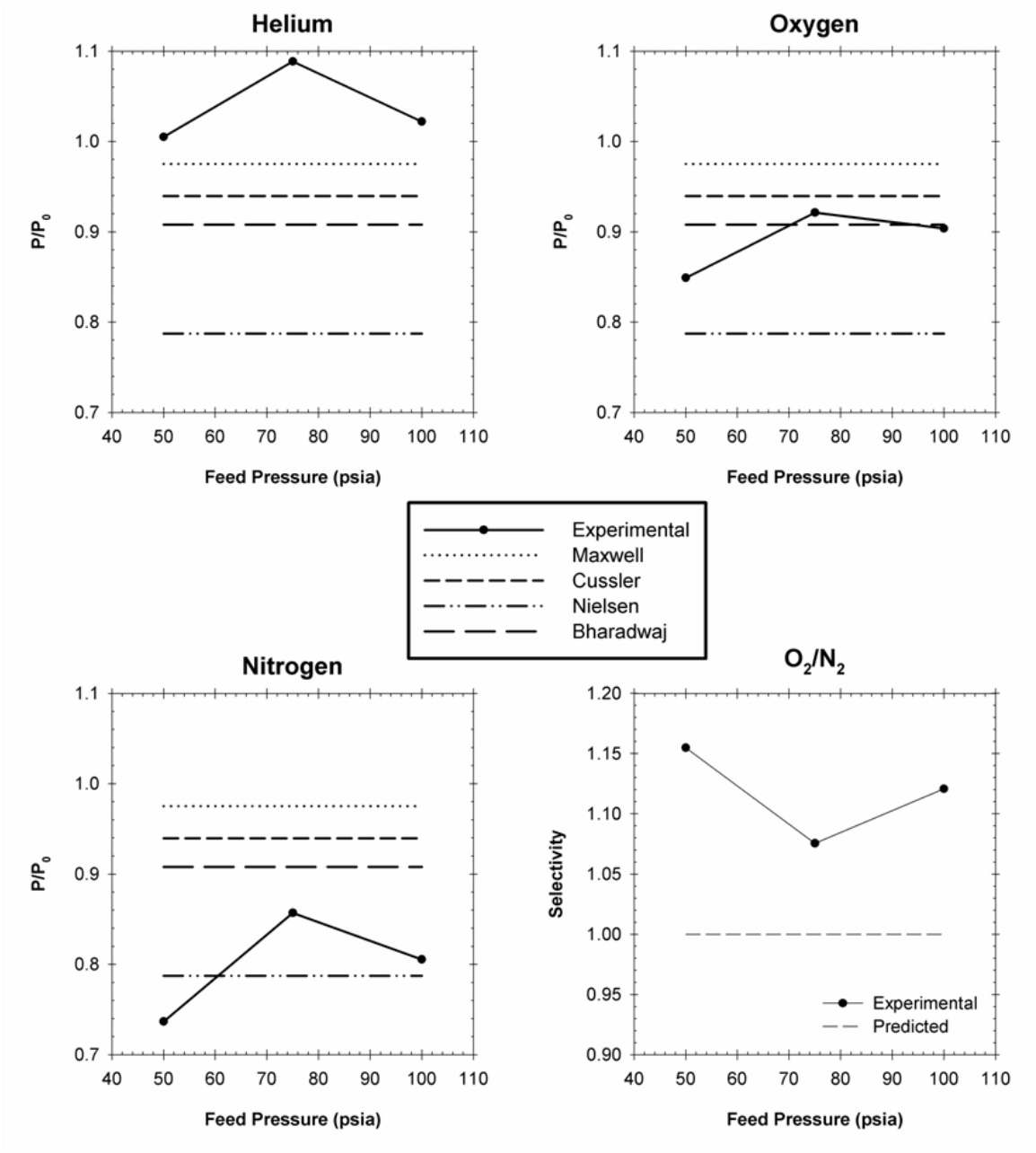

Figure 5.11: Average P/P_0 and α/α_0 values for Torlon®-Laponite® RD nanocomposite films containing 3wt% nanoclay filler at different feed pressures compared to predicted values using various transport models. Filler particle aspect ratio was assumed to be 30 for model calculations and S=0 for the Bharadwaj model.

5.5 Characterization of Torlon®-Laponite® RD Dense Film Membranes Containing 5wt% Nanoclay

Continuing our investigation on the effects of nanoclay loading in the Torlon® matrix, we produced and tested nanocomposite films containing 5wt% Laponite® RD. In these samples it was our objective to further prove that increasing barrier content shows a greater decrease in membrane permeability while maintaining an exfoliated and dispersed inorganic phase. Unlike the previous membranes containing 3wt% nanoclay, wherein the average permeability depression was less than that of 1wt% containing films, the membranes containing 5wt% nanoclay by-and-large showed a greater depression in permeability than the initial case. These results support our hypothesis that increased nanoclay loading results in greater permeability depression. TEM images show supporting evidence that our membrane formation techniques create a well exfoliated and dispersed system of nanoclays in the organic phase.

5.5.1 Permeability of Hybrid Membranes Containing 5wt% Nanoclay

Permeability and selectivity results of the 5wt% hybrid films compared to pure polymer values are shown in Figure 5.12 and the average values are reiterated in Table 5.6 for convenience. For all of the gas penetrants tested there is a clear decrease in permeability for the hybrid films compared to the pure polymer film. This trend is on par with the results shown for the first system containing 1wt% nanoclay. Furthermore, the O_2/N_2 permselectivity deviations are much more consistent with expectations, unlike the membranes containing 3wt% nanoclay. This conclusion is more clearly elucidated in Table 5.7 whereby we have reported the ratio of the hybrid membrane transport properties with those of the pure polymer membrane (P/P_0 and α/α_0).

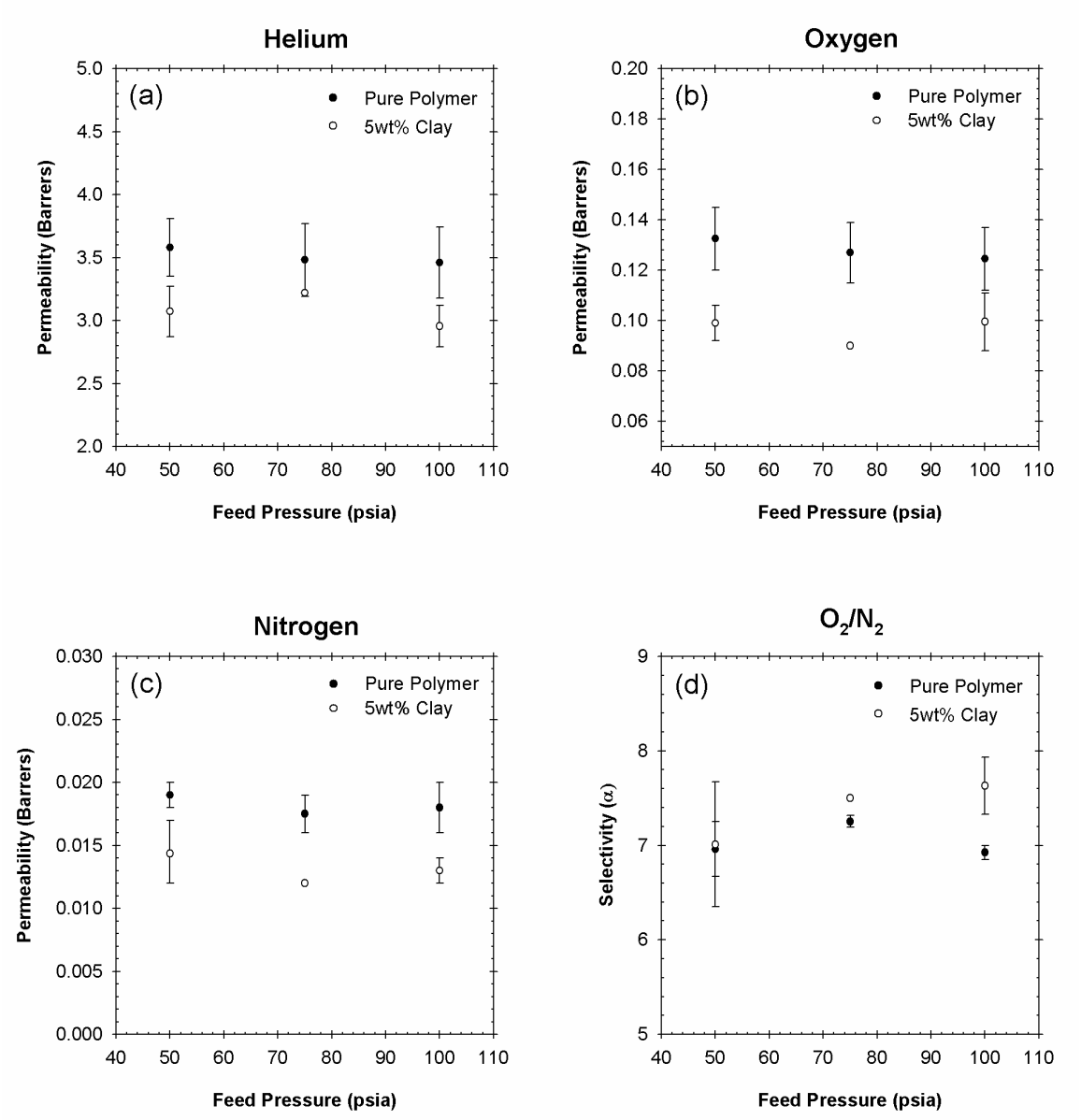

Figure 5.12: Permeability properties of Torlon®-Laponite® RD nanocomposite dense film membranes containing 5wt% nanoclay filler. (a) Helium (b) Oxygen (c) Nitrogen (d) O_2/N_2 Selectivity

Table 5.6: Average Permeability (Barrers) & Selectivity values for Torlon®-Laponite® RD nanocomposite films containing 5wt% nanoclay filler at different feed pressures.

Feed Gas	Feed Pressure		
	50 psia	*75 psia*	*100 psia*
Helium	3.07 ±0.20	3.22	2.96 ±0.16
Oxygen	0.099 ±0.007	0.090	0.099 ±0.012
Nitrogen	0.014 ±0.003	0.012	0.013 ±0.001
O_2/N_2 Selectivity	7.07 ±0.66	7.50	7.62 ±0.30

It is necessary to insert an explanation related to the data uncertainty bars presented in Figure 5.12. The reader will see that data points representing a feed pressure of 75psia do not have associated error bars. This particular hybrid composition was studied early in this work. During the early phase of development we focused on permeation measurements at 50 and 100psia. Measurements at 75psia were performed on one sample to show consistency in the permeability values. It has been shown in previous sections that there is no discernable trend in the data that would lead to alternative conclusions related to permeability versus feed pressure in these systems.

The data from Table 5.6 has been normalized by the data from Table 5.1 and represented in Table 5.7 as P/P_0 and α/α_0 for each test gas and feed pressure. Trends from these data will be displayed and revisited in Section 5.5.

Table 5.7: Average P/P_0 and α/α_0 values for Torlon®-Laponite® RD nanocomposite films containing 5wt% nanoclay filler at different feed pressures.

Feed Gas	Feed Pressure		
	50 psia	*75 psia*	*100 psia*
Helium	0.86	0.92	0.86
Oxygen	0.75	0.71	0.80
Nitrogen	0.76	0.69	0.72
O_2/N_2 Selectivity	1.01	1.03	1.10

5.5.2 Microscopic Characterization of Hybrid Membranes Containing 5wt% Nanoclay

In Sections 5.2.2 and 5.3.2 we presented TEM images confirming that the nanoclays in a hybrid membrane containing 3wt% filler are exfoliated. The same observation is made when the films have 5wt% loading. Figure 5.13 is a darkfield (hence the reverse contrast) TEM image showing the nanoclays are exfoliated and disordered in the membrane. Unfortunately, the image also signifies that there is flocculation. The dark gray patches correspond to pure polymer, whereas the white cloud groupings are the flocculated particles. Generally, the presence of large floccs is undesired in a hybrid membrane and may lead to defective transport properties.[11,12] However, we found that the measured permeabilities were within the expected range. This suggests that the floccs may contribute to the permeability suppression. We will revisit this concept in Chapter 6.

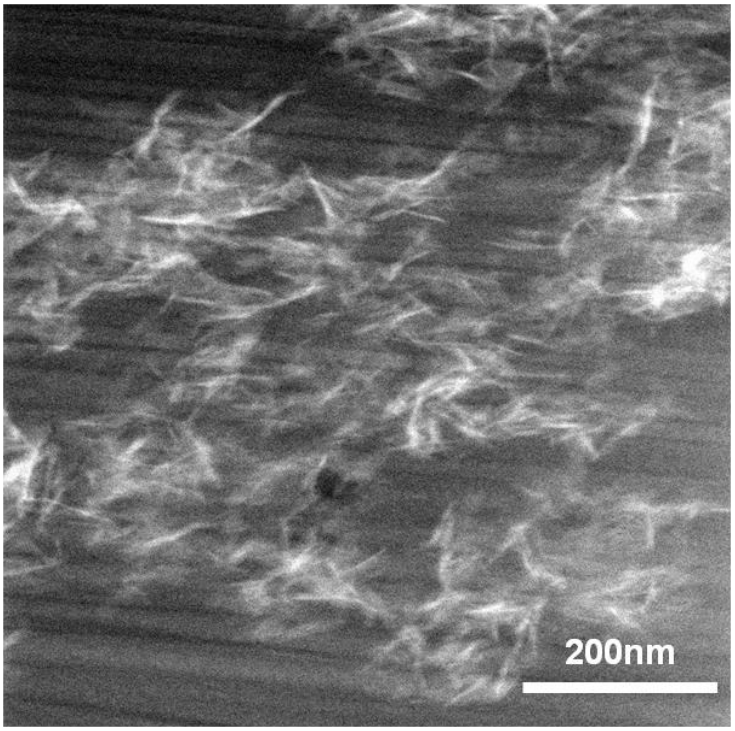

Figure 5.13: Transmission electron micrograph of Torlon®-Laponite® RD hybrid membrane containing 5wt% nanoclay filler showing evidence of good exfoliation and the presence of flocculation

5.5.3 Comparison of Experimental Permeation Results to Model Permeability Predictions

Overall, our experimental permeabilities values agree well with model predictions. Unlike the previous case, helium exhibits permeability reductions that outperform Maxwell model predictions for rigid spheres; but the measured values are greater than that of oxygen and nitrogen. Data for oxygen and nitrogen permeation lies within the bound of the Nielsen and Bharadwaj equations, which is very promising. We do, however, see that the O_2/N_2 selectivity is higher (~10%) than the ideal value. This suggests that there are molecular level discrepancies in the membrane that have an apparent selectivity. Such anomalies will be discussed in the next section. Normalized permeability and selectivity trends for Torlon® hybrid membranes containing 5wt% nanoclay filler are presented along with model predictions in Figure 5.14 below.

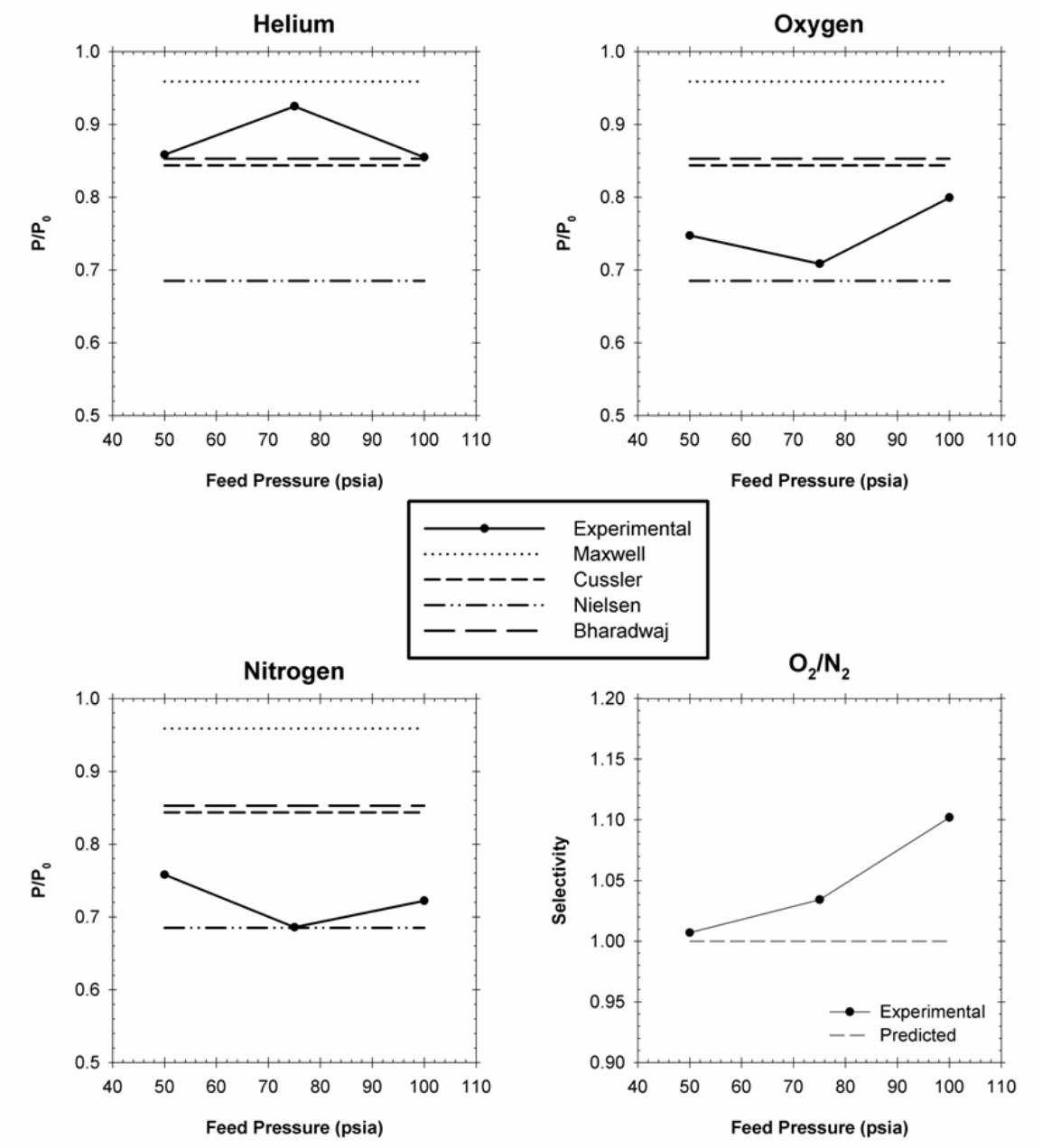

Figure 5.14: Average P/P_0 and α/α_0 values for Torlon®-Laponite® RD nanocomposite films containing 5wt% nanoclay filler at different feed pressures compared to predicted values using various transport models. Filler particle aspect ratio was assumed to be 30 for model calculations and S=0 for the Bharadwaj model.

5.6 Analysis of Permeability Trends with Respect to Gas Penetrant

Throughout this Chapter we have alluded to a series of unexpected trends related to the permeabilities and permselectivities of the hybrid membranes studied in this work. It is our intention in this section to provide a possible explanation of these trends based on the observations of hybrid membranes as presented in the literature. The average permeability and selectivity of each case study have been combined and are presented in Figure 5.15 below.

The most critical observation from these data pertains to the trend in O_2/N_2 selectivity for all hybrid membranes. More specifically, the increase of the hybrid membrane permselectivity with respect to the pure polymer demonstrates that there may be additional membrane physical characteristics unaccounted for in the base assumptions. Similar observations have been made and discussed by others in the literature.[10,13] Current thoughts on these trends are associated with localized polymer chain immobilization within the membrane at the particle interface.[14]

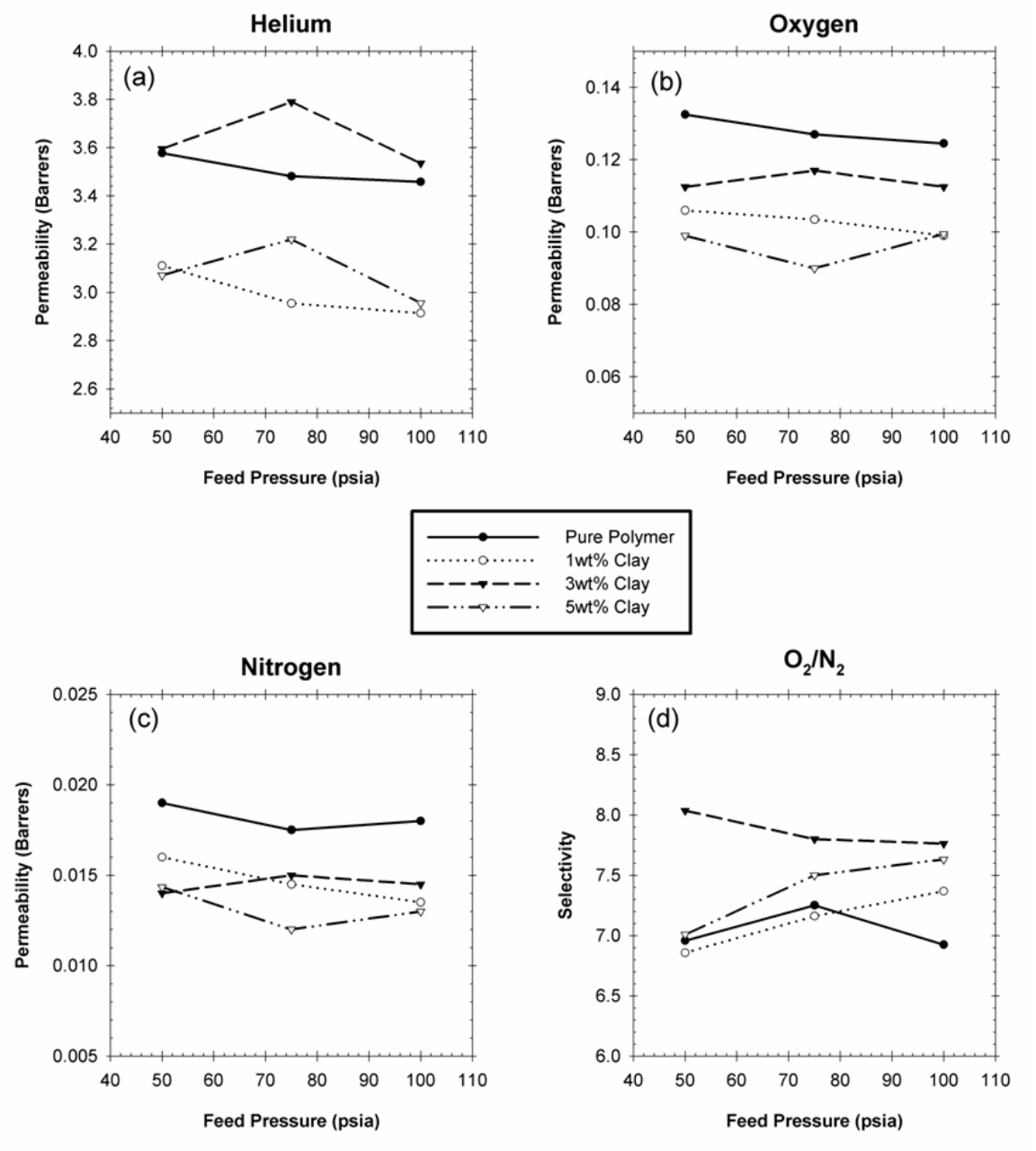

Figure 5.15: Comparison of average Permeability and Selectivity properties of Torlon® and Torlon®-Laponite® RD nanocomposite dense film membranes containing different nanoclay loadings. (a) Helium (b) Oxygen (c) Nitrogen (d) O_2/N_2 Selectivity

5.6.1 Permeability Trends in Torlon®-Laponite® RD Dense Film Membranes as a Function of Gas Penetrant Kinetic Diameter

It was shown in Figure 5.15 that permselectivity increased in hybrid membranes compared to pure polymer values. These results show that solution diffusion in the nanocomposite does not coincide with the standard assumption wherein permselectivity is constant and permeability decreases. Similar observations, however, have been shown in the mixed matrix membrane literature and are often attributed to polymer chain immobilization; which for our purposes is related to the *zone of influence* around the particles.[9,10] For further analysis, we can decouple the permeability versus pressure results and plot P/P_0 as a function of the kinetic diameter of the gas penetrant. These data are shown in Figures 5.16-5.18 for each case study (wt% filler).

According to the trends shown in Figure 5.16 regarding penetrant kinetic diameter, the evidence for the nanocomposite films containing 1wt% filler is not as clear as the other samples. It is safe to say that for membranes containing very low volume fractions of filler that any permselectivity contribution effects due to the polymer-particle interfacial discontinuities are obscured in experimental uncertainty. However, when the filler loading is higher a la Figure 5.17 and 5.18, the trend is more apparent.

On average, there is a 20% decrease in P/P_0 between helium and nitrogen and 10% for oxygen and nitrogen. This strongly suggests that there are two unequal permeable phases in the membrane (we still maintain the assumption that the clay is impermeable). Furthermore, based on the observations it is evident that the proposed zone of influence is denser than the bulk and therefore the permselectivity increases. A cartoon depicting this concept is shown in Figure 1.5.

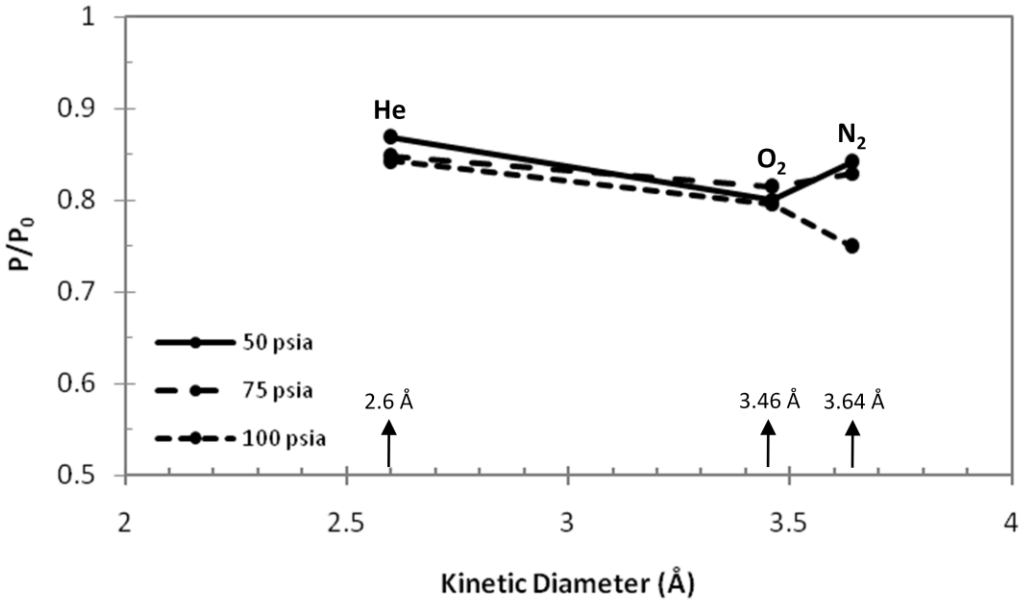

Figure 5.16: Permeability depression in Torlon®-Laponite® RD hybrid membrane containing 1wt% nanoclay as a function of kinetic diameter of gas penetrant.

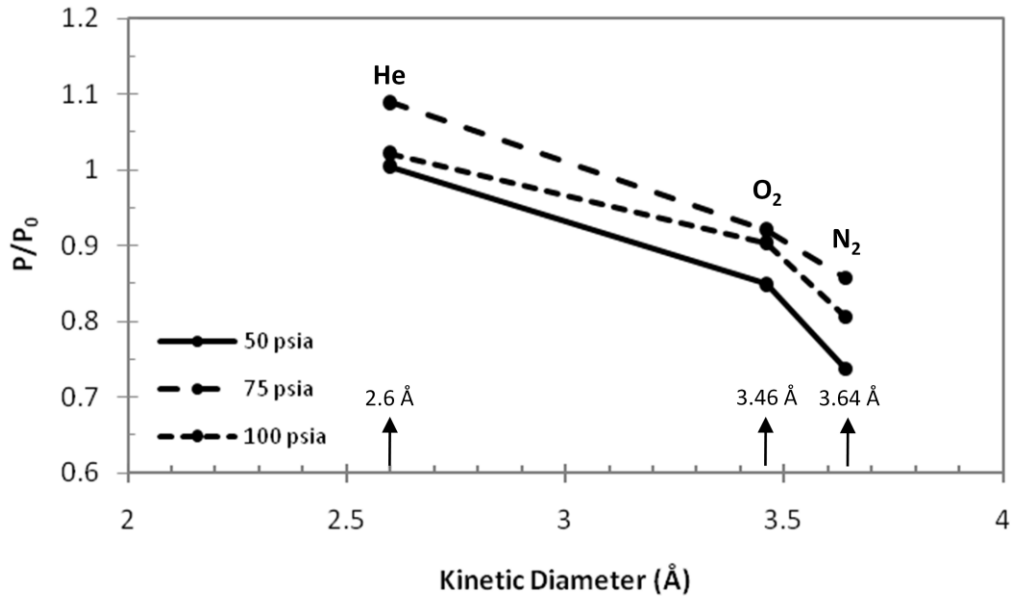

Figure 5.17: Permeability depression in Torlon®-Laponite® RD hybrid membrane containing 3wt% nanoclay as a function of kinetic diameter of gas penetrant.

If these data were to display the opposite trends (i.e. increasing P/P_0 with increasing kinetic diameter) then it would be evidence of a *leaky interface* morphology which is counterintuitive to the noticeable depressions in permeability that have been observed. In other words, a rigidified matrix at the polymer-particle interface has beneficial properties for nanocomposite membranes containing impermeable filler. Additional studies may be conducted using additional penetrants to fully uncover any trends associated with kinetic diameter.

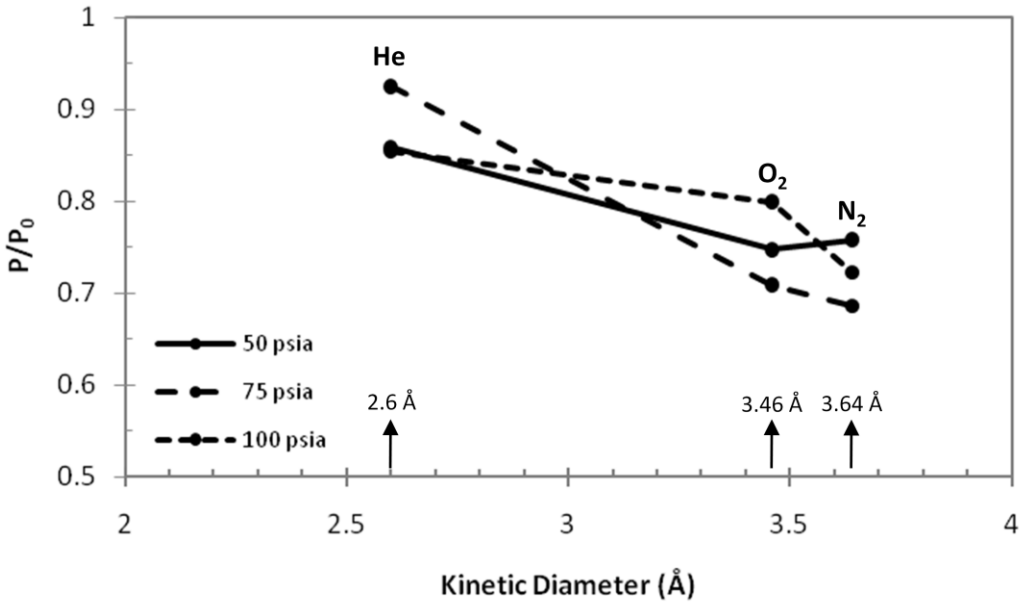

Figure 5.18: Permeability depression in Torlon®-Laponite® RD hybrid membrane containing 5wt% nanoclay as a function of kinetic diameter of gas penetrant.

5.6.2 Gas Sorption in Torlon®-Laponite® RD Hybrid Dense Film Membranes

It was shown that the kinetic diameter of the gas penetrant affects the observed permeability. We have hypothesized that this observation is related to the rigidified matrix concept. To further understand if the zone of influence is significant we have used pressure decay sorption to probe the solubility of gas in the hybrid membrane and

compared these results with the pure polymer membrane. These measurements were made using carbon dioxide as a test gas. Attempts were made using oxygen and nitrogen as penetrants, but it was found that the sorption capacity was below the measurable limit for the equipment and conditions that we were using. Furthermore, tests were carried from low to sufficiently high pressures (~250psia) to ensure that the isotherm reached steady state to accurately fit parameters using the dual-mode sorption model (see Eq. 2.7).

To know the base values of each material, we measured the sorption capacity for a pure Torlon® film and unmodified Laponite® RD. Sorption isotherms for these materials are presented in Figure 5.19 and the corresponding Henry's and Langmuir sorption parameters are given in Table 5.8. Since the clay materials are impermeable, sorption occurs in the micropore region (gallery spaces) of the tactoids.[15,16]

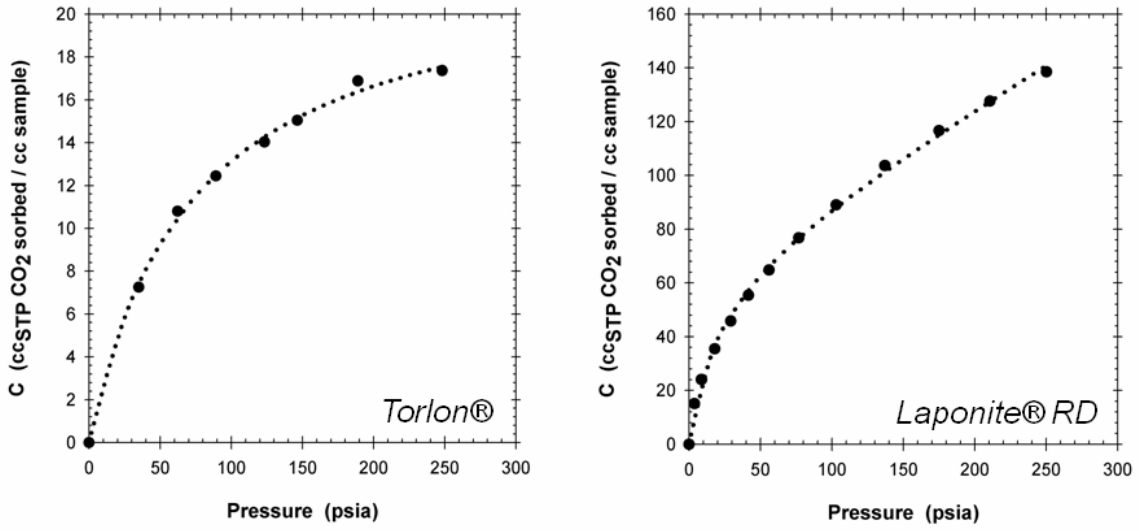

Figure 5.19: Sorption isotherms for carbon dioxide in a Torlon® dense film and unmodified Laponite® RD powder

Table 5.8: Henry's and Langmuir sorption parameters for CO_2 in Torlon® and Laponite® RD

Parameter	Torlon®	Laponite® RD
k_D	0	0.316
C'_H	22.662	66.991
b	0.014	0.046

Using the sorption parameters obtained for the pure components independently we can calculate the expected isotherm for the hybrid material. There are two possible approaches to calculate the expected hybrid membrane sorption capacity. If we assume that the clay filler does not contribute to sorption in the hybrid material, then the concentration in the hybrid membrane, C, may be estimated based on reduced polymer volume fraction and the pure polymer properties (C_0), as demonstrated by Equation 5.1.

$$C = C_0 \cdot (1-\phi) \qquad \text{Eq. 5.1}$$

Alternatively, we may also account for the observed sorption capacity in the clay, C_D, and include it into our estimation. Assuming that the sorption properties of the materials are additive and based on intrinsic volume fraction (ϕ) contributions, we can make our estimation using Equation 5.2.

$$C = C_0 \cdot (1-\phi) + C_D \cdot \phi \qquad \text{Eq. 5.2}$$

Sorption measurements were repeated in the pressure range of interest on the hybrid films. The data and fitted curves are shown in Figure 5.20. Predicted values for the hybrid materials based on Equations 5.1 and 5.2 are also shown ($\phi = 0.028$). Calculated dual-mode sorption parameters for the hybrid membrane, based on experimental data, are presented in Table 5.9.

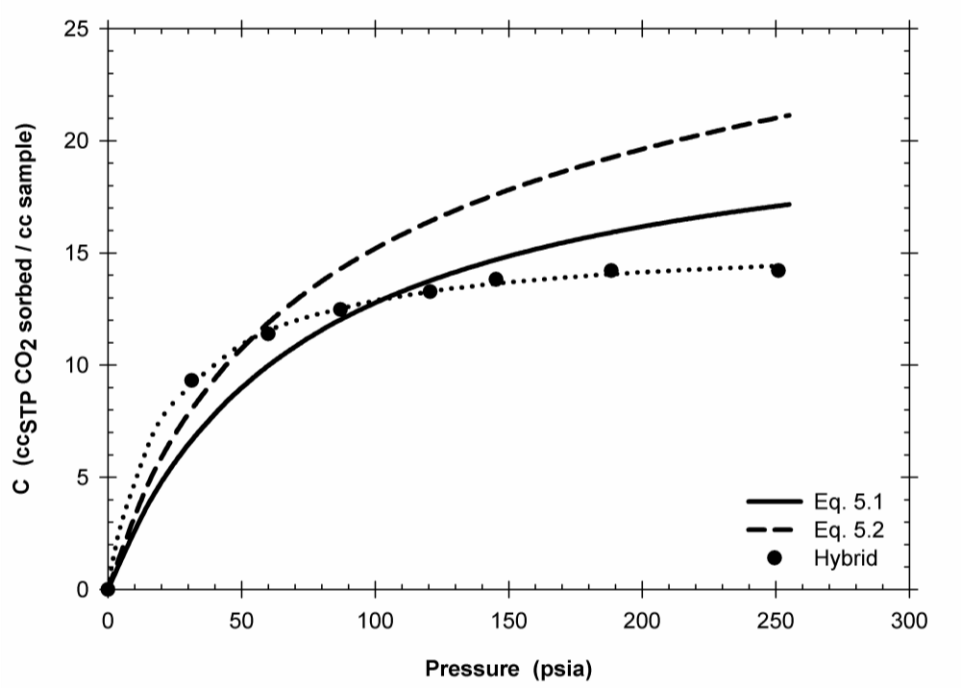

Figure 5.20: Sorption isotherm for carbon dioxide in Torlon® hybrid films containing 5wt% nanoclay filler. Predicted trends based on contribution assumptions for pure polymer and clay particles are plotted as well.

Table 5.9: Henry's and Langmuir sorption parameters for CO_2 in hybrid Torlon® membranes containing 5wt% Laponite® RD filler

Parameter	Torlon-5wt% Laponite® RD
k_D	0
C'_H	15.667
b	0.046

Interestingly, the hybrid membranes exhibit sorption capacities at higher pressures are lower than either of the predictions at higher pressures. This trend indicates that the volume fraction of the filler material may be higher (upwards of 5x) than assumed. Alternatively, the overall (bulk) polymer density in the hybrid membrane may be lower than the pure polymer version, thereby reducing the sorption capacity. If the latter scenario is true, then our argument regarding the zone-of-influence around the filler may

be true. Additional measurements on hybrid membranes containing different filler loadings may further elucidate these observations.

5.7 Summary & Conclusions

We have shown significant evidence proving that Torlon® and unmodified Laponite® RD nanocomposite membranes yield desirable transport properties – even when the volume fraction of filler is kept very low. These transport properties (permeability and selectivity) as a function of nanoclay loading are reviewed in Figure 5.21 as a final summary. (For the reader's reference, mass and equivalent volume fractions in these membranes are as follows: 1wt% = 0.6v%, 3wt% = 1.7v%, 5wt% = 2.8v%)

Permeability measurements and supporting TEM images were used to verify our initial hypothesis that a polyamide-imide material would create a well adhered interface with the nanoclay. The likely route for this absorption is cationic coordination via *d*-complexes, although there is the possibility of hydrogen bonding between the amide groups in the polymer backbone with the electron deficient Si-O-Si surface group of the nanoclay.[1,17,18] This hypothesis is further verified by evidence that permeability is a function of increasing penetrant kinetic diameter which corresponds with the rigidified matrix concept whereby polymer density is higher at the particle interface than the bulk.

Based on the results presented in this portion of our work, it can be safely concluded that methods developed to create hybrid solutions for nanocomposite membrane formation may be further exploited for the manufacture of asymmetric hollow fiber membranes. Moreover, these methods may be applicable to non-membrane based organic-inorganic composites.

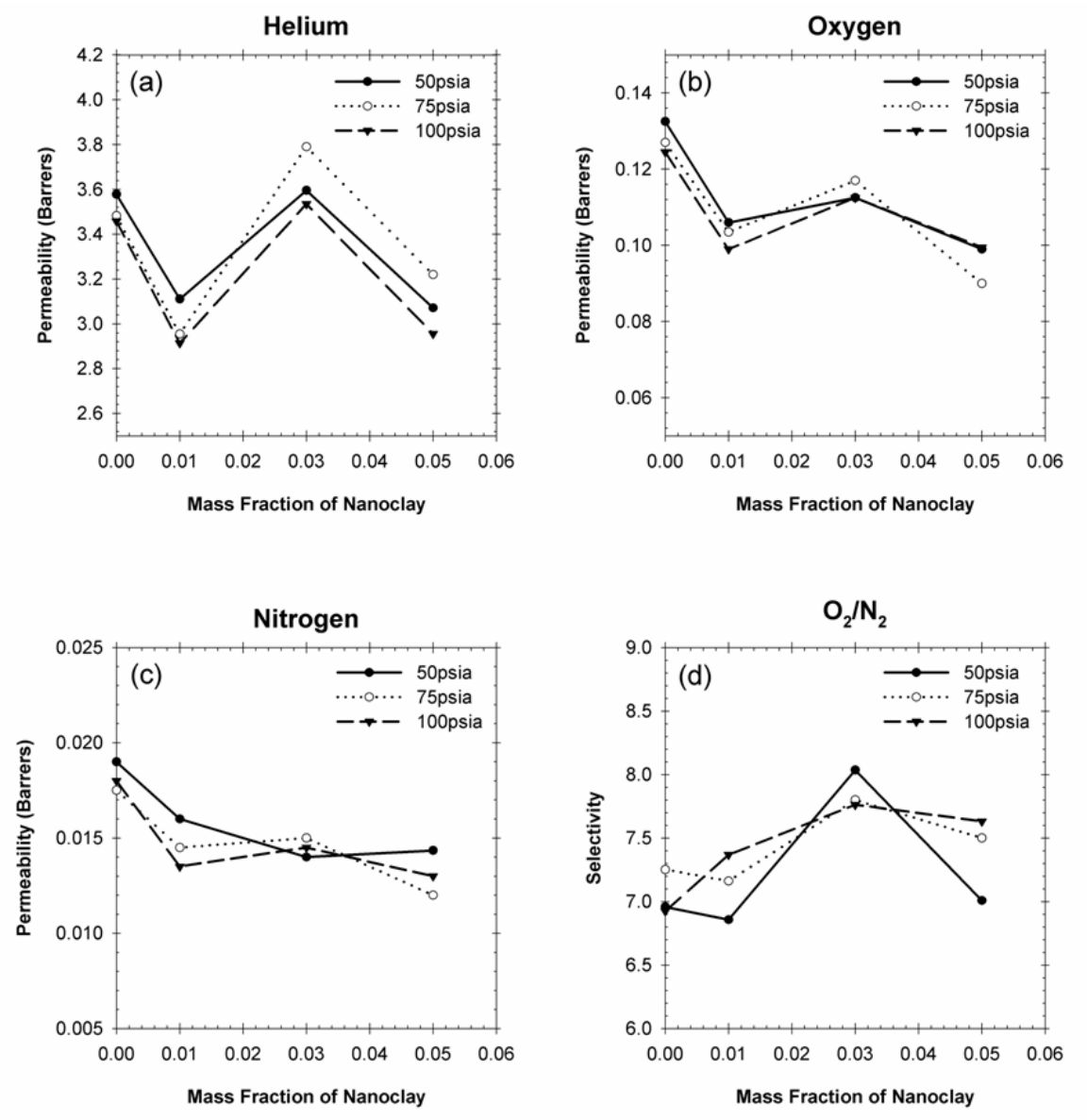

Figure 5.21: Permeability Properties of Torlon® and Torlon®-Laponite® RD Nanocomposite Dense Film Membranes as a Function of Nanoclay Loading. (a) Helium (b) Oxygen (c) Nitrogen (d) O_2/N_2 Selectivity

5.8 References

1. M. Kosuri, "Polymeric Membranes for Super Critical Carbon Dioxide ($scCO_2$) Separations," *PhD Dissertation*, Georgia Institute of Technology, 2009.

2. M. Kosuri and W.J. Koros, "Defect-free Asymmetric Hollow Fiber Membranes from Torlon, a Polyamid-imide, for High Pressure CO_2 Separations," *Journal of Membrane Science* **320** (1-2), 65-72 (2008).

3. R. Chafin II, "Torlon and Silicalite Mixed Matrix Membranes for Xylene Isomer Purification," *PhD Dissertation*, Georgia Institute of Technology, 2007.

4. D.R. Paul and L.M. Robeson, "Polymer Nanotechnology: Nanocomposites," *Polymer* **49** (15), 3187-3204 (2008).

5. S. Pavlidou and C. Papaspyrides, "A Review on Polymer-Layered Silicate Nanocomposites," *Progress in Polymer Science* **33** (12), 1119-1198 (2008).

6. A. Mourchild, A. Delville, J. Lambard, E. Lecolier, and P. Levitz, "Phase Diagram of Colloidal Dispersions of Anisotropic Charged Particles: Equilibrium Properties, Structure, and Rheology of Laponite Suspensions," *Langmuir* **11** (6), 1942-1950 (1995).

7. T. Pinnavaia and G. Beall (eds), *Polymer-Clay Nanocomposites*. (John Wiley & Sons, Inc., New York, NY, 2000).

8. T. Moore, "Effects of Materials, Processing, and Operating Conditions on the Morphology of Gas Transport Properties of Mixed Matrix membranes," *PhD Dissertation*, University of Texas - Austin, 2004.

9. T. Moore, R. Mahajan, D. Vu, and W.J. Koros, "Hybrid Membrane Materials Comprising Organic Polymers with Rigid Dispersed Phases," *AIChE Journal* **50** (2), 311-321 (2004).

10. T. Moore and W.J. Koros, "Non-Ideal Effects in Organic-Inorganic Materials for Gas Separation Membranes," *Journal of Molecular Structure* **739** (1-3), 87-98 (2005).

11. G. Choudalakis, A. Gotsis, "Permeability of Polymer/Clay Nanocomposites: A Review," *European Polymer Journal* **45** (4), 967-984 (2009).

12. A. Manninen, H. Naguib, A. Nawaby, and M. Day, "CO_2 Sorption and Diffusion in Polymethyl Methacrylate-Clay Nanocomposites," *Polymer Engineering and Science* **45** (7), 904-914 (2005).

13. L. Khounlavong and V. Ganesan, "Influence of Interfacial Layers Upon the Barrier Properties of Polymer Nanocomposites," *Journal of Chemical Physics* **130** (10), 12 (2009).

14. K. Wang, S. Liang, J. Deng, H. Yang, Q. Zhang, Q. Fu, X. Dong, D. Wang, and C. Han, "The Role of Clay Network on Macromolecular Chain Mobility and Relaxation in Isotactic Polypropylene/Organoclay Nanocomposites," *Polymer* **47** (20), 7131-7144 (2006).

15. R. Aringhieri, "Nanoporosity Characteristics of Some Natural Clay Minerals and Soils," *Clays and Clay Minerals* **52** (6), 700-704 (2004).

16. L. Aylmore, "Gas Sorption in Clay Mineral Systems," *Clay and Clay Materials* **22**, 175-183 (1974).

17. S. Yariv and H. Cross (eds), *Organo-Clay Complexes and Interactions*. (Marcel Dekker, Inc., New York, NY, 2002).

18. N. Schamp and J. Huylebroeck, "Adsorption of Polymers on Clays," *Journal of Polymer Sicence: Polymer Symposia* **42** (2), 553-562 (1973).

CHAPTER 6

CELLULOSE ACETATE-LAPONITE® RD HYBRID DENSE FILM MEMBRANES

6.1 Overview

Cellulose Acetate was chosen as a prototype polymer for this work because of its hydrophilic constituents and commercial relevance.[1] In this chapter we will present the reader with two firm conclusions: (1) the preparation procedures presented in Chapter 3 are in fact effective for the manufacture of hybrid membranes and (2) these membranes exhibit desirable permeation properties thereby proving the efficacy of the polymer-filler matching. Dense film permeation measurements are the basis for these conclusions, but are complemented by microscopic characterization. We will also compare the performance of these hybrid membranes with the predicted performance according to the mathematical models.

Permeation measurements of the hybrid dense films containing 1wt% nanoclay suggest that the polymer and particle are miscible – or at least partially. TEM micrographs provided further evidence that the preparation procedure yields a membrane with exfoliated nanoplatelet filler. These results did, however, present some reproducibility issues and therefore have been removed to Appendix D. This chapter will focus on the films containing 3wt% and 5wt% nanoclay loadings and their gas transport properties.

6.2 Characterization of Cellulose Acetate Dense Films: A Control Study

Transport properties for cellulose acetate membranes is very well known and discussed in depth throughout the literature.[2-4] These properties are also quite consistent as we

observed independently of this study. In other words, casting solvent and appropriate drying conditions will generally produce results that are in good agreement with accepted results for the base polymer, which provides good control films using the procedures developed for the nanocomposite films.

Unlike the subsequent hybrid films, we did not use any microscopic techniques to characterize these films, since the control films contain no filler material, and microscopy characterization would be meaningless.

6.2.1 Permeability of Control Membranes

Casting solutions for the control membranes were made using the shear mixing protocol previously discussed. We did, however, neglect the first two mixing stages since there is no inorganic filler to disperse. After casting, the films were subjected to the same drying/annealing protocol that was used for the hybrid membranes. Permeabilities and selectivities as a function of feed pressure for the three test gases are presented in Figure 6.1. These results are further illustrated in Table 6.1 for convenient comparison.

Table 6.1: Average Permeability (Barrers) & Selectivity Values for Cellulose Acetate Control Film at Different Feed Pressures.

Feed Gas	**Feed Pressure**		
	50 psia	*75 psia*	*100 psia*
Helium	14.75 ±1.87	14.55 ±2.14	14.27 ±2.38
Oxygen	0.681 ±0.044	0.659 ±0.077	0.650 ±0.064
Nitrogen	0.115 ±0.002	0.109 ±0.007	0.108 ±0.008
O_2/N_2 Selectivity	5.92 ±0.27	6.04 ±0.32	6.02 ±0.12

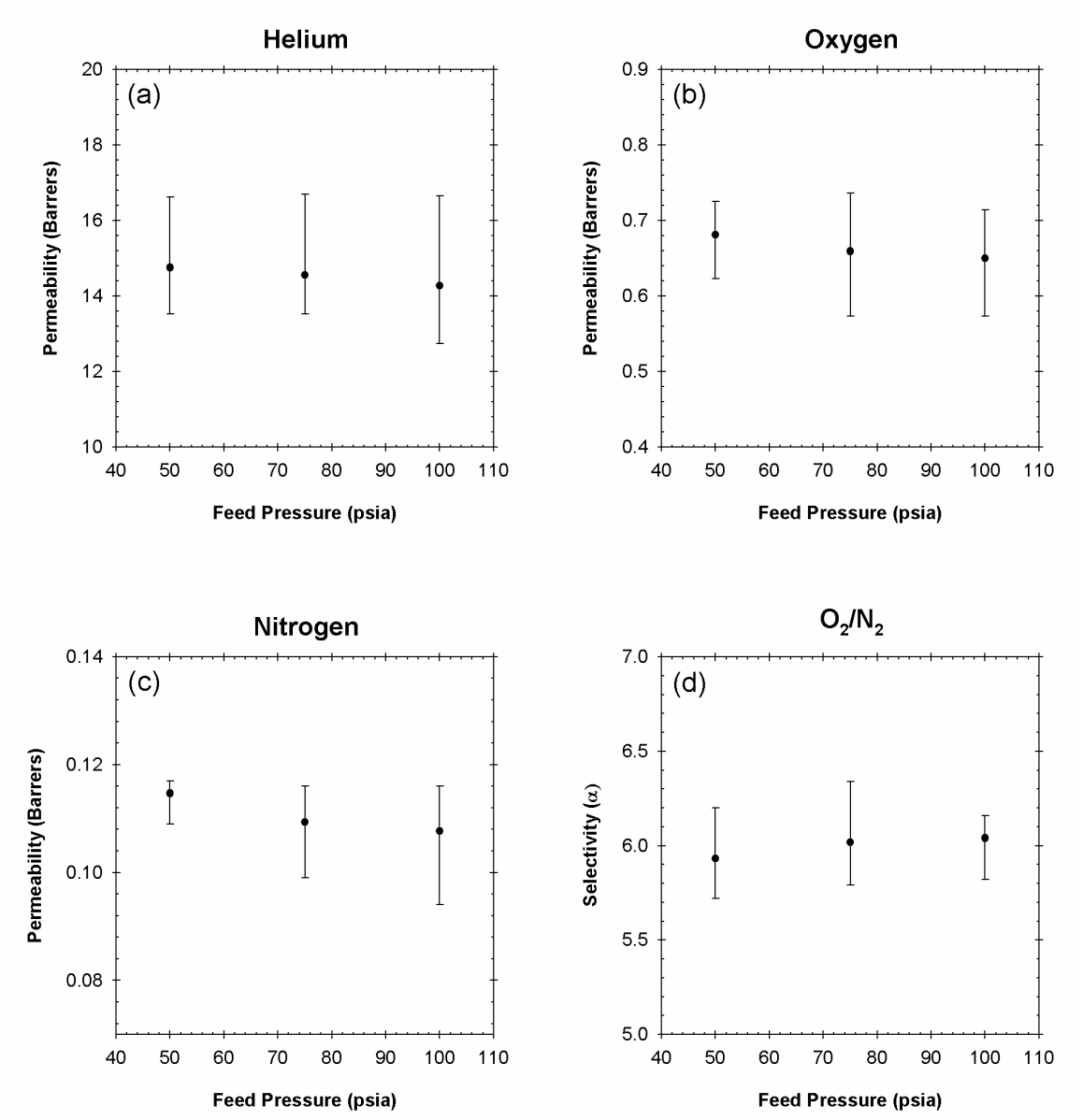

Figure 6.1: Permeability properties of Cellulose Acetate dense film membranes. (a) Helium (b) Oxygen (c) Nitrogen (d) O_2/N_2 Selectivity

6.3 Characterization of Cellulose Acetate-Laponite® RD Dense Film Membranes Containing 3wt% Nanoclay

It is expected that a hybrid membrane containing 3wt% Laponite® RD in cellulose acetate should exhibit permeability depressions between ~10-20% according to mathematical predictions. We cast and characterized such films and found our permeation results compared well with predicted values. Agreement with the model model predictions suggests that the hybrid membranes are comprised of highly exfoliated and dispersed filler.

6.3.1 Permeability of Hybrid Membranes Containing 3wt% Nanoclay

We found that hybrid membranes with 3wt% nanoclay filler showed very promising permeation results. For all penetrants and pressures the permeabilities were reduced significantly. Moreover, the variability in the measurements was quite small compared to pure polymer films. The average permeabilities and selectivities are presented in Table 6.2. Additionally, the permeability trends for each penetrant are plotted in Figure 6.2 along with the corresponding pure polymer values.

Table 6.2: Average Permeability (Barrers) & Selectivity Values for Cellulose Acetate-Laponite® RD Nanocomposite Films Containing 3wt% Nanoclay Filler at Different Feed Pressures.

Feed Gas	**Feed Pressure**		
	50 psia	*75 psia*	*100 psia*
Helium	11.72 ±0.05	11.78	11.60 ±0.18
Oxygen	0.562 ±0.018	0.558	0.542 ±0.012
Nitrogen	0.096 ±0.003	0.095	0.094 ±0.001
O_2/N_2 Selectivity	5.85 ±0.01	5.87	5.76 ±0.04

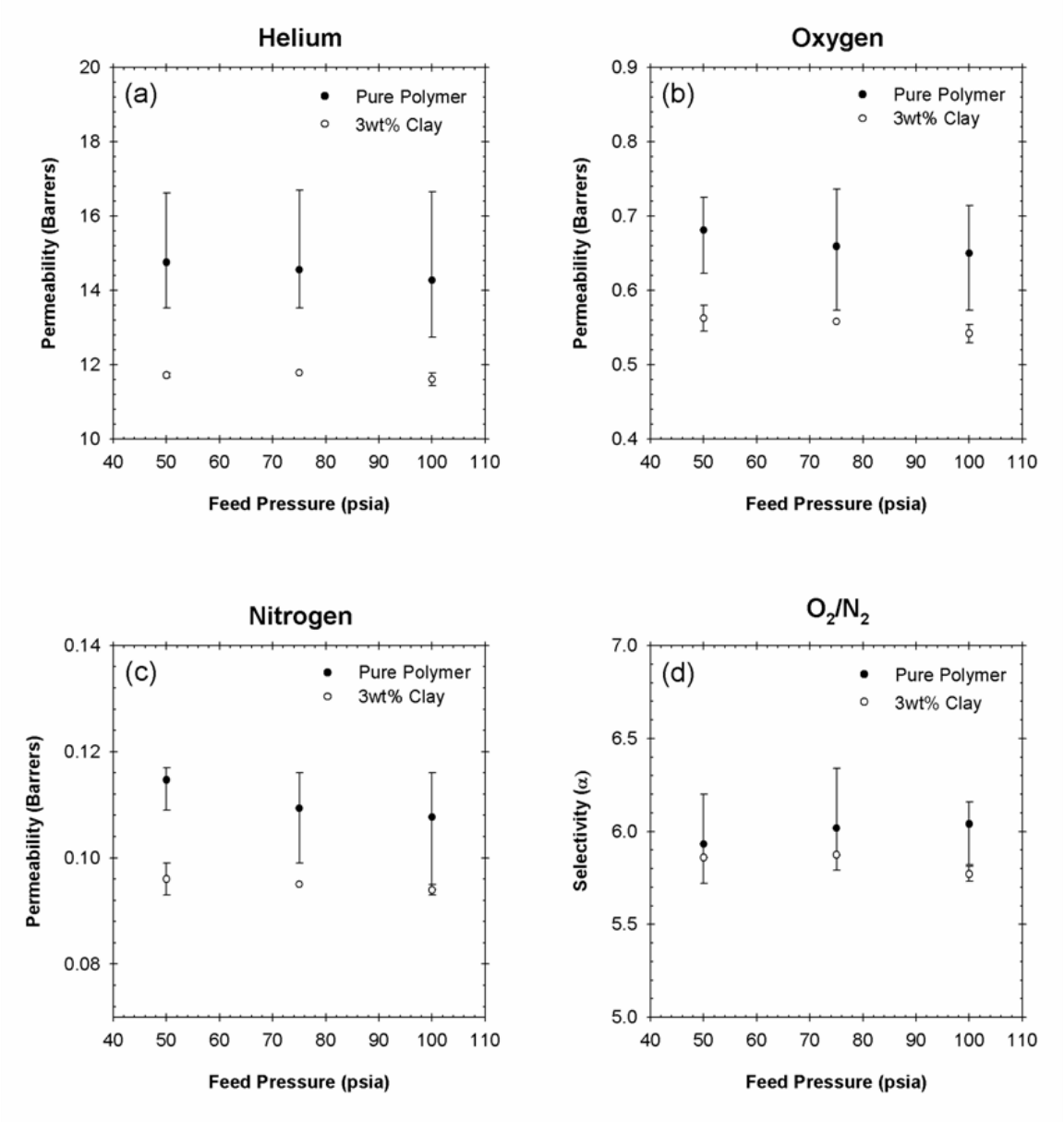

Figure 6.2: Permeability properties of Cellulose Acetate-Laponite® RD nanocomposite dense film membranes containing 3wt% nanoclay filler. (a) Helium (b) Oxygen (c) Nitrogen (d) O_2/N_2 Selectivity

Error bars are not available for permeabilities corresponding to a feed pressure of 75psia. Early in this work we only considered feed pressure of 50 and 100psia. Measurements at 75psia were added to more confidently represent permeability trends with respect to increasing feed pressure. We see that the data at 75psia is in line with the other values. Measurements on other hybrid films support the existence of a trend.

In the previous hybrid membrane tests for Torlon® presented in Chapter 5 it was observed that there was a trend in the permeability reduction with respect the gas penetrant kinetic diameter. We will consider these effects in a later section. For the time being, we have presented the normalized permeabilities and selectivities in Table 6.3.

Table 6.3: Average P/P_0 and α/α_0 values for Cellulose Acetate-Laponite® RD nanocomposite films containing 3wt% nanoclay filler at different feed pressures.

Feed Gas	**Feed Pressure**		
	50 psia	*75 psia*	*100 psia*
Helium	0.79	0.81	0.81
Oxygen	0.83	0.85	0.83
Nitrogen	0.84	0.87	0.87
O_2/N_2 Selectivity	0.99	0.98	0.96

Ideally, the incorporation of impermeable filler into a polymer matrix should affect the permeability of all penetrants equally. According to the values reported in Table 6.3, we have a membrane that presents near-ideal permeation properties. The normalized selectivities are very close to one which indicates that the presence of the filler material does not introduce permselective anomalies. Individual values for normalized permeability further support this conclusion. All values for P/P_0 are within a 5% range of the mean value.

6.3.2 Comparison of Experimental Permeation Results to Model Permeability Predictions

When we compare our measured permeabilities (normalized) with the selected models we see that our data are bounded by predicted values using the Nielsen and Bharadwaj equations. These results are presented in Figure 6.3. It is very encouraging that the measured values closely match predicted values. This suggests that the filler is highly exfoliated and dispersed. Microscopic characterization was used to probe the membrane morphology even further. These results are presentd in Section 6.5 of this chapter.

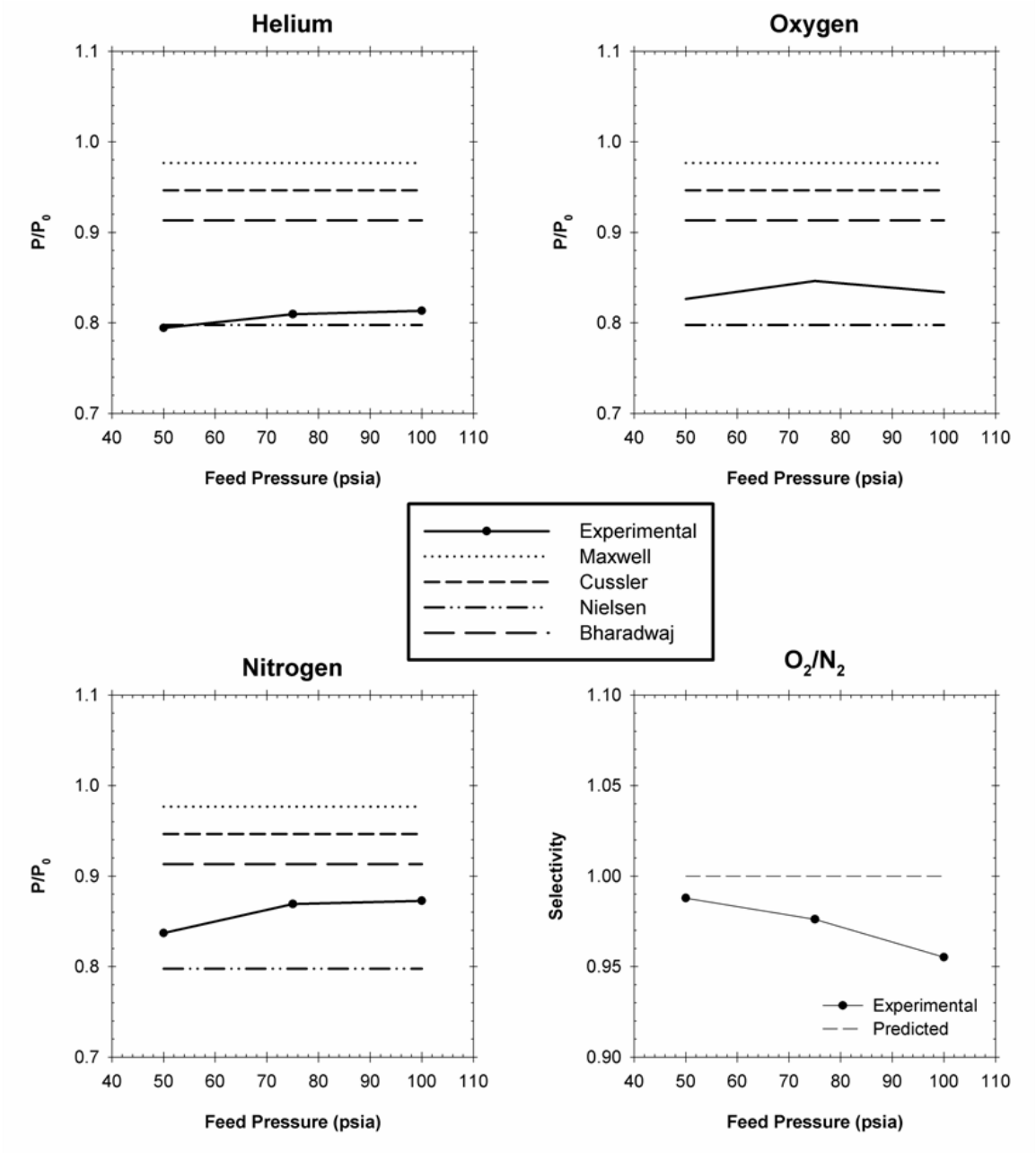

Figure 6.3: Average P/P_0 and α/α_0 values for Cellulose Acetate-Laponite® RD nanocomposite films containing 3wt% nanoclay filler at different feed pressures compared to predicted values using various transport models. Filler particle aspect ratio was assumed to be 30 for model calculations and S=0 for the Bharadwaj model.

6.4 Characterization of Cellulose Acetate-Laponite® RD Dense Film Membranes Containing 5wt% Nanoclay

Transitioning from 3wt% to 5wt% filler should greatly increase the effects on transport properties of the hybrid membranes. Model predictions show expected permeability depressions on the order of ~15-30%. This was proven to be a correct assumption – largely. Comparing experimental values to model predictions showed very good agreement.

6.4.1 Permeability of Hybrid Membranes Containing 5wt% Nanoclay

The measured permeabilities for dense films containing 5wt% Laponite® RD in a cellulose acetate matrix show considerable depression compared to pure polymer values. Reductions between 15~30% were observed for different penetrants at different feed pressures. These values are well outside the range of error. Nitrogen showed the largest depression and helium the least. Calculated ideal permselectivities were consistent at all feed pressures, but are observed to be slightly higher (~3%) than average pure polymer values.

Permeability versus feed pressure plots are shown in Figure 6.4 with pure polymers plotted for reference. Average permeability and selectivity values are displayed in Table 6.4 for convenience.

Table 6.4: Average Permeability (Barrers) & Selectivity Values for Cellulose Acetate-Laponite® RD Nanocomposite Films Containing 5wt% Nanoclay Filler with Different Feed Pressures.

Feed Gas	**Feed Pressure**		
	50 psia	*75 psia*	*100 psia*
Helium	12.33 ±0.19	12.22 ±0.18	12.23 ±0.22
Oxygen	0.490 ±0.006	0.496 ±0.004	0.501 ±0.007
Nitrogen	0.078 ±0.001	0.079 ±0.003	0.080 ±0.004
O_2/N_2 Selectivity	6.28 ±0.11	6.28 ±0.15	6.26 ±0.19

Following the same format as the previous sections, we have calculated normalized permeability and selectivity values to elucidate any trends. These data are presented in Table 6.5 below. As was the case for data presented in Chapter 5, for hybrid films containing 5wt% filler in a Torlon® matrix (see Table 5.7), we see a trend whereby the permeability depression decreases as a function of penetrant kinetic diameter. Our observations suggest that there are anomalous macro- or micro-defects contributing to the membrane performance. We will revisit this issue in Sections 6.4.

Table 6.5: Average P/P_0 and α/α_0 values for Cellulose Acetate-Laponite® RD nanocomposite films containing 5wt% nanoclay filler at different feed pressures.

Feed Gas	**Feed Pressure**		
	50 psia	*75 psia*	*100 psia*
Helium	0.836	0.840	0.857
Oxygen	0.721	0.752	0.771
Nitrogen	0.676	0.727	0.747
O_2/N_2 Selectivity	1.067	1.038	1.032

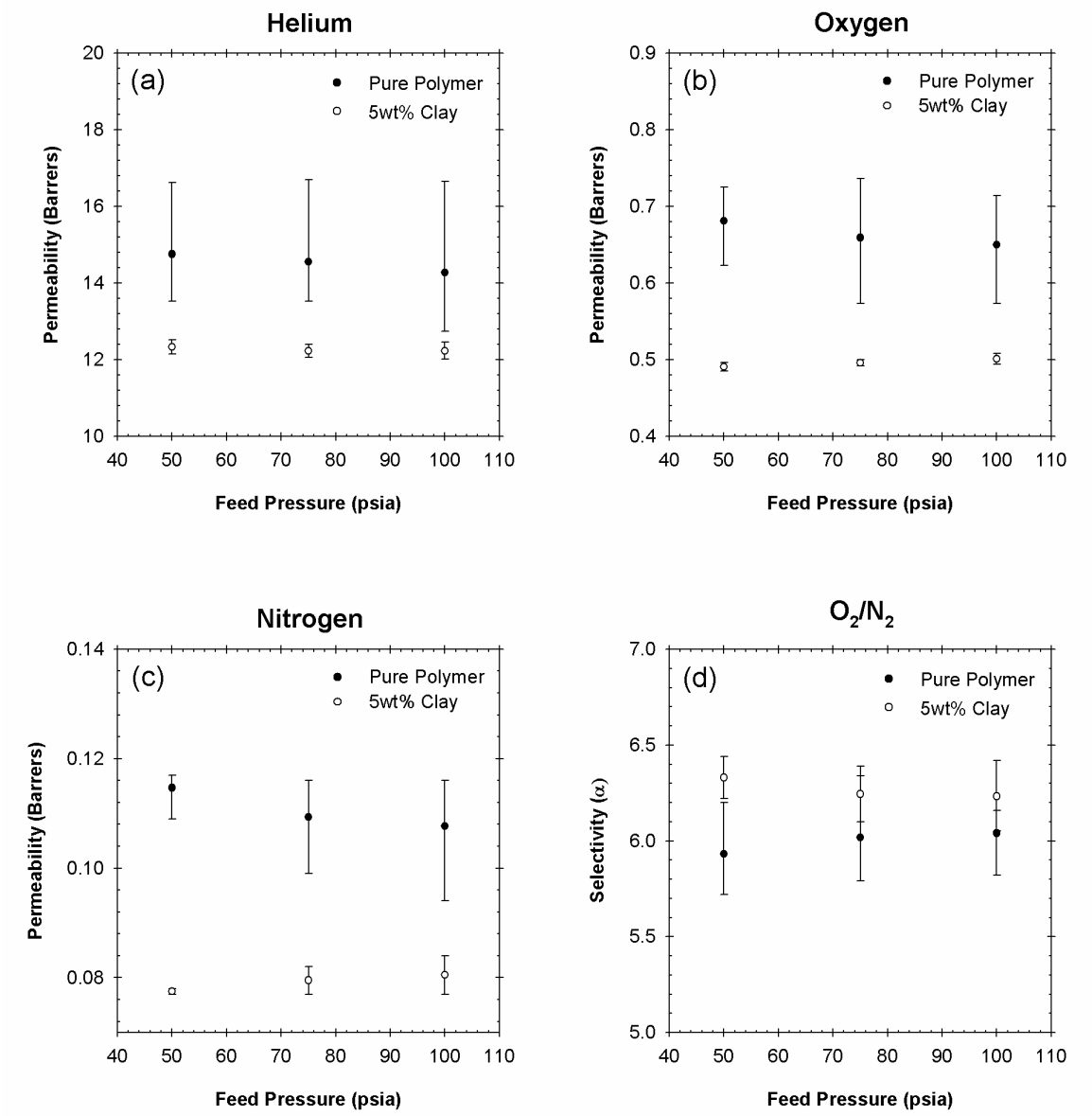

Figure 6.4: Permeability properties of Cellulose Acetate-Laponite® RD nanocomposite dense film membranes containing 5wt% nanoclay filler. (a) Helium (b) Oxygen (c) Nitrogen (d) O_2/N_2 Selectivity

6.4.2 Comparison of Experimental Permeation Results to Model Permeability Predictions

In the previous example we found that our experimental values were within the bounds of the various model predictions. The same observations have been made for hybrid films presented in this section. Figure 6.5 shows the corresponding plots for average normalized permeabilities with respect to the model predictions for these films.

We should note that that the normalized experimental permeabilities for oxygen and nitrogen are different, which is unexpected. Recall that the model predictions assume that the permeability for all penetrants will be effects equally because filler geometry is the only influencing variable. As such, P/P_0 is constant. From the data we see that the permeability of the larger penetrant, nitrogen, is effected more dramatically. This evidence indicates that there are non-uniformities in the membrane that selectively effect permeability. We will discuss this observation in greater detail in the next section.

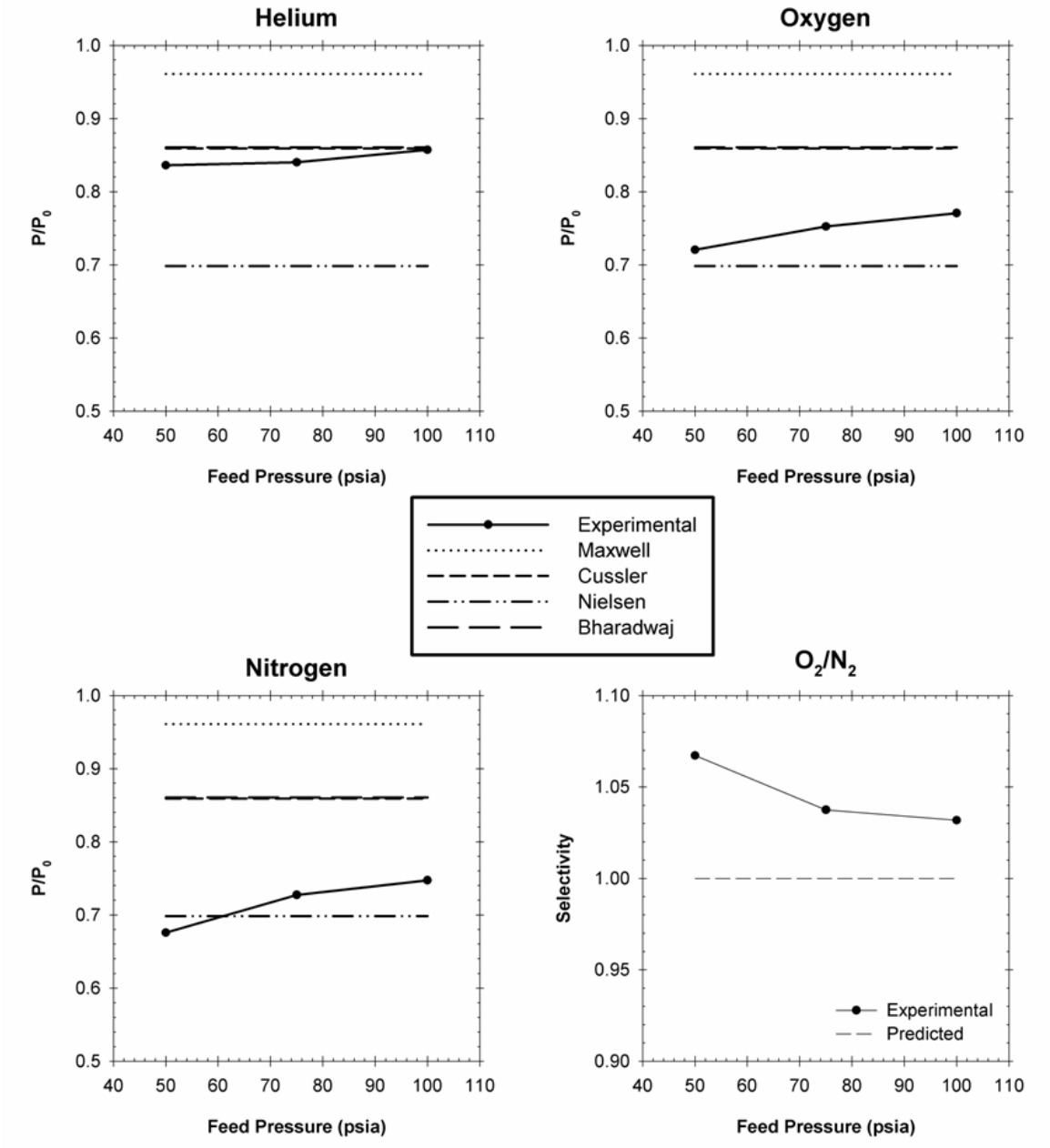

Figure 6.5: Average P/P_0 and α/α_0 values for Cellulose Acetate-Laponite® RD nanocomposite films containing 5wt% nanoclay filler at different feed pressures compared to predicted values using various transport models. Filler particle aspect ratio was assumed to be 30 for model calculations and S=0 for the Bharadwaj model.

6.5 Analysis of Permeability Trends with Respect to Gas Penetrant

In the previous sections we commented on apparent trends in permeability depression for each hybrid loading. It was observed that normalized permeability in the hybrid membranes is a function of the penetrant kinetic diameter. We would like to expand on this topic and discuss the observation further. For convenience we have combined the permeability and selectivity measurements for all membrane types tested and presented the average values in Figure 6.6.

Upon first glance, the permeability data does not provide any significant insight because the trends as a whole do not exhibit any particular pattern. However, if we look closely at the selectivity data we can see that there are some anomalies with respect to expected values. Films with 3wt% nanoclay filler follow a trend that closely matches pure polymer – as expected. On the other hand, films with 5wt% nanoclay filer exhibit a slightly higher permselectivity than the pure polymer. This suggests that there may be physical characteristics that are illustrated by this trend.[5,6]

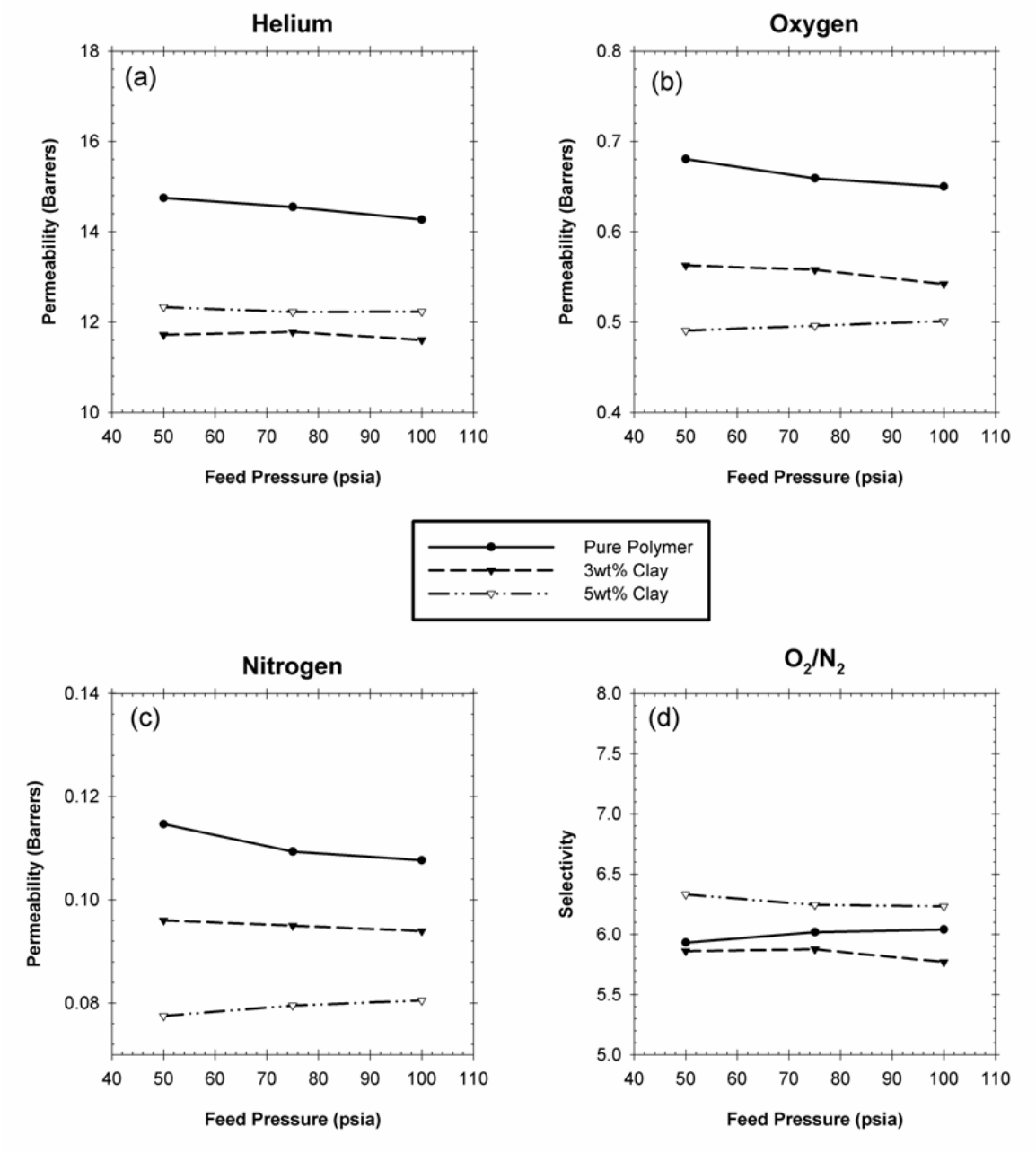

Figure 6.6: Comparison of Average Permeability Properties of Cellulose Acetate and Cellulose Acetate-Laponite® RD Nanocomposite Dense Film Membranes Containing Different Nanoclay Loadings. (a) Helium (b) Oxygen (c) Nitrogen (d) O_2/N_2 Selectivity

6.5.1 Permeability Trends in Cellulose Acetate-Laponite® RD Dense Film Membranes as a Function of Gas Penetrant Kinetic Diameter

In the event that angstrom sized defects exist at the polymer-platelet interface, gas penetrants of different sizes may magnify this effect through permeation measurements.[7-9] In this study, permeation values for films containing 5wt% nanoclay filler suggest that such an analysis is possible. On the other hand, films containing 3wt% filler exhibit a more ideal trend. For the purposes of these analyses we have plotted averaged P/P_0 as a function of gas penetrant kinetic diameter for each filler fraction. These data are shown in Figures 6.7 and 6.8.

Dense films with 3wt% filler did not show such a significant deviation from the expected value (see Figure 6.7). In fact, one could suggest that the opposite effect occurred because there is a slight increase in the normalized permeability with increasing kinetic diameter. Such an effect would be a result of Knudsen based diffusion and therefore an indication that there are nano-sized defects.[10] This is not impossible, but we do not believe that the observed variability is significant enough to confidently make this claim.

On the hand, a negative slope exists in the trends shown in Figure 6.8 as a function of increasing gas penetrant kinetic diameter for the membranes containing 5wt% nanoclay filler. Between helium and oxygen there is a decrease in P/P_0 of ~10%. Then, between oxygen and nitrogen the change is on the order of ~5%. This trend suggests that there are non-uniformities at the polymer-particle interface. As suggested earlier, such an apparent non-uniformity creates a more selective membrane. In all likelihood the apparent non-uniformity is due to a *zone of influence* around the particle and the platelet surface. While it is possible that independent interactions exist between the gases (oxygen and nitrogen) and platelet, sorption studies suggest that the clay is non-selectively sorbing (see Section 6.4.2). This suggests that there is in fact the polymer is not uniform throughout the system and potentially “structured” near the platelet surface. Pressure-decay gas sorption is used to further elucidate these results.

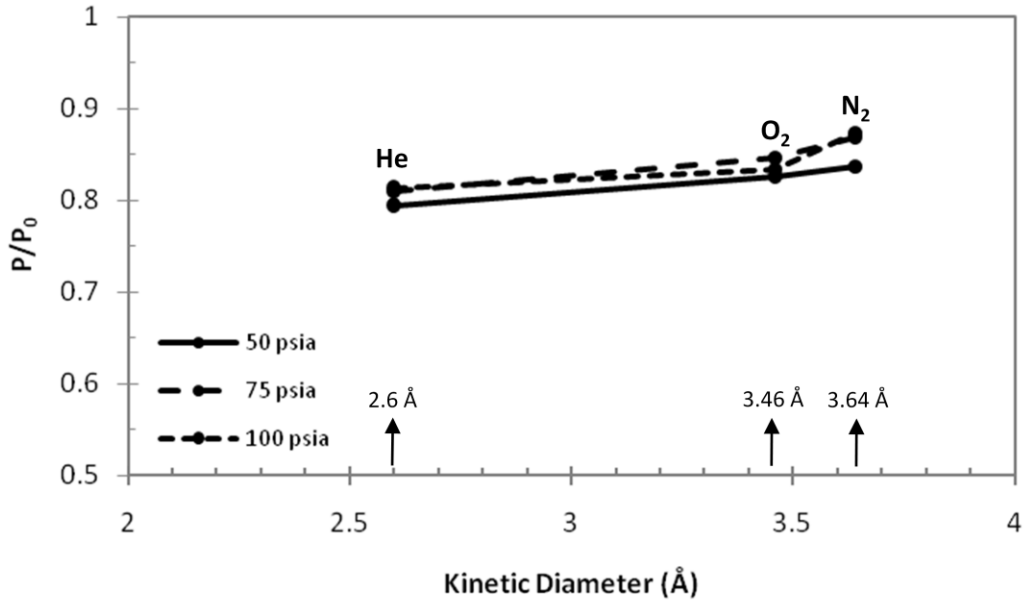

Figure 6.7: Permeability depression in Cellulose Acetate-Laponite® RD hybrid membrane containing 3wt% nanoclay as a function of kinetic diameter of gas penetrant.

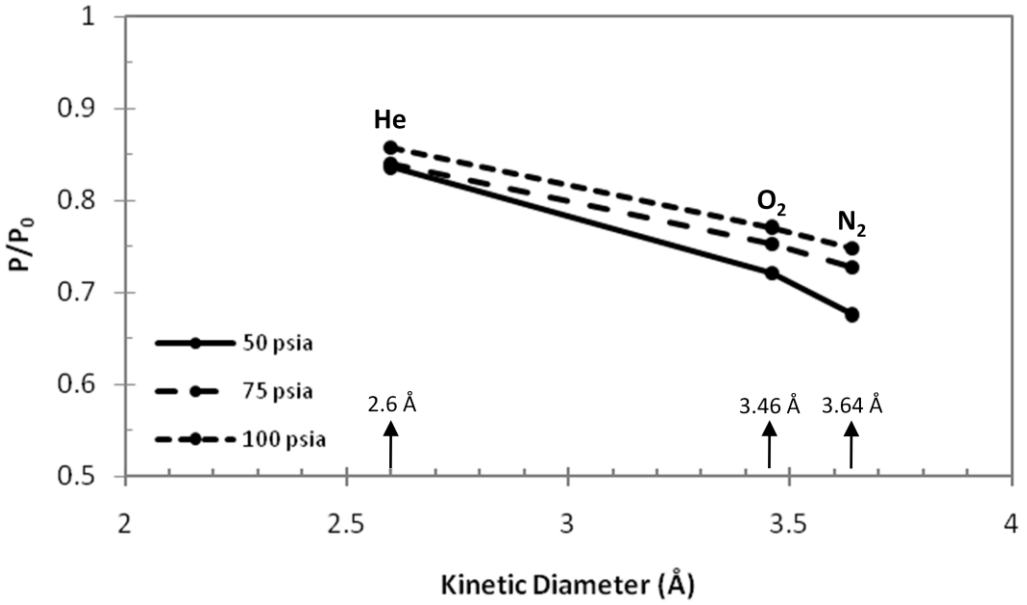

Figure 6.8: Permeability depression in Cellulose Acetate-Laponite® RD hybrid membrane containing 5wt% nanoclay as a function of kinetic diameter of gas penetrant.

6.5.2 Gas Sorption in Cellulose Acetate-Laponite® RD Hybrid Dense Film Membranes

In the previous section we presented evidence that suggests that packing disruptions may exist in the hybrid membranes, especially in the zone of influence around the filler material. We have used pressure decay sorption measurements to probe the hybrid membrane and base materials in order to improve our understanding of the permeation phenomena. Sorption tests were conducted on pure polymer films, unmodified clay and hybrid membranes containing 5wt% nanoclay filler. Hybrid membranes with different loadings were not considered due to time limitations.

Oxygen and nitrogen sorption isotherms for pure polymer film and as-received, unexfoliated clay are shown in Figure 6.9. Henry's and Langmuir dual-mode sorption parameters (see Eq. 2.7) for these isotherms and materials are presented in Table 6.6. We should note that measurements were not carried out at high pressures because it is outside of the range of interest. The unexfoliated clay exhibited a Henry's only regime such that the concentration, C_D, is the product of the Henry's coefficient, k_D, and the feed pressure, p_i. Moreover, the clay does not appear to have a solubility selectivity in this pressure range.

Table 6.6: Henry's and Langmuir sorption parameters for Cellulose Acetate and Laponite® RD

	Cellulose Acetate		Laponite® RD	
Parameter	*Oxygen*	*Nitrogen*	*Oxygen*	*Nitrogen*
k_D	0	0	0.105	0.108
C'_H	18.637	11.86	-	-
b	0.003	0.004	-	-

As shown in Chapter 5, we can use the sorption parameters obtained for the pure components to predict the isotherm for the hybrid material. We also noted in the previous chapter that there are two approaches to predicting these isotherms. Discussion regarding the two approaches is provided in Section 5.5.2 as well as the governing equations.

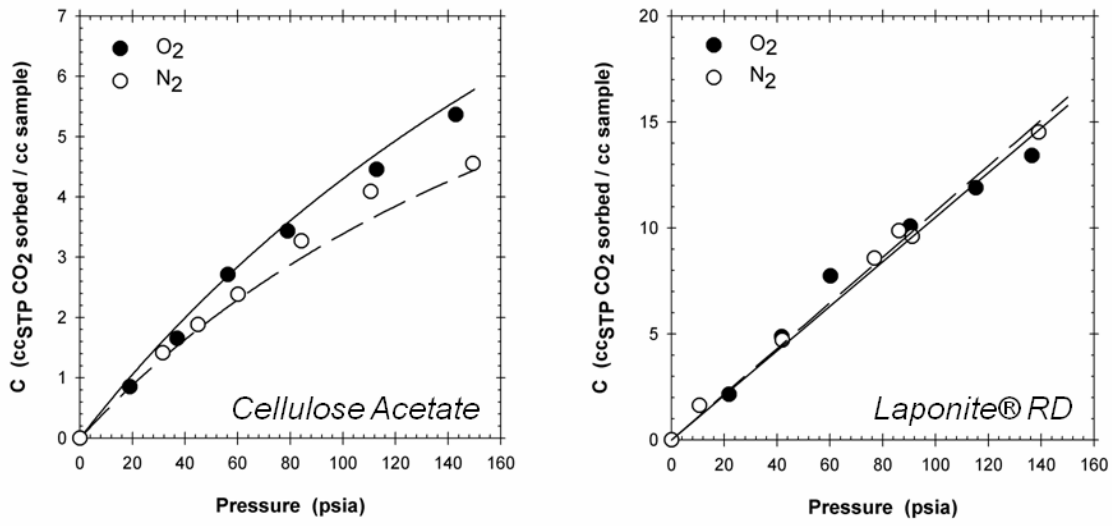

Figure 6.9: Sorption isotherms for oxygen and nitrogen in a Cellulose Acetate dense films and unmodified Laponite® RD powder.

Sorption measurements were repeated in the pressure range of interest on the hybrid films. The data and fitted curves for oxygen and nitrogen measurements are shown in Figure 6.10. Predicted values for the hybrid materials based on Equation 5.1 are also shown. Calculated dual-mode sorption parameters for the hybrid, based on experimental data, are presented in Table 6.7.

Table 6.7: Dual-Mode sorption parameters for hybrid Cellulose Acetate membrane containing 5wt% Laponite® RD filler

Cellulose Acetate – 5wt% Laponite® RD		
Parameter	*Oxygen*	*Nitrogen*
k_D	0.018	0.037
C'_H	5.504	1.175
b	0.007	0.022

Experimental and predicted values for oxygen sorption in the hybrid membrane are in good agreement which would indicate that the membrane is homogenous. Nitrogen isotherms, on the other hand, deviate between experimental and predicted values. This

is likely a result of proposed non-uniformities in the hybrid membrane because it was shown that the neat clay does not selectively sorb this gas pair. We see further evidence of these apparent anomalies when comparing diffusion coefficients in each system (neat and hybrid).

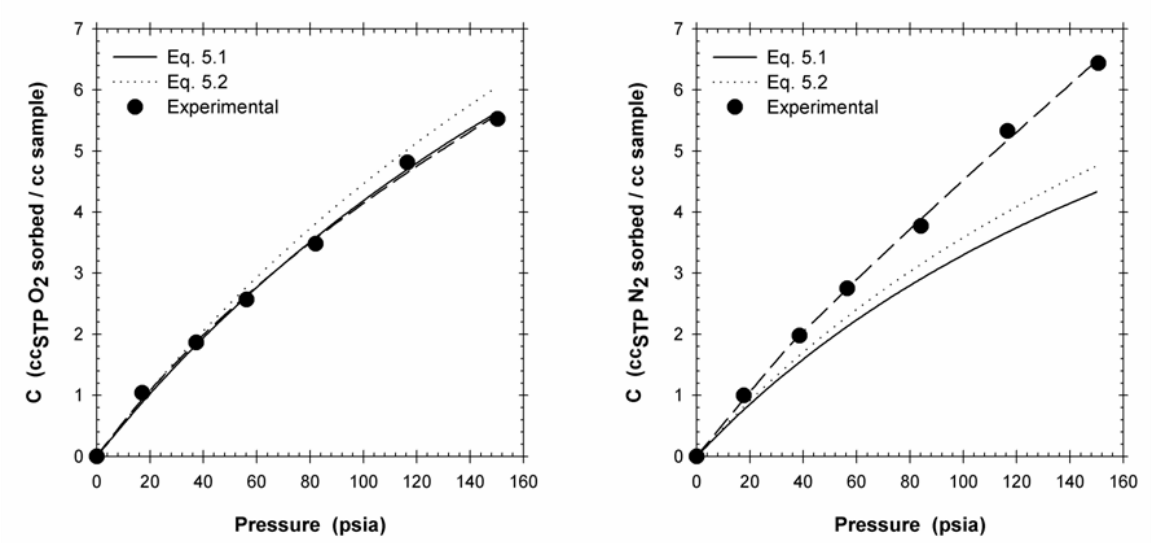

Figure 6.10: Sorption isotherms for oxygen and nitrogen in a Cellulose Acetate hybrid films containing 5wt% nanoclay filler. Predicted trends based on additive contributions for pure polymer and clay particles are plotted as well.

6.5.3 Penetrant Diffusion in Pure and Hybrid Membranes

First, we will maintain our assumption that the clay filler is impermeable. This is certainly true, so the normalized diffusion coefficients (D/D_0) should be the same in an ideal polymer-platelet nanocomposite. We have, however, already shown that the solubility is not consistent with predicted values. Using the solubility values calculated from dual-mode trends and experimental permeation values, we have calculated the diffusion coefficient of oxygen and nitrogen in the pure polymer and hybrid membranes. These values are reported in Table 6.8.

Two conclusions are immediate based on the data in Table 6.8. Diffusive selectivity between the two membranes is different and the ratio of pure and hybrid coefficients is not equal for each gas. We have graphically represented these observations in Figure 6.11. In the figure it is made more apparent that the depression in diffusivity for nitrogen is significantly higher than oxygen in the hybrid membrane. This is supported by the increase in diffusive selectivity. A logical explanation for this observation is the rigidified matrix concept that we introduced in Chapter 1. According to the literature, chain immobilization around the filler is likely responsible for this phenomenon.[7-9]

Additional sorption and permeation measurements with different penetrants and pressures – as well as different filler loadings – should be completed to develop a better understanding of this trend.

Table 6.8: Oxygen and nitrogen diffusion coefficients for Cellulose Acetate and Cellulose Acetate hybrid films containing 5wt% Laponite® RD as calculated from permeability and sorption measurements. All values reported in [cm^2/s]

	Cellulose Acetate		**Laponite® RD**	
Pressure (psia)	D_{O2} (cm^2/s)	D_{N2} (cm^2/s)	D_{O2} (cm^2/s)	D_{N2} (cm^2/s)
50	$7.24 \cdot 10^{-9}$	$1.50 \cdot 10^{-9}$	$5.28 \cdot 10^{-9}$	$8.17 \cdot 10^{-10}$
75	$7.46 \cdot 10^{-9}$	$1.54 \cdot 10^{-9}$	$5.78 \cdot 10^{-9}$	$8.71 \cdot 10^{-10}$
100	$7.81 \cdot 10^{-9}$	$1.65 \cdot 10^{-9}$	$6.24 \cdot 10^{-9}$	$9.15 \cdot 10^{-10}$

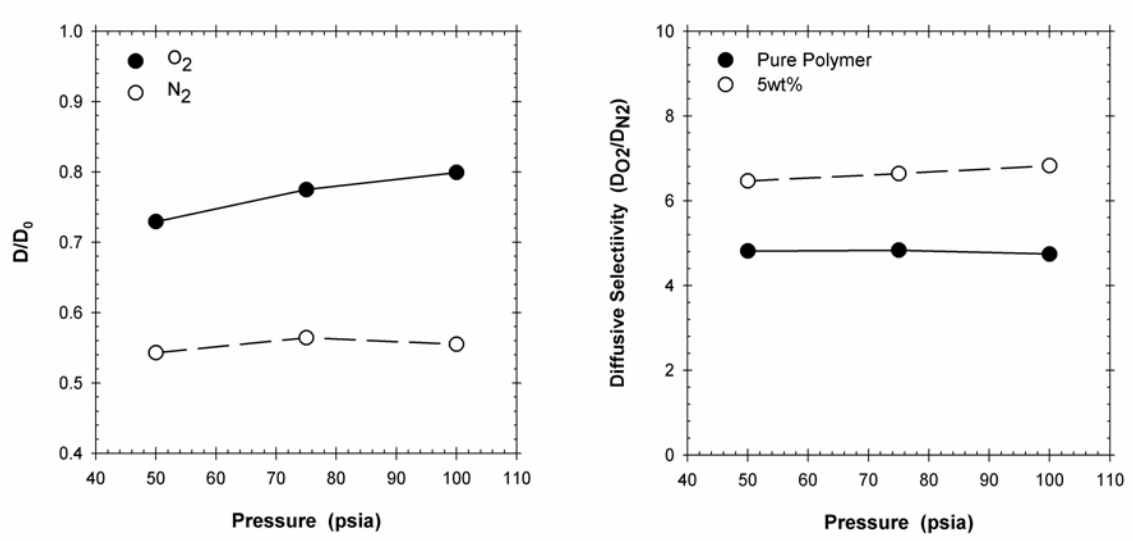

Figure 6.11: Data for oxygen and nitrogen diffusion in Cellulose Acetate and Cellulose Acetate hybrid films containing 5wt% Laponite® RD as calculated from permeability and sorption measurements. (i) Normalized diffusion coefficients for oxygen and nitrogen (ii) Diffusive selectivity in pure and hybrid membranes

6.6 Microscopic Characterization and Analysis of Cellulose Acetate-Laponite® RD Hybrid Membranes

It has been shown that a cellulose acetate hybrid membranes with nanoclay filler exhibit promising permeation properties. These transport properties suggest that the nanoplatelets are well exfoliated and that the polymer is well adhered to the particle surface. The TEM images presented as Figures 6.12 support this conclusion. When compared to model predictions the transport properties compared very well. These near perfect results raised suspicion. The Nielsen model, for instance, assumes that the platelets are evenly dispersed and aligned orthogonal to the direction of transport.[11] Alternatively, the Bharadwaj model accounts for incongruities in the particle orientation – but it is still assumed that the particles are evenly distributed within the matrix.[12] Realistically, it was unlikely that our membranes satisfied these assumptions. We used transmission electron microscopy (TEM) to probe the membrane morphology to consider this additional aspect.

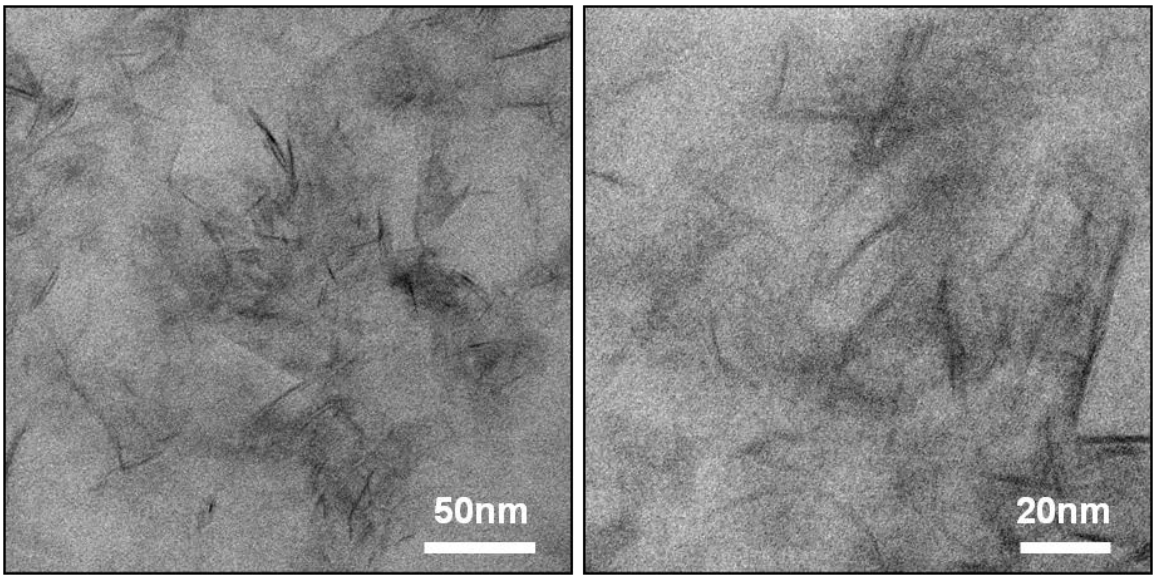

Figure 6.12: Transmission electron micrographs showing exfoliated nanoclays in a cellulose acetate hybrid membrane containing 5wt% filler

The TEM images presented in Chapter 5 and those presented here in Figure 6.12 show strong evidence of nanoplatelet exfoliation. Moreover, we see that these platelets do not have a consistent orientation in the matrix. This would suggest that platelet morphology does satisfy the model constraints. If we look at these materials from a more global perspective, however, the TEM images suggest otherwise. In Figures 6.13 and 6.14 we have presented two images corresponding to cellulose acetate films with 3wt% Laponite® RD filler. This microscopic evidence suggests that the permeation reductions are likely due to expansive floccs in the polymer matrix. Coincidently the contributing effect of these floccs is roughly equivalent to the other extreme wherein the platelets are solitary in the matrix.

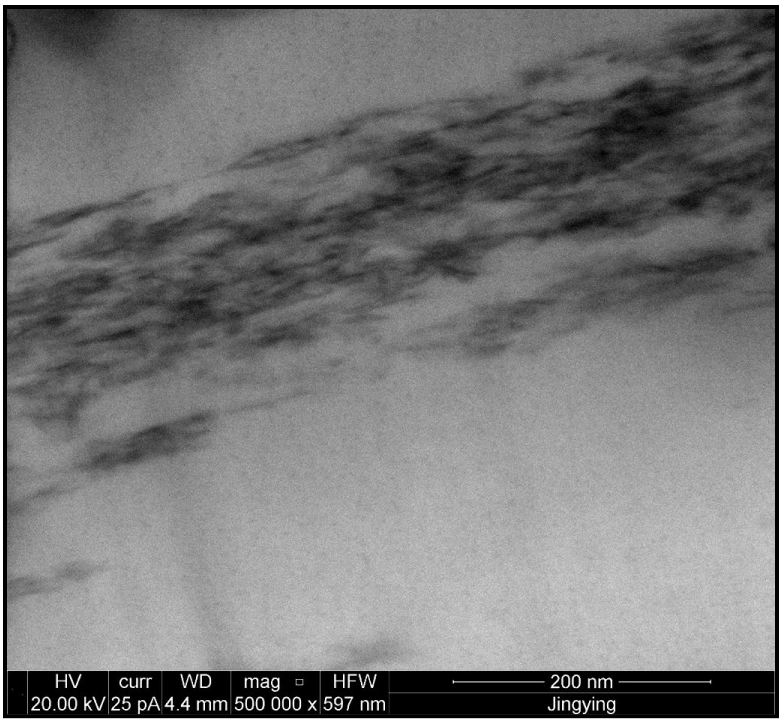

Figure 6.13: Transmission electron micrograph of Cellulose Acetate-Laponite® RD nanocomposite film containing 3wt% nanoclay filler showing evidence of flocculation.

In Figure 6.13 we present a highly magnified image of the membrane morphology. The dark "milky way" band in the image represents the clays and the light gray portion is the polymer matrix. Based on the density and size of the dark band the clays are severely flocculated. This morphology is reminiscent of complex flocc structure evidenced by Pignon, et al for Laponite® RD nanoclays.[13] On a plus side, if polymer is well incorporated into the flocc micro/macropores and if the polymer is well adhered then the flocc will significantly influence the permeability (as observed). Reducing the magnification may provide further insight into the general morphology of the nanocomposite.

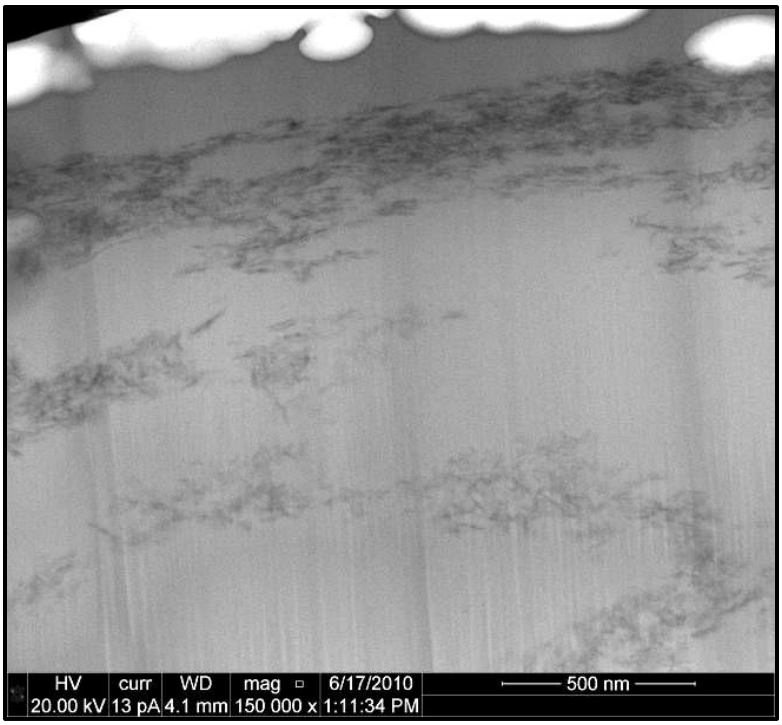

Figure 6.14: Transmission electron micrograph of Cellulose Acetate-Laponite® RD nanocomposite film containing 3wt% nanoclay filler showing a dispersed phase of amorphous floccs/agglomerates.

When the magnification is reduced (Figure 6.14), we see that the flocc morphology is quite prevalent. This supports the previous observation that the nanoclays are in fact not well dispersed in the polymer matrix. Although this result is slightly discouraging, it does not refute the permeation measurements. Based on the TEM micrographs we can see that the permeability depressions are predominately a result of extended floccs in the polymer matrix.

After seeing these flocc effects in the cellulose acetate hybrid films, we decided to look at the Torlon® hybrid films with the same perspective. A similar flocc morphology was observed at lower magnifications as shown in Figure 6.15. Despite this observation, we are still confident that the hybrid membrane transport properties are accurate, which is our ultimate objective.

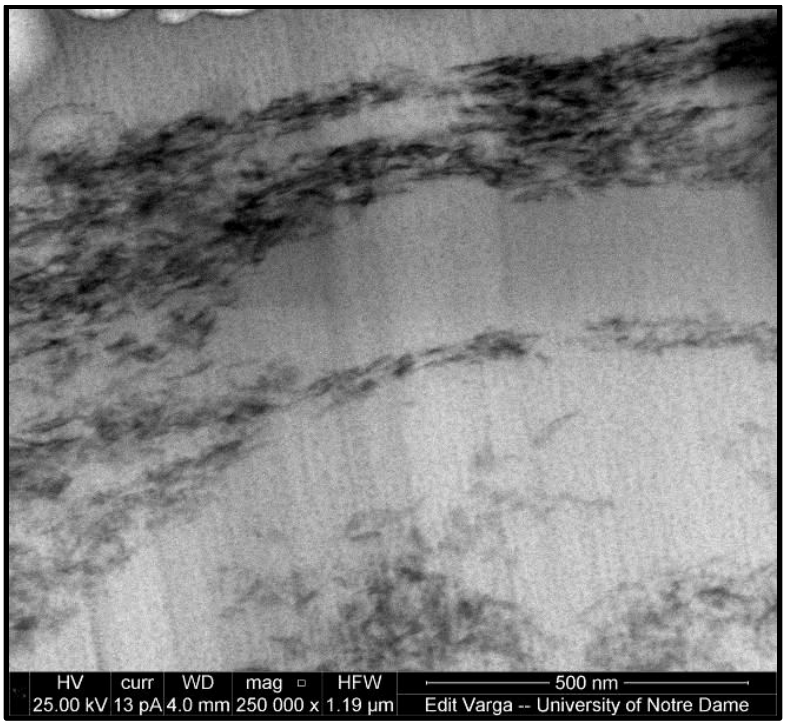

Figure 6.15: Transmission electron micrograph of Torlon®-Laponite® RD nanocomposite film containing 3wt% nanoclay filler showing evidence of large agglomerate formation. The highlighted area outlines a fibrous aggregate microstructure.

6.7 Summary & Conclusions

It has been shown that cellulose acetate and unmodified Laponite® RD can be combined to form a hybrid membrane that exhibits significant depressions in permeability while maintaining selectivity within an acceptable range. Furthermore, this was achieved at very low loadings. (Average permeability values as a function of loading are presented in Figure 6.16 as a recap.) There is still some uncertainty in adhesion between the polymer and filler, although good transport properties suggest that sufficient adhesion has been achieved. Analysis of solubility measurements and diffusion calculations provides evidence that the polymer is adhered; in fact it may be immobilized near the particle surface. Large particle floccs were observed by TEM in some samples, which imply that the exfoliation and dispersion process may need improvement to achieve the best possible results.

Despite any formation uncertainties, effective membranes were produced. This is sufficient evidence to support our claims that a purely solution based membrane can be produced using commercially available materials – without material modification. We believe that this process can be extended to other systems if the materials are carefully chosen. Formation of asymmetric membranes will be the final test to prove the efficacy and scalability of the process and materials.

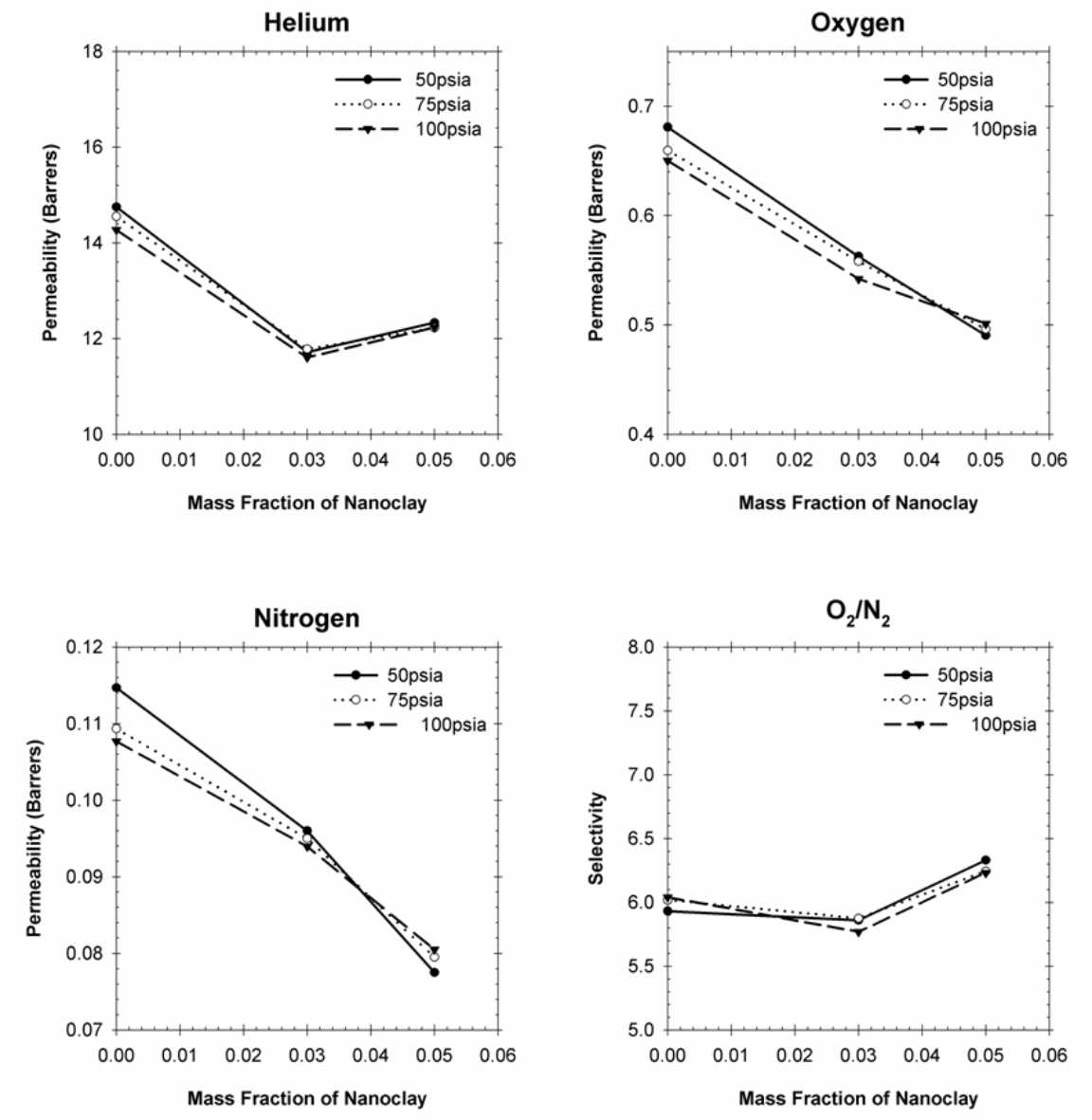

Figure 6.16: Permeability Properties of Cellulose Acetate and Cellulose Acetate-Laponite® RD Nanocomposite Dense Film Membranes as a Function of Nanoclay Loading. (a) Helium (b) Oxygen (c) Nitrogen (d) O_2/N_2 Selectivity

6.8 References

1. Y. Lim and A. Mohammed, "Effect of Solution Chemistry on Flux Decline During High Concentration Protein Ultrafiltration Through a Hydrophillic Membrane," *Chemical Engineering Journal* **159** (1-3), 91-97 (2010).

2. P. Mercea, "Gas Permeation Through Asymmetrical Cellulose Acetate Membranes," *Revista De Chimie* **43** (3-4), 121-128 (1992).

3. S. Stern, "Polymers for Gas Separation: The Next Decade," *Journal of Membrane Science* **94** (1), 1-65 (1994).

4. E. Sada, H. Kumazawa, J. Wang, and M. Koizumi, "Separation of CO_2 By Asymmetric Hollow Fiber Membrane of Cellulose Acetate," *Journal of Applied Polymer Science* **45** (12), 2181-2186 (1992).

5. L. Khounlavong and V. Ganesan, "Influence of Interfacial Layers Upon the Barrier Properties of Polymer Nanocomposites," *Journal of Chemical Physics* **130** (10), 12 (2009).

6. K. Wang, S. Liang, J. Deng, H. Yang, Q. Zhang, Q. Fu, X. Dong, D. Wang, and C. Han, "The Role of Clay Network on Macromolecular Chain Mobility and Relaxation in Isotactic Polypropylene/Organoclay Nanocomposites," *Polymer* **47** (20), 7131-7144 (2006).

7. T. Moore, R. Mahajan, D. Vu, and W.J. Koros, "Hybrid Membrane Materials Comprising Organic Polymers with Rigid Dispersed Phases," *AIChE Journal* **50** (2), 311-321 (2004).

8. T. Moore, "Effects of Materials, Processing, and Operating Conditions on the Morphology of Gas Transport Properties of Mixed Matrix membranes," *PhD Dissertation*, University of Texas - Austin, 2004.

9. T. Moore and W.J. Koros, "Non-Ideal Effects in Organic-Inorganic Materials for Gas Separation Membranes," *Journal of Molecular Structure* **739** (1-3), 87-98 (2005).

10. R. Barrer, *Diffusion in and Through Solids*. (Cambridge University Press, New York, NY, 1951).

11. L. Nielsen, "Models for the Permeability of Filled Polymer Systems," *Journal of Macromolecular Science: Part A, Pure & Applied Chemistry* **1** (5), 929-942 (1967).

12. R. Bharadwaj, "Modeling the Barrier Properties of Polymer-Layered Silicate Nanocomposites," *Macromolecules* **34** (26), 9189-9182 (2001).

13. F. Pignon, A. Magnin, J-M. Piau, B. Cabane, P. Lindner, and O. Diat, "Yield Stress Thixotropic Clay Suspensions: Investigations of Structure by Light, Neutron, and X-Ray Scattering," *Physical Review E* **56** (3), 3281-3289 (1997).

CHAPTER 7

CELLULOSE ACETATE - LAPONITE® RD HYBRID ASYMMETRIC HOLLOW FIBER MEMBRANES

7.1 Overview

As a final test to determine the efficacy of our preparation methods and to confirm the scalability of the process we applied the techniques developed in this work to the formation of asymmetric hollow fiber membranes. It was our objective to produce membranes that exhibited the desired selective separation of oxygen and nitrogen, as exhibited by the dense film study presented in Chapter 5. Unfortunately, it was found the fibers produced in this portion of the study were highly defective and therefore we are unable to put the argument to rest. We, however, did show that we could use the preparation methods to create hybrid dopes for fiber spinning. More importantly, we have evidence that suggests that we have achieved the desired orientation of nanoplatelets within the polymer matrix of the hollow fibers. Significant optimization in the dope composition – as it relates to the ternary phase diagram – is needed to complete this study; but this was outside the scope and timeline of this project.

7.2 Production of Hybrid Asymmetric Hollow Fiber Membranes Comprising of Cellulose Acetate and Laponite® RD Nanoclay Filler

A review of the mechanism that dictates asymmetric hollow fiber membrane formation was presented in Chapter 2. Moreover, the general procedure for preparing spin dopes was discussed in Chapter 3. Before discussing the results from our hollow fiber spinning study, we would like to provide some more details regarding the spinning process and

post-spin procedures. Details related to fiber test module construction and testing have been provided in-depth elsewhere.[1-3]

7.2.1 Dual Layer (Composite) Spinning

Typical asymmetric hollow fiber membranes for gas separation processes are produced using a single layer spinneret. In other words, the fiber is comprised of one material (this may include polymer blends) throughout. This is quite sufficient for most applications. However, if one is interested in using an expensive polymer material or a hybrid matrix of polymer and inorganic filler, a dual layer fiber may be a better choice.[4-6] Dual layer fibers provide the user with several advantages, including: (1) lower material costs when considering expensive, high performance polymers and/or hybrid membranes (2) flexibility in creating a dope that yields a valuable membrane but does not possess desirable mechanical properties for fiber spinning (3) adaptable substructure morphology for improved transport properties. For the purposes of our work, we will utilize advantages (1) and (2) from this list.

A complete cartoon depicting the dual layer hollow fiber spinning process is shown in Figure 7.1 as well as an inset image demonstrating the geometry of a composite spinneret as seen from the outlet. During the spinning process three components – bore fluid, core dope and sheath dope – are co-extruded through the composite spinneret. The extrudate then continues along a typical trajectory wherein it passes through an air gap to create a vitrified layer followed by a quench bath to complete phase separation and finally onto a take-up drum for collection.[7] In this procedure we are able utilize a tailored sheath dope for the membrane and a robust core dope for mechanical strength.

In this work we investigated the effects of air gap height, extrusion rates, take-up rates, spinning temperatures (includes spinneret, pumps and delivery lines) and quench bath temperature. The sheath dope, which contained the nanoplatelet filler, was designed based on the procedures discussed in the previous chapters. It should be noted that due to the quantity of water necessary for nanoclay exfoliation, the polymer

concentrations were lower than typical spin dopes (therefore the viscosity was also lower). Core dopes were comprised of the same polymer thereby ensuring interfacial miscibility between the sheath and core layers. Applied compositions of the core dopes were tailored to create a highly porous substructure and provide stable lines during the spinning process.

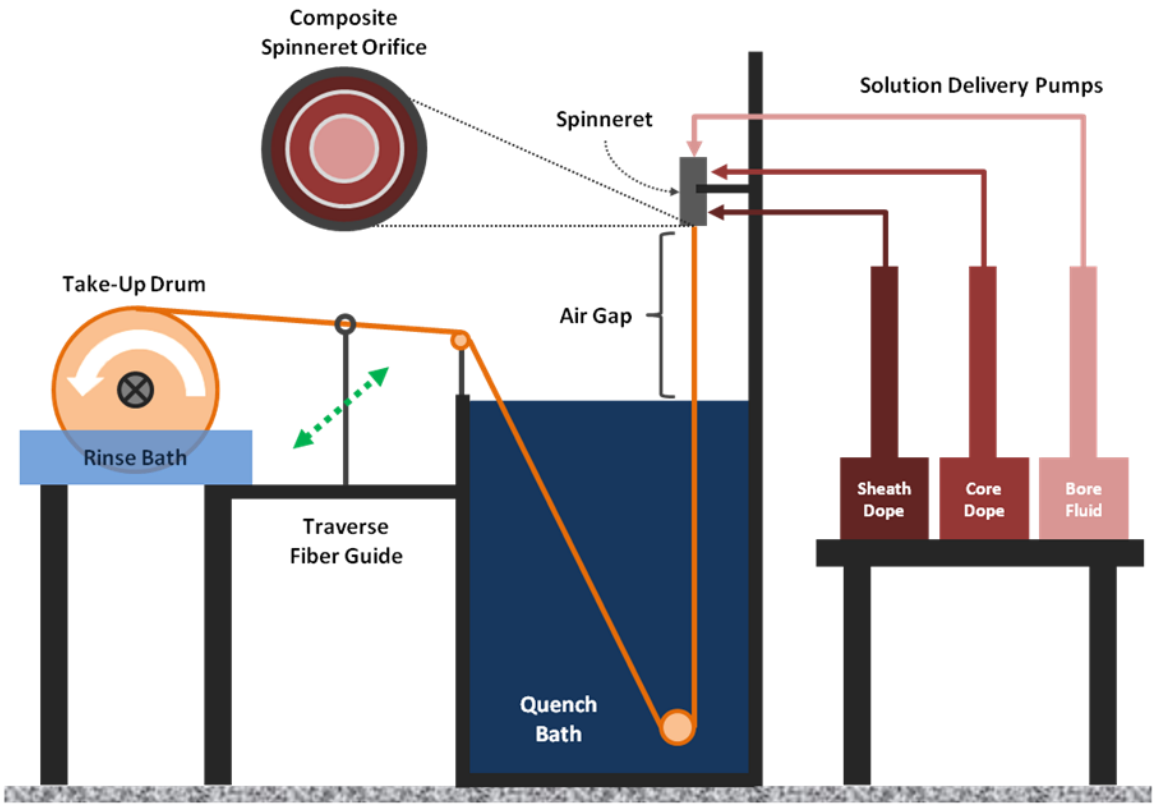

Figure 7.1: Cartoon depicting composite hollow fiber spinning apparatus. The orange line represents the spin line and fiber spinning process.

7.2.2 Solvent Exchange

Traditionally in the Koros Research Group, a three-step solvent exchange process has been used in post-spin fiber processing.[2,3] (The necessity for the solvent exchange process was described in Chapter 2.) The first stage is a multi-day soak in deionized water, followed by a short term soak in methanol to remove the water and completed by

a hexane soak to remove the methanol. Researchers have reported that this process is not appropriate for cellulose acetate asymmetric membranes.[8-10] Rather, a series of solvent dilutions produce improved performance in the membranes. Following the lead of these researchers we adapted our solvent exchange process to mimic theirs. See Figure 7.2 for a schematic illustration. After solvent exchange, the fibers were first air dried to remove a bulk of the hexane and then dried in a vacuum oven at 100ºC for 1 hour to remove all residual solvents.

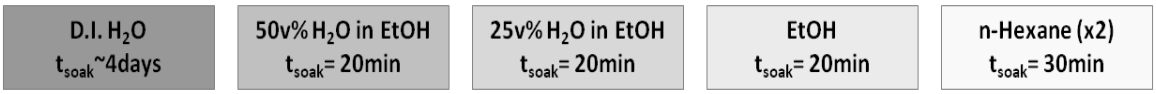

Figure 7.2: Flow chart outlining the solvent exchange process used for hybrid dual layer asymmetric hollow fiber membranes. Order of operations is listed from left to right.

7.3 Effect of Preparation Methods on Membrane Performance

In the very early stages of this work it was discovered that using the correct blend of water and polar solvent we could achieve an exfoliated dispersion of nanoclays. This dispersion could then be used to create a hybrid dope for membrane manufacture. Our original dispersion method was soon proven to be ineffective at creating dense films with desirable properties. These results lead to the development of improved mixing and dispersion methods which have been the focus of the previous discussions.

Regardless of the developments that were made, we also applied the original exfoliation and dispersion process to the formation of asymmetric hollow fiber membranes. These fibers were not successful for selective separations. We then extended the high shear mixing process to dope formulation with the hopes that the membrane performance would improve. Again, these fibers did not exhibit attractive permselectivities.

7.3.1 Comparison of Exfoliation/Dispersion Methods and Separation Performance

When the co-solvent exfoliation process was first conceived we used a magnetic stir bar in a round bottom flask for the exfoliation and dilution/dispersion steps (see Method 3 in Figure 4.6). Polymer was then added to the clay-solvent suspension and allowed to mix using a low shear method. This method was very promising at first because it produced optically transparent hybrid dopes. After further developments we found that high shear mixing produced a dope that yielded dense nanocomposite membranes with desired performance, which the initial "stir-bar" method did not. Regardless, we spun hollow fibers using the first method (while working in parallel to optimize hybrid dense films). Upon improving the preparation technique we re-created the first hybrid spin to determine if the new method produced asymmetric fibers with enhanced separation performance. Core and sheath dope compositions for these fibers are listed in Table 7.1

Table 7.1: Core and sheath dope compositions (based on mass fraction in %) used to spin hybrid cellulose acetate asymmetric hollow fiber containing 3wt% Laponite® RD filler in the sheath layer after formation.

Core Dope		Sheath Dope	
Component	*Mass Fraction (%)*	*Component*	*Mass Fraction (%)*
Cellulose Acetate	16.8	Cellulose Acetate	13.3
PVP*	3.2	Laponite® RD	0.7
NMP	70.2	DMSO	67.3
Water	9.8	Acetone**	11.2
		Water	7.5

*Polyvinylpyrrolidone (PVP) was used as a pore forming agent to create substructure with minimal transport resistance and to reduce macrovoid formation.
**Acetone was used as the volatile component (b.p. ~ 56ºC) for skin layer formation.

Since there was no prior experience in the Koros Group and limited literature related to spinning dopes of this nature, we were required to explore a variety of variables during the spinning process.[11] Adjustment of any one spinning parameter may improve the separation performance of a membrane; however, air gap and temperature generally

have the greatest influence.[1,12] In Table 4.2 we have listed the major spinning parameters that were considered during the spinning process and their corresponding range of interest. A bore fluid with composition of 15wt% water in NMP was primarily used in both spin sets. The fiber take-up rate was set to 42 m/min for all states collected.

Table 7.2: Spinning parameters that were considered for this investigation and the ranges that were used for each respective spin.

Spinning Parameter	Low Shear Mixing	High Shear Mixing
Air Gap	13-30 cm	12-40 cm
Core Flow Rate	180-240 ml/hr	200-300 ml/hr
Sheath Flow Rate	18-90 ml/hr	5-30 ml/hr
Spinneret Temperature	40-75ºC	45ºC
Quench Bath Temperature	30-45ºC	25-50ºC

After completing the solvent exchange process on the spun fibers, we made test modules for gas permeance measurements. Helium, oxygen and nitrogen were used as test gases using a feed pressure of 50psig and test temperature of 35ºC. For all modules in this study we found that the helium permeance was outside the measurable range (extremely high) of our equipment. This was the initial indication that the fibers were highly defective. Oxygen and nitrogen permeance measurements verified this conclusion. Both test gases had very high fluxes through all modules tested. The ideal selectivity for O_2/N_2 in cellulose acetate is 5-6.[13] We were not able to achieve selectivities substantially higher than the Knudsen limit of 0.94.[14] In summary, we were unable to produce a defect-free asymmetric hollow fiber membrane using either the high shear or the low shear preparation technique. But regardless of separation performance we have shown that the high shear mixing process (and the low shear process) can be used to spin hollow fibers.

The reactive post-treatment technique was used on the modules produced from the high shear prepared fibers. [15,16] It is possible that molecular pin-hole defects may be the

cause of the poor separation performance. In optimum cases, the post-treatment process can patch these holes and increase the permselectivity. Unfortunately, it was found that this technique did not improve the permselectivity. This result further verifies our initial conclusion that the fibers are highly defective.

7.3.1.1 Microscopic Evaluation of Hybrid Hollow Fibers Containing 3wt% Nanoclay Filler

We found that all of the fibers spun – using either preparation method – were highly defective for selective gas transport. This fact notwithstanding, we have still shown that hollow fibers containing nanoplatelet fillers may be produced. Figures 7.3 and 7.4 show a series of scanning electron micrographs (SEM) for the *low shear* and *high shear* fibers respectively. Using SEM we were able to confirm that the fibers are (1) hollow (2) concentric (3) exhibit a desirable substructure morphology and (4) demonstrate miscibility between the core and sheath layers. Microscopic analysis of the fibers outer surface was also used to explore the possible source of defective gas transport.

Photographic evidence suggests that both preparation methods contributed to the manufacture of hollow fibers with acceptable morphologies. Figures 7.3a and 7.4a provide an overview of the fiber morphology. We can see that the fibers are round, indicating that phase separation in the quench bath was sufficient, because there was no fiber collapse. Also the bore of the fiber is free of protruding polymer debris – a side effect of improper bore fluid composition.[15] Macrovoids are present in both spins (see Figures 7.3a,b and 7.4c) though, which is undesirable for the mechanical integrity of the membrane. These macrovoids do not protrude into the sheath layer, but rather have an even radial limit. The macrovoid boundary coincides with the interfacial region between the sheath and core layers. Figures 7.3d and 7.4d highlight the interfacial region more clearly. In these images we see a gradient in the apparent porosity of the fiber substructure, indicating that the two layers are highly miscible. In the event that the layers in a composite fiber are not miscible, a clear delineation is present and in extreme cases of incompatibility a gap between the layers may occur.[4]

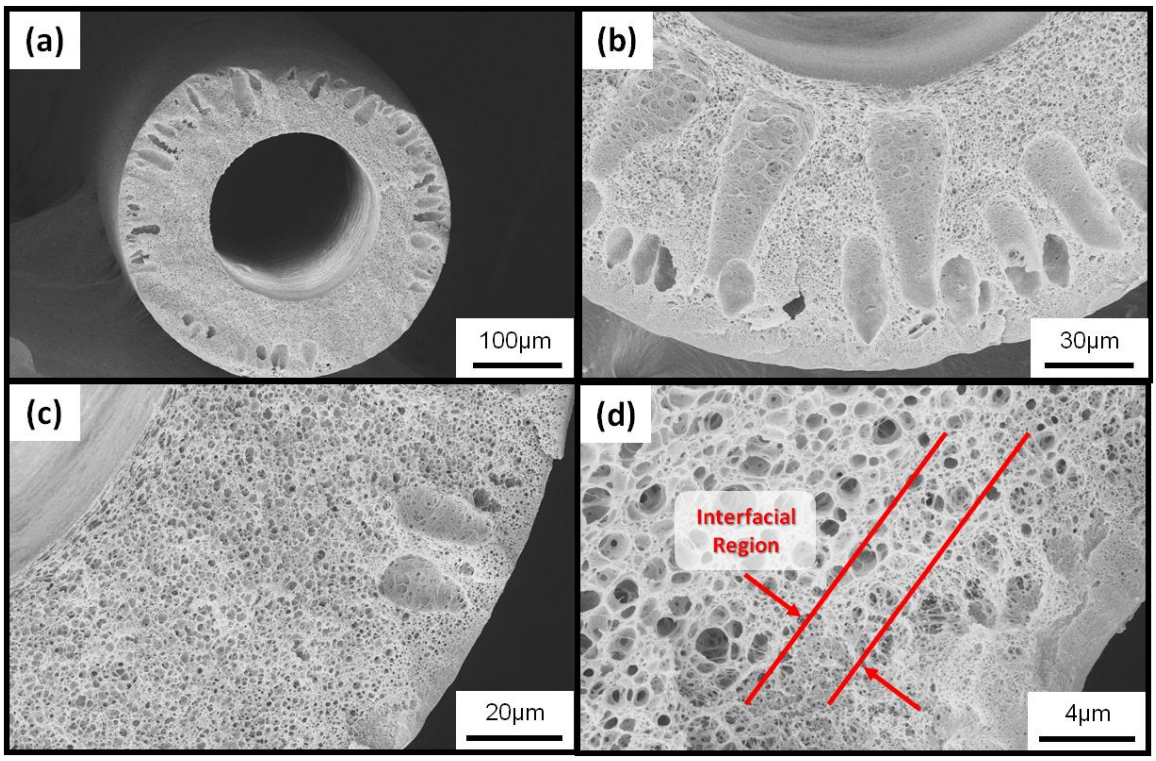

Figure 7.3: Scanning electron micrographs of Cellulose Acetate-Laponite® RD hybrid asymmetric hollow fiber membrane containing 3wt% nanoclay filler. Fibers were produced using a dope that was prepared using a *low shear* mixing technique. (a) broad view of fiber showing concentricity (b) evidence of substructure macrovoids (c) uniform substructure porosity (d) interfacial region between sheath and core layers

Albeit we applied a post-treatment technique to the hollow fiber modules, the fibers were still found to be highly defective. If defects in the skin layer are sufficiently large then the typical post-treatment procedure cannot improve the separation performance. Upon inspection of the outer surface, we see that the skin layer had numerous defects. One such micron sized defect is highlighted in Figure 7.5. This defect penetrates the skin layer, which provides a non-selective outlet for gas molecules during transport tests. Alternatively, in Figure 7.6 we observe that there is an array of non-surface penetrating defects. Dimples or divots in the fiber surface are highlighted in Figure 7.6a and 7.6b. Morphology of this nature suggests that the phase separation kinetics are mismatched.[17] This may pertain to vitrification issues in the air gap (slow or fast solvent evaporation) or

phase separation in the quench bath. Regardless of the root cause, the presence of such defects will have a negative impact of the permselectivity.

Further developments are necessary to produce a defect free hollow fiber membrane. Wide ranges of spinning parameters were explored in this work, but to no avail. Modification of the spinning dope may produce hollow fiber membranes with desirable transport properties. One such alteration was explored.

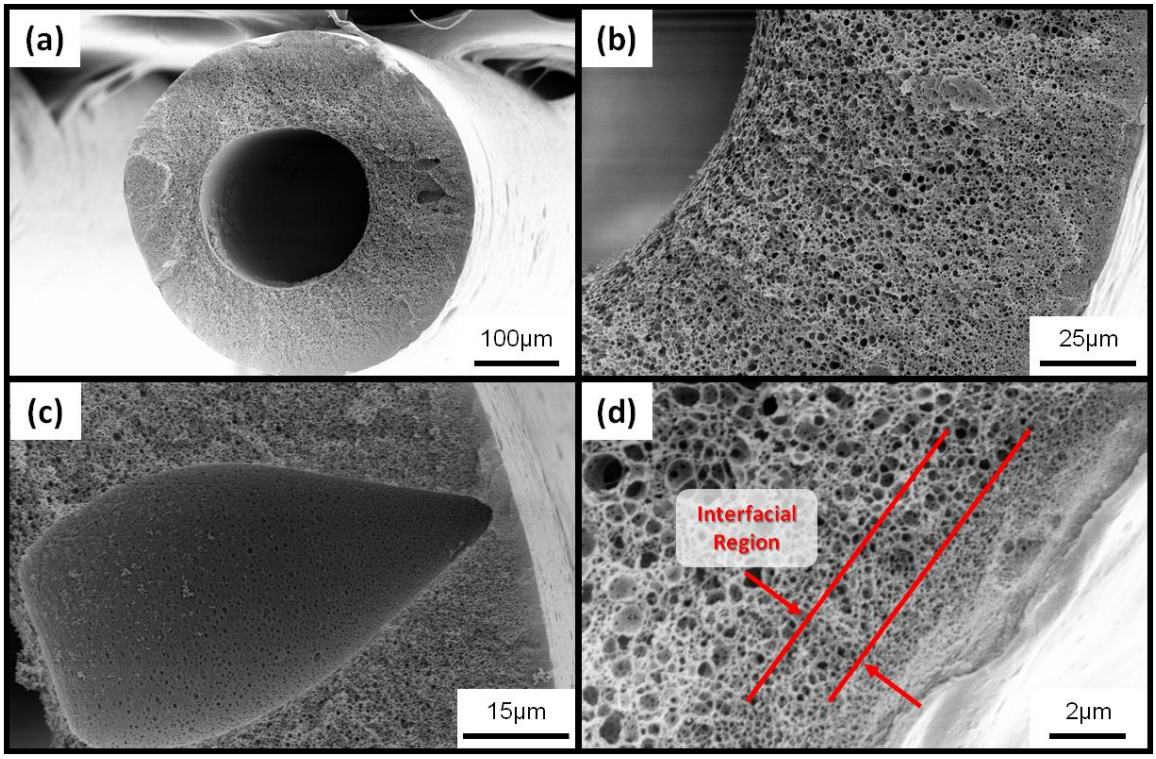

Figure 7.4: Scanning electron micrographs of Cellulose Acetate-Laponite® RD hybrid asymmetric hollow fiber membrane containing 3wt% nanoclay filler. Fibers were produced using a dope that was prepared using a *high shear* mixing technique. (a) broad view of fiber showing concentricity (b) uniform substructure porosity (c) evidence of a large substructure macrovoid (d) interfacial region between sheath and core layers

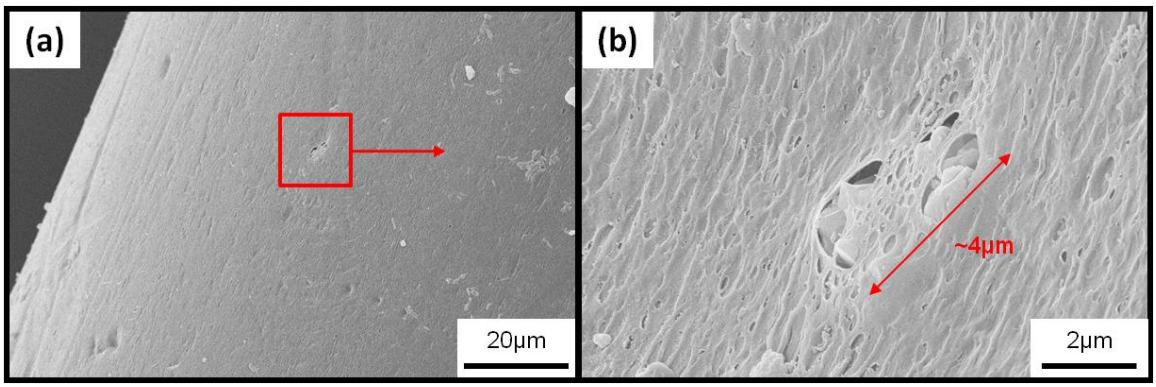

Figure 7.5: Scanning electron micrographs of Cellulose Acetate-Laponite® RD hybrid asymmetric hollow fiber membrane containing 3wt% nanoclay filler. Fibers were produced using a dope that was prepared using a *low shear* mixing technique. (a) broad view of fiber skin layer with visible defects (b) magnified images illustrating micron size skin defect

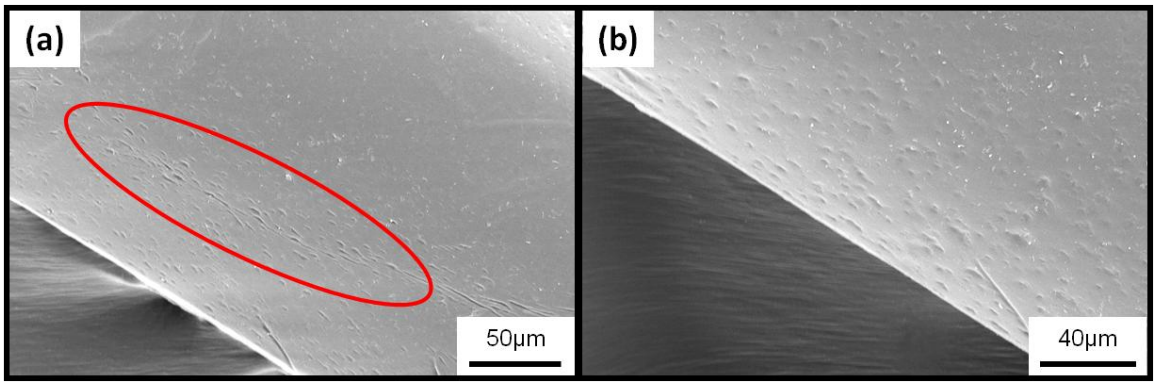

Figure 7.6: Scanning electron micrographs of Cellulose Acetate-Laponite® RD hybrid asymmetric hollow fiber membrane containing 3wt% nanoclay filler. Fibers were produced using a dope that was prepared using a *high shear* mixing technique. (a) divots in the fiber skin layer (b) alternative perspective of surface roughness

7.3.2 Effect of Volatile Solvent Concentration on Separation Performance

In the previous section we showed that an asymmetric hollow fiber membrane containing nanoclay filler could be produced; but the gas transport properties of these fibers were disappointing. A final attempt was made in this study to produce asymmetric hollow fiber membranes with desirable separation performance. Typical hollow fiber membrane production strives to make the skin layer as thin as possible. A thinner skin layer will

increase productivity and ideally retain selectivity because the mass transfer resistance reduces as a function of thickness. However, in order to prove the fundamental applicability of our approach we opted to attempt to produce a very thick skin layer. This morphology is not ideal, but if successful would validate the scalability of this work. The concentration of volatile solvent in the sheath dope was increased from 11wt% to 19wt% in hopes that we may produce a very thick skin. Complete dope compositions for the core and sheath components are shown in Table 7.3. We also increased the clay content from 3wt% to 5wt% (w.r.t. the polymer). It was hypothesized that higher barrier content may generate more significant decreases in permeance; even if small defects are present.

Table 7.3: Core and sheath dope compositions (based on mass fraction in %) used to spin hybrid cellulose acetate asymmetric hollow fiber containing 5wt% Laponite® RD filler in the sheath layer after formation.

Core Dope		**Sheath Dope**	
Component	*Mass Fraction (%)*	*Component*	*Mass Fraction (%)*
Cellulose Acetate	23.0	**Cellulose Acetate**	14.55
NMP	70.0	**Laponite® RD**	0.45
$LiNO_3$ *	7.0	**DMSO**	61.0
		Acetone**	19.0
		Water	5.0

*Lithium nitrate was used as a pore forming agent. Studies by Dhaval Bhandari in the Koros Group showed that this core dope composition produced a highly porous substructure with good mechanical characteristics during the spinning process. A bore fluid composition of 20% water in NMP was used in this case.

In addition to increasing the volatile component content, efforts were made to increase the skin layer thickness by using higher air gaps during the spin process. A longer residence time in the air gap can induce greater solvent evaporation and drive the dope closer into the polymer rich region where vitrification occurs.[12] Parameters that were varied during the spin process are shown in Table 7.4. Temperatures for the spinneret assembly and the quench bath were maintained at 50ºC throughout the experiment.

Table 7.4: Spinning parameters that were considered for this investigation and the ranges that were used in the process.

Spinning Parameter	
Air Gap	10-35 cm
Core Flow Rate	200-320 ml/hr
Sheath Flow Rate	20-50 ml/hr
Take-up Rate	25-30 m/min

Similarly to the previously discussed hybrid fibers, we employed the same solvent exchange, drying and module fabrication procedures. Permeance tests were conducted using the same protocols that were outlined previously. Unlike before, we were able to measure helium permeance in all modules; but the values were unacceptably high. Oxygen and nitrogen measurements followed suit with exceptionally large permeances for all modules in the study. The permselectivity for this gas pair matched Knudsen diffusion limits. Since the permeance values were found to be orders of magnitude higher than desired it was decided that a post-treatment step would not provide the necessary amelioration.

7.3.2.1 Microscopic Evaluation of Hybrid Hollow Fibers Containing 5wt% Nanoclay Filler

It was shown in Section 7.2.1.1 that hybrid hollow fibers could be produced and that they exhibited positive morphological characteristics. Similar microscopic evidence is presented here to validate the apparent properties of hybrid hollow fibers containing 5wt% nanoclay. In Figure 7.7a-c we present SEM images of the fiber cross section. Clearly, we see that the fibers are round and concentric – as before. The substructure pore size is slighter lower than the previous case; but in this example the core dope was a different composition. As a result of this smaller pore size, the transition layer between the sheath and core dopes is less prevalent. We have illustrated the likely region of interfacial mixing in Figure 7.7c.

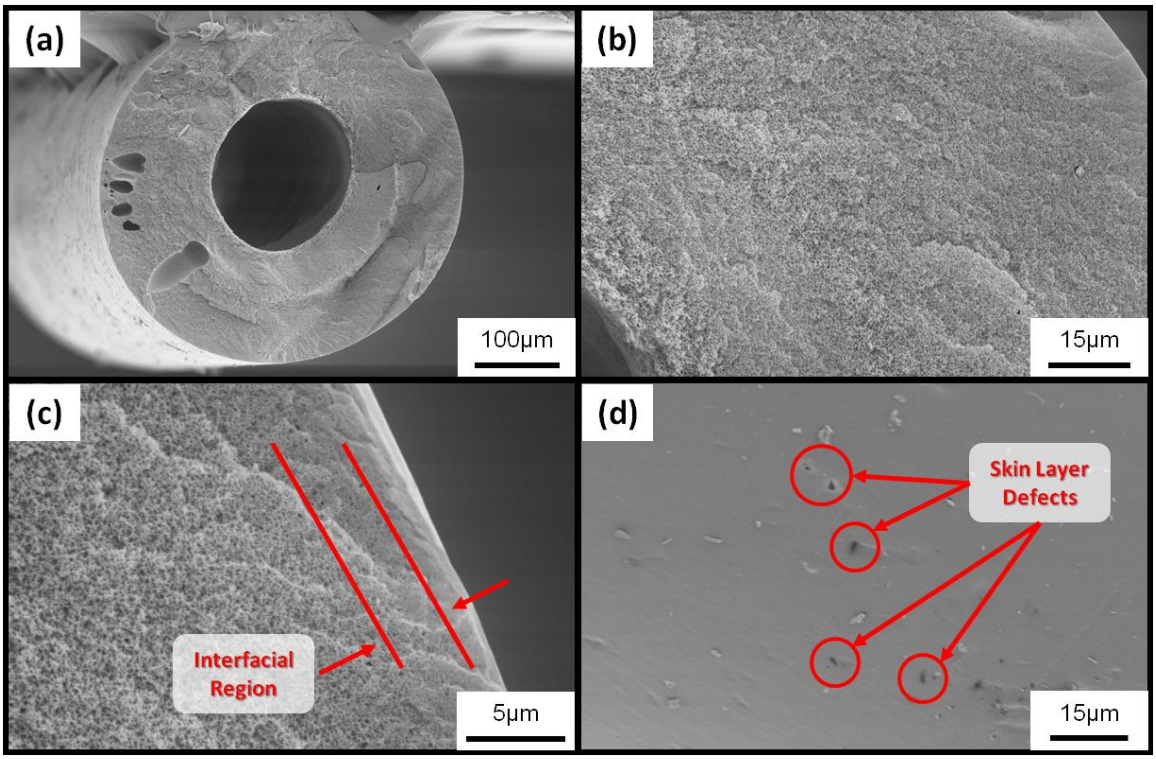

Figure 7.7: Scanning electron micrographs of Cellulose Acetate-Laponite® RD hybrid asymmetric hollow fiber membrane containing 3wt% nanoclay filler. Fibers were produced using a dope that was prepared using a *high shear* mixing technique. (a) broad view of fiber showing concentricity (b) uniform substructure porosity (c) interfacial region between sheath and core layers (d) evidence of a surface defects

A surface analysis was conducted to determine if any improvements had been made in the skin layer topography. Unfortunately, micron sized skin layer defects were quite evident (see Figure 7.7d). Further dope optimization is necessary in order to produce an asymmetric hollow fiber membrane with a defect free skin layer.

7.4 Orientation of Nanoplatelets in an Asymmetric Hollow Fiber Membrane

In Chapter 1 we discussed the necessity of nanoplatelet orientation in the polymer matrix in order to achieve optimum transport properties. Preferably, the platelets should be aligned perpendicular to the direction of transport to achieve maximum enhancement.[18,19] According to the rotational theory described by Macosko, orientation

of prolate and oblate particles will occur if the shear stress applied to a system overcomes Brownian induced randomization.[20] TEM images presented in Chapters 5 and 6 suggest that the particle orientation is anisotropic in the membrane; albeit exfoliated. This morphology is not surprising in the dense film membranes because insignificant shear is applied during the film casting process. During the spinning process shear forces increase due to the viscosity of the dope, extrusion rate and the narrow channel in the spinneret. We hypothesized that the shear forces in the spinneret during extrusion would provide enough stress to align the nanoplatelets axially (as depicted in Figure 1.8).

TEM images of our hybrid hollow fibers were provided by Dr. Sunho Cho while he was still a researcher at the University of Minnesota. These images – shown in Figure 7.TEM – provide very strong evidence that the nanoplatelet fillers experience alignment in the desired direction. In the figure we have denoted the radial direction (R) which was determined based on additional images at low magnification. The dark striations observed in image (a) demonstrate that the platelets are exfoliated.[21] Moreover, these striations are predominately perpendicular to the signified radial direction. Image (b) in this figure provides similarly supporting evidence in that the dark striations have a prevailing orientation in the radial direction. This image also indicates that we do not have perfect dispersion. The dark mass in the southeast portion of the image corresponds to a large agglomerate of nanoplatelets; which is not terribly surprising. Fibers produced using the low shear preparation methods were used for this characterization.

Regardless of the presence of particle agglomerates, the image clearly demonstrates that nanoplatelet fillers readily orient during the fiber spinning process – despite the degree of agglomeration. If defect free membranes were obtained, the observed particle orientation would suggest that reductions in gas transport would be obtained. Or in the case of molecular sieving nanoplatelets, we would see an increase in productivity and efficiency.

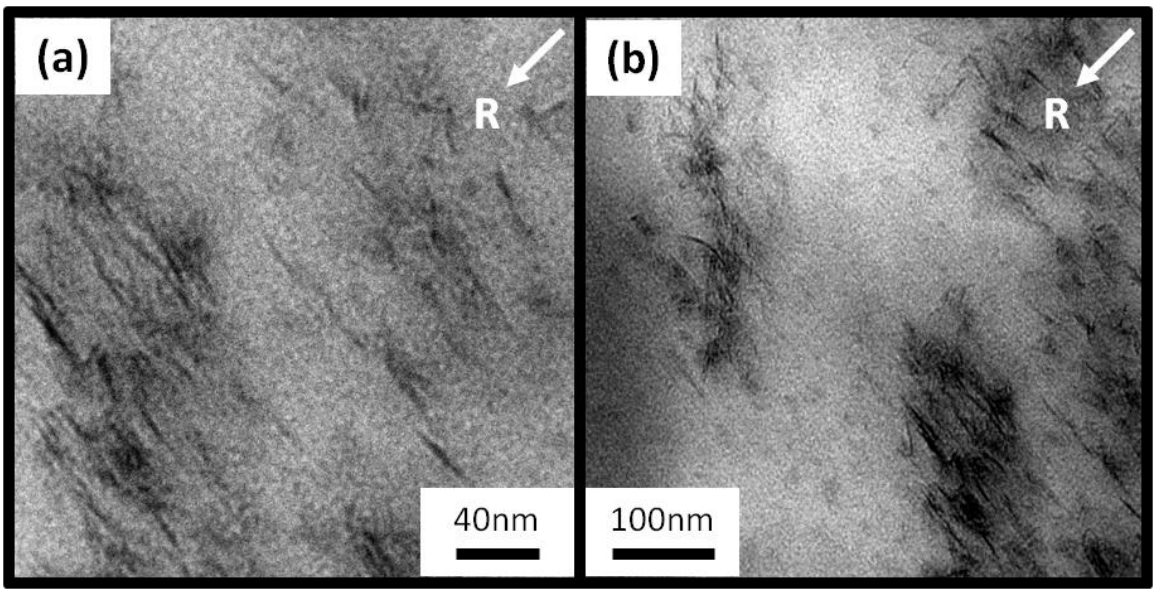

Figure 7.8: TEM images depicting nanoplatelet orientation within the polymer matrix of a hybrid asymmetric hollow fiber membrane. (a) Magnified view of the exfoliated platelets. (b) Lower magnification perspective illustrating the presence of particle agglomerates with reasonably well aligned orientation. Vector "R" represents radial direction of fiber.

Regardless of the presence of particle agglomerates, the image clearly demonstrates that nanoplatelet fillers readily orient during the fiber spinning process – despite the degree of agglomeration. If defect free membranes were obtained, the observed particle orientation would suggest that reductions in gas transport would be obtained. Or in the case of molecular sieving nanoplatelets, we would see an increase in productivity and efficiency.

7.5 Summary & Conclusions

We have clearly demonstrated that hybrid asymmetric hollow fiber membranes containing nanoplatelets are realizable and that the scalability of the preparation procedure has been validated. Moreover, we have presented evidence that suggests particle orientation in the hollow fiber is attainable during the spinning process. Unfortunately we were unable to produce defect free hollow fiber membranes using our methods. However, this result does not detract from the value of our main conclusions.

It is the opinion of the authors that hybrid hollow fibers with decreased permeabilities are achievable through careful spin dope and spin condition optimization. Due the timeline of this work and the necessity to thoroughly investigate hybrid dense film membranes, we were unable to dedicate the time towards this optimization. As a suggestion to future researchers, we would recommend investigating the phase boundary in the sheath dope and/or optimizing the co-solvent ratios used for nanoclay exfoliation in order to reduce the water content and therefore increase the polymer concentration.

7.6 References

1. S. Carruthers, G. Ramos, and W.J. Koros, "Morphology of Integral-Skin Layers in Hollow-Fiber Gas-Separation Membranes," *Journal of Applied Polymer Science* **90** (2), 399-411 (2003).

2. S. Husain, "Mixed Matrix Dual Layer Hollow Fiber Membranes for Natural Gas Separation," *PhD Dissertation*, Georgia Institute of Technology, 2006.

3. D. Wallace, "Crosslinked Hollow Fiber Membranes for Natural Gas Purification and Their Manufacture from Novel Polymers," *PhD Dissertation*, University of Texas - Austin, 2004.

4. T. He, M. Mulder, H. Strathmann, and M. Wessling, "Preparation of Composite Hollow Fiber Membranes: Co-extrusion of Hydrophilic Coatings onto Porous Hydrophobic Support Structures," *Journal of Membrane Science* **207** (2), 143-156 (2002).

5. J. Shieh, T. Chung, R. Wang, M. Srinivasan, and D.R. Paul, "Gas Separation Performance of Poly(4-vinylpyridine)/Polyetherimide Composite Hollow Fibers," *Journal of Membrane Science* **182** (1-2), 111-123 (2001).

6. S. Husain and W. J. Koros, "Mixed Matrix Hollow Fiber Membranes Made with Modified HSSZ-13 Zeolite in Polyetherimide Polymer Matrix for Gas Separation," *Journal of Membrane Science* **288** (1-2), 195-207 (2007).

7. S. Pesek and W.J. Koros, "Aqueous Quenched Asymmetric Polysulfone Hollow Fibers Prepared by Dry/Wet Phase Separation," *Journal of Membrane Science* **88** (1), 1-19 (1994).

8. B. Minhas, T. Matsuura, and S. Sourirajan, "Formation of Asymmetric Cellulose Acetate Membranes for the Separation of Carbon Dioxide-Methane Gas Mixtures," *Industrial & Engineering Chemistry Research* **26** (11), 2344-2348 (1987).

9. J. Hao and S. Wang, "Influence of Quench Medium on the Structure and Gas Permeation Properties of Cellulose Acetate Membranes," *Journal of Applied Polymer Science* **68** (8), 1269-1276 (1996).

10. X. Jie, Y. Cao, J-J. Qin, and Y. Quan, "Influence of Drying Method on Morphology and Properties of Asymmetric Cellulose Hollow Fiber Membrane," *Journal of Membrane Science* **246** (2), 157-165 (2005).

11. K. Wang, S. Foo, and T. Chung, "Mixed Matrix PVDF Hollow Fiber Membranes with Nanoscale Pores for Desalination through Direct Contact Membrane Distillation," *Industrial & Engineering Chemistry Research* **48** (9), 4474-4483 (2009).

12. D. Clausi and W.J. Koros, "Formation of Defect-Free Polyimide Hollow Fiber Membranes for Gas Separations," *Journal of Membrane Science* **167** (1), 79-89 (2000).

13. S. Stern, "Polymers for Gas Separations: The Next Decade," *Journal of Membrane Science* **94** (1), 1-65 (1994).

14. R. Barrer, *Diffusion in and Through Solids*. (Cambridge University Press, New York, NY, 1951).

15. M. Kosuri, "Polymeric Membranes for Super Critical Carbon Dioxide ($scCO_2$) Separations," *PhD Dissertation*, Georgia Institute of Technology, 2009.

16. O.M. Ekiner, R.A. Hayes, and P. Manos, U.S. Patent No. 5,091,216 (1992).

17. S. Carruthers, "Integral-skin Formation in Hollow Fiber Membranes for Gas Separations," *PhD Dissertation*, University of Texas - Austin, 2001.

18. E.L. Cussler, "Membranes Containing Selective Flakes," *Journal of Membrane Science* **52**, 275-288 (1990).

19. J.R. Johnson and W.J. Koros, "Utilization of Nanoplatelets in Organic-Inorganic Hybrid Separation Materials: Separation Advantages and Formation Challenges," *Journal of Taiwan Insitute of Chemical Engineers* **40** (3), 268-275 (2009).

20. C. Macosko, *Rheology Principles, Measurements and Applications*. (Wiley-VCH, Inc., New York, 1994).

21. D.R. Paul and L.M. Robeson, "Polymer Nanotechnology: Nanocomposites," *Polymer* **49** (15), 3187-3204 (2008).

CHAPTER 8

SUMMARY, CONCLUSIONS & FUTURE DIRECTIONS

8.1 Overview

This work has culminated in the development of a procedure that led to the successful formation of dense film and asymmetric hybrid membranes containing impermeable nanoplatelet fillers. The dense film membranes demonstrated successful depression in gas permeability with evidence of an exfoliated nanoclay filler. Asymmetric hollow fiber membranes produced using the same preparation techniques did not exhibit the anticipated permeation properties, but did show evidence of desired platelet orientation. Further studies are necessary to optimize the preparation procedure in order to produce defect-free asymmetric hollow fiber membranes. Additional characterization may provide further insight into the fundamental morphology and mechanical properties of these hybrid membranes.

8.2 Summary & Conclusions

The overarching goal of this project was to *develop an engineering understanding of the principles governing production of polymer-nanoplatelet hybrid asymmetric hollow fiber membranes and their applications in efficient gas separations.* We developed a series of objectives that, if successfully accomplished, would allow us to achieve this goal. These objectives are reiterated below for the reader's convenience. A summary of the project results are provided afterwards, with the primary conclusions in **bold** font.

1. *Develop a method(s) to successfully exfoliate and disperse inorganic nanoplatelets into a polymer solution for membrane formation.*

2. *Produce and characterize hybrid dense film membranes to verify the efficacy of the preparation techniques developed.*
3. *Spin and characterize hybrid asymmetric hollow fiber membranes containing exfoliated and dispersed nanoplatelet filler materials.*

There has been extensive research in the area of polymer-nanoplatelet hybrid materials. Moreover, many authors have been successful at producing gas separation membranes. Typically these reports have utilized melt blending, *in situ* polymerization or solution blending. Few, however, have utilized solution blending for creating membranes via phase inversion. And to date, there have not been any reports regarding the fabrication of asymmetric membranes containing nanoplatelet filler materials. **In this work we have developed a solution-based procedure for the formation of polymer-nanoplatelet membranes that is applicable to dense and asymmetric membranes.** The latter results indicate that the process can be applied in a realistic membrane formation platform. We also examined the diversity of the process by using an alternate polymer matrix, which was also successful. At this time, we have not extended the platform to other filler materials or to polymers beyond Torlon® and cellulose acetate; however, we believe that the results from this work strongly indicate that the methods are flexible, diverse and scalable.

A blend of polar organic solvents and water was used to successfully create an exfoliated system of nanoclays *in situ*. This success was verified using simple free swelling tests and rheological evaluation. Implementation of a high shear mixing protocol enabled us to effectively incorporate a polymer and create a homogenous blend of platelets in the host matrix. Rheological measurements verified that we had achieved a high degree of exfoliation – especially when compared to traditional mixing methods like sonication and low shear stirring. These conclusions were valid for both polymer systems of interest. In fact, the rheology data strongly suggests that cellulose acetate surface sorbs to the nanoclays while in solution.

As noted above, two polymers with very different characteristics were explored to prove the versatility of the formation process. Torlon®, a polyamide-imide, is a robust polymer with excellent intrinsic barrier properties as well as durable mechanical properties. **We were able to produce hybrid dense film membranes containing significant mass fractions of unmodified Laponite® RD in a Torlon® matrix.** Based on the permeation studies, it is apparent that the polymer and clay produce an organic-inorganic interface that is desirable for achieving desirable transport properties. Pressure decay sorption measurements suggest the possible existence of non-uniformities in the polymer phase based on the deviations from predicted values for the hybrid membranes. This observation is further supported by unexpected variations in permselectivities. Further studies are necessary to confirm this observation. Despite slight anomalies in the transport properties, we showed via transmission electron micrographs (TEM) that the preparation technique does produce an exfoliated clay system. Conversely, lower magnification images suggest that the nanoplatelet fillers are not perfectly exfoliated or perhaps not perfectly dispersed in the polymer matrix – despite the fact that the measured values correspond reasonably with predicted values.

Cellulose acetate was also used to create hybrid membranes. This polymer has significant industrial relevance in gas and liquid separations. Proving that our techniques could be used to produce effective hybrid membranes from this polymer further supported our conclusion that the process is versatile. **Permeation studies showed that these hybrid dense film membranes produced considerable permeability depressions that agreed well with predicted values.** This fact notwithstanding, TEM images showed evidence that the nanoclay filler is not perfectly dispersed in the polymer matrix. Diffusion coefficients were calculated using sorption and permeation data. We confirmed that the hybrid membrane does greatly decrease the rate of diffusion (as expected based on tortuosity arguments). However, we did find that the diffusive selectivity is different between pure and hybrid materials. As was the case with Torlon® hybrid materials, the cellulose acetate materials appear to have non-uniformities in the polymer phase. It is very likely that there is a *zone of influence*

around the particles or in the interstices of any flocculated species that is leading to these small deviations.

Based on the success of the cellulose acetate hybrid dense films, we investigated the scalability of the process and produced asymmetric hollow fiber membranes using cellulose acetate and Laponite® RD. **We successfully produced dual-layer hollow fibers containing 3wt% and 5wt% nanoclay in the sheath layer.** Scanning electron microscopy (SEM) images provided proof that the fibers were concentric and that the sheath-core layer interface was homogenous. More importantly, TEM images show evidence that the nanoplatelets were aligned orthogonal to the radial direction (the direction of transport) within the polymer matrix. This confirmed our initial hypothesis that the shear forces in the spinneret during the spinning process would be sufficient for the orientation of high aspect ratio fillers. Unfortunately, none of the fibers produced in this work exhibited desirable transport properties. Despite this set back, we strongly believe that through processing and spinning optimization one could produce defect-free asymmetric hollow fiber membranes.

The efficacy, versatility and scalability of our preparation procedures have been successfully demonstrated in this work. We have developed a fundamental understanding towards the production of polymer-nanoplatelet membranes using commercially relevant materials and an efficient production process. These accomplishments serve as an excellent platform for future work in the development of advanced hybrid membranes.

8.3 Future Directions

Throughout the course of this project significant progress was made in the development of preparation procedures for the formation of polymer-nanoplatelet hybrid membranes. These membranes showed desirable transport properties – even exceeding mathematical predictions. Although we have successfully achieved the original objectives, there are opportunities for growth in this field. Nanoplatelet exfoliation,

dispersion and membrane formation techniques proved effective for the materials used in this project, but the data suggests that there is room for improvement. Optimizing the processing techniques and membrane formation procedures may lead to membranes with even better transport properties. Hollow fiber spinning, specifically, requires significant optimization in order to produce defect-free membranes. Additional characterization techniques may provide further support of our findings and lead to new insights into the properties of these materials as well. Finally, understanding organic-inorganic relationships can improve our fundamental understanding of these hybrid systems and ultimately allow the end user to anticipate material compatibility prior to membrane formation.

8.3.1 Exfoliation, Dispersion and Incorporation

The preparation procedures used in this work for creating hybrid membranes containing an exfoliated, dispersed phase of nanoplatelets in a polymer matrix were successful. Through a combination of a carefully chosen aqueous organic solvent and high shear mixing we created an exfoliated suspension of nanoclays. Polymer was added to this suspension with the aid of additional high shear mixing. Although this process was successful, we did not explore all of the possible combinations of aqueous solvent(s) nor did we consider studying alternative mixing protocols. It is likely that through careful optimization that hybrid membranes with improved filler dispersion and even nanoclay exfoliation may be possible. Moreover, there are potential methods for increasing the filler content without sacrificing polymer dissolvability.

In Chapter 3 we used rheological measurements to qualitatively determine an aqueous organic solvent blend that would be suitable for both exfoliation and polymer dissolution. We believe that this solvent ratio can be fine tuned to reduce the water content, thereby enabling greater polymer dissolution. Rheological measurements can be used to study the efficacy of alternative solvent blends. Small angle x-ray scattering (SANS) and small angle neutron scattering (SANS) may also be used as complementary characterization techniques to quantify nanoplatelet exfoliation. These tools can also be used to

characterize the hybrid dopes after polymer addition. In combination with a solvent investigation, it would be wise to also study alternative mixing protocols. Rather than reducing the water content in the exfoliating medium, we can increase it to improve exfoliation. Based on our previously defined constraints this would typically be counterproductive.

Although not reported here, we successfully produced hybrid membranes using a hydrophobic polyimide, Matrimid®, for the host matrix. These membranes did not have desirable transport properties though; this is likely due to poor polymer-clay adhesion. These casting solutions could not be prepared using the standardized method discussed in this work due to the hydrophobicity of the polymer. To overcome this limit, we greatly reduced the amount of polymer that was added to the aqueous organic clay suspension. Reducing the polymer content allowed us to produce a dope that was in the one phase region of the ternary diagram. Consequently, this dope was very dilute (low viscosity) and could not be used in its current state to cast dense films. Therefore, the solution was intentionally coagulated in water. After removing the water and drying the precipitate, we were left with a polymer-nanoclay composite that could then be re-dissolved in the solvent choice because the clay was stabilized and dispersed in the polymer phase. We believe that this technique may be a valid approach for creating composites using more hydrophobic polymers. Recent literature shows a similar technique that may be even more beneficial for creating bulk nanocomposite polymers. Yun, *et al* have used spray drying technology to create polymer-clay nanocomposite microspheres from dilute solution.[1] This technology is very scalable and promotes increased filler loadings.

8.3.2 Membrane Formation

Drying and annealing conditions can significantly influence the properties of a polymeric membrane.[2-5] This is even more evident in hybrid materials.[6,7] Early in our work we identified a multi-day procedure with temperature ramps and soaks that yielded hybrid membranes with desirable transport properties. Once the method was identified we did

not explore other possibilities for the sake of consistency and due to time constraints. Investigating alternative drying procedures may lead to improved membrane properties and/or expedited time to completion (the current method requires +4 days in a vacuum oven). This idea also applies to hollow fiber membranes. It is possible to repair minor skin layer defects using elevated temperature annealing procedures.

8.3.3 Asymmetric Hollow Fibers

In the final portion of our study we were able to successfully produce asymmetric hollow fiber membranes containing nanoplatelet fillers, but they were highly defective for selective gas permeation. Hollow fiber spinning and the production of defect-free membranes is challenging in its own right and incorporating inorganic filler adds another variable. Regardless, through careful dope and spin condition optimization it is possible to produce defect-free membranes. From our results we suspect that the first step would be to increase the polymer concentration in the sheath dope to promote skin layer formation. To do this, however, would require increasing the total clay content in solution in order to maintain a desirable polymer-to-platelet ratio. Improved exfoliation and dispersion techniques may be required to produce the necessary dope composition (see Section 7.2.1).

8.3.4 Hybrid Membrane Characterization

A review of polymer-nanoplatelet composite literature indicates that there is a wide variety of techniques that may be used to characterize these materials.[8,9] For our purposes we focused on gas transport measurements and transmission electron microscopy (TEM). Additional characterization tools may complement the results that we obtained or even provide new insight into our observations. Thermal and x-ray based techniques are the most commonly used.[9] Nuclear magnetic resonance (NMR), Fourier transform infrared spectroscopy (FTIR) and SANS have also been used.[8] Any or all of these characterization tools, combined with gas transport measurements, may provide supporting information that can lead to more conclusive statements regarding the preparation and formation techniques.

Both wide and small angle x-ray scattering (WAXS and SAXS) have been used to characterize exfoliation of nanoplatelet materials. The intrinsic tactoid structure of nanoplatelet materials show Bragg peaks in the lower range of 2θ (2-15º) that typically correspond to the gallery spacing between individual platelets. Once exfoliated, these peaks will disappear into the very low range and are only visible with SAXS. Moreover, WAXS measurements of a nanocomposite samples can provide information regarding the degree of exfoliation in the hybrid. If the intrinsic Bragg peaks are no longer visible then there it is highly likely that the platelets are exfoliated. The same conclusion applies if the peaks are visible but shifted into the very low range.

Diffential scanning calorimetry (DSC) and dynamic mechanical analysis (DMA) are also valuable tools for characterizing nanocomposites. DSC studies are focused on measuring the shift in glass transition temperature (T_g) of the composite compared to the pure polymer. The movement of the T_g can provide information regarding the interface between the polymer and filler and qualitatively the degree of exfoliation. DMA studies provide similar information, but the measurement principles are different. In this case the mechanical properties are measured (modulus, tensile strength, thermal expansion) under a variety of constraints.

8.3.5 Organic-Inorganic Interactions

It has been stressed throughout this work that adhesion between the polymer and filler is critical for producing a membrane with enhanced properties. Due the extensive research the field of polymer-clay composites, there have been significant advancements in the knowledge polymer-clay interactions. Numerous authors have proposed mechanisms for organic-inorganic adhesion for a wide variety of materials. However, as new materials are developed and new material pairs are investigated, it is important to reconsider the potential interactions.[10] Molecular simulations are widely used as an investigatory tool to predict the interactions between organic and inorganic materials. They may also be used to explain empirical results. An alternative

experimental technique is atomic force microscopy. We will discuss these two approaches as they pertain to polymer-nanoplatelet hybrid systems in detail below.

8.3.5.1 Molecular Simulations

All of the conclusions from our study were based on experimental results and observations. Ultimately, experimental studies are necessary to prove the value of any material. However, molecular simulations may be used to pre-screen materials to predict the material properties. With respect to polymer-nanoplatelet materials there have been significant investigations related to predicting the morphology of these systems.[11-14] Scocchi, *et al*, in particular, have shown that molecular simulations can predict characteristics in macro- and micro-domains that match well with experimental data. Regarding our work, we believe that molecular simulations may provide insight into the observed polymer-platelet interactions – especially the proposed *zone of influence* effects.

8.3.5.2 Atomic Force Microscopy

There are techniques reported in the literature for quantifying interaction energies between solid and amorphous (e.g. polymers, biological specimens) materials using atomic force microscopy (AFM). These measurements provide insight into the potential interactions between two materials based on attraction/repulsion forces. Various authors have reported successful measurements between polymer and inorganic materials. The techniques for conducting these measurements vary, but one approach that has shown recent success is the *colloidal probe technique*.[15-19] In this manner, a spherical inorganic particle (d~2-20μm) is attached to the AFM cantilever or probe tip. The polymer, on the other hand, is coated on a glass or silicone substrate. This modified probe is then used to measure forces between the attached particle and the coating substrate.[15] We propose that a modified version of this method could be useful in quantifying interactions between polymer and nanoplatelets. A cartoon of the experimental setup is shown in Figure 8.1.

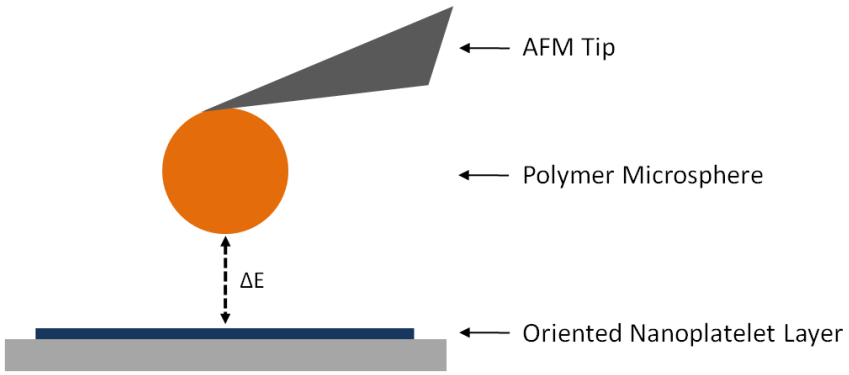

Figure 8.1: Experimental schematic for measuring polymer-nanoplatelet interactions via AFM

Unlike the work of previous authors, we propose to attach a polymer microsphere to the AFM tip rather than the inorganic particle. This is primarily motivated by the high aspect ratio geometry of the inorganic phase. Producing polymer microspheres is a well established process and has even been proven viable for polyimide materials.[20,21] Furthermore, literature reports show that exfoliated nanoclays in solution will align into a flat geometry on a substrate if the suspending medium is removed.[22,23] Fundamentally, this approach is similar to the current colloidal probe approach.

Recently there have been reports of attaching polymer microspheres to the AFM tip.[24,25] However, to our knowledge this has procedure has not been implemented to measure the interactions between organic and nanoplatelet materials. If implemented and successful, this approach could have applicability in other organic-inorganic systems.

8.4 References

1. S. Yun, D. Attard, V. Lo, J. Davis, H. Li, B. Latella, F. Tsvetkov, H. Noorman, S. Moricca, R. Knott, H. Hanley, M. Morcom, G. Simon G. Gadd, "Spray-Dried Microspheres as a Route to Clay/Polymer Nanocomposites," *Journal of Applied Polymer Science* **108** (3), 1550-1556 (2007).

2. M. Das, "Membranes for Olefin/Paraffin Separations," *PhD Dissertation*, Georgia Institute of Technology, 2009.

3. R. Chafin, J. Lee, W.J. Koros, "Effects of Casting and Post Casting Annealing on Xylene Isomer Transport Properties of Torlon Films," *Polymer* **51** (15), 3462-3471 (2010).

4. F. Zhou, W.J. Koros, "Study of Thermal Annealing on Matrimid Fiber Performance in Pervaporation of Acetic Acid and Water Mixtures," *Polymer* **47** (1), 280-288 (2006).

5. J. Wind, S. Sirard, D. Paul, P. Green, K. Johnston, W.J. Koros, "Carbon Dioxide-Induced Plasticization of Polyimide Membranes: Pseudo-Equilibrium Relationships of Diffusion, Sorption, and Swelling," *Macromolecules* **36** (17), 6433-6441 (2003).

6. T. Moore, "Effects of Materials, Processing, and Operating Conditions on the Morphology of Gas Transport Properties of Mixed Matrix membranes," *PhD Dissertation*, University of Texas - Austin, 2004.

7. R. Adams, C. Carson, J. Ward, R. Tannenbaum, W.J. Koros, "Metal Organic Framework Mixed Matrix Membranes for Gas Separations," *Microporous and Mesoporous Materials* **131** (1-3), 13-20 (2010).

8. S. Pavlidou, C. Papaspyrides, "A Review on Polymer-Layered Silicate Nanocomposites," *Progress in Polymer Science* **33** (12), 1119-1198 (2008).

9. D.R. Paul, L.M. Robeson, "Polymer Nanotechnology: Nanocomposites," *Polymer* **49** (15), 3187-3204 (2008).

10. S. Yariv, H. Cross (ed), *Organo-Clay Complexes and Interactions*. (Marcel Dekker, Inc., New York, NY, 2002).

11. G. Scocchi, P. Posocco, J-W. Handgraaf, J. Fraaije, M. Fermeglia, S. Pricl, "A Complete Multiscale Modelling Approach for Polymer–Clay Nanocomposites," *Chemistry - A European Journal* **15** (31), 7586-7592 (2009).

12. G. Scocchi, P. Posocco, M. Fermeglia, S. Pricl, "Polymer-Clay Nanocomposites: A Multiscale Molecular Modeling Approach," *Journal of Physical Chemistry: Part B* **111** (9), 2143-2151 (2007).

13. G. Scocchi, P. Posocco, A. Danani, S. Pricl, M. Fermeglia, "To the Nanoscale, and Beyond! Multiscale Molecular Modeling of Polymer-Clay Nanocomposites," *Fluid Phase Equilibria* **261** (1-2), 366-374 (2007).

14. Q. Zeng, A. Yu, G. Lu, "Multiscale Modeling and Simulation of Polymer Nanocomposites," *Progress in Polymer Science* **33** (2), 191-269 (2008).

15. J-H. Lee, B. Thio, T-H. Bae, J. Meredith, "Role of Lewis Basicity and van der Waals Forces in Adhesion of Silica MFI Zeolites (010) with Polyimides," *Langmuir* **25** (16), 9101-9107 (2009).

16. B. Thio, J-H. Lee, J. Meredith, A. Keller, "Measuring the Influence of Solution Chemistry on the Adhesion of Au Nanoparticles to Mica Using Colloid Probe Atomic Force Microscopy," *Langmuir* **26** (17), 13995-14003 (2010).

17. B. Thio, J. Meredith, "Measurement of Polyamide and Polystyrene Adhesion with Coated-Tip Atomic Force Microscopy," *Journal of Colloid and Interface Science* **314** (1), 52-62 (2007).

18. K. Feldman, T. Tervoort, P. Smith, N. Spencer, "Toward a Force Spectroscopy of Polymer Surfaces," *Langmuir* **14** (2), 372-378 (1998).

19. J. Nalaskowski, J. Drelich, J. Hupka, J. MIller, "Adhesion between Hydrocarbon Particles and Silica Surfaces with Different Degrees of Hydration as Determined by the AFM Colloidal Probe Technique," *Langmuir* **19** (13), 5311-5317 (2003).

20. Z. Chai, Z. Xiao, S. Xuefei, "Preparation of Polymer Microspheres from Solutions " *Journal of Polymer Science: Part B: Polymer Physics* **41** (2), 259-165 (2002).

21. K. Soppimath, A. Kulkarni, T. Aminabhavi, C. Bhaskar, "Cellulose Acetate Microspheres Prepared by O/W Emulsification and Solvent Evaporation Method," *Journal of Microencapsulation* **18** (6), 811-817 (2001).

22. E. Balnois, S. Durand-Vidal, P. Levitz, "Probing the Morphology of Laponite Clay Colloids by Atomic Force Microscopy," *Langmuir* **19** (17), 6633-6637 (2003).

23. T. Szabo, J. Wang, A. Volodin, C. van Haesendonck, I. Dekany, R. Shoonheydt, "AFM Study of Smectites in Hybrid Langmuir-Blodgett Films: Saponite, Wyoming Bentonite, Hectorite, and Laponite," *Clays and Clay Minerals* **57** (6), 706-714 (2009).

24. E. Glynos, V. Koutsos, W. McDicken, C. Moran, S. Pye, J. Ross, V. Sboros, "Nanomechanics of Biocompatible Hollow Thin-Shell Polymer Microspheres," *Langmuir* **25** (13), 7514-7522 (2009).

25. J. Ally, E. Vittorias, A. Amirfazili M. Kappl, E. Bonaccurso, C. McNamee, H. Butt, "Interaction of a Microsphere with a Solid-Supported Liquid Film," *Langmuir* **26** (14), 11797-11803 (2010).

THIS PAGE INTENTIONALLY LEFT BLANK.

APPENDIX A

POLYETHERIMIDE-ORGANOCLAY NANOCOMPOSITES

A.1 Overview

In Chapter 3 of this work we indicated that we had attempted to create polymer-nanoplatelet hybrid materials using conventional methods. Despite the abundant success reported throughout the literature, we found that we were unable to incorporate organo modified submicron nanoclays into a polymer matrix using solution blending procedures. At the time of this work we had not made any of the advancements that lead to the eventual success of this project. For the reader's benefit, our study regarding organoclays is presented in full detail in this appendix.

A.2 Current Investigation

In this section of the thesis we will report initial attempts to produce asymmetric hollow fiber membranes containing nanoplatelets. The fibers and composites reported focus on the incorporation of impermeable model nanoplatelet materials (nanoclays) rather than actual molecular sieving nanoplatelets. Numerous molecular sieving nanoplatelets have been identified as potential filler materials in membrane applications[1,2]; however these materials are difficult to synthesize in the quantities needed for hollow fiber production. Nanoclays have been extensively studied as filler materials in polymer matrices for a variety of applications.[3] These materials have similar characteristics as the permeable nanoplatelets and are widely available. The purposes of the reported investigation are twofold. One, we want to study the addition of a nanoplatelet fillers to the hollow fiber membrane platform and to determine the processing effects. Second, we wanted to develop processing techniques using model materials that could be applied to a hybrid system containing molecular sieving nanoplatelets at a later date.

A.2.1 Surface Modification of Nanoplatelets

Many techniques have been used to produce traditional nanoclay-polymer composites.[3,4] Surface modification of clays is commonly used to aid in particle exfoliation and dispersion. This approach is generally combined with melt-blending or *in situ* polymerization in order to incorporate the filler into the polymer matrix. There have been reports in the literature that show surface modified nanoclays can be dispersed in certain halogenated solvents with limited mechanical energy input.[5,6] We have investigated the application their findings in the asymmetric hollow fiber format.

A.3 Materials and Methods

For this study inexpensive impermeable layered silicates (clays), rather than molecular sieving nanoplatelets, were used. This work was conducted in collaboration with other research groups who have focused on the synthesis and incorporation of molecular sieving nanoplatelets into polymer matrices. The clay nanoplatelet materials were identified as models to enable developing the fundamental basis in this area before utilizing the exotic molecular sieving nanoplatelets.

A.3.1 Materials

Clays are naturally occurring layered silicate materials that exhibit similar geometric characteristics as the molecular sieving nanoplatelets of interest. For this work we chose to use a synthetic hectorite, Laponite® RD (Southern Clay Products, USA), as our model nanoplatelet material. A single layer of Laponite® RD is ~1nm thick with a diameter of 25-30nm.[7] Like many other clays, a sheet of Laponite® RD is comprised of three layers – tetrahedral:octahedral:tetrahedral (TOT). This crystal structures leads to a net negative charge on the particle faces. Sodium (Na^+) cations stabilize the surface charge via a shared ionic bond in the interstitial space between the layers. Laponite® RD readily disperses in water and forms a transparent suspension of uniform particles.

A polyetherimide (2,2-bis[4-(3,4-dicarboxyphenoxy)phenyl] propane dianhydride - 1,3-phenylenediamine) under the trade name Ultem® 1000 (GE Plastics, USA) has received

attention as a valuable membrane material.[8] This material has been used to produce dense films as well as asymmetric hollow fiber membranes that exhibit favorable O_2/N_2 selectivities. The polymer used in these experiments has a weight average molecular weight of 50,000-60,000 g/mol.

Anhydrous n-methyl-2-pyrrolidone (NMP), tetrahydrofuran (THF), chloroform and ethanol were used as solvents during the investigation and were used as received from Sigma-Aldrich Co. The salt, $LiNO_3$ was used as the non-solvent component in the membrane solution and was received from Sigma-Aldrich Co. Dimethyl dihydrogenated tallow quaternary ammonium hydroxide (DMDT) was generously provided by Akzo-Nobel Inc. (USA) and used to surface modify Laponite® RD particles.

A.3.2 Particle Surface Modification

A 1wt% dispersion of Laponite® RD was prepared by mixing the as-received clays in a flask containing a solution of 50wt% DI water and 50wt% ethanol. The particles readily exfoliated in this solution. Using reported literature values for the cation exchange capacity (CEC) of Laponite® RD[9,10], a mass of DMDT equaling twice the CEC was added to the clay dispersion and allowed to mix for 24 hours on a heated stir plate (T=80°C). A water cooled reflux column was used to prevent solvent losses. During the treatment stage the particles would precipitate inside the flask. Treated particles were collected from the solution using a vacuum filter apparatus equipped with a stirrer to prevent dense filter cake formation. To remove excess surfactant, a two-stage rinse procedure was used. First, the filtrate was re-dispersed in excess methanol (methanol volume ~ initial dispersion solvent) and allowed to mix for 24 hours on a heated stir plate (T=80°C). Particles were collected again using the same filtration set-up as before. Methanol rinsed particles were then re-dispersed in n-hexane. This dispersion was allowed to reflux at 55°C for 24 hours. After the final rinse step, the dispersion was poured into an open glass dish on the same heated stir plate wherein the n-hexane rapidly evaporated. Surface treated particles remained as a fine off-white powder.

The two rinse steps (methanol and n-hexane) were chosen specifically. It was observed that if only water or ethanol was used to rinse the modified particles, followed by heated drying in a dish, a dense cake would form. A dense cake means that the particles are very "tightly" agglomerated. Methanol has a lower surface tension than water or ethanol and n-hexane is even lower yet. By slowly decreasing the surface tension of the solvent on the particles we were able to produce larger agglomerates, but with lower density (i.e. not as tightly packed). We believed that "loose" agglomerates would be easier to exfoliate in a solvent system than the former case.

A.3.3 Solution Development & Membrane Formation

Preparation and formation of asymmetric hollow fiber membranes has been discussed at length in the literature so for the sake of brevity we will not discuss the process here. The cloud-point technique was used to determine the composition of the hybrid solution used to produce the reported asymmetric hollow fibers.[11] These fibers were made using previously reported methods for so-called dry-wet hollow fiber spinning. Fibers were not made using the surface modified particles; syringe extrusion tests (described in detail later) were used to determine if the hybrid solution would demonstrate the characteristics required to spin fibers at a later date.

Unmodified Laponite® RD was incorporated into the reported asymmetric hollow fiber membranes. The desired quantity of clays was added to the required quantity of NMP. A high-powered sonication horn (Dukane Ultra 1000 Auto-Trac, Dukane Corp., USA) was used to mix the dispersion. The mixture was sonicated for five minutes and allowed to rest for 10 minutes (to allow cooling); this procedure was repeated a total of five times. Next, the required mass of $LiNO_3$ was added to the dispersion and the entire vessel was placed inside a standard sonication bath (Branson 1510, Bransonic Inc., USA) and allowed to sonicate for 45 minutes. Tetrahydrafuran was then added followed by the Ultem® 1000 polymer. Both the clays and polymer were dried overnight in a vacuum oven at 100°C. The polymer solution was allowed to mix slowly on a roller device until the polymer had completely dissolved (~3 days).

For the syringe test solutions, modified Laponite® RD was dispersed in a desired quantity of chloroform and allowed to mix in a sonication bath for 24 hours. A water cooled reflux column was used to prevent solvent losses. Following the dispersion step, Ultem® 1000 was added to the solution and mixed using the procedure described above. An aliquot of the polymer solution was placed into a 5 ml syringe and this solution was extruded into a beaker of methanol at room temperature to induce phase separation.

A.3.4 Characterization

A.3.4.1 Scanning Electron Microscopy (SEM)

SEM was used as the primary characterization technique in order to determine the efficacy of the clay exfoliation within the polymer matrix. Images were taken using a JEOL 1530 (JEOL, Japan) machine. Samples were prepared by soaking a 2 cm long section of fiber in n-hexane for 2 minutes. The section was then removed from the solvent and placed in a dish containing liquid N_2 and allowed to soak for 2 minutes. Precision tweezers were used to fracture the fiber while submersed.

A.3.4.2 X-ray Diffraction (XRD)

Powder XRD was used to investigate the effects of the surface modification process. A PANalytical X'Pert PRO (PANalytical, Netherlands) fitted with a Ni-filter and a Cu Kα radiation source. The nanoclays were modified in small batches so a shallow, quartz-bottomed sample pan was used to conserve material.

A.3.4.3 Thermal Gravimetric Analysis (TGA)

TGA was used to verify that the DMDT surfactant was present on the surface of the clays after the treatment process. A N_2 gas sweep was used during the TGA measurements. The measurements were made using a Netzsch STA 409 PC TGA (Netzsch Instruments Inc., USA).

A.3.4.4 Gas permeation

Permeation measurements were conducted on the asymmetric hollow fibers. Fiber module preparation and testing procedures are reported elsewhere.[12,13]

A.4 Results & Discussion

A.4.1 Asymmetric Hollow Fibers Containing Unmodified Laponite® RD Filler

Two hypotheses were made prior to spinning these fibers. First, we hypothesized that NMP could swell the clay stacks such that polymer could intercalate and exfoliate the layers. Water has a Snyder Polarity Index of P'=10.2 [14] and as a solvent readily exfoliates Laponite® RD particles. Amongst common solvents for advanced polymer, NMP has a higher Snyder Polarity Index value at P'=6.7 (for n-hexane P'=0.1). Second, as noted in Figure 4, we assumed that the nanoplatelets would orient in the desired direction due to the high shear forces applied within the spinneret during the fiber spinning process.

The composition of the hybrid solution used to spin the asymmetric hollow fibers is shown in Table A.1. Within the spinning solution, the clay loading appears low because we are interested in the ratio of polymer and filler. The as-spun fibers have an estimated nanoclay loading of 2.5wt%.

Table A.1: Spinning solution composition

Component	wt% Loading
Ultem® 1000	**31.2**
Laponite® RD	**0.8**
n-methyl-2-pyrrolidone	**3.5**
tetrahydrofuran	**51.6**
$LiNO_3$	**12.9**

It was found that the direct dispersion process used does not produce the desired state of complete exfoliation. On the other hand, the presence of the particles in the spinning solution did not interfere with fiber formation. Figure A.1a is scanning electron micrograph showing the cross-sectional area of one of the as-spun fibers. Here we can see that the fiber is concentric, has a clear bore passage and the desired porous substructure. In the same image we have highlighted an area containing large particulates. A magnified image of this area is shown in Figure A.1b. This image clearly suggests that all of the dispersed Laponite® RD particles did not exfoliate as desired. Furthermore, we see that the particles are not evenly distributed throughout the fiber. Additional SEM images (not shown here) yield the same results.

Despite the failure to fully exfoliate the clay filler, permeation test modules were prepared using the as-spun fibers. During the spinning process the air gap was greatly varied in order to change the thickness of the permselective layer. Unfortunately, all of the fibers tested were non-selective for the standard gases tested (N_2, O_2, and He); indicating defects in the skin layer.

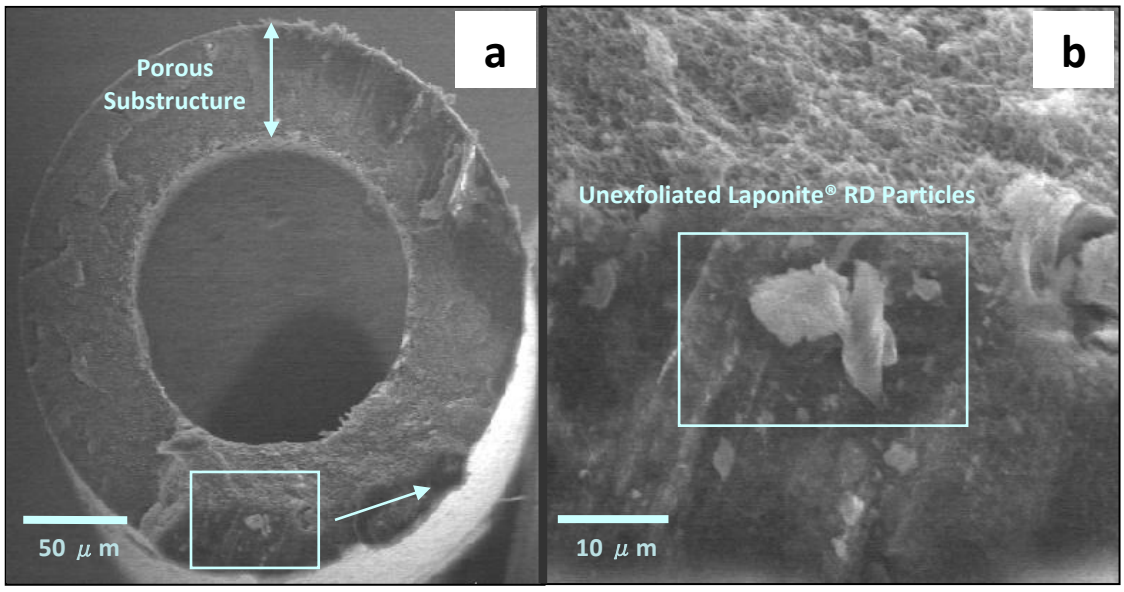

Figure A.1: (a) asymmetric hollow fiber with 2.5wt% nanoclay filler (b) magnified image of unexfoliated Laponite® RD within the Ultem® 1000 matrix

Very little clay material (seemingly less than 2.5wt%) is visible in Figure A.1, so we consider two possible scenarios to explain this observation. One, it is possible that the particles remained so large within the hybrid solution that they were removed by the coarse 90μm sintered metal filter that was in place upstream from the spinneret. Figure A.2a shows an SEM image of the as-received particles. Notice that there is a broad distribution of sizes, but that a bulk of the material is present as large crystals. These larger particles, if not exfoliated during the dispersion process, would be easily removed by the in-line filter. On the other hand, a second scenario may be that a majority of the particles were indeed exfoliated in the system. If this were true, then the nanoplatelets would not be visible under standard SEM measurements. Transmission electron microscopy (TEM) images must be taken to clarify which of these scenarios is most likely. We have not pursued this characterization at this point because, as noted, the fibers were shown to be highly defective with the permeation experiment. It is, however, our expectation that adequate exfoliation was not achieved, so we decided to seek an alternate parallel path while resolving the situation with regard to the platelets highlighted in Figure A.1. Even if some of the clay is unexfoliated and is captured by the pre-filter, it would be difficult to detect since the clay is present at very low loadings initially.

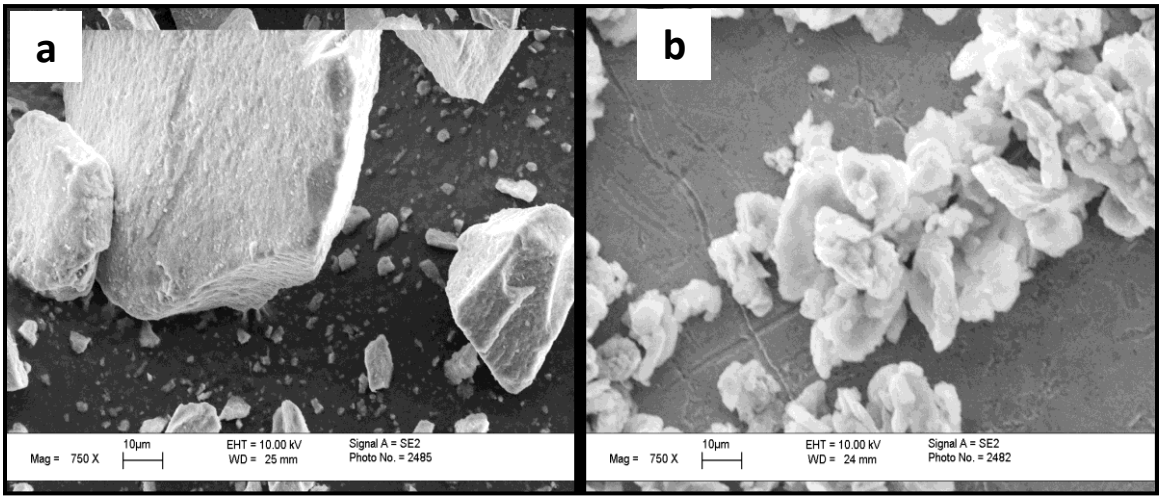

Figure A.2: (a) as-received Laponite® RD deposited on carbon tape (b) nanoclays treated with DMDT

A.4.2 Surface Modification of Laponite® RD

Two characterization techniques were used to determine the efficacy of the surface modification process prior to forming a new dope with the particles treated according to Section A.1.1. A TGA plot is shown in Figure A.3. The lower curve corresponds to as-received Laponite® RD. Assuming the absence of any organic material, the broadly sweeping curve represents the loss of atmospherically adsorbed water. The upper curve corresponds to a sample of Laponite® RD that was treated with DMDT. Initially, there is a small water loss followed by a plateau then a drastic drop in mass. The latter drop is due to desorption of the DMDT surfactant at high temperatures. An XRD spectrum is shown in Figure A.4. A comparative analysis was completed to ensure that the surface modification process did not alter the crystal structure of the particles. The top spectrum corresponds to the as-received Laponite® RD and the lower spectrum corresponds to the surface modified clays. We see that the two spectra have identical primary peaks. Conducting small-angle x-ray scattering (SAXS) analysis would be a valuable additional study. SAXS analysis would allow us to probe the interstitial d-spacing between the particles and quantify the degree of exfoliation. These data have not been collected as of yet.

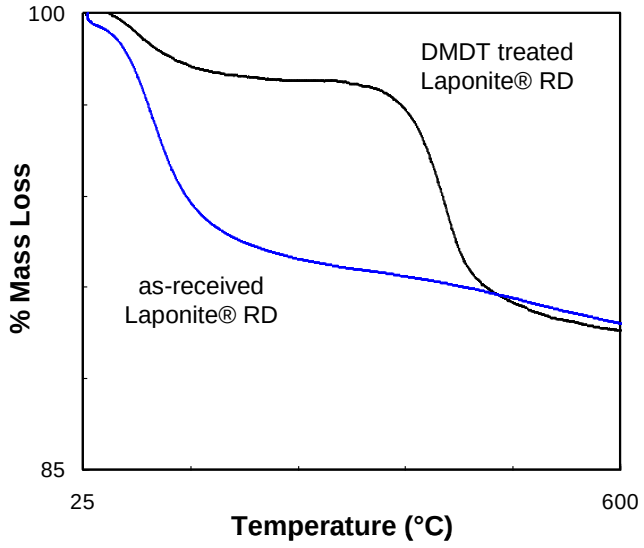

Figure A.3: TGA analysis of treated vs. as-received Laponite® RD

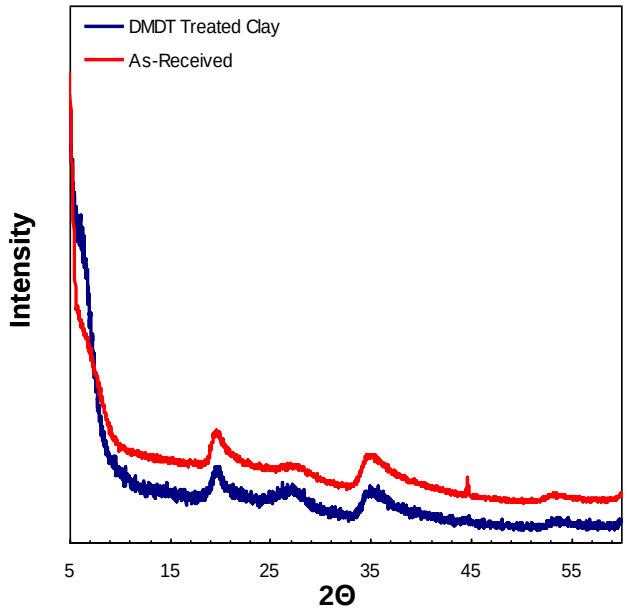

Figure A.4: XRD pattern comparing treated and untreated Laponite® RD

A.4.3 Syringe Extrusion Tests

Spinning asymmetric hollow fibers is a time intensive process. We completed syringe extrusion tests as a preliminary examination with the modified clays. These tests allow us to quantify the efficacy of the solution preparation process. Moreover, during the extrusion we can qualitatively determine, via visual observations, if the prepared solution will have the characteristics (viscosity, rate of phase separation, etc) needed to complete the dry-wet spinning process. This was particularly important in this case because methanol is required for the coagulation step. The coagulation bath used in our spinning operation is greater than 80 liters; a large amount of methanol would be wasted if the spinning solution were not viable.

The solution used for these tests was 30wt% solids (polymer and clays) with the balance comprising chloroform. Polymer and modified clays were loaded at a ratio of 95wt% polymer and 5wt% clays, respectively. Unlike the solution used in the first experiment with the unmodified clays, we did not add phase-inducing salt for this investigation. Our

primary objective was to determine if the modified clays would exfoliate during the solution preparation process.

A cross-sectional SEM image of the extrudate is shown in Figure A.5a. In this image we see large particulates throughout the fiber. When the image is magnified (Figure 9b) we see that the particulates are still quite large. Comparing Figure 9b with Figure A.5b, we can clearly see that little exfoliation has occurred. Moreover, unlike the previously discussed hollow fibers, it appears that the surface area scan corresponds roughly to the original loading (5wt%), thereby suggesting that no significant amount of the modified clays had been exfoliated. These images clearly show that the proposed exfoliation process was ineffective.

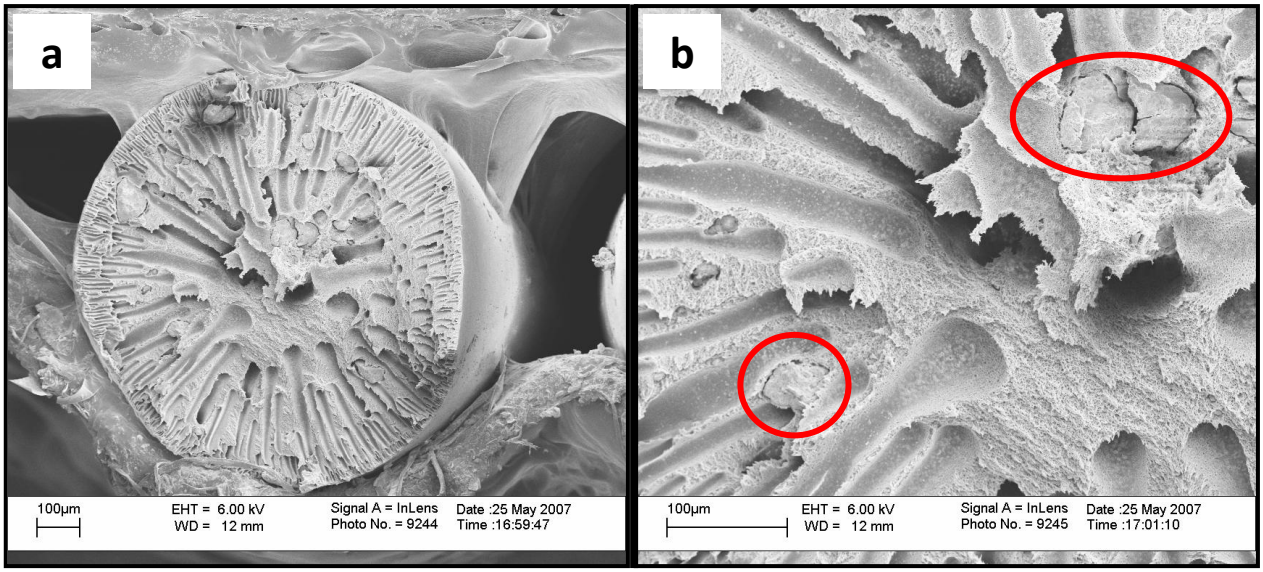

Figure A.5: (a) syringe extrusion with 5wt% nanoclay (b) magnified image highlighting agglomerated Laponite® RD particles within the Ultem® 1000 matrix

A.5 Summary & Conclusions

It was shown that the choice of solvent used to disperse these materials is not straightforward. We are currently investigating alternative solvent systems that may be used to readily exfoliate and disperse these materials and have the capability of adding a polymer that is favorable for membrane formation.

Surface modified materials have been successfully used throughout the literature, but we have shown that simple mixing procedures are not adequate for creating primarily organic solvent dispersion of these materials suitable for forming realistic membranes with high performance polymers. It is worthwhile to investigate the possibility of incorporating modified nanoplatelets into a polymer matrix via melt-blending or *in situ* polymerization prior to the preparation of the fiber spinning solution. The as-produced composite matrix could potentially be added directly to solvent, eliminating the need for additional complex mixing prior to fiber formation. We have also begun to look into these options.

Hybrid membranes containing molecular sieving fillers have the potential to extend the separation benefits provided by the polymeric membrane platform. Molecular sieving nanoplatelet materials add further benefits through processing and productivity advantages. These materials, however, introduce additional challenges that are not applicable to membrane systems that use A_r~1 materials. The work presented here is a first glance at the challenges and attempts made at introducing nanoplatelet materials into an asymmetric hollow fiber.

A.6 References

1. E.L. Cussler, "Membranes Containing Selective Flakes," *Journal of Membrane Science* **52**, 275-288 (1990).

2. H-K Jeong, W. Krych, H. Ramanan, S. Nair, E. Marand, and M. Tsapatsis, "Fabrication of Polymer/Selective-Flake Nanocomposite Membranes and Their Use in Gas Separation," *Chemistry of Materials* **16** (20), 3838-3845 (2004).

3. F. Hussain, M. Hojjati, M. Okamoto, and R. E. Gorga, "Review Article: Polymer-Matrix Nanocomposites, Processing, Manufacturing, and Application: An Overview," *Journal of Composite Materials* **40** (17), 1511-1575 (2006).

4. T.J. Pinnavaia and G.W. Beall, *Polymer-Clay Nanocomposites*. (John Wiley & Sons, Ltd., New York, 2000).

5. D. Ho, R. Briber, and C. Glinka, "Characterization of Organically Modified Clayes Using Scattering and Microscopy Techniques," *Chemistry of Materials* **13** (5), 1923-1931 (2001).

6. D. Ho and C. Glinka, "Effects of Solvent Solubility Parameters on Organoclay Dispersions," *Chemistry of Materials* **15** (6), 1309-1312 (2003).

7. M. Kroon, W. L. Vos, and G. H. Wegdam, "Structure and Formation of a Gel of Colloidal Disks," *Physical Review E* **57** (2), 1962-1970 (1998).

8. S. Husain and W. J. Koros, "Mixed Matrix Hollow Fiber Membranes Made with MHSSZ-13 Zeolite in Polyetherimide Polymer Matrix for Gas Separation," *Journal of Membrane Science* **288** (1-2), 195-207 (2007).

9. N. N. Herrera, J. M. Letoffe, J. L. Putaux, L. David, and E. Bourgeat-Lami, "Aqueous Dispersions of Silane-Functionalized Laponite Clay Platelets. A First Step Toward the Elaboration of Water-Based Polymer/Clay Nanocomposites," *Langmuir* **20** (5), 1564-1571 (2004).

10. N. N. Herrera, J. M. Letoffe, J. P. Reymond, and E. Bourgeat-Lami, "Silylation of Laponite Clay Particles with Monofunctional and Trifunctional Vinyl Alkoxysilanes," *Journal of Materials Chemistry* **15** (8), 863-871 (2005).

11. M. R. Kosuri and W. J. Koros, "Defect-free Asymmetric Hollow Fiber Membranes from Torlon®, a Polyamide-imide Polymer, for High-Pressure CO_2 Separations," *Journal of Membrane Science* **320** (1-2), 65-72 (2008).

12. S.C. Pesek, "Aqueous Quenched Asymmetric Polysulfone Flat Sheet and Hollow Fiber Membranes Prepared by Dry/Wet Phase Separation," *PhD Dissertation*, University of Texas - Austin, 1993.

13. D. Q. Vu, W. J. Koros, and S. J. Miller, "High Pressure CO_2/CH_4 Separation using Carbon Molecular Sieve Hollow Fiber Membranes," *Industrial & Engineering Chemistry Research* **41** (3), 367-380 (2002).

14. A. Barton, *Handbook of Solubility Parameters and Other Cohesion Parameters*. (CRC Press, Inc., Boca Raton, FL, 1983), 1st ed.

APPENDIX B

PREPARATION OF POLYMER NANOCOMPOSITE SAMPLES VIA FOCUSED ION BEAM (FIB) MILLING FOR TRANSMISSION ELECTRON MICROSCOPY (TEM) CHARACTERIZATION

B.1 Overview

A fortuitous relationship was formed with Dr. Alexander Moukasian and Ms. Tatyana Orlova at the University of Notre Dame (ND) during the course of this investigation. This team was responsible for the TEM images presented in this work. Due to the organic nature of polymer materials, it is often difficult to prepare and characterize polymers and polymer composites for TEM analysis. Borrowing from their vast experiences in materials characterization, the ND team developed a procedure for preparing polymer-nanoplatelet samples for TEM characterization. Their methods are faster and more reproducible than traditional ultramicrotomy methods. In this appendix we would like to provide the reader with a glimpse at the technique they used.

B.1 FIB Milling

We should preface that we are not claiming to be experts in the field of FIB milling. If the reader would like to know more about the subject, please refer to the abundance of literature on the subject.[1,2] Our objective is to present a simplified perspective of the complex, yet elegant procedure that was used by the ND team. A similar technique was reported by Hashemi, *et al* in 2006.[3] Based on the quality of the TEM images obtained, we believe the technique developed and implemented by the ND team is an improvement on the previously reported method. The procedure will be described stepwise with corresponding images for each step.

Step 1

A large piece of the membrane is loaded into the FIB chamber as a starting point. Next, bulk material is removed around a small strip of the membrane as shown in Figure B.1. This is the starting point for the TEM sample. The second milling step relieves the sample from the bulk via an undercut and two side cuts (Figure B.2). The sample can now be captured and transferred.

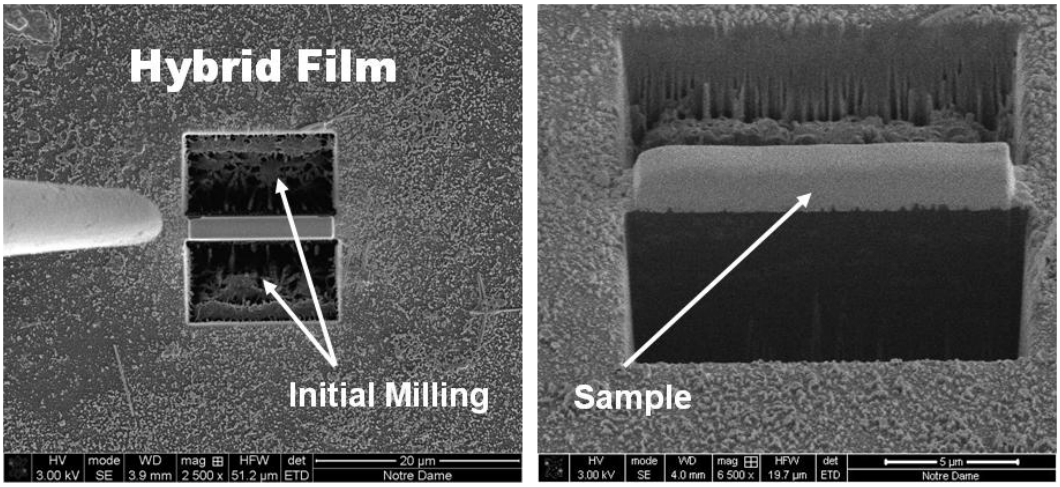

Figure B.1: Top view of hybrid film after initial milling and a side view of the initial sample

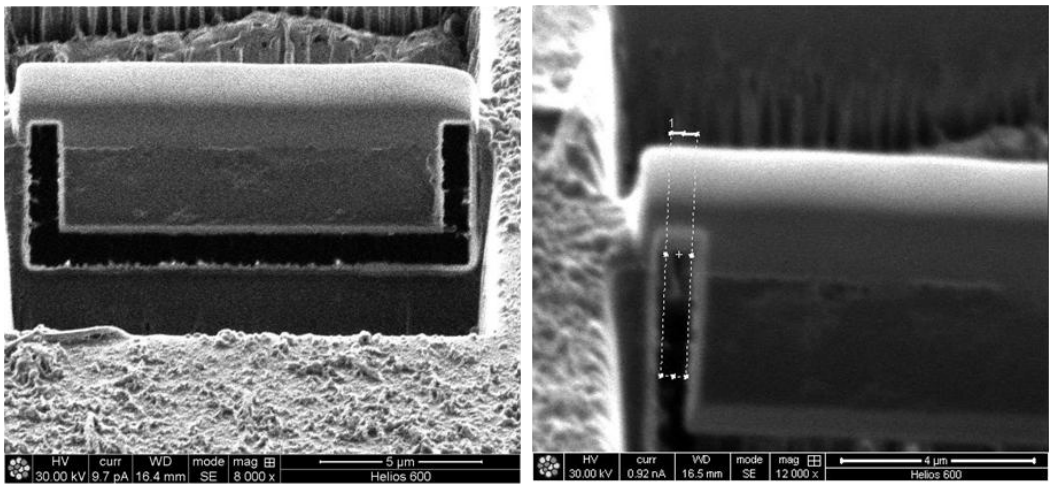

Figure B.2: Undercut of sample after bulk milling and a view of sample prior to the final side cut.

Step 2

Once the primary milling is complete, the sample is ready for removal from the bulk. An omni probe is used to transfer the sample in the chamber to the TEM grid. Platinum spot welding is used to attach the sample to omni probe. The weld point and the omni probe tip have been identified in Figure B.3.

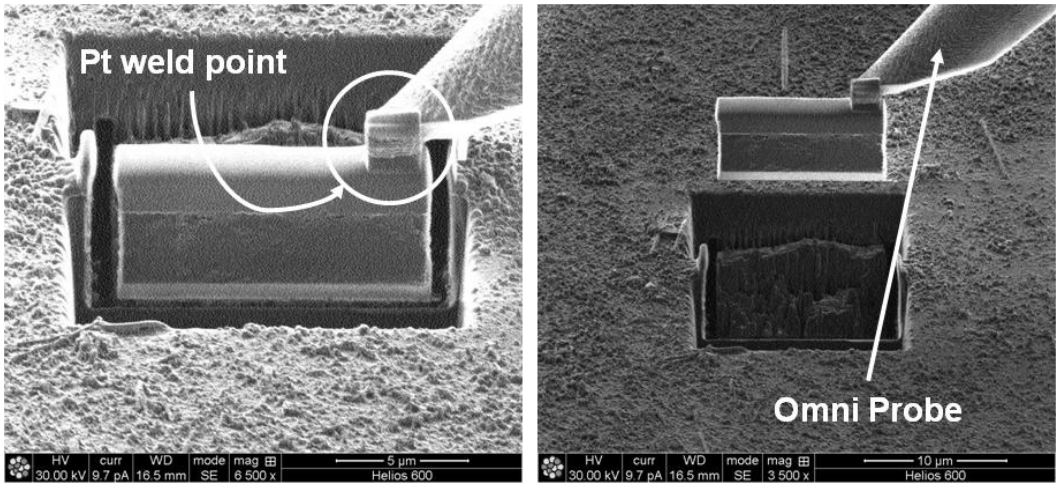

Figure B.3: Removal of the film sample after milling using an omni probe with a Pt spot weld

Step 3

After removing the sample from the bulk material it is transferred to the TEM grid using the omni probe. The sample grid and sample are shown in Figure B.4. A second platinum weld is used to secure the sample to the TEM grid. The weld holding the omini probe is destroyed so that the probe can be removed. Figure B.5 shows the sample welded to the grid and after the omni probe has been retracted.

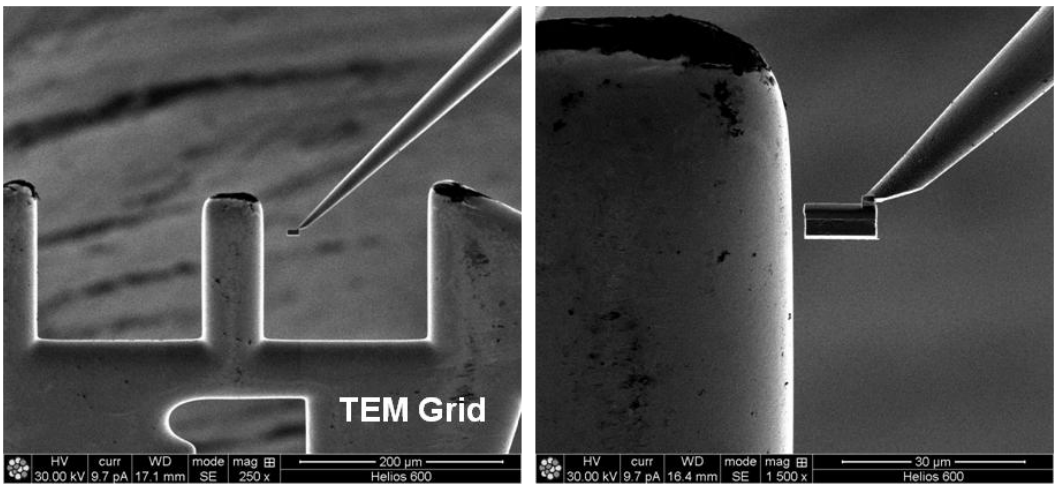

Figure B.4: Transfer of sample to TEM grid using omni probe. Image on the right is a magnified perspective of the sample and grid.

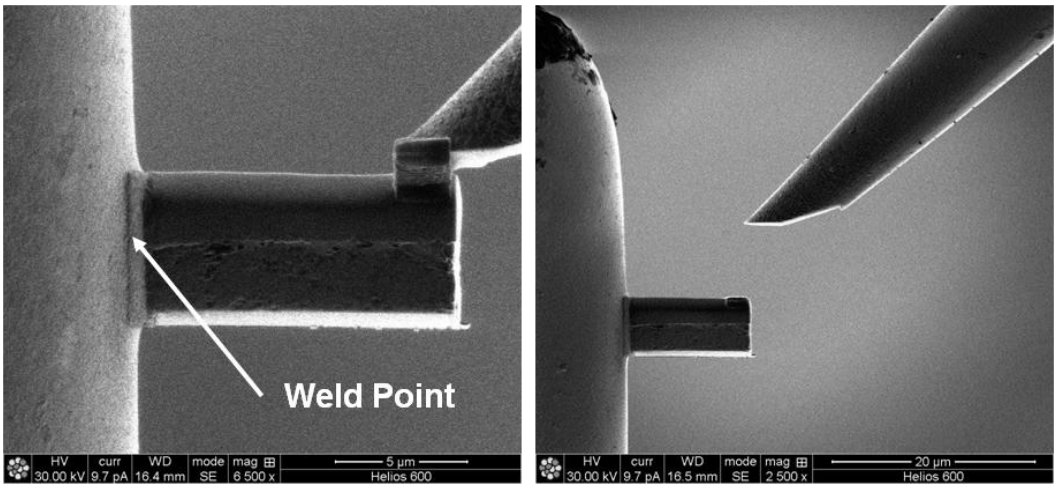

Figure B.5: Attached sample to TEM grid after Pt welding and retraction of omni probe

Step 4

To perform TEM characterization the sample must be sufficiently thin (ℓ<1µm). As we can see in Figure B.6, the sample is several microns thick (see top view). Therefore, the sample that was cut from the bulk must thinned down via additional milling. In Figure B.7 we see the sample after the thinning process.

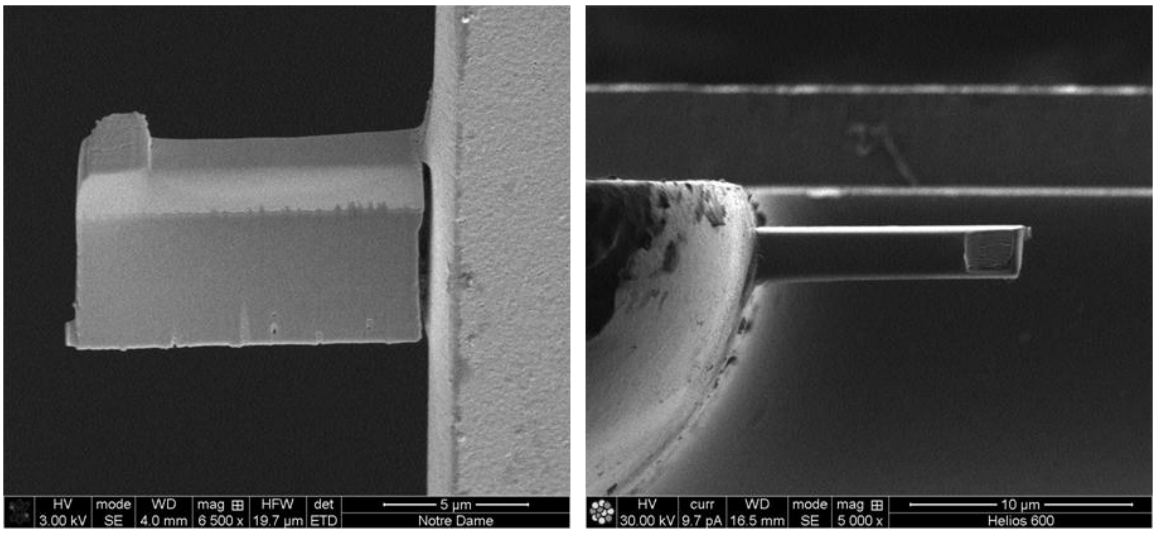

Figure B.6: Side and top views of sample before thinning.

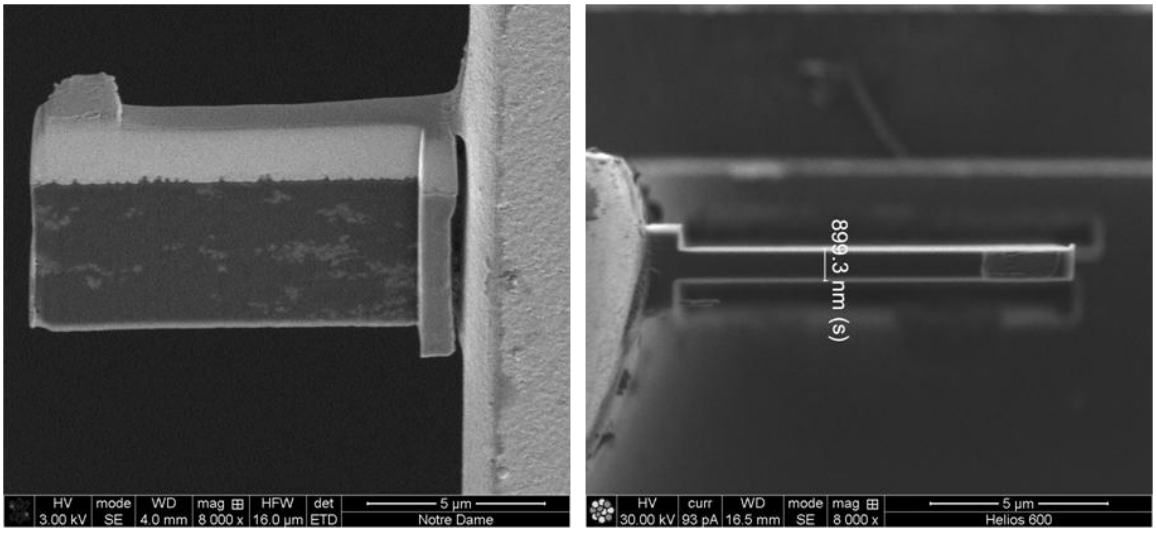

Figure B.7: Side and top views of sample after thinning.

B.3 References

1. N. Yao (ed), *Focused Ion Beam Systems: Basics and Applications*. (Cambridge University Press, New York, NY, 2010), 1st ed.

2. L. Giannuzzi and F. Stevie (eds), *Introduction to Focused Ion Beams: Instrumentation, Theory, Techniques and Practice* (Springer, New York, NY, 2005).

3. S. Hashemi, R. Sahraian, P. Lafleur, and K. Stoeffler, "Focus Ion Beam Preparation of Transmission Electron Microscope Sample in Polymer Clay Nanocomposite," *Iranian Polymer Journal* **15** (7), 539-545 (2006).

APPENDIX C

SUPPLEMENTAL RHEOLOGICAL DATA

C.1 Overview

A thorough discussion regarding the rheological properties of polymer-nanoclay dopes was provided in Chapter 4. The effects of mixing protocols and the contributions of nanoclay loadings were investigated with respect to viscosity under increasing shear conditions. In the write-up we made note that reverse measurements were made to see the hysteresis under decreasing shear, but that these data were not presented at the time for the sake of clarity in the figures. Furthermore, as we will see here, these data did not change the outcome of the analyses made previously. In this appendix we will provide a full disclosure of the hysteresis. Also, details regarding the methods of graphical data representation will be elucidated.

C.2 Data Compilation

All of the viscosity studies presented in Chapter 4 were reported in terms of viscosity or relative viscosity (η_r). To obtain these values we measured the viscosities of polymer-nanoclay dopes (η) and their respective suspending media – the "solvent" phase (η_s) – which consisted of polymer, solvent and non-solvent. Measurements for every dope and solvent were repeated by loading a new sample into the cell. Numerous measurements would be necessary to complete a proper error analysis and to claim that the data were statistically relevant. However, based on the objectives of these studies we only repeated these measurements once to ensure that there were no anomalies.

Once all of the measurements were completed, the data were averaged using Equation C.1 and the method described below. We should preface that this approach was not

necessary for the samples in the mixing study because those data were reported in terms of viscosity. In that case, the measured values were averaged. The high and low values were reported as the error bars in the plots, which represents a conservative error estimate.

$$\bar{\eta}_r = \overline{\left(\frac{\eta}{\eta_s}\right)} = \overline{\left(\frac{\eta^1}{\eta_s^1} + \frac{\eta^2}{\eta_s^2} + \frac{\eta^1}{\eta_s^2} + \frac{\eta^2}{\eta_s^1}\right)} \qquad \text{Eq. C.1}$$

In this equation η and η_s are the dope and solvent viscosities, respectively. On the right hand side of the equation, the superscript (1,2) denotes the measurement number. The relative viscosity for each data set was calculated from the individual parts and averaged as shown. When the data was plotted we used the high and low values as calculated from the parts in the right hand side of Equation C.1.

Additional tests are necessary in order to claim statistical relevance. However, from the data we gathered, we see that the error from average is not disconcerting. All of the plots are presented in the following two sections.

C.3 Viscosities of Samples Prepared Using Different Dispersion Methods

In the following two subsections we have presented the viscosity plots with hysteresis for each preparation technique used, with respect to the polymer. These data may are associated with the results and discussion presented in Section 4.1.2, where it was found that the high shear mixing procedure created a dope with improved exfoliation compared to sonication and low shear (rolling) mixing methods. The measured samples were designed to represent a dope that could be used to cast a film wherein the final membrane would have a 5wt% loading of Laponite® RD in a polymer matrix. Mass fractions for polymer, clay, NMP, DMSO and water were 9.5%, 0.5%, 80%, 5% and 5% respectively.

C.3.1 Cellulose Acetate-Laponite® RD Dopes

Viscosity profiles for each mixing method are shown in Figures C.1-C.3. Closed circles represent viscosity as shear rate is increased and open circles represent viscosity as shear rate is decreased. In Figures C.1 and C.2 there is a slight deviation in the hysteresis curves compared to the initial values. Figure C.3, on the other hand shows a larger deviation in the hysteresis. This is likely a product of platelet alignment at high shear rates. If the platelets are sufficiently exfoliated, at high shear they will align with the shear field to minimize resistance. However, when the shear is decreased the platelets will disorder and continue with random orientation. The deviation in the hysteresis corresponds to this effect. Note that when shear rate is sufficiently low, the viscosity approaches the initial value, indicating that the orientation is randomized.

C.3.2 Torlon®-Laponite® RD Dopes

Viscosity profiles for each mixing method are shown in Figures C.4-C.6. Closed circles represent viscosity as shear rate is increased and open circles are the reverse. Unlike the previous section where a deviation was observed in one example, the trends in these samples were quite consistent throughout.

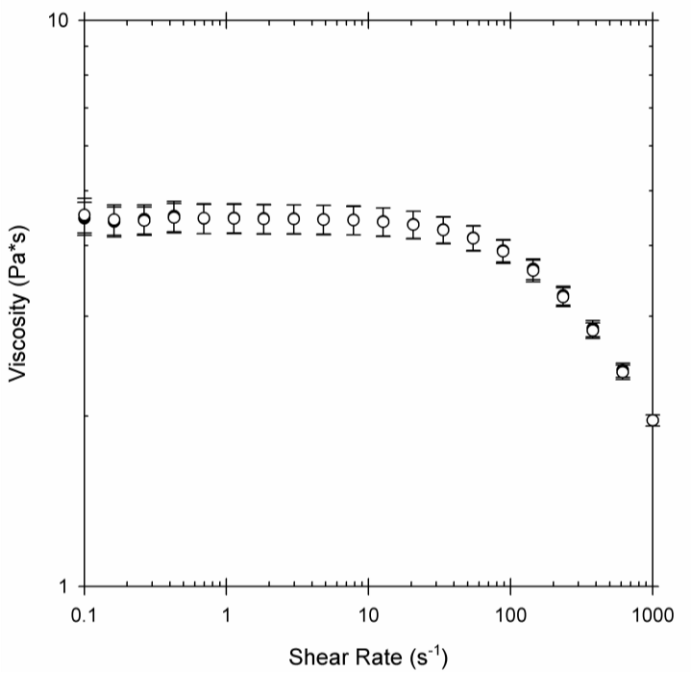

Figure C.1: Viscosity profile of cellulose acetate hybrid dopes prepared using low shear mixing.

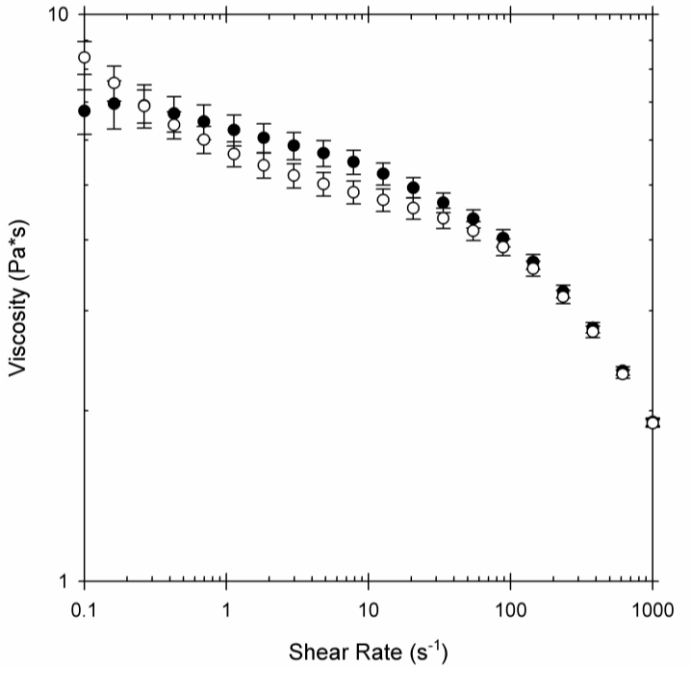

Figure C.2: Viscosity profile of cellulose acetate hybrid dopes prepared using sonication mixing.

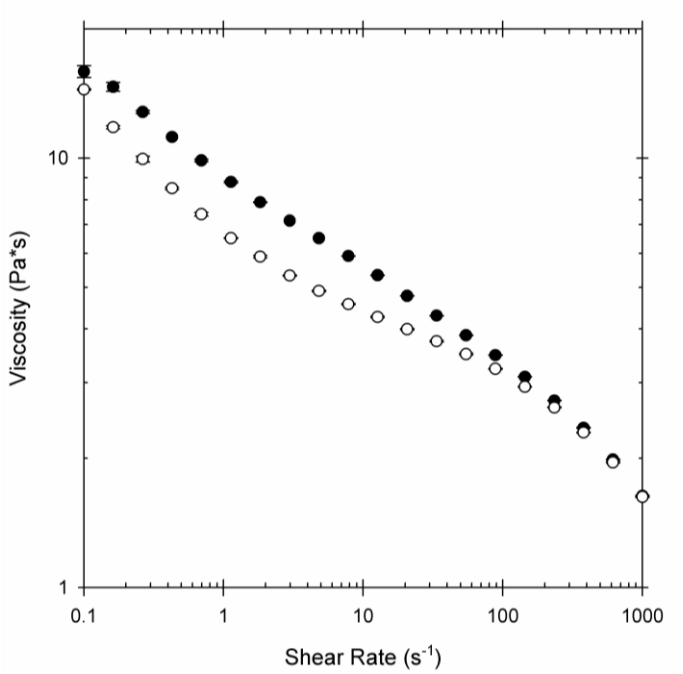

Figure C.3: Viscosity profile of cellulose acetate hybrid dopes prepared using high shear mixing.

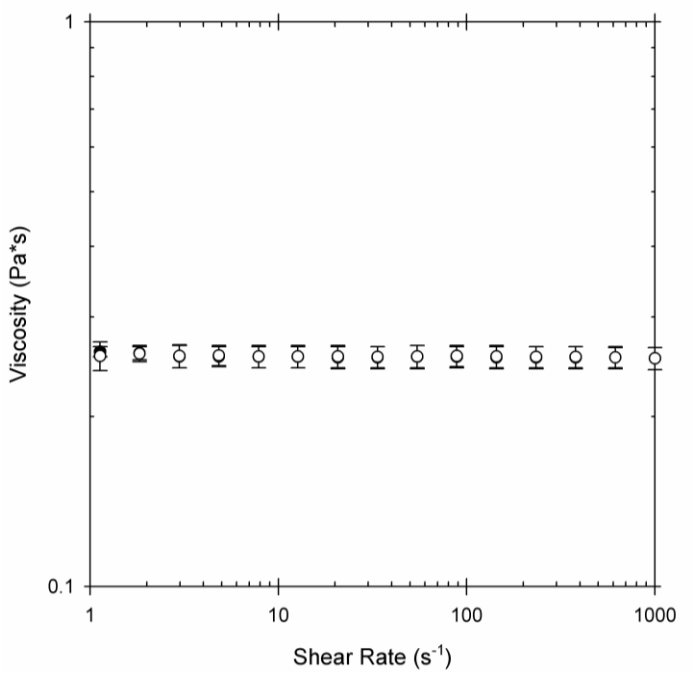

Figure C.4: Viscosity profile of Torlon® hybrid dopes prepared using low shear mixing.

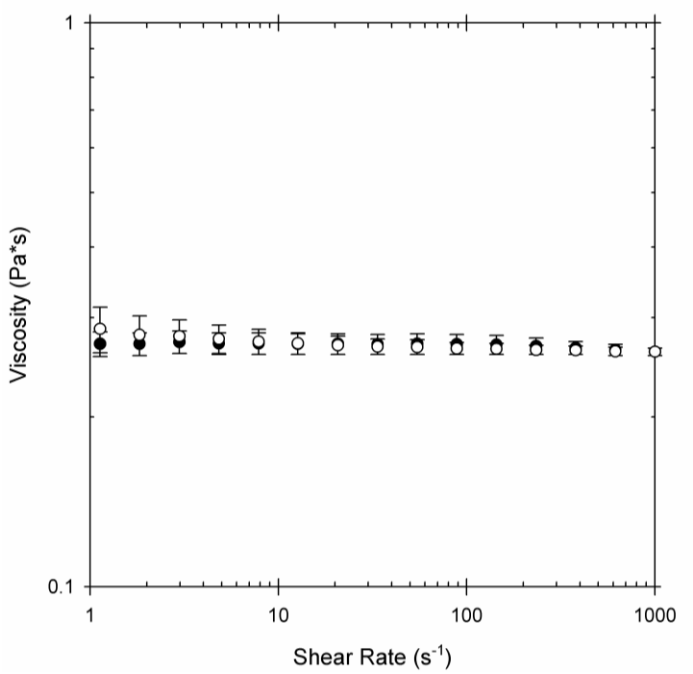

Figure C.5: Viscosity profile of Torlon® hybrid dopes prepared using sonication mixing.

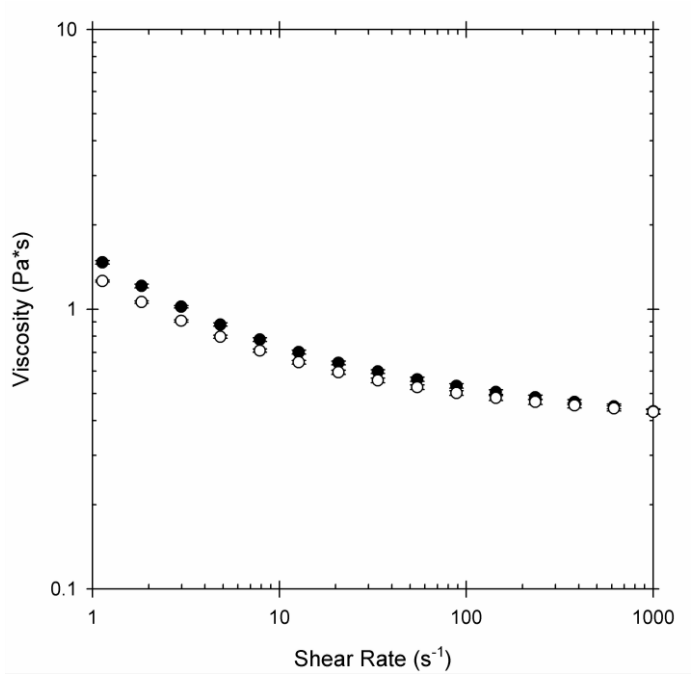

Figure C.6: Viscosity profile of Torlon® hybrid dopes prepared using high shear mixing.

C.4 Viscosities of Samples Containing Different Loading of Nanoclay

Plots presented in the following two subsections are associated with the results and discussion presented in Chapter 4, Section 4.2. Previously we reported the relative viscosities of solutions containing different nanoclay loadings. We found that the solvent solution (polymer, solvent, non-solvent) did not exhibit any deviations in the hysteresis, and therefore have been omitted from this report. Therefore in the following sections we have reported the measured viscosities and their respective hysteresis trends for the dopes containing nanoclay. Compositions for these dopes were reported in Tables 4.3 and 4.4 in Chapter 4. For all figures in this section, closed circles represent viscosity as shear rate is increased and open circles represent viscosity as shear rate is decreased.

C.4.1 Cellulose Acetate-Laponite® RD Dopes

Plots corresponding to the viscosities for the cellulose acetate dopes are presented in Figures C.7-C.9. Dopes containing 0.1wt% and 0.3wt% nanoclay (Figures C.7 and C.8) did not show any deviations in the hysteresis that was not within the error of the measurements. Conversely, the dope containing 0.5wt% (Figure C.9) did show a deviation. We should not that Figure C.9 is a replicate of Figure C.3, but has been re-presented for consistency. An explanation of the observed deviation was given prior in Section C.2.1.

C.4.2 Torlon®-Laponite® RD Dopes

Figures C.10-C.12 correspond to hybrid Torlon® dopes containing different nanoclay loadings. In all cases we do not see any deviations in the hysteresis that are outside the reported error. Please note that Figure C.12 is a replicate of Figure C.6 and has been re-presented here for consistency.

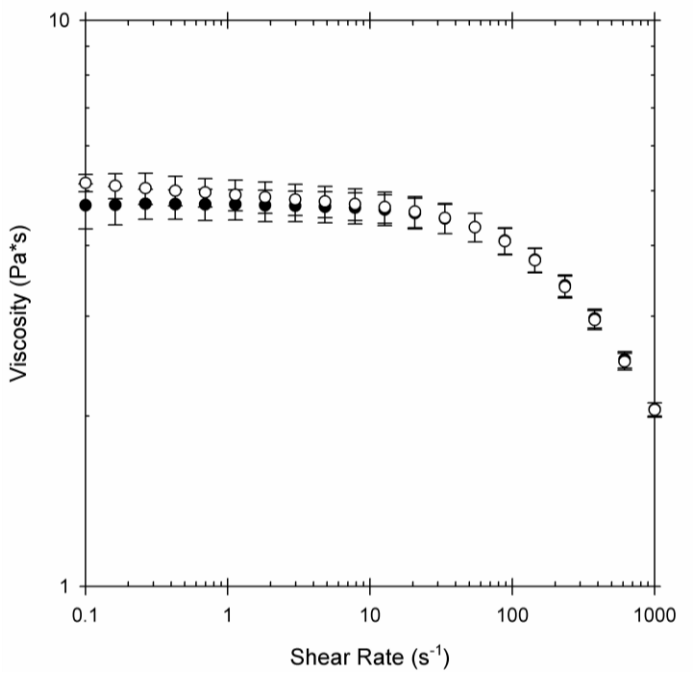

Figure C.7: Viscosity profile of hybrid dopes containing 9.9wt% Cellulose Acetate and 0.1wt% nanoclay dissolved in DMSO, NMP and water

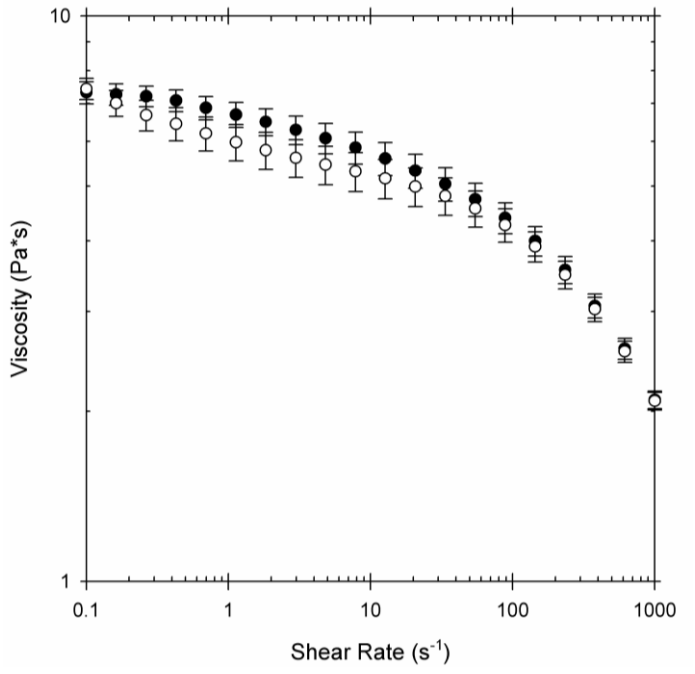

Figure C.8: Viscosity profile of hybrid dopes containing 9.7wt% Cellulose Acetate and 0.3wt% nanoclay dissolved in DMSO, NMP and water

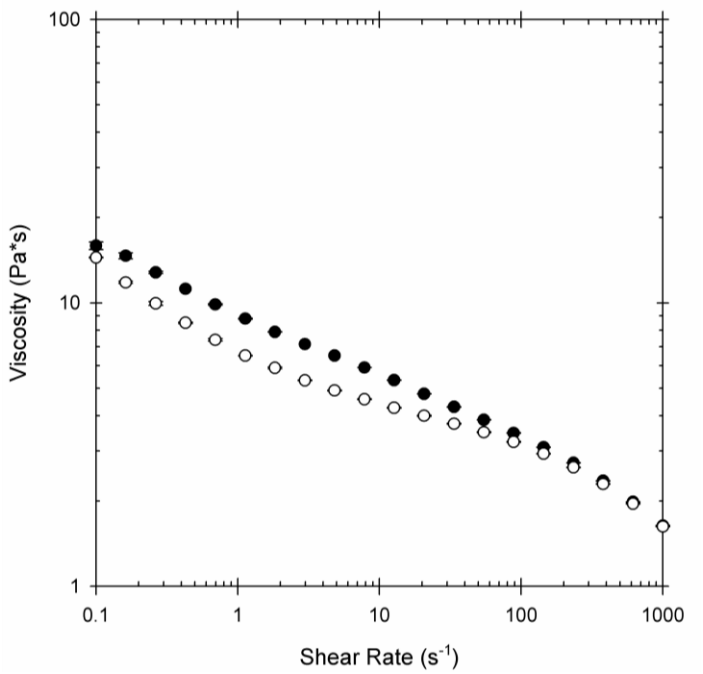

Figure C.9: Viscosity profile of hybrid dopes containing 9.5wt% Cellulose Acetate and 0.5wt% nanoclay dissolved in DMSO, NMP and water

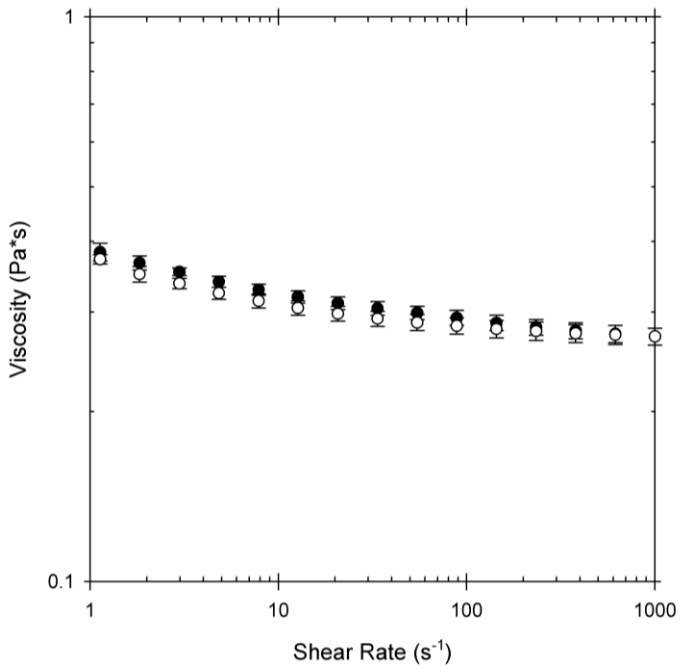

Figure C.10: Viscosity profile of hybrid dopes containing 9.9wt% Torlon® and 0.1wt% nanoclay dissolved in DMSO, NMP and water

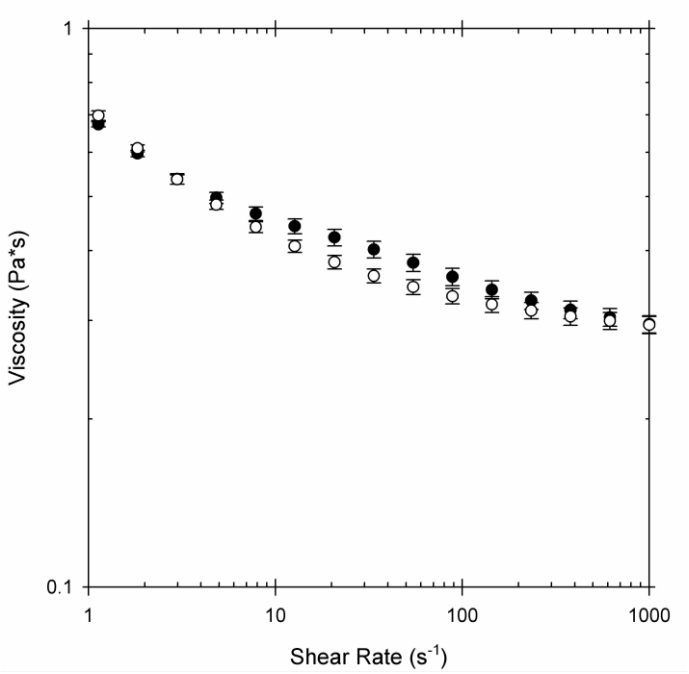

Figure C.11: Viscosity profile of hybrid dopes containing 9.7wt% Torlon® and 0.3wt% nanoclay dissolved in DMSO, NMP and water

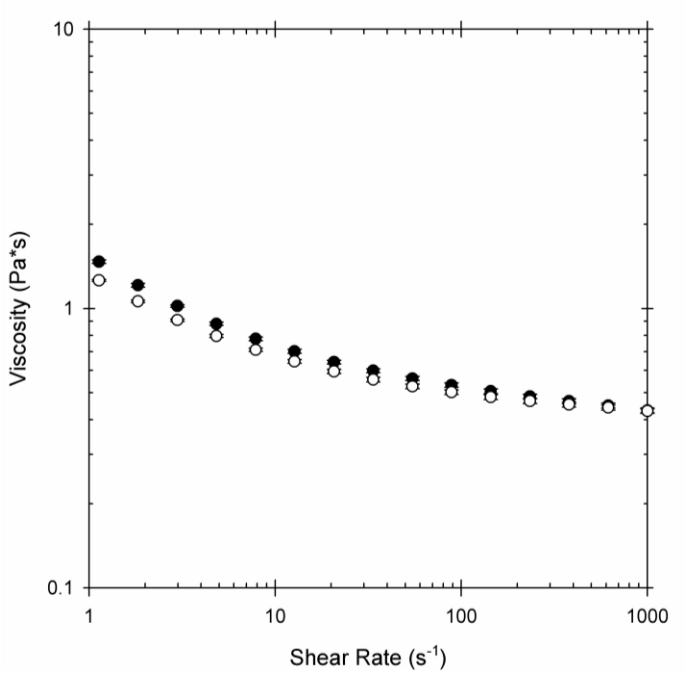

Figure C.12: Viscosity profile of hybrid dopes containing 9.5wt% Torlon® and 0.5wt% nanoclay dissolved in DMSO, NMP and water

APPENDIX D

CELLULOSE ACETATE HYBRID DENSE FILM MEMBRANES CONTAINING 1WT% LAPONITE® RD FILLER

D.1 Overview

In Chapter 5 we presented data for Torlon® hybrid membranes containing 1wt%, 3wt% and 5wt% nanoclay filler. Furthermore, in Chapter 6 we presented data for cellulose acetate hybrid membranes containing 3wt% and 5wt% nanoclay filler. These samples showed significant depression in permeability, as anticipated. However, unlike the Torlon® materials, we had significant difficult obtaining reproducible results for cellulose acetate membrane containing 1wt% filler. In fact, out of dozens of tests we were only able to measure permeability depression in one sample; and this was only evident in one sample gas. Despite the inconsistency, we believe that the data is reasonable and provides a valuable perspective.

D.2 Characterization of Hybrid Dense Film Membranes

Films containing 1wt% Laponite® RD presented challenges in conducting permeation measurements. Numerous attempts were made to produce films that showed permeability reductions. Several films were cast using the preparation and formation procedure developed in this work, but we still found that it was difficult to reproduce transport properties. The permeation properties that were measured are presented in Section D.1.1. Comparisons with mathematical models are presented for consistency.

D.2.1 Permeation Tests

Nanocomposite permeation measurements were made using the same protocol and conditions as the pure polymer film. We observed permeation reduction in one sample out of dozens tested. The permeabilities and associated selectivities for this film are presented solitary in Table D.1. Transport trends are also showed in conjunction with pure polymer values in Figure D.1. (Refer to Chapter 6 for details regarding pure polymer dense films.)

From the data plotted in Figure D.1a it would appear that the hybrid membrane does not exhibit the desired transport properties because the helium permeabilities are higher than the pure polymer membrane. If only these data were considered, then we would conclude that the nanoclays are poorly exfoliated and/or the polymer-clay adhesion is meager. However, if we consider the oxygen permeability we see a slight decrease in permeability compared to the average pure polymer values. These results are promising for the nanocomposite performance. Further analyses of the nitrogen permeation data provide evidence that there is adhesion between the polymer and filler.

Table D.1: Permeability (Barrers) & Selectivity values for Cellulose Acetate-Laponite® RD nanocomposite films containing 1wt% nanoclay filler at different feed pressures.

Feed Gas	**Feed Pressure**		
	50 psia	*75 psia*	*100 psia*
Helium	16.72	16.78	16.85
Oxygen	0.627	0.637	0.646
Nitrogen	0.080	0.089	0.084
O_2/N_2 Selectivity	7.84	7.16	7.69

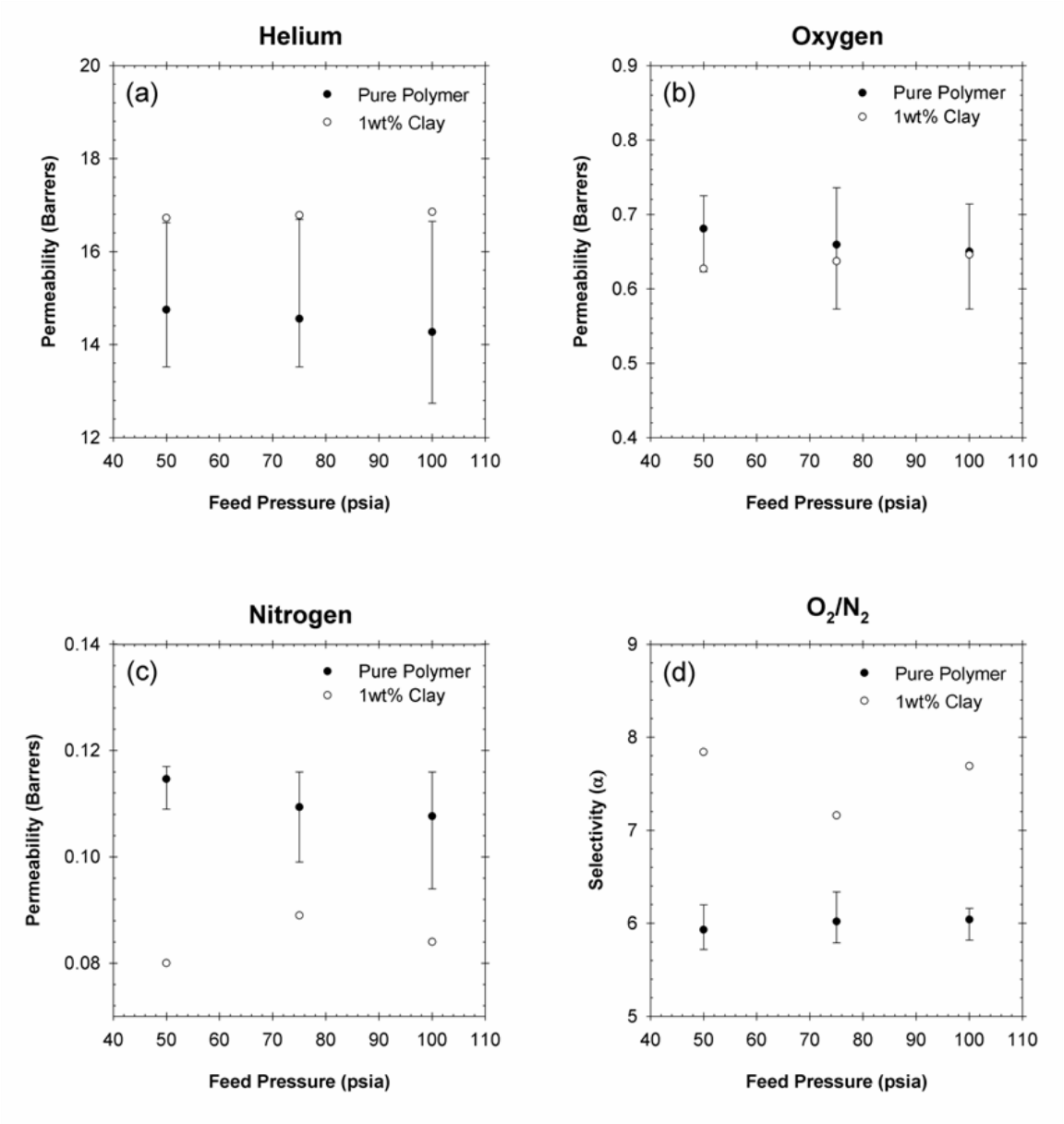

Figure D.1: Permeability properties of Cellulose Acetate-Laponite® RD nanocomposite dense film membranes containing 1wt% nanoclay filler. (a) Helium (b) Oxygen (c) Nitrogen (d) O_2/N_2 Selectivity

To more clearly see the differences between the pure polymer and hybrid membranes, we have presented normalized permeabilities and selectivities in Table D.2. Pure polymer permeation/selectivity is denoted by the naught subscript. A clear trend is visible wherein the normalized permeability decreases as a function of penetrant kinetic diameter (see Table 3.3). As a result the O_2/N_2 selectivity in the hybrid membrane is greater than that of the pure polymer; this does not agree with the base assumptions for hybrid barrier membranes. These trends will be discussed further in Section D.1.4.

Table D.2: Average P/P_0 and α/α_0 values for Cellulose Acetate-Laponite® RD nanocomposite films containing 1wt% nanoclay filler at different feed pressures.

Feed Gas	Feed Pressure		
	50 psia	*75 psia*	*100 psia*
Helium	1.13	1.15	1.18
Oxygen	0.92	0.97	0.97
Nitrogen	0.70	0.81	0.78
O_2/N_2 Selectivity	1.32	1.19	1.27

D.2.2 Microscopic Characterization

Despite the inconsistencies in the transport data, we wanted to characterize the nanoscale morphology of the hybrid membranes. Transmission electron microscopy was used to investigate the exfoliation and dispersion of nanoclays in the matrix. Example images are presented in Figure D.2.

The images in Figure D.2 show substantial evidence that the lamellae are exfoliated within the polymer matrix. These images also suggest that there is particle flocculation, as evidenced by the darker mass in the bottom right of the second image. Existence of floccs is not in these types of membranes. Floccs may even contribute to the poor permeation properties. It has been shown that nanoclay floccs may contain “holes” in the interstitial spaces where polymer does not exist. If true, then these holes would act as non-selective, low-resistance channels for molecular transport. [1,2]

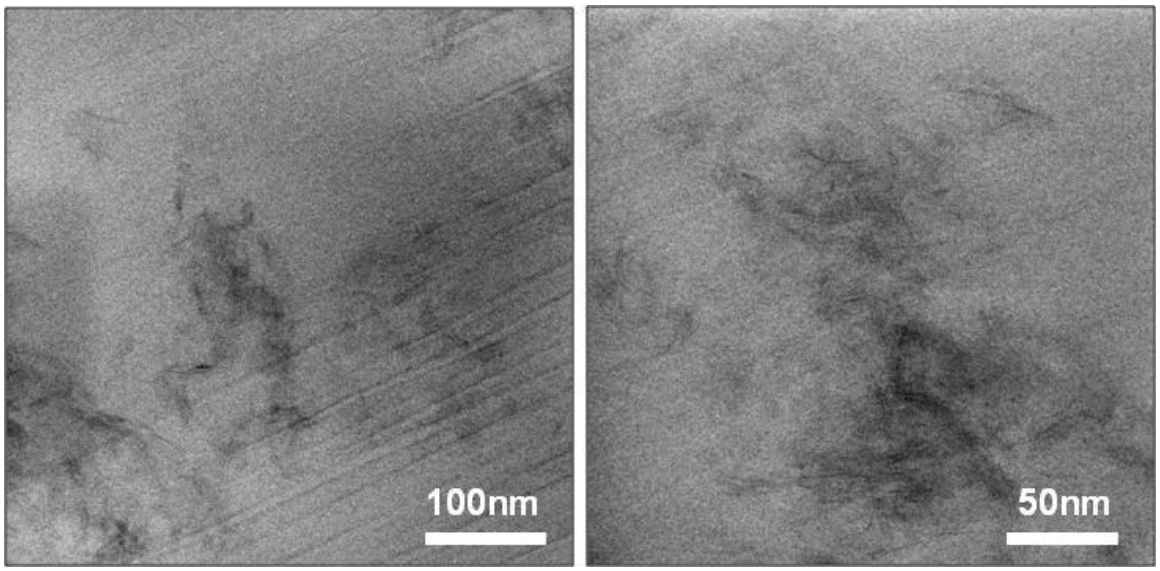

Figure D.2: Transmission electron micrographs of exfoliated (left) and flocculated (right) nanoclays in a cellulose acetate hybrid membrane containing 1wt% filler

Although the TEM images show evidence of well exfoliated nanoclay filler, it is likely that there are numerous defects (floccs, interfacial delamination) in the membranes that lead to the undesirable transport properties. This may be aggravated by the low loading of filler. In Chapter 6 we showed that floccs existed in the higher loading films, yet permeability depressions were achieved. These depressions may be supported by "bulk" type effects of floccs in the membranes, as discussed earlier. At the low loadings presented here these "bulk" effects may not be achievable.

D.2.3 Comparison of Experimental Permeation Results to Model Permeability Predictions

Four equations (Eqs. 2.12, 2.13, 2.17, 2.18) were identified in Chapter 2 as candidates for the prediction of polymer-platelet hybrid membrane transport properties. When we compare our experimental values with these models we do not see any groundbreaking trends. During the permeation analysis of the hybrid film containing 1wt% nanoclay filler we concluded that there are morphological characteristics that contribute to the

unmatched permeability trends. Plotting these data against model values (see Figure D.3) supports this conclusion.

It should be noted that the models were solved with the assumption that the aspect ratio of the filler is 30. This is the idealized value reported in the literature for a single Laponite® RD platelet. Additionally, volume fraction (ϕ_{vol}) used in the model solutions were equal to that of the membrane. For the Bharadwaj equation (Eq. 2.18) it was assumed that the orientation factor (S) was equal to zero – corresponding to an anisotropic orientation of platelets in the polymer matrix.

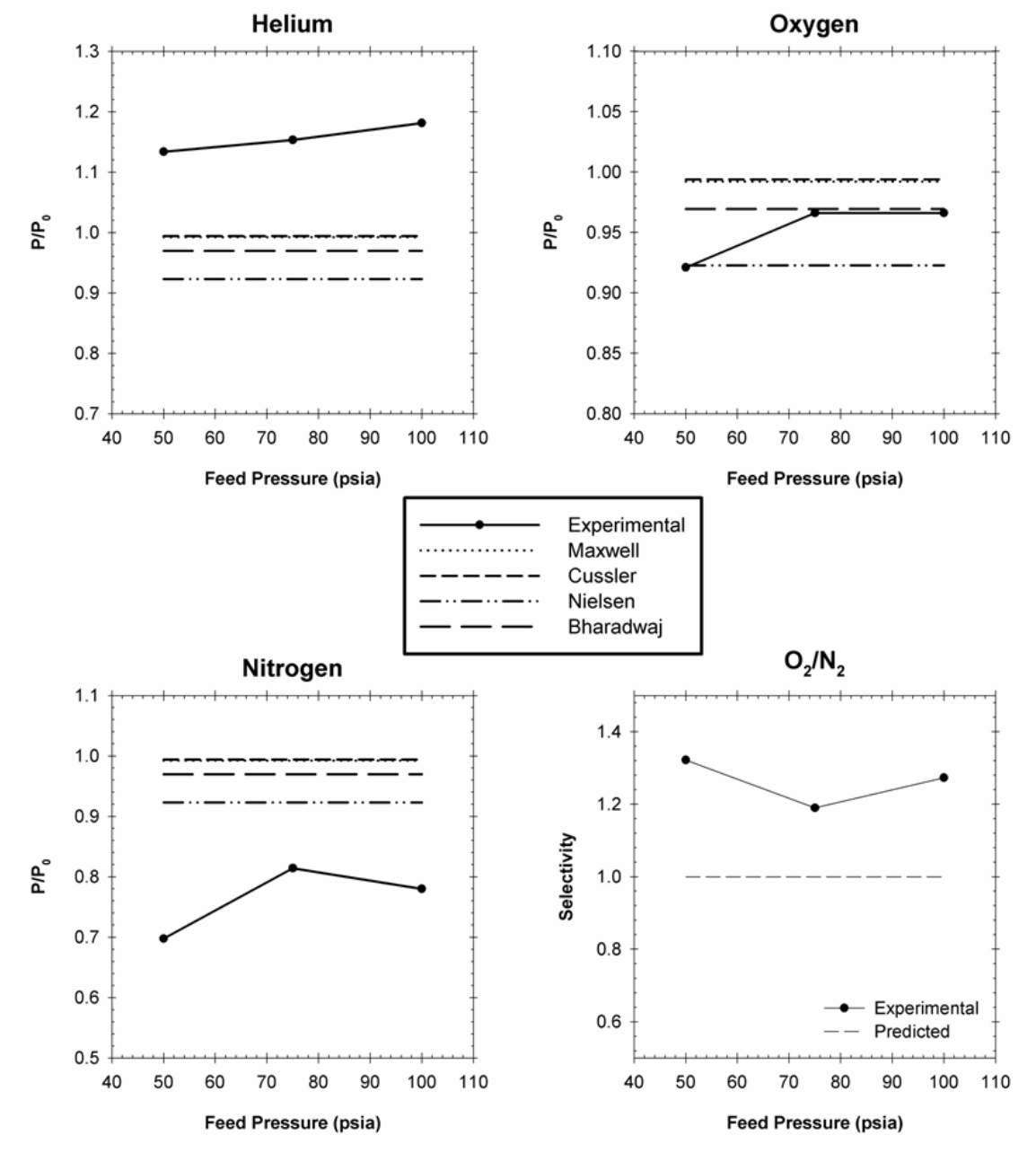

Figure D.3: Average P/P_0 and α/α_0 values for Cellulose Acetate-Laponite® RD nanocomposite films containing 1wt% nanoclay filler at different feed pressures compared to predicted values using various transport models. Filler particle aspect ratio was assumed to be 30 for model calculations and S=0 for the Bharadwaj model.

D.2.4 Permeability Trends as a Function of Gas Penetrant Kinetic Diameter

It was previously prefaced that the permeation measurements for films containing 1wt% nanoclay filler were not reproducible; despite numerous attempts. Data in Figure D.4 may provide an explanation. We see that P/P_0 values for helium are greater than one and oxygen values are very near one. Nitrogen, on the other hand, has a significant deviation from one. This trend indicates two possible morphologies: (1) defects exist in the membrane that are selective for nitrogen or (2) a zone of influence exists around the filler phase that has a greater effect on the larger gas. Regardless, the average ideal selectivity increased more than 20% over pure polymer. To some this may appear like a serendipitous success – increased selectivity with little change in permeability (for the fast gas). We cannot say with confidence that this is true since the data was not reproducible. Meanwhile, we can confidently say that there are defects in the measured film. Further permeation studies are needed to draw additional conclusions.

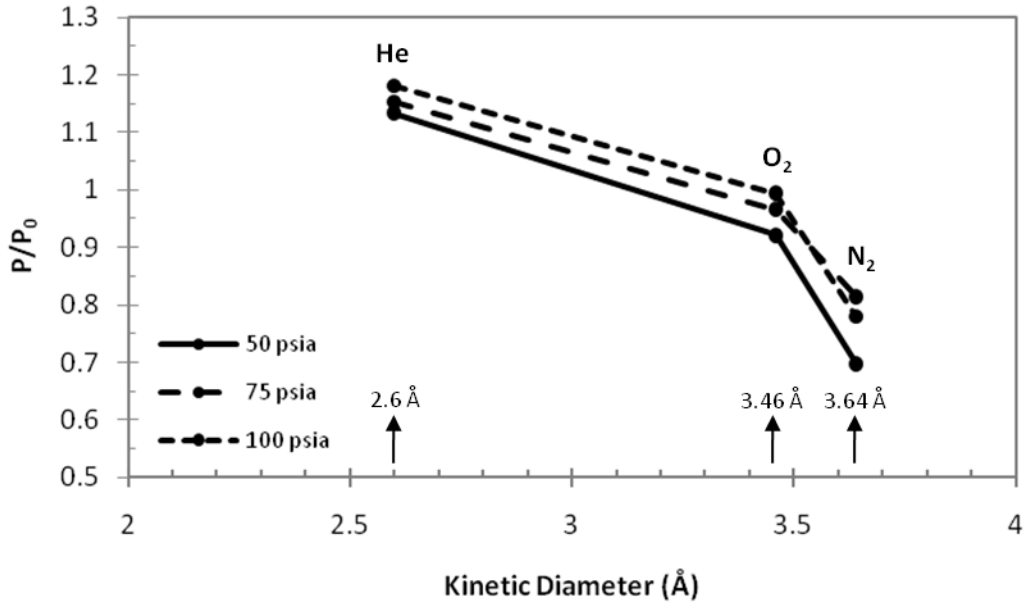

Figure D.4: Permeability depression in Cellulose Acetate-Laponite® RD hybrid membrane containing 1wt% nanoclay as a function of kinetic diameter of gas penetrant.

D.3 Summary & Conclusions

Throughout the course of this work it was quite common to face difficulties in repeatedly masking defect free membranes for permeation tests. In some cases this was a product of large particulates in the films; however there were other cases were no defect was apparent by eye. The TEM images presented in Figure D.2 proves that the hybrid membranes do contain an exfoliated system of nanoclays, but also that floccs are present. We hypothesize that a combination of interfacial and flocc defects, combined with the low loading of clay in the hybrid membrane, are the source of the difficulties reproducibly testing these films. Optimization of the dope preparation procedures may improve the reproducibility. Regardless of these data, it was shown that cellulose acetate hybrid films with higher loadings were successful and reproducible.

D.4 References

1. G. Choudalakis, A. Gotsis, "Permeability of Polymer/Clay Nanocomposites: A Review," *European Polymer Journal* **45** (4), 967-984 (2009).

2. A. Manninen, H. Naguib, A. Nawaby, and M. Day, "CO_2 Sorption and Diffusion in Polymethyl Methacrylate-Clay Nanocomposites," *Polymer Engineering and Science* **45** (7), 904-914 (2005).

CONSOLIDATED BIBLIOGRAPHY

A consolidated list of the cited literature is provided below, in alphabetical order by first author, for the reader's convenience.

R. Adams, C. Carson, J. Ward, R. Tannenbaum, W.J. Koros, 2010: Metal Organic Framework Mixed Matrix Membranes for Gas Separations. *Microporous and Mesoporous Materials*, **131,** 13-20.

J. Ally, E. Vittorias, A. Amirfazili M. Kappl, E. Bonaccurso, C. McNamee, H. Butt, 2010: Interaction of a Microsphere with a Solid-Supported Liquid Film. *Langmuir*, **26,** 11797-11803.

R. Aringhieri, 2004: Nanoporosity Characteristics of Some Natural Clay Minerals and Soils. *Clays and Clay Minerals*, **52,** 700-704.

L. Aylmore, 1974: Gas Sorption in Clay Mineral Systems. *Clay and Clay Materials*, **22,** 175-183.

R.W. Baker, 2004: *Membrane Technology and Applications.* 2nd ed. John Wiley & Sons, Inc.

R.W. Baker, 2006: Membrane Technology in the Chemical Industry: Future Directions. *Membrane Technology in the Chemical Industry*, 2nd ed., S. P. Nunes, and K.-V. Pienemann, Eds., WILEY-VCH, 305-335.

E. Balnois, S. Durand-Vidal, P. Levitz, 2003: Probing the Morphology of Laponite Clay Colloids by Atomic Force Microscopy. *Langmuir*, **19,** 6633-6637.

R. Barrer, 1951: *Diffusion in and through Solids.* Cambridge University Press.

A. Barton, 1983: *Handbook of Solubility Parameters and Other Cohesion Parameters.* CRC Press, Inc.

D. Bhandari, 2010: Hollow Fiber Sorbents for the Desulfurization of Pipeline Natural Gas. PhD Dissertation, Chemical & Biomolecular Engineering, Georgia Institute of Technology.

R. Bharadwaj, 2001: Modeling the Barrier Properties of Polymer-Layered Silicate Nanocomposites. *Macromolecules*, **34,** 9189-9182.

R.H.B. Bouma, A. Checchetti, G. Chidichimo, and E. Drioli, 1997: Permeation Through a Heterogeneous Membrane: The Effect of the Dispersed Phase. *Journal of Membrane Science*, **128,** 141-149.

D. Breck, 1974: *Zeolite Molecular Sieves: Structure, Chemistry, and Use.* Robert E. Krieger Publishing Co.

G. Brindley, K. Wiewiora, A. Wiewiora, 1969: Intracrystalline Swelling of Montmorillonite in Some Water-Organic Mixtures. *The American Mineralogist*, **54,** 1635-1644.

D. Burgentzle, J. Duchet, J. Gerard, A. Jupin, B. Fillon, 2004: Solvent-Based Nanocomposite Coatings I. Dispersion of Organophillic Montmorillonite in Organic Solvents. *Journal of Colloid and Interface Science*, **278,** 26-39.

S. Carruthers, 2001: Integral-Skin Formation in Hollow Fiber Membranes for Gas Separations. PhD Dissertation, Chemical Engineering, University of Texas - Austin.

S. Carruthers, G. Ramos, and W.J. Koros, 2003: Morphology of Integral-Skin Layers in Hollow-Fiber Gas-Separation Membranes. *Journal of Applied Polymer Science*, **90,** 399-411.

R. Chafin II, 2007: Torlon and Silicalite Mixed Matrix Membranes for Xylene Isomer Purification. PhD Dissertation, Chemical & Biomolecular Engineering, Georgia Institute of Technology.

R. Chafin, J. Lee, W.J. Koros, 2010: Effects of Casting and Post Casting Annealing on Xylene Isomer Transport Properties of Torlon Films. *Polymer*, **51,** 3462-3471.

Z. Chai, Z. Xiao, S. Xuefei, 2002: Preparation of Polymer Microspheres from Solutions *Journal of Polymer Science: Part B: Polymer Physics*, **41,** 259-165.

J. Chang, T. Jang, K. Ihn, and G. Sur, 2003: Poly(Vinyl Alcohol) Nanocomposites with Different Clays: Pristine Clays and Organoclays. *Journal of Applied Polymer Science*, **90,** 3208-3214.

S.-H. Chang, M. Ryan, R. Gupta, B. Swiatkiewicz, 1991: The Adsorption of Water Soluble Polymers on Mica, Talc, Limestone, and Various Clay Minerals. *Colloids and Surfaces*, **59,** 59-70.

L. Cheng, D. Lin, K. Yang, 2000: Formation of Mica-Intercalated Nylon-6 Nanocomposite Membranes by Phase Inversion Method. *Journal of Membrane Science*, **172,** 157-166.

S. Choi, and Coauthors, 2008a: Layered Silicates by Swelling of Amh-3 and Nanocomposite Membranes. *Angewandte Chemie-International Edition*, **47,** 552-555.

S. Choi, J. Coronas, J. Sheffel, E. Jordan, W. Oh, S. Nair, D. Shantz, M. Tsapatsis, 2008: Layered Silicate by Proton Exchange and Swelling in Amh-3. *Microporous and Mesoporous Materials*, **115,** 75-84.

S.H. Choi, J.Q. Coronas, Z.P. Lai, D. Yust, F. Onorato, and M. Tsapatsis, 2008b: Fabrication and Gas Separation Properties of Polybenzimidazole (Pbi)/Nanoporous Silicates Hybrid Membranes. *Journal of Membrane Science*, **316,** 145-152.

G. Choudalakis, A. Gotsis, 2009: Permeability of Polymer/Clay Nanocomposites: A Review. *European Polymer Journal*, **45,** 967-984.

T.S. Chung, L.Y. Jiang, Y. Li, and S. Kulprathipanja, 2007: Mixed Matrix Membranes (Mmms) Comprising Organic Polymers with Dispersed Inorganic Fillers for Gas Separation. *Progress in Polymer Science*, **32,** 483-507.

D. Clausi, and W.J. Koros, 2000: Formation of Defect-Free Polyimide Hollow Fiber Membranes for Gas Separations. *Journal of Membrane Science*, **167,** 79-89.

D. Clausi, W.J. Koros, 2000: Formation of Defect-Free Polyimide Hollow Fiber Membranes for Gas Separations. *Journal of Membrane Science*, **167,** 79-89.

J. Coronas, 2010: Present and Future Synthesis Challenges for Zeolites. *Chemical Engineering Journal*, **156,** 236-242.

J. Crank, G. Park, 1968: *Diffusion in Polymers.* Academic Press, Inc.

E.L. Cussler, 1990: Membranes Containing Selective Flakes. *Journal of Membrane Science*, **52,** 275-288.

M. Das, 2009: Membranes for Olefin/Paraffin Separations. PhD Dissertation, Chemical & Biomolecular Engineering, Georgia Institute of Technology.

P. de Gennes, 1980: Conformations of Poymers Attached to an Interface. *Macromolecules*, **13,** 1069-1075.

P. de Gennes, 1987: Polymers at an Interface: A Simplified View. *Advances in Colloid and Interface Science*, **27,** 189-209.

P. Dubin, P. Tong, Ed., 1993: *Colloid-Polymer Interactions*. American Chemical Society.

O.M. Ekiner, R.A. Hayes, and P. Manos, 1992: Reactive Post Treatment for Gas Separation Membranes. E. I. Du Pont de Nemours and Company, L'Air Liquide, S.A.

K. Feldman, T. Tervoort, P. Smith, N. Spencer, 1998: Toward a Force Spectroscopy of Polymer Surfaces. *Langmuir*, **14,** 372-378.

I. Frankel, and H. Brenner, 1993: Taylor Dispersion of Orientable Brownian Particles in Unbounded Homogeneous Shear Flows. *J. Fluid Mech.*, **255,** 129-156.

G. Fredrickson, J. Bicerano, 1999: Barrier Properties of Oriented Disk Composites. *Journal of Chemical Physics*, **110,** 2181-2188.

C.V. Funk, and D.R. Lloyd, 2008: Zeolite-Filled Microporous Mixed Matrix (Zeotips) Membranes: Prediction of Gas Separation Performance. *Journal of Membrane Science*, **313,** 224-231.

L. Giannuzzi, and F. Stevie, Eds., 2005: *Introduction to Focused Ion Beams: Instrumentation, Theory, Techniques and Practice* Springer.

E. Glynos, V. Koutsos, W. McDicken, C. Moran, S. Pye, J. Ross, V. Sboros, 2009: Nanomechanics of Biocompatible Hollow Thin-Shell Polymer Microspheres. *Langmuir*, **25,** 7514-7522.

E. Goddard, B. Vincent, Ed., 1984: *Polymer Adsorption and Dispersion Stability*. Amercian Chemical Society.

J. Hao, and S. Wang, 1996: Influence of Quench Medium on the Structure and Gas Permeation Properties of Cellulose Acetate Membranes. *Journal of Applied Polymer Science*, **68,** 1269-1276.

S. Hashemi, R. Sahraian, P. Lafleur, K. Stoeffler, 2006: Focus Ion Beam Preparation of Transmission Electron Microscope Sample in Polymer Clay Nanocomposite. *Iranian Polymer Journal*, **15,** 539-545.

S. Hashemifard, A. Ismail, T. Matsuura, 2010: A New Theoretical Gas Permeability Model Using Resistance Modeling for Mixed Matrix Membrane Systems. *Journal of Membrane Science*, **350,** 259-268.

T. He, M. Mulder, H. Strathmann, and M. Wessling, 2002: Preparation of Composite Hollow Fiber Membranes: Co-Extrusion of Hydrophilic Coatings onto Porous Hydrophobic Support Structures. *Journal of Membrane Science*, **207,** 143-156.

N.N. Herrera, J.M. Letoffe, J.P. Reymond, and E. Bourgeat-Lami, 2005: Silylation of Laponite Clay Particles with Monofunctional and Trifunctional Vinyl Alkoxysilanes. *Journal of Materials Chemistry*, **15,** 863-871.

N.N. Herrera, J.M. Letoffe, J.L. Putaux, L. David, and E. Bourgeat-Lami, 2004: Aqueous Dispersions of Silane-Functionalized Laponite Clay Platelets. A First Step toward the Elaboration of Water-Based Polymer/Clay Nanocomposites. *Langmuir*, **20,** 1564-1571.

D. Ho, and C. Glinka, 2003: Effects of Solvent Solubility Parameters on Organoclay Dispersions. *Chemistry of Materials*, **15,** 1309-1312.

D. Ho, R. Briber, and C. Glinka, 2001: Characterization of Organically Modified Clayes Using Scattering and Microscopy Techniques. *Chemistry of Materials*, **13,** 1923-1931.

W. Ho, Ed., 1992: *Membrane Handbook*. Springer.

R. Hunter, 1991: *Foundations of Colloid Science.* Vol. 1, Oxford University Press.

S. Husain, 2006: Mixed Matrix Dual Layer Hollow Fiber Membranes for Natural Gas Separation. PhD Dissertation, Chemical & Biomolecular Engineering, Georgia Institute of Technology.

S. Husain, and W.J. Koros, 2007: Mixed Matrix Hollow Fiber Membranes Made with Modified Hssz-13 Zeolite in Polyetherimide Polymer Matrix for Gas Separation. *Journal of Membrane Science*, **288,** 195-207.

F. Hussain, M. Hojjati, M. Okamoto, and R.E. Gorga, 2006: Review Article: Polymer-Matrix Nanocomposites, Processing, Manufacturing, and Application: An Overview. *Journal of Composite Materials*, **40,** 1511-1575.

H.-K. Jeong, W. Krych, H. Ramanan, S. Nair, E. Marand, and M. Tsapatsis, 2004: Fabrication of Polymer/Selective-Flake Nanocomposite Membranes and Their Use in Gas Separation. *Chemistry of Materials*, **16,** 3838-3845.

L.Y. Jiang, T.S. Chung, and S. Kulprathipanja, 2006: Fabrication of Mixed Matrix Hollow Fibers with Intimate Polymer-Zeolite Interface for Gas Separation. *Aiche Journal*, **52,** 2898-2908.

X. Jie, Y. Cao, J.-J. Qin, and Y. Quan, 2005: Influence of Drying Method on Morphology and Properties of Asymmetric Cellulose Hollow Fiber Membrane. *Journal of Membrane Science*, **246,** 157-165.

J.R. Johnson, W.J. Koros, 2009: Utilization of Nanoplatelets in Organic-Inorganic Hybrid Separation Materials: Separation Advantages and Formation Challenges. *Journal of Taiwan Insitute of Chemical Engineers*, **40,** 268-275.

Y.C. Ke, and P. Stroeve, 2005: *Polymer-Layered Silicate and Silica Nanocomposites.* ELSEVIER Inc.

L. Khounlavong, and V. Ganesan, 2009: Influence of Interfacial Layers Upon the Barrier Properties of Polymer Nanocomposites. *Journal of Chemical Physics*, **130,** 12.

J. Koo, 2006: *Polymer Nanocomposites.* McGraw Hill.

W.J. Koros, Ed., 1990: *Barrier Polymers and Structures*. American Chemical Society.

W.J. Koros, 2004: Evolving Beyond the Thermal Age of Separation Processes: Membranes Can Lead the Way. *AIChE Journal*, **50,** 2326.

W.J. Koros, Fleming, G., 1993: Membrane-Based Gas Separation. *Journal of Membrane Science*, **83,** 1-80.

M. Kosuri, 2009: Polymeric Membranes for Super Critical Carbon Dioxide ($Scco_2$) Separations. PhD Dissertation, Chemical & Biomolecular Engineering, Georgia Institute of Technology.

M. Kosuri, and W.J. Koros, 2008: Defect-Free Asymmetric Hollow Fiber Membranes from Torlon, a Polyamid-Imide, for High Pressure Co_2 Separations. *Journal of Membrane Science*, **320,** 65-72.

M. Kroon, 1998: Structure and Formation of a Gel of Colloidal Disks. PhD Dissertation, Physics, Universiteit van Amsterdam.

S.S. Kulkarni, S.M. Tambe, A.A. Kittur, and M.Y. Kariduraganavar, 2006: Preparation of Novel Composite Membranes for the Pervaporation Separation of Water-Acetic Acid Mixtures. *Journal of Membrane Science*, **285,** 420-431.

W. Lawrence, Ed., 1965: *Clay-Water Systems*. Alfred University.

E.S.H. Leach, A. Hopkinson, K. Franklin, and J.S. van Duijneveldt, 2005: Nonaqueous Suspensions of Laponite and Montmorillonite. *Langmuir*, **21,** 3821-3830.

J.-H. Lee, B. Thio, T-H. Bae, J. Meredith, 2009: Role of Lewis Basicity and Van Der Waals Forces in Adhesion of Silica Mfi Zeolites (010) with Polyimides. *Langmuir*, **25,** 9101-9107.

A. Leite, L. Maia, E. Araujo, H. Lira, 2009: Nylon 6/Brazilian Clay Membranes Prepared by Phase Inversion. *Journal of Applied Polymer Science*, **113,** 1488-1493.

N. Li, A. Fane, W. Ho, T. Matsuura, Ed., 2008: *Advanced Membrane Technology and Applications*. John Wiley & Sons, Inc.

S. Liff, N. Kumar, G. McKinley, 2007: High-Performance Elastomeric Nanocomposites Via Solvent-Exchange Processing. *Nature Materials*, **6,** 76-83.

Y. Lim, and A. Mohammed, 2010: Effect of Solution Chemistry on Flux Decline During High Concentration Protein Ultrafiltration through a Hydrophillic Membrane. *Chemical Engineering Journal*, **159,** 91-97.

J. Liu, T-H. Bae, W. Qiu, S. Husain, S. Nair, C. Jones, R. Chance, W.J. Koros, 2009: Butane Isomer Transport Properties of 6fda-Dam and Mfi-6fda-Dam Mixed Matrix Membranes. *Journal of Membrane Science*, **343,** 157-163.

L. Liu, and Coauthors, 2009: New Crystalline Layered Zinc Phosphate with 10-Membered-Ring Channels Perpendicular to Layers. *Inorganic Chemistry*, **48,** 4598-4600.

C. Lu, Y-M. Mai, 2005: Influence of Aspect Ratio on Barrier Properties of Polymer-Clay Nanocomposites. *Physical Review Letters*, **95,** 088303/088301-088303/088304.

C. Macosko, 1994: *Rheology Principles, Measurements and Applications.* Wiley-VCH, Inc.

S. Maheshwari, E. Jordan, S. Kumar, F.S. Bates, R.L. Penn, D.F. Shantz, and M. Tsapatsis, 2008: Layer Structure Preservation During Swelling, Pillaring, and Exfoliation of a Zeolite Precursor. *Journal of the American Chemical Society*, **130,** 1507-1516.

A. Manninen, H. Naguib, A. Nawaby, and M. Day, 2005: Co_2 Sorption and Diffusion in Polymethyl Methacrylate-Clay Nanocomposites. *Polymer Engineering and Science*, **45,** 904-914.

J. Mark, Ed., 1999: *Polymer Data Handbook*. 1st ed. Oxford University Press.

S. Matteucci, R.D. Raharjo, V.A. Kusuma, S. Swinnea, and B.D. Freeman, 2008: Gas Permeability, Solubility, and Diffusion Coefficients in 1,2-Polybutadiene Containing Magnesium Oxide. *Macromolecules*, **41,** 2144-2156.

J. Maxwell, 1873: *A Treatise on Electricity and Magnetism.* Vol. 1, Clarendon Press.

M. McAlpine, N. Hudson, J. Liggat, R. Pethrick, D. Pugh, and I. Rhoney, 2006: Study of the Factors Influencing the Exfoliation of an Organically Modified Montmorillonite in Methyl Methacrylate/Poly(Methyl Methacrylate) Mixtures. *Journal of Applied Polymer Science*, **99,** 2614-2626.

J. Meng, X. Hu, F. Boey, and L. Lin, 2005: Effect of Layered Nano-Organosilicate on the Gel Point Rheology of

Bismaleimide/Diallylbisphenol a Resin. *Polymer*, **46,** 2766-2776.

P. Mercea, 1992: Gas Permeation through Asymmetrical Cellulose Acetate Membranes. *Revista De Chimie*, **43,** 121-128.

T. Merkel, B. Freeman, R. Spontak, Z. He, I. Pinnau, P. Meakin, A. Hill, 2002: Ultrapermeable, Reverse-Selective Nanocomposite Membranes. *Science*, **296,** 519-522.

V.B. Meyer-Rochow, and J. Gal, 2003: Pressures Produced When Penguins Pooh—Calculations on Avian Defaecation *Polar Biology*, **27,** 56-58.

B. Minhas, T. Matsuura, and S. Sourirajan, 1987: Formation of Asymmetric Cellulose Acetate Membranes for the Separation of Carbon Dioxide-Methane Gas Mixtures. *Industrial & Engineering Chemistry Research*, **26,** 2344-2348.

T. Moore, 2004: Effects of Materials, Processing, and Operating Conditions on the Morphology of Gas Transport Properties of Mixed Matrix Membranes. PhD Dissertation, Chemical Engineering, University of Texas - Austin.

T. Moore, S. Damle, P. Williams, and W.J. Koros, 2004a: Characterization of Low Permeability Gas Separation Membranes and
Barrier Materials: Design and Operation Considerations. *Journal of Membrane Science*, **245,** 227-231.

T. Moore, R. Mahajan, D. Vu, and W.J. Koros, 2004b: Hybrid Membrane Materials Comprising Organic Polymers with Rigid Dispersed Phases. *AIChE Journal*, **50,** 311-321.

T. Moore, W.J. Koros, 2005: Non-Ideal Effects in Organic-Inorganic Materials for Gas Separation Membranes. *Journal of Molecular Science*, **739,** 87-98.

A. Mourchild, A. Delville, J. Lambard, E. Lecolier, and P. Levitz, 1995: Phase Diagram of Colloidal Dispersions of Anisotropic Charged Particles: Equilibrium Properties, Structure, and Rheology of Laponite Suspensions. *Langmuir*, **11,** 1942-1950.

M. Mulder, 2003: *Basic Principles of Membrane Technology.* 2nd ed. Kluwer Academic Publishers Group.

J. Nalaskowski, J. Drelich, J. Hupka, J. MIller, 2003: Adhesion between Hydrocarbon Particles and Silica Surfaces with Different Degrees of Hydration as Determined by the Afm Colloidal Probe Technique. *Langmuir*, **19,** 5311-5317.

D. Napper, A. Netschey, 1971: Studies of the Steric Stabilization of Colloidal Particles. *Journal of Colloid and Interface Science*, **37,** 528-535.

R. Nelson, 1988: *Dispersing Powders in Liquids.* Elsevier.

A. Newman, G. Brown, 1987: *Chemistry of Clays and Clay Minerals.* John Wiley & Sons.

L. Nielsen, 1967: Models for the Permeability of Filled Polymer Systems. *Journal of Macromolecular Science: Part A, Pure & Applied Chemistry*, **1,** 929-942.

O. Olabisi, Ed., 1997: *Handbook of Thermoplastics*. Marcel Dekker, Inc.

S. Olejnik, A. Posner, and J. Quirk, 1974: Swelling of Montmorillonite in Polar Organic Liquids. *Clays and Clay Minerals*, **22,** 361-365.

I. Omole, 2008: Crossliked Polyimide Hollow Fiber Membranes for Aggressive Natural Gas Feed Streams. PhD Dissertation, Chemical & Biomolecular Engineering, Georgia Institute of Technology.

M. Onikata, M. Kondo, N. Hayashi, and S. Yamanaka, 1999: Complex Formation of Cation-Exchanged Montrmorillonites with Propylene Carbonate: Osmotic Swelling in Aqueous Electrolyte Solutions. *Clays and Clay Minerals*, **47,** 672-677.

R. Pal, 2007: *Rheology of Particulate Dispersions and Composites.* Vol. 136, CRC Press.

R. Pal, 2008: Permeation Models for Mixed Matrix Membranes. *Journal of Colloid and Interface Science*, **317,** 191-198.

J. Park, H. Lee, D. Chae, W. Oh, J. Yeh, Y. Deng, and J. Yeum, 2009: Electrospinning and Characterization of Poly(Vinyl Alcohol)/Chitosan Oligosaccharide/Clay Nanocomposite Nanofibers in Aqueous Solutions. *Colloid and Polymer Science*, **287,** 943-950.

D.R. Paul, L.M. Robeson, 2008: Polymer Nanotechnology: Nanocomposites. *Polymer*, **49,** 3187-3204.

S. Pavlidou, C. Papaspyrides, 2008: A Review on Polymer-Layered Silicate Nanocomposites. *Progress in Polymer Science*, **33,** 1119-1198.

S. Pesek, 1993: Aqueous Quenched Asymmetric Polysulfone Flat Sheet and Hollow Fiber Membranes Prepared by Dry/Wet Phase Separation. PhD Dissertation, Chemical Engineering, University of Texas - Austin.

S. Pesek, and W.J. Koros, 1994: Aqueous Quenched Asymmetric Polysulfone Hollow Fibers Prepared by Dry/Wet Phase Separation. *Journal of Membrane Science*, **88,** 1-19.

J. Petropoulos, 1985: A Comparative Study of Approaches Applied to the Permeability of Binary Composite Polymeric Materials. *Journal of Polymer Science: Polymer Physics*, **23,** 1309-1324.

F. Pignon, A. Magnin, J.-M. Piau, B. Cabane, P. Lindner, and O. Diat, 1997: Yield Stress Thixotropic Clay Suspensions: Investigations of Structure by Light, Neutron, and X-Ray Scattering. *Physical Review E*, **56,** 3281-3289.

I. Pinnau, B. Freeman, Ed., 1999: *Membrane Formation and Modification*. American Chemical Society.

T.J. Pinnavaia, and G.W. Beall, 2000: *Polymer-Clay Nanocomposites.* John Wiley & Sons, Ltd., 349 pp.

C. Pizzey, S. Klein, E. Leach, J. van Duijneveldt, and R. Richardson, 2004: Suspensions of Colloidal Plates in a Nematic Liquid Crystal: A Small Angle X-Ray Scattering Study. *Journal of Physics - Condensed Matter*, **16,** 2479-2495.

M. Porter, 1991: *Handbook of Industrial Membrane Technology.* William Andrew Publishing.

J. Ramsay, S. Swanton, and J. Bunce, 1990: Swelling and Dispersion of Smectite Clay Colloids: Determination of Structure by Neutron Diffraction and Small-Angle Neutron Scattering. *Journal of the Chemical Society, Faraday Transactions*, **86,** 3919-3926.

S. Ray, M. Okamota, 2003: Polymer/Layered Silicate Nanocomposites: A Review from Preparation to Processing. *Progress in Polymer Science*, **28,** 1539-1641.

I. Rhoney, S. Brown, N. Hudson, and R. Pethrick, 2004: Influence of Processing Method on the Exfoliation Process for Organically Modified Clay Systems I. Polyurethanes. *Journal of Applied Polymer Science*, **91,** 1335-1343.

P. Rittigstein, and J.M. Torkelson, 2006: Polymer-Nanoparticle Interfacial Interactions in Polymer Nanocomposites: Confinement Effects on Glass Transition Temperature and Suppression of Physical Aging. *J. Polym. Sci. Pt. B-Polym. Phys.*, **44,** 2935-2943.

L.M. Robeson, 1993: Correlation of Separation Factor Versus Permeability for Polymeric Membranes. *Journal of Membrane Science*, **62,** 165-185.

L.M. Robeson, 2008: The Upper Bound Revisited. *Journal of Membrane Science*, **320,** 390-400.

M. Rubinstein, and R. Colby, 2003: *Polymer Physics.* Oxford University Press.

E. Sada, H. Kumazawa, J. Wang, and M. Koizumi, 1992: Separation of Co_2 by Asymmetric Hollow Fiber Membrane of Cellulose Acetate. *Journal of Applied Polymer Science*, **45,** 2181-2186.

C. Sanchez, B. Julian, P. Belleville, M. Popall, 2005: Applications of Hybrid Organic-Inorganic Nanocompsites. *Journal of Materials Chemistry*, **15,** 3559-3592.

N. Schamp, and J. Huylebroeck, 1973: Adsorption of Polymers on Clays. *Journal of Polymer Sicence: Polymer Symposia*, **42,** 553-562.

G. Scocchi, P. Posocco, A. Danani, S. Pricl, M. Fermeglia, 2007a: To the Nanoscale, and Beyond! Multiscale Molecular Modeling of Polymer-Clay Nanocomposites. *Fluid Phase Equilibria*, **261,** 366-374.

G. Scocchi, P. Posocco, J-W. Handgraaf, J. Fraaije, M. Fermeglia, S. Pricl, 2009: A Complete Multiscale Modelling Approach for Polymer–Clay Nanocomposites. *Chemistry - A European Journal*, **15,** 7586-7592.

G. Scocchi, P. Posocco, M. Fermeglia, S. Pricl, 2007b: Polymer-Clay Nanocomposites: A Multiscale Molecular Modeling Approach. *Journal of Physical Chemistry: Part B*, **111,** 2143-2151.

D. Sen, H. Kalipcilar, and L. Yilmaz, 2007: Development of Polycarbonate Based Zeolite 4a Filled Mixed Matrix Gas Separation Membranes. *Journal of Membrane Science*, **303,** 194-203.

P.o. Separations, 1998: *Separation Technologies for the Industries of the Future.* National Academy Press.

J.A. Sheffel, and M. Tsapatsis, 2007: A Model for the Performance of Microporous Mixed Matrix Membranes with Oriented Selective Flakes. *Journal of Membrane Science*, **295,** 50-70.

J. Shieh, T. Chung, R. Wang, M. Srinivasan, and D.R. Paul, 2001: Gas Separation Performance of Poly(4-Vinylpyridine)/Polyetherimide Composite Hollow Fibers. *Journal of Membrane Science*, **182,** 111-123.

S. Shu, 2007: Engineering the Performance of Mixed Matrix Membranes for Gas Separations. PhD Dissertation, Chemical & Biomolecular Engineering, Georgia Institute of Technology.

K. Soppimath, A. Kulkarni, T. Aminabhavi, C. Bhaskar, 2001: Cellulose Acetate Microspheres Prepared by O/W Emulsification and Solvent Evaporation Method. *Journal of Microencapsulation*, **18,** 811-817.

S. Stern, 1994: Polymers for Gas Separations: The Next Decade. *Journal of Membrane Science*, **94,** 1-65.

H. Stretz, D. Paul, R. Li, H. Keskkula, P. Cassidy, 2005: Intercalation and Exfoliation Relationships in Melt-Processed Poly(Styrene-*Co*-Acrylonitrile)/Montmorillonite Nanocomposites. *Polymer*, **46,** 2621-2637.

T. Szabo, J. Wang, A. Volodin, C. van Haesendonck, I. Dekany, R. Shoonheydt, 2009: AFM Study of Smectites in Hybrid Langmuir-Blodgett Films: Saponite, Wyoming Bentonite, Hectorite, and Laponite. *Clays and Clay Minerals*, **57,** 706-714.

B. Theng, 1982: Clay-Polymer Interactions: Summary and Perspectives. *Clays and Clay Minerals*, **30,** 1-10.

B. Thio, J-H. Lee, J. Meredith, A. Keller, 2010: Measuring the Influence of Solution Chemistry on the Adhesion of Au Nanoparticles to Mica Using Colloid Probe Atomic Force Microscopy. *Langmuir*, **26,** 13995-14003.

B. Thio, J. Meredith, 2007: Measurement of Polyamide and Polystyrene Adhesion with Coated-Tip Atomic Force Microscopy. *Journal of Colloid and Interface Science*, **314,** 52-62.

M. Tsapatsis, and W. Fan, 2010: A New, yet Familiar, Lamellar Zeolite. *ChemCatChem*, **2,** 246-248.

S. Tunc, O. Duman, 2010: Preparation and Characterization of Biodegradeable Methyl Cellulose/Montmorillonite Nanocomposite Films. *Applied Clay Science*, **48,** 414-424.

H. van Olphen, 1977: *An Introduction to Clay Colloid Chemistry.* 2nd ed. John Wiley & Sons, Ltd.

B.R. Vaughn, and E. Marand, 2008: Transport Properties of Polymer-Aluminophosphate Nano-Composites Prepared by Simple Mixing. *Journal of Membrane Science*, **310,** 197-207.

J. Vermant, S. Ceccia, M. Dolgovskij, P. Maffettone, C. Macosko, 2007: Quantifying Dispersion of Layered Nanocomposites Via Melt Rheology. *Journal of Rheology*, **51,** 429-450.

D.Q. Vu, W.J. Koros, and S.J. Miller, 2002: High Pressure Co2/Ch4 Separation Using Carbon Molecular Sieve Hollow Fiber Membranes. *Industrial & Engineering Chemistry Research*, **41,** 367-380.

W. Wakeham, E. Mason, 1979: Diffusiontthrough Multiperforate Laminae. *Industrial & Engineering Chemistry Fundamentals*, **18,** 301-305.

D. Wallace, 2004: Crosslinked Hollow Fiber Membranes for Natural Gas Purification and Their Manufacture from Novel Polymers. PhD Dissertation, Chemical Engineering, University of Texas - Austin.

C. Wang, W.M. Hua, Y.H. Yue, and Z. Gao, 2007: Delaminated Microporous Aluminophosphate-Filled Polyvinyl Alcohol Membrane for Pervaporation of Aqueous Alcohol Solutions. *Microporous and Mesoporous Materials*, **105,** 149-155.

K. Wang, S. Foo, and T. Chung, 2009: Mixed Matrix Pvdf Hollow Fiber Membranes with Nanoscale Pores for Desalination through Direct Contact Membrane Distillation. *Industrial & Engineering Chemistry Research*, **48,** 4474-4483.

K. Wang, and Coauthors, 2006: The Role of Clay Network on Macromolecular Chain Mobility and Relaxation in Isotactic Polypropylene/Organoclay Nanocomposites. *Polymer*, **47,** 7131-7144.

J. Ward, 2009: Crosslinkable Mixed Matrix Membranes for the Purification of Natural Gas. PhD Dissertation, Chemical & Biomolecular Engineering, Georgia Institute of Technology.

R. Weast, Ed., 1986: *Crc Handbook of Chemistry and Physics*. 67th ed. CRC Press, Inc.

N. Willenbacher, 1996: Unusual Thixotropic Properties of Aqueous Dispersions of Laponite Rd. *Journal of Colloid and Interface Science*, **182,** 501-510.

J. Wind, S. Sirard, D. Paul, P. Green, K. Johnston, W.J. Koros, 2003: Carbon Dioxide-Induced Plasticization of Polyimide Membranes: Pseudo-Equilibrium Relationships of Diffusion, Sorption, and Swelling. *Macromolecules*, **36,** 6433-6441.

H. Winter, 1999: Soft Polymeric Materials near the Transition from Liquid to Solid State. *Korea-Australia Rheology Journal*, **11,** 275-278.

H. Winter, and F. Chambon, 1986: Analysis of Linear Viscoelasticity of a Crosslinking Polymer at the Gel Point. *Journal of Rheology*, **30,** 367-382.

B. Xu, Q. Zheng, Y. Song, Y. Shangguan, 2006: Calculating Barrier Properties of Polymer/Clay Nanocomposites: Effects of Clay Layers. *Polymer*, **47,** 2904-2910.

Y. Yampolskii, I. Pinnau, B. Freeman, Ed., 2006: *Materials Science of Membranes for Gas and Vapor Separation*. John Wiley & Sons Inc.

N. Yao, Ed., 2010: *Focused Ion Beam Systems: Basics and Applications*. 1st ed. Cambridge University Press.

S. Yariv, and H. Cross, Eds., 2002: *Organo-Clay Complexes and Interactions*. Marcel Dekker, Inc.

C. Yaws, Ed., 1998: *Chemical Properties Handbook*. 1st ed. McGraw-Hill Professional.

S. Yun, D. Attard, V. Lo, J. Davis, H. Li, B. Latella, F. Tsvetkov, H. Noorman, S. Moricca, R. Knott, H. Hanley, M. Morcom, G. Simon G. Gadd, 2007: Spray-Dried Microspheres as a Route to Clay/Polymer Nanocomposites. *Journal of Applied Polymer Science*, **108,** 1550-1556.

Q. Zeng, A. Yu, G. Lu, 2008: Multiscale Modeling and Simulation of Polymer Nanocomposites. *Progress in Polymer Science*, **33,** 191-269.

L. Zhang, C. Jahns, B. Hsiao, and B. Chu, 2003: Synchrotron Saxs/Waxd and Rheological Studies of Clay Suspensions in Silicone Fluid. *Journal of Colloid and Interface Science*, **266,** 339-345.

F. Zhou, W.J. Koros, 2006: Study of Thermal Annealing on Matrimid Fiber Performance in Pervaporation of Acetic Acid and Water Mixtures. *Polymer*, **47,** 280-288.

C.M. Zimmerman, A. Singh, and W.J. Koros, 1997: Tailoring Mixed Matrix Composite Membranes for Gas Separations. *Journal of Membrane Science*, **137,** 145-154.

VITA

J.R. Johnson was born betwixt the picturesque Blue, Wallowa and Elkhorn Mountain ranges in LaGrande, Oregon on 1 October 1981, the son of Anthony Johnson and Merri Compton. During his youth, the family moved around the state including exotic locations like Jordan Valley and Halfway. They briefly settled in Veneta, a suburb of Eugene, where J.R. attended elementary school. When he was twelve, the family moved to the correct side of state and settled in Baker City. He graduated from Baker Senior High School in May of 2000. After high school, J.R. decided to depart the great Northwest and ventured to New England where he attended Worcester Polytechnic Institute in Worcester, Massachussetts. During his undergraduate program J.R. studied abroad extensively; completing projects in London (U.K.), Windhoek (Namibia) and at the E&J Gallo Wineries (Modesta, CA). J.R. graduated with a B.Sc. in Chemical Engineering in May of 2004. His educational palate not sate, he enrolled in the School of Chemical and Biomolecular Engineering at the Georgia Institute of Technology in the fall of 2004. Upon entering the graduate program, J.R. was fortunate enough to have the opportunity to pursue his Doctorate of Philosophy under the guidance of Dr. W.J. Koros. While completing his thesis, J.R. began working as the Lab Manager for the Koros Research Group. J.R. culminated his graduate school experience when he defended his PhD in the fall of 2010. After graduating, J.R. will continue his tenure in the Koros Research Group as the Lab Director and as a Research Engineer for some time. Then, who knows…